STRUCTURE AND DESIGN OPTIMISATION OF COMPOSITES FOR NOISE SUPPRESSION IN VEHICLES

MATTHEW K. LING

APRIL 1992

A thesis submitted in partial fulfilment of the requirements of the Council for National Academic Awards for the degree of Doctor of Philosophy

Sheffield City Polytechnic in collaboration with I.C.I. Polyurethanes Group, Brussels, funded by the National Advisory Body for Public Sector Higher Education

STRUCTURE AND DESIGN OPTIMISATION OF COMPOSITES FOR NOISE SUPPRESSION IN VEHICLES

MATTHEW K. LING

Multi-layered noise control systems are used worldwide in the automotive industry to control vehicles interior noise quality. These composites, which include moulded, and slabstock, polyurethane foam cored carpet systems, are intended to attenuate the ingress of airborne noise and suppress the radiation of structure-borne noise. However, little information has been published on their performance characteristics and the optimisation of their design.

This thesis reviews previous theoretical work on the dynamics of panel vibration and the airborne acoustic insulation and the structure-borne isolation provided by composite systems. Mathematical models are developed for the acoustic behaviour of unbonded multilayer foam cored carpet composites as experienced on the experimental test rig. The models identify the important material and system parameters governing behaviour. These models, together with experimental evidence are used to optimise the design of the polyurethane foam core and rank the foam materials in order of performance. The experimental and theoretical studies are not intended for vehicle interior noise prediction purposes.

The experimental facility uses a horizontal steel test panel, 1mm thick, about 1mx1m, and provides acoustic and vibration excitation. Data are obtained for the effective damping (loss factor) of the 4C panel and the insertion loss (IL) of foam cored composites for both vibration and airborne excitation. The intensity method was used to measure the transmitted noise. The precision of the insertion loss measurements was shown to be better than 1.7dB for frequencies below 4kHz. For airborne excitation reproducibility was better than 1.5dB (f<2kHz). For vibration excitation the reproducibility was less. This was attributed to the coupling method used. Experimental and theoretical studies are divided into three sections: (i) loss factors, (ii) vibration insertion loss and (iii) airborne insertion loss.

Particular attention is given to airborne insertion loss since the precision of measurement allows a detailed analysis to be made. It is shown that IL passes through a minimum governed primarily by the modulus and thickness of the foam core and the surface density of the septum and steel substrate. The level of the IL depends in a complex way on material and design parameters, including the damping of the foam core. The damping of the septum mass is shown to have little effect upon behaviour.

The design optimisation procedure described in the thesis takes account of the loudness of vehicle interior noise at relatively high frequencies (f>500Hz) and the annoyance of discrete tonal noise at relatively low frequencies. It is shown that for a particular incident noise spectrum the carpet composite can be designed to provide the most acceptable noise quality in a vehicle. For a typical large volume production vehicle the optimum resonance frequency is predicted to be about 300Hz. Ways of achieving this frequency with different combinations of design parameters are described.

ACKNOWLEDGEMENTS

The author would like thank the following people for their assistance with this work.

Dr. N.C. Hilyard of Sheffield City Polytechnic for his guidance and supervision of the project. Dr A Cunningham, Mr M Walker, and Mr S Nebesniak of ICI Ltd for the supply of experimental materials. Mr R Rodwell of Gracey & Associates for his advice on intensity measurement techniques. Thanks are also due to other colleagues at Sheffield City Polytechnic and the Building Research Establishment, Watford who have helped in this work.

The photographs of the experimental test facility are reproduced with kind permission of ICI Ltd and Alan Godfrey Photography of Codicote, Hitchin.

Finally, the author would like to thank his family, especially his wife Claire. The support and encouragement they have given has been invaluable.

'When I applied my mind to know wisdom...then I saw all the work of God' Ecclesiastes $8^{16,17}$

ADVANCED STUDIES

Viscoelasticity and the Physics of Foams : A Series of Tutorials by Dr. N. C. Hilyard, Sheffield City Polytechnic, 1987

Wordstar: An Introductory Course, Sheffield City Polytechnic, 1987

Lotus 123: An Introductory Course, Sheffield City Polytechnic, 1987

Sixth Conference on Teaching of Noise and Vibration, Sheffield City Polytechnic, 1988

Noise In and Around Buildings, Autumn Conference, Institute of Acoustics, Windermere, 1988

Acoustics '90, Spring Conference, Institute of Acoustics, Southampton, 1990

Cellular Polymers, An International Conference, RAPRA Technology Ltd., London, 1991

CRAC SERC Graduate School, University of Sheffield, 2-7 April 1992

Glossary of Symbols

a	Panel side length
A	Equivalent room absorption
A_i, A_t	Incident and transmitted pressure amplitudes
A_m, B_m, C_m, D_m	Panel vibration constants
B	Bending stiffness
c_0	Velocity of sound in air
C_B	Velocity of flexural waves
C_L	Velocity of longitudinal waves
d	Thickness of foam layer
e_2	Ratio of elastic moduli
E'	Storage modulus
E^*	Complex modulus, $E^*=E'(1+j\eta)$
f	Frequency
f_c	Critical frequency
f_n	Band centre frequency
f_R	Resonant frequency
F	Force
F_2	Surface pressure-intensity field indicator
F_3	Global pressure-intensity field indicator
g	Acceleration due to gravity $9.81 ms^{-2}$
$g_1(\alpha)$, $g_2(\alpha)$	Radiation efficiency variables
G_x, G_y	Mode frequency variables
h	Panel thickness
h_2	Ratio of layer thicknesses
H_1, H_2	Layer thicknesses
H_x, H_y	Mode frequency variables
I	Intensity
I_{p0}	Residual intensity
I_i, I_t	Incident and transmitted intensity
I_0	Intensity reference level
j	Complex operator $\sqrt{-1}$
k	Wave number
K	Error factor (intensity measurement)
K^*	Bulk stiffness modulus (complex)
K'	Bulk stiffness modulus (real)
l, m, n	Integer variables
L_d	Dynamic capability index
L_{IL}	Insertion loss
m_s	Surface or area density (kgm^{-2})
m_{s1}	Panel surface density
m_{s2}	Septum surface density
m_{seff}	Effective system surface density
m_t	Total mass of system
p_n	Pressure wave
Q	Bulk elastic coefficient for porous material
R_1	Flow resistivity
R_2	Approximately $1.2R_1$
$R_{composite}$	Transmission loss of composite
R_{steel}	Transmission loss of steel
S	Panel area
t	Time
t_1, t_2, t_3	Thickness
T_g	Glass transition temperature
T_{60}	Reverberation time
u	Particle velocity
U	Panel perimeter

$\langle v^2 \rangle$	Space time average mean square velocity
w	Transverse displacement
W_{rad}	Power radiated
x	Axial direction
x_1, x_2	Transmission functions
Y	Porosity
z_0	Specific impedance of air
z_1, z_2, z_3, z_4	Impedance of composite layers
z_T	Terminating impedance
α	Panel mode variable
η	Loss factor
γ	Ratio of specific heats
Γ	Propagation constant
ϵ	Error
δ_{pI0}	Residual pressure-intensity index
δ_{pI}	Local pressure-intensity index
Δ_{pI}	Global pressure-intensity index
∂	Partial differential operator
θ	Angle of incidence
λ	Wavelength
λ_c	Critical wavelength
π	Pi = 3.141..
ϕ	Phase angle
ρ	Density
ρ_0	Density of air
ρ	Complex density of PUR foam
ρ_{tot}	Total density of foam structure and septum
ν	Poisson's ratio
σ_{rad}	Radiation efficiency
τ	Transmissibility coefficient
ω	Angular frequency
Ω	Non-dimensional frequency factor
DMS	Dynamic Mechanical Spectrometer
DMTA	Dynamic Mechanical Thermal Analysis
FEM	Finite Element Model
HHF	High Hysteresis Foam
HR	High Resilient (foam)
IL	Insertion Loss
MDI	Diphenylmethane-4-4-Diisocyanate
PUR	Polyurethane
SEA	Statistical Energy Analysis
SEM	Scanning Electron Microscope
SPL	Sound Pressure Level
SRI	Sound Reduction Index
TDI	Toluene Diisocyanate
TL	Transmission Loss
VE	Viscoelastic
VIBIL	Insertion Loss for vibration excitation

INDEX

1. INTRODUCTION

There has been increasing concern in recent years, throughout the automotive industry, of the importance of interior noise and its effect upon vehicle occupants. Multilayered noise control systems are widely used in production vehicles to reduce interior noise levels. Traditionally, these systems have fibrous felt cores but increasingly moulded polyurethane (PUR) foam backed carpets are being used. They provide the manufacturer with a single unit moulded car carpet, enabling easy and cheaper installation. However, little information has been published on their performance characteristics or their design optimisation.

This thesis reports on work that examines the theoretical and experimental response of these foam cored carpet systems, in order to identify the factors that affect system noise insulation performance. Evaluation of the noise insulation characteristics of the composite is insufficient in itself to assess performance for vehicle noise control because design optimisation of the system is not possible without consideration of the vehicle noise spectrum and the response of the occupant to the noise.

Whilst this work is concerned with the control of noise radiated into the vehicle compartment, no attempt has been made to predict vehicle interior noise levels. The final interior noise level and spectrum results from a combination of all the noise control measures being used, the particular configuration of mechanical components and the compartment geometry. It is thus outside the scope of this project. However, the general concepts of vehicle noise and

vibration are discussed.

This chapter begins with a discussion of the acoustical and vibrational characteristics of vehicles. Noise and vibration sources are identified and methods for interior noise control reviewed. In the final section the scope of the work is presented, and the theoretical and experimental methodologies described.

1.1 Acoustic and Vibration Characteristics of a Vehicle Compartment

The acoustic characteristics of a vehicle compartment are extremely complex. The geometry of the vehicle compartment causes cavity resonances, i.e. standing waves are created laterally and longitudinally. These cause a fluctuating sound level, consisting of high and low pressure levels (Priede, 1970, Raff *et al*, 1973). Careful design of the compartment is required to ensure that the nodal points (i.e. pressure minima) occur in the plane of the head position. Analysis and design is normally carried out using the finite element method (FEM), (Craggs, 1972, 1986, 1988) or more recently by statistical energy analysis (SEA), (Walsh *et al* 1990). The principle resonances for a car are in the region of 80-90, 130-140 and 150-160 Hz (Priede *et al*, 1970).

The vibrational characteristics of a vehicle compartment are also complex and differ between cars and heavy goods vehicles (HGV). In a car the vehicle cavity forms an integral part of the vehicle structure, and is thus subjected to many stresses and forces. A truck has a cab which is a self-contained unit and placed on the

load bearing chassis. The work by Priede (1971) and Talbot *et al* (1975) has shown that for a car the dominant cavity vibration is caused by ring modes (nos. 2, 3 and 4) which produce the body resonances in the 80Hz region.

1.2 Characteristics of the Noise and Vibration Sources in Vehicles

Noise entering a vehicle can be divided into two categories (a) airborne and (b) structure-borne. This is shown in Fig. 1.

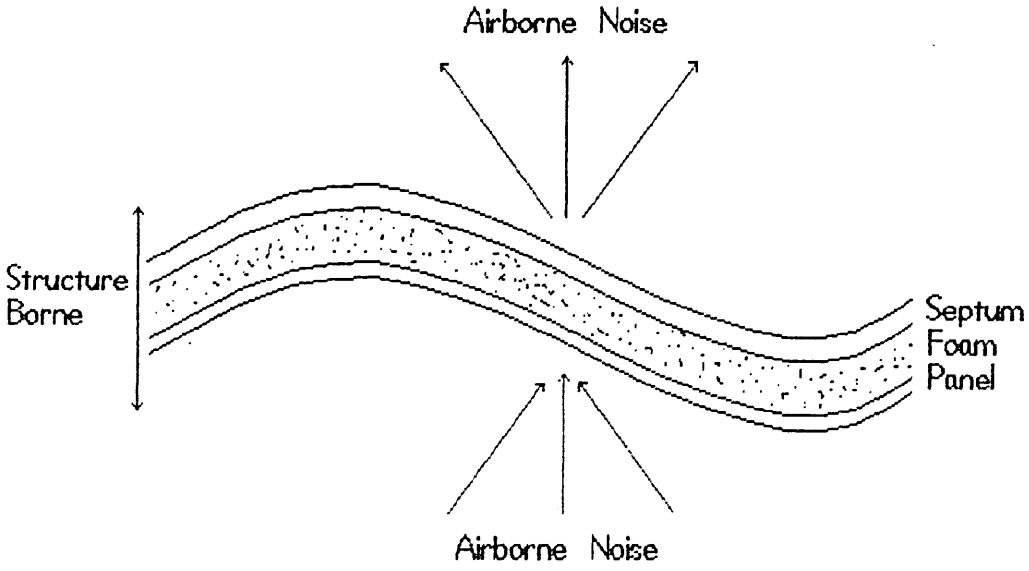

Fig. 1 Noise and vibration transmission in a vehicle

Rhodes (1988) reported that below 500 Hz the structure borne noise is the dominant component, whilst above 500 Hz the airborne noise is the dominant contributor to interior vehicle noise.

Airborne noise arises from the engine, road/tyre and aerodynamic noise. The structure-borne noise originates from vibration caused by

excitation forces transmitted through the suspension mounts. This vibration is then re-radiated from the car panels into the compartment. A typical internal noise spectra for a small saloon car is illustrated in Fig. 2.

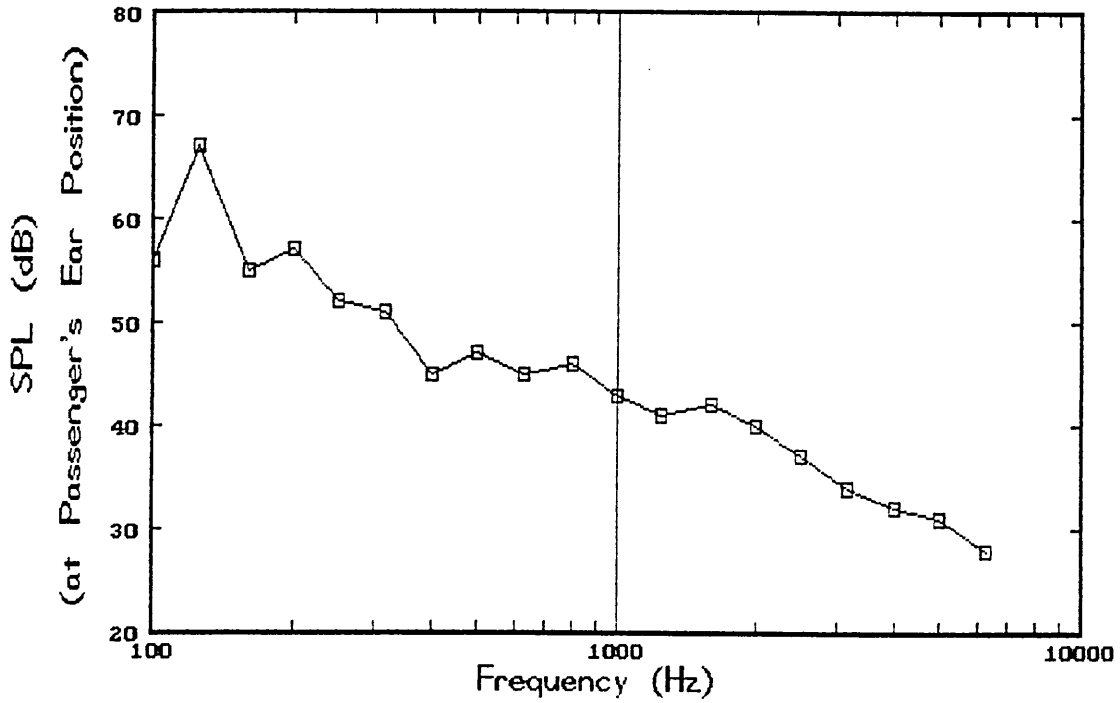

Fig. 2 Typical interior noise spectra in saloon car (4500 r.p.m.)

The dominant source that needs to be considered is the engine noise. The sound level generated depends upon a number of parameters. These are primarily engine speed, engine capacity and engine load (Priede, 1971, Jha, 1976). The engine noise consists of discrete frequency components due to combustion noise. The frequency values are related to the engine speed E, and are given by ½E, E, 2E, 4E Hz; where E is the engine speed in revolutions per second. For an engine speed of 4500 r.p.m. the principal components occur at 37.5, 75, 150 and 300 Hz. It is the discrete component nature of the engine combustion noise that also makes it the most subjectively annoying to the vehicle occupant. The situation is further complicated by the fact

that these frequency components coincide with the principle cavity resonances. This causes the resonant modes to be excited and results in the characteristic low-frequency vehicle 'boom'. Aerodynamic and tyre/road noise are broadband sources. They do not contribute greatly to interior noise annoyance, the noise principally affecting speech intelligibility. The response of the vehicle occupant to noise is discussed further in Chapter 6. A typical sound pressure distribution within a car compartment is shown in Fig. 3. It is seen that the principle radiating surfaces are the bulkhead and the transmission tunnel.

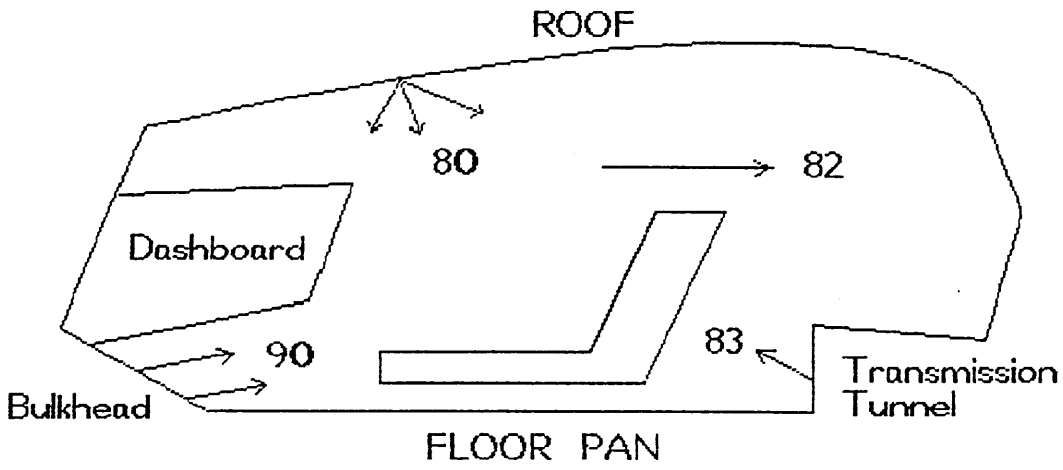

Fig. 3 Internal sound pressure distribution in a saloon car (after Gahlau, 1987)

1.3 Control of Interior Vehicle Noise

This can be carried out by three approaches. All three methods can be applied together as part of a complete noise control package.

1.3.1 Reduction of Noise at Source

Careful design of automotive components e.g. engine and drive-train enable source noise to be reduced. Recent developments have been reported by Priede (1985), Richmond *et al* (1987), and French (1989). The majority of analysis and design of components is through the use of finite elements to model the vibrational behaviour.

1.3.2 Reduction of Noise Within Vehicle

This can be achieved by introducing acoustic absorbents into the car compartment. These take the form of the headliner, carpet and other trim items. The aim is to reduce the reflected acoustic energy and thus the overall sound levels. The design of the cavity is also required to obtain optimum shape. The work by Craggs *et al* (1989) reported that an absorptive lining would cause a change in the damping factor. Craggs also found that the absorptive lining was not reactive, such that damped waves were propagated in the lining affecting SPL's in other cavity locations. This causes a shift in the resonant frequencies of the enclosure.

If control of interior noise is targeted towards the most subjectively annoying part of the internal noise, i.e. the cavity resonances and the engine combustion noise, the technique of active (or adaptive) noise cancellation can be used (Elliott *et al*, 1988, Nelson *et al*, 1987). The method relies on the deterministic nature of the noise signal enabling the characteristic of the signal to be predicted. By the introduction of a sound wave in antiphase, the noise is reduced. In a vehicle this can be carried out using the car

stereo system (Tyler, 1990). Research in the area of active noise control is being applied to panel vibration, thus being relevant to vehicle panels and bulkhead vibration (Pan *et al*, 1990).

1.3.3 Reduction of Transmitted Noise and Vibration

Careful design of vehicle components (i.e. engine mounts and suspension) can reduce transmitted vibration. This requires examination of the basic system response e.g. Hemingway (1986). Vibration can also be reduced by active (adaptive) engine and suspension mounts (Servotest, 1988, Foag, 1989).

Airborne noise enters the vehicle compartment through the panels and the bulkhead. The introduction of sound reduction materials in the sound path reduces the interior noise. This can be applied to the floor-pan and the bulkhead. A typical under-carpet barrier system was illustrated in Fig. 1. It consists of the steel floorpan, decoupling layer and a heavy layer. The carpet is placed upon the heavy septum layer. The decoupling layer is made either from a fibrous felt or a polymer foam. Increasingly, moulded units are being used with water blown PUR foams. These are CFC free, and offer the opportunity of one step assembly, thus reducing costs, and provide the acoustic engineer with the design flexibility needed to tailor the composite to meet the needs of a particular type of vehicle (Ling *et al*, 1991). With the latest moulded units, the systems are unbonded to the floorpan. Little work has been published on the experimental and theoretical behaviour of these systems to noise and vibration. A better understanding of the system behaviour is required to optimise the under-carpet treatment, thus providing higher noise reduction

with optimum use of materials.

1.4 Scope of the Work

The previous sections have discussed how vehicle interior noise is the result of structural and airborne excitation from a number of different sources. Reduction of this noise can be achieved by a combination of improved vehicle design, noise control within the compartment and reduction of transmitted noise and vibration. The performance of three layered PUR cored composites used for this last method is reported in this work.

The purpose of the work was threefold; (a) to develop theoretical models that would predict the system behaviour (b) to investigate experimentally the behaviour of under-carpet composite systems when subjected to noise and vibration and (c) to optimise the system design. By approaching the work in this manner the relationship between material and functional properties would be established and related to optimal composite design, resulting in new foam formulations by the collaborating company. Improved under-carpet noise control systems could thus be developed for the automotive industry.

1.4.1 Theoretical Methodology

The aim of the theoretical investigation is to examine the factors that influence system behaviour. The two different types of system excitation present in a vehicle require that two approaches are taken; one for structure-borne excitation and one for airborne noise. Rather than use transmission loss to characterise the sound

insulation performance of the carpet composites, system insertion loss is used.

1.4.1.1 Structure-Borne Excitation

A number of workers (e.g. Cremer *et al* 1988, Ver *et al* 1988) have shown for structurally excited panels that radiated noise is related to panel vibration. Reduction of panel vibration is therefore potentially a method of reducing vehicle interior noise. Chapter 2 develops the theory of Oberst (1954) to predict the influence on panel damping of the foam composite. Empirical formaulae, based on Plunt's data (1991) for system damping are then combined with a simple lumped parameter model of the system to predict the vibration response. By incorporating the expressions for vibration of point excited panels given by Cremer *et al* (1988) , the radiated noise can be predicted with and without the composite. The system insertion loss can thus be predicted. The model is used with material data to predict composite insertion loss. The data varies one material or system parameter whilst keeping other properties constant. From the predictions the influence of system and material design parameters are identified.

1.4.1.2 Airborne Excitation

The principles of sound transmission are introduced in Chapter 2. A model is then developed from the transmission line theory of Beranek *et al* (1949) to predict the insertion loss of the composite when subjected to airborne noise. By evaluating the layer impedances an expression for the overall attenuation is obtained. The model is

used with material data to predict composite insertion loss. As with the structure-borne excitation above, the predictions are obtained with one material or system parameter varied whilst keeping other properties constant. From these predictions the influence of system and material design parameters are identified.

1.4.2 Experimental Methodology

The experimental studies were conducted to establish the validity of the theoretical work. The development of a small scale test facility to investigate the vibrational and acoustic characteristics of the composites is discussed in Chapter 3. Existing facilities for the measurement of transmission loss characteristics were considered unsuitable. The test facility was designed to measure the insertion loss and effective loss factor properties of unbonded, horizontal systems. (Experimental composites were constructed from foam materials supplied by the collaborating company). The facility consists of a massive box with a steel panel in an aperture on the top surface. Excitation is provided by either a mechanical shaker or a loudspeaker inside the sending chamber. Radiated noise from the panel or panel and composite is measured using an intensity probe and 1/3 octave real time analyser. The use of intensity measurement minimises restrictions on the laboratory sound field and environment that would otherwise exist if sound pressure measurements were made. Other material properties were obtained using the methods in Table 1 below. These are discussed in Chapter 4.

Property	Method	Comments
Dynamic Modulus and Loss Factor	BMW	Resonance method Test piece loaded area 50mmx50mm, 1<f<250Hz
Air Flow Resistance	BS4443	Test piece circular Radius=60mm

Table 1 Methods of foam core characterisation

1.5 Design Optimisation

Generally, design optimisation is the process whereby a system is made to satisfy a set of criteria. The criteria might be to obtain the 'best performance' from a specific system (which means that the term 'best performance' needs to be defined). When an optimisation procedure is applied to vehicle composites three factors need to be considered. They are: (a) the vehicle noise spectrum (b) the insulation of the composite and (c) the response of the occupant to the noise. These factors are discussed in Chapter 6, where a general optimisation model is developed, and design solutions made for a set of criteria.

1.6 Experimental Materials

The experimental materials were supplied by the collaborating company, ICI Ltd. The polyurethane (PUR) foams provided were viscoelastic (VE), high resiliency (HR) and high hysteresis (HH). They were cold cured, water blown and wholly MDI (4-4'-diphenylmethane diisocyanate and 4-4'-diisocyanato diphenylmethane) foams. They were manufactured

to cover a wide range of mechanical properties (density, modulus etc). The structure and mechanical properties of the experimental materials is discussed in Chapter 4.

2. THEORETICAL

2.1 Introduction

To understand the behaviour of noise reduction treatments and determine ways of optimising system performance it is necessary to understand how noise is radiated by vibrating panels, excited either by airborne acoustic noise or by structure-borne vibration noise, and how this vibration and acoustic transmission path is influenced by the foam composite. This chapter identifies the essential features of structural vibration, vibration damping and sound transmission relevant to the system under investigation based on published information. Theoretical models are then developed to predict the insertion loss of multilayered panels.

When considering the vibration of structures and the radiated noise it is necessary to identify the types of wave that exist and their significance in the particular application under consideration. This is the starting point of the review given below. It continues by examining the parameters which govern the damping of panel vibration and the acoustic power radiated by a point vibration excited panel. These concepts are then combined with vibration transmissibility theory to produce a simple model representation of the insertion loss behaviour of a foam composite for a vibration excited panel. The second half of the chapter concentrates on the development of a mathematical model for airborne noise transmission and the insertion loss of the viscoelastic foam composite. This is based on the transmission line approach of Beranek *et al*(1949) and other workers. Predictions of the influence of system design parameters and foam material properties are given and these are compared

with experimental measurements in Chapter 5. The main purpose of the two models developed here is to explain the behaviour observed with the experimental test facility. This has been designed to rank foam composites in terms of noise insulation performance and not for the prediction of vehicle interior noise.

2.2 Waves in Structures

Four types of mechanical waves exist in a structure. They are: longitudinal, shear, torsional and bending. Our interest is mainly in radiated sound. This includes the case of transmitted sound, where airborne excitation of a structure results in vibration and subsequent re-radiation of sound at a different point. In the case of a panel, airborne excitation will vibrate one side, transferring energy into the panel. This causes vibration of the opposite side, and subsequent re-radiation of the sound. There are many more flexural modes than longitudinal modes in structures at low frequencies. This means that little direct contribution is made to the radiated sound by longitudinal, torsional or shear waves, e.g. Smith *et al* (1965) and Cremer *et al* (1988). However, they can be important in the transfer and redistribution of energy. Bending waves are thus the most important in our analysis, as they couple more readily with the incident sound field. The velocity of flexural (bending) waves in a thin panel is given by;

$$C_B = \omega^{1/2} \left[\frac{B}{m_{s1}}\right]^{1/4} \qquad (ms^{-2}) \qquad \langle 1 \rangle$$

where B is the bending stiffness (Nm)
m_{s1} is the panel surface density (kgm^{-2}).
$\omega=2\pi f$ is the angular frequency, f is the frequency in Hz

A thin panel is a panel where the effects due to wave types other than bending waves can be neglected. This is the case where the thickness of the plate is less than one sixth the bending wavelength (Cremer, 1988). Where the thickness $h=\lambda/6$ the error due to transverse waves is 10%. Thus for the materials in this study, for a thickness of 18mm the above equation is valid for frequencies below 2800Hz to an accuracy of 10%.

2.3 Free Harmonic Vibration of Panels

The behaviour of a steel panel is similar to any other mechanical system in that when it is excited it exhibits many natural modes of vibration, or resonances. These occur at frequencies specific to the system. The mode frequencies depend upon factors such as geometry (e.g. dimensions, boundary conditions) and material properties (e.g. elastic modulus, panel density, Poisson's ratio). The most exhaustive reviews of panel vibration are those carried out by Leissa (1969, 1973, 1977), whilst a rigorous mathematical analysis was made by Mindlin (1956). A simpler approach to obtaining the system response is by treating the panel as many mass-spring-damper systems. The superposition of the individual responses gives the overall system response, Smith *et al* (1965). Initially we are concerned with a knowledge of the modes of vibration. The classical equation of thin plate motion is attributed to Love (1927);

$$B\nabla^4 w + m_{s1}\frac{\partial^2 w}{\partial t^2} = 0 \qquad \langle 2 \rangle$$

where w is the transverse displacement,
$\nabla^4 = \nabla^2.\nabla^2$
B is the panel bending stiffness (Nm), $B=Eh^3/(1-\nu^2)$,
E is Young's modulus,

h is the panel thickness
ν is the Poisson's ratio

and, $\nabla^2 = \frac{\partial^2}{\partial x^2} + \frac{\partial^2}{\partial y^2}$

The test facility described in Chapter 3 uses a rectangular panel in its aperture, so the analysis here concentrates on the behaviour of a square panel with all four edges clamped. There are in fact twenty-one sets of boundary conditions that exist for a rectangular panel. If a sinusoidal time response is assumed for free vibration we obtain the Voigt (1893) solution;

$$w = [A_m \sin(k^2-\alpha^2)^{\frac{1}{2}}y + B_m \cos(k^2-\alpha^2)^{\frac{1}{2}}y + C_m \sinh(k^2-\alpha^2)^{\frac{1}{2}}y + D_m(k^2-\alpha^2)^{\frac{1}{2}}y]\sin\alpha x \qquad \langle 3 \rangle$$

where $K^4 = m_{s1}\omega^2/B$
and $\alpha = m\pi/a \quad m=1,2\ldots \quad (k^2 > \alpha^2)$

By applying boundary conditions as explained by Young (1950), solutions for this can be obtained. The fundamental frequencies of a simply supported square plate of side length a are given by;

$$f_{mn} = \frac{1}{\pi}.\left[\frac{B}{m_{s1}}\right]^{\frac{1}{2}}[(m\pi/a)^2 + (n\pi/a)^2] \qquad \langle 4 \rangle$$

The panel under consideration has all edges clamped (C-C-C-C). The first mode frequency is given by Gahlin, the second by Leissa (1969) and the remaining modes by Warburton (1954);

$$f_{1,1} = \frac{18}{\pi a^2}.\left[\frac{B}{m_{s1}}\right]^{\frac{1}{2}} \qquad \langle 5 \rangle$$

$$f_{1,2} = \frac{73}{2\pi a^2}.\left[\frac{B}{m_{s1}}\right]^{\frac{1}{2}} \qquad \langle 6 \rangle$$

$$f_{m,n} = \frac{\Omega h \pi}{a^2} \cdot \left[\frac{Eg}{48\rho\,(1-\nu^2)}\right]^{\frac{1}{2}} \qquad \langle 7 \rangle$$

The non-dimensional frequency factor, Ω, for a square plate is given by;

$$\Omega^2 = 2G_x^4 + 2(\nu H_x H_y + (1-\nu) J_x J_y) \qquad \langle 8 \rangle$$

The variables in this equation are given in Table 2;

m,n	G_x, G_y	H_x, J_x, H_y, J_y
2	1.506	1,248
3,4	$m-\frac{1}{2}$	$(m-\frac{1}{2})^2[1-2/(1-2/(\pi(m-\frac{1}{2}))]$

Table 2 Mode frequency variables for clamped square plate

For the test panel in these studies the predicted mode frequencies are as shown in Table 3. It is seen that the panel has a high number of modes. These are often closely spaced e.g. modes (4,5) and (6,1). This has implications for the measurement of panel loss factor as discussed in Chapter 3.

m	n	Gx	Hx	Jx	Gy	Hy	Jy	Ω2	Freq.(Hz)
1	1								11.48
1	2			(see text)					23.40
2	1								23.40
2	2	1.51	1.25	1.25	1.51	1.25	1.25	13.40	54.63
2	3	1.50	1.30	1.30	2.50	4.66	4.66	56.19	111.85
3	2	2.50	4.66	4.66	1.50	1.30	1.30	56.19	111.85
3	3	2.50	4.66	4.66	2.50	4.66	4.66	121.53	164.50
2	4	1.50	1.30	1.30	3.50	10.02	10.02	181.08	200.80
4	2	3.50	10.02	10.02	1.50	1.30	1.30	181.08	200.80
4	3	3.50	10.02	10.02	2.50	4.66	4.66	282.50	250.80
3	4	2.50	4.66	4.66	3.50	10.02	10.02	282.50	250.80
2	5	1.50	1.30	1.30	4.50	17.39	17.39	460.16	320.09
5	2	4.50	17.39	17.39	1.50	1.30	1.30	460.16	320.09
4	4	3.50	10.02	10.02	3.50	10.02	10.02	501.00	333.99
5	3	4.50	17.39	17.39	2.50	4.66	4.66	611.10	368.87
3	5	2.50	4.66	4.66	4.50	17.39	17.39	611.10	368.87
5	4	4.50	17.39	17.39	3.50	10.02	10.02	908.59	449.78
4	5	3.50	10.02	10.02	4.50	17.39	17.39	908.59	449.78
6	1	5.50	26.75	26.75	0.50	-0.07	-0.07	911.47	450.49
1	6	0.50	-0.07	-0.07	5.50	26.75	26.75	911.47	450.49
2	6	1.50	1.30	1.30	5.50	26.75	26.75	989.41	469.36
6	2	5.50	26.75	26.75	1.50	1.30	1.30	989.41	469.36
3	6	2.50	4.66	4.66	5.50	26.75	26.75	1203.34	517.62
6	3	5.50	26.75	26.75	2.50	4.66	4.66	1203.34	517.62
5	5	4.50	17.39	17.39	4.50	17.39	17.39	1424.62	563.21
4	6	3.50	10.02	10.02	5.50	26.75	26.75	1601.26	597.10
6	4	5.50	26.75	26.75	3.50	10.02	10.02	1601.26	597.10
1	7	0.50	-0.07	-0.07	6.50	38.11	38.11	1779.92	629.53
7	1	6.50	38.11	38.11	0.50	-0.07	-0.07	1779.92	629.53
7	2	6.50	38.11	38.11	1.50	1.30	1.30	1888.84	648.51
2	7	1.50	1.30	1.30	6.50	38.11	38.11	1888.84	648.51
3	7	2.50	4.66	4.66	6.50	38.11	38.11	2179.21	696.57
7	3	6.50	38.11	38.11	2.50	4.66	4.66	2179.21	696.57
6	5	5.50	26.75	26.75	4.50	17.39	17.39	2255.18	708.61
5	6	4.50	17.39	17.39	5.50	26.75	26.75	2255.18	708.61
4	7	3.50	10.02	10.02	6.50	38.11	38.11	2699.03	775.21
7	4	6.50	38.11	38.11	3.50	10.02	10.02	2699.03	775.21
6	6	5.50	26.75	26.75	5.50	26.75	26.75	3261.10	852.12
7	5	6.50	38.11	38.11	4.50	17.39	17.39	3520.29	885.34
5	7	4.50	17.39	17.39	6.50	38.11	38.11	3520.29	885.34
6	7	5.50	26.75	26.75	6.50	38.11	38.11	4739.01	1027.22
7	6	6.50	38.11	38.11	5.50	26.75	26.75	4739.01	1027.22
7	7	6.50	38.11	38.11	6.50	38.11	38.11	6475.17	1200.73

Table 3 Mode frequencies for 0.87 x 0.87m clamped square plate

2.4 Damping of Panels

Damping is characterised by the loss factor, η, which is the proportion of vibratory energy lost per radian cycle of vibration. Panel damping has been studied by a number of workers, e.g. Utley *et al*

(1973), Ver *et al* (1988), and Cremer *et al* (1988). Measurement techniques have been described by Plunkett (1959) and Zhu *et al* (1989) and are discussed in Chapter 3. Damping of clamped panels is due to three main factors. (1) Internal material damping. (2) Radiation damping due to coupling of the panel vibrations with the surrounding medium. This can be neglected where the medium is air, Smith (1965) and Fahy (1985). (3) Boundary damping which is due to energy losses caused by edge conditions and discontinuities.

Tarnoczy (1970) reported results for a steel plate (area=$2m^2$, thickness=2mm). For the steel plate with clamped edges the loss factor decreased with frequency from a value of $\eta=5x10^{-2}$ at 30Hz to $\eta=1.15x10^{-3}$ at 1 kHz. The attachment of a 5mm damping layer caused a an increase in loss factor with frequency from $\eta=3x10^{-2}$ at 30Hz to $\eta=9x10^{-2}$ at1kHz. Bies *et al* (1980) reported measurements on a point supported steel plate (area=$0.2m^2$, thickness=1mm). Loss factors increased with frequency from $\eta=0.015$ at 400Hz to $\eta=0.02$ at 5kHz. With the addition of a damping treatment, the loss factor similarly increased with frequency. Their measurements also demonstrated that damping values obtained from the reverberant decay method are slightly lower than those from the steady state method. These differences were thought to be due to the plate not being in steady state equilibrium during reverberant decay. More recently Plunt (1991) presented loss factors for carpet treatments using the power injection method. Data was presented for two systems. The first a steel + foam + septum of $7.5kgm^{-2}$, and the second of steel + foam + carpet of $0.8kgm^{-2}$. The loss factor was observed to decrease with increasing frequency. For the foam + septum values ranged from 1.0 at 100Hz to 0.7 at 2kHz. The foam + carpet gave values from 0.5 at

125 Hz to 0.01 at 2kHz. The panel was framed, but it is not stated whether the foam and septum were bonded to the steel panel. Plunt's data for a 0.8mm steel panel were also presented. The values of loss factor are higher than those of Bies and Tarnoczy, with a value of approximately 0.07 over the frequency range. The results of Tarnoczy, Bies *et al* and Plunt are compared in Fig. 4.

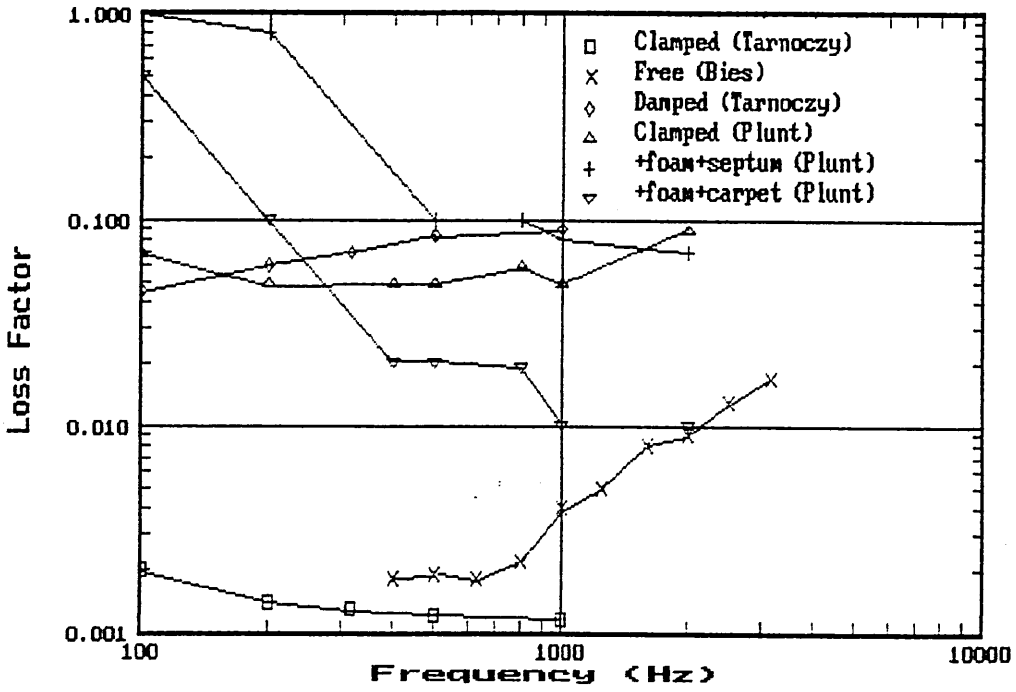

Fig. 4 Comparison of measured loss factors for steel panels

The vibration of a panel can be reduced by the application of damping treatments. These take the form of spot treatments, where damping is applied to vibrational antinodes (i.e. where the velocity is at a maximum). This works well for specific modes, but where many modes co-exist the benefit is reduced. This would occur, for example, in the system being considered here as the excitation is by random noise; where complete panel treatments need to be applied. This was described by Oberst (1952), and Ross *et al* (1959). This can

be achieved by the attaching of a viscoelastic (VE) layer to the panel, as illustrated in Fig. 5a. When the panel flexes, the VE layer is subjected to extensional and compression deformation. This causes energy to be dissipated, reducing the overall vibration amplitude.

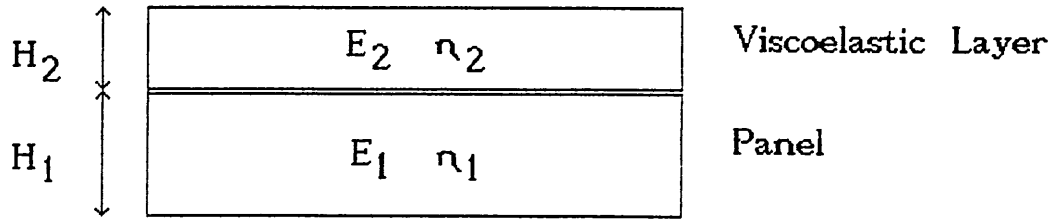

Fig 5 (a) Unconstrained layer damping

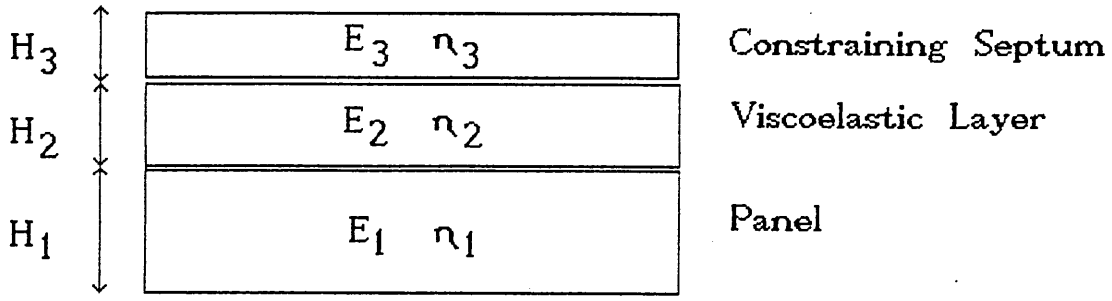

Fig 5 (b) Constrained layer damping

The extra damping produces a system with a composite damping factor given by;

$$\eta = \frac{\eta_2}{1 + 1/(e_2 h_2 (3+6h_2+4h_2^2)} \qquad \langle 9 \rangle$$

where η_2 is the loss factor of VE layer
$e_2 = E_2/E_1$, the ratio of the elastic moduli
$h_2 = H_2/H_1$, the ratio of layer thicknesses

The composite loss factor thus depends upon geometry (i.e. h_2), and material properties (i.e. η_2 and e_2).

The addition of a constraining layer on the viscoelastic material introduces shear as well as the bending and extensional deformation in the layers. This three layer system is similar to the composite used in this work except the layers are bonded. It is illustrated in fig. 5b. The composite damping is given by;

$$\eta = \frac{\eta_2 YX}{1 + (2+Y)X + (1+Y)(1+\eta_2^2)X^2} \qquad \langle 10 \rangle$$

The stiffness parameter Y is given by;

$$1/Y = \frac{1 + e_3 h_3^3}{12 h_{31}^2} \left(1 + \frac{1}{e_3 h_3}\right) \qquad \langle 11 \rangle$$

where the ratios $e_3=E_3/E_1$, $h3=H_3/H_1$, $h_{31}=H_{31}/H_1$ and $H_{31}=H_2+(H_1+H_3)/2$

The stiffness parameter,X is given by;

$$X = \frac{G_2}{k^2 H_2} \left(\frac{1}{E_1 H_1} + \frac{1}{E_3 H_3}\right) \qquad \langle 12 \rangle$$

where k is the wave number $k=2\pi/\lambda$

The shear modulus G_2 (Cremer, 1988) is:

$$G_2 = E_2/2(1+\nu) \qquad \langle 13 \rangle$$

where ν is the Poisson's ratio. This equals approximately zero for foams in compression and 0.25 when in tension (Hilyard *et al*, 1990). For bending waves the wavelength is related to the bending wavespeed from Eqn. <1> by;

$$\lambda_B = [4\pi^2 B/f^2 m_{s1}]^{1/4} \qquad \langle 14 \rangle$$

The bending stiffness, B is given by Nilsson (1990) as;

$$B = E_3H_3(H_2-x_0)^2 + E_2(H_2^3-3H_2^2x_0+3H_2x_0^2)/3 + E_1H_1x_0^2 \quad \langle 15 \rangle$$

where the neutral axis, x_0 is given by;

$$x_0 = H_2(E_3H_3+E_2H_2/2)/(E_1H_1+E_2H_2+E_3H_3) \quad \langle 16 \rangle$$

2.5 Radiation Efficiency

The ability of a panel to radiate sound into a medium is described by it's radiation impedance and radiation efficiency. The impedance is a complex quantity. The imaginary part is frequency dependent; but if the panel is radiating into air it's effect is negligible; reducing the modal frequencies only slightly. However, radiation resistance cannot be ignored, because the dissipated energy is often of the same order as that dissipated internally, Smith (1965). In practice, the radiation efficiency is easier to use than radiation resistance. The radiation efficiency is affected by the panel dimensions, and also the supports and constraints. If a stiffened panel is used the radiation efficiency is increased, but the vibration velocity may also be reduced, and thus greater sound radiation does not necessarily result. Radiation efficiency, σ_{rad}, is defined for a panel by Ver *et al* (1988) in Eqn. <17>.

$$\sigma_{rad} = \frac{W_{rad}}{\rho_0 c_0 S \langle v \rangle^2} \quad \langle 17 \rangle$$

where W_{rad} is the power radiated (W)
S is the panel area (m^2)
$\langle v \rangle^2$ the space time average mean square panel velocity (m^2s^{-2})

$\rho_0 c_0$ is the specific acoustic impedance of air (the product of air density and speed of sound in air)

For a simply supported panel Ver *et al* (1988) give the expression for the radiation efficiency as;

$$\sigma_{rad} = \lambda_c^2 \, g_1(\alpha)/S + U\lambda_c \, g_2(\alpha)/S \qquad f<f_c \qquad <18>$$

$$\text{where, } g_1(\alpha) = \frac{8\,(1-2\alpha^2)}{\pi^4\,\alpha(1-\alpha^2)^{1/2}} \qquad f<f_c/2 \qquad <19>$$

$$g_2(\alpha) = \frac{(1-\alpha^2)\,\ln[(1+\alpha)/(1-\alpha)] + 2\alpha}{4\pi^4\,(1-\alpha^2)^{3/2}} \qquad <20>$$

$$\alpha = (f/f_c)^{1/2} \qquad <21>$$

For a panel with all the edges clamped, the radiation efficiency is doubled, i.e. a clamped panel radiates sound twice as efficiently than one with free edges.

Another expression for radiation efficiency given by Cremer (1988) is in Eqn. <22>. This is for a point excited, weakly damped panel.

$$\sigma_{rad} = \frac{U\lambda_c}{\pi^2 S}\,[f/f_c]^{1/2} \qquad f<f_c \qquad <22>$$

2.6 Point Excitation

A point excited panel exhibits different behaviour from that of a panel undergoing free (natural) vibration. The point excitation acts as a power input. This input force excites bending waves which propagate through the panel. If the system is infinite, they travel indefinitely. If there are boundaries the wave energy is reflected and combines with the incident wave energy to form standing waves. Thus with many reflections and superposition of waves the result is

a reverberant vibration field away from the excitation point, and a direct, or near field close to the excitation point. If the panel is lightly damped the reverberant wave field is the dominant one.

Panel behaviour is somewhat predictable. If the input is a sinusoid, the velocity at a particular point will go through a series of minima and maxima according to whether a natural mode is excited. The dominating modes are the ones whose natural frequencies are closest to the excitation frequency. The characteristics, (frequency, magnitude, phase etc.), of these displacement maxima and minima depend upon the panel geometry, the excitation position, and the position at which the response is determined.

2.6.1 Power Input by Point Excitation

The mechanical power input into a panel created by a point force is;

$$W_{in} = F_{rms}^2 \, Re[z] \qquad \langle 23 \rangle$$

where z is the input impedance of the panel, and is defined as the ratio of the applied force and panel velocity. The input power is;

$$W_{in} = F_{rms}^2/(2.3 \, \sigma_{rad} \, c_L \, h^2) \qquad \langle 24 \rangle$$

In this investigation the choice of using single point excitation for structure-borne noise was made for three reasons. It is more easily treated theoretically, and readily implemented experimentally (McGary, 1986). Thirdly, in a vehicle the mounting of the primary vibration sources (i.e. engine, suspension and drive-train) is

closer to being point mounted than line mounted.

2.6.2 Sound Radiation by Point Excited Panel

As mentioned above the sound radiation from a panel into a medium is governed by the radiation efficiency, which depends strongly upon boundary conditions. The power radiated from a point excited panel is given by Cremer (1988) in Eqn. <25>. It is derived for the case of an infinite panel. The effect of clamping the edges is to increase double the radiation efficiency (Ver, 1988). The total radiation is the sum of the contributions of the near-field and far-field panel vibration .

$$W_{rad} = \underbrace{\frac{\rho c k^2 F_{rms}^2}{2\pi\omega^2 m_{s1}^2}}_{\text{Near-field}} + \underbrace{\rho c S \langle v^2 \rangle \sigma_{rad}}_{\text{Reverberant Field}} \qquad \langle 25 \rangle$$

F_{rms}^2 is the mean square exciting force

By substituting for σ_{rad} and the equation between exciting force and mean square velocity we obtain;

$$W_{rad} = \frac{\rho F^2}{2\pi m_{s1}^2} \left(1 + \frac{U}{2Sk_b\eta}\right) \qquad \langle 26 \rangle$$

This is independent of frequency except for k_b. By examining this equation Cremer states that the radiated power is only significantly reduced by extra damping if $2\eta k_b S/U<1$. For the steel test panel this would mean that increasing the loss factor beyond $\eta=0.05$ at 100 Hz and $\eta=0.007$ at 5kHz will have little effect on reducing sound radiation. This has implications in the choice of PUR foams. High hys-

teresis (HHF) foams have high loss factors (typically η>0.8) but are more difficult to process. In contrast viscoelastic (VE) foams have lower damping (typically $\eta\approx$0.4) but are easier to manufacture. Thus the fact that above a certain level, (illustrated in Fig. 6), increasing the damping will have little effect in reducing sound radiation affects which PUR foam is best to use on grounds of processability. The other implication of the theoretical power radiation equation above is that the system radiation becomes increasingly dominated by the near field vibration rather than the reverberant vibration field with increasing system damping.

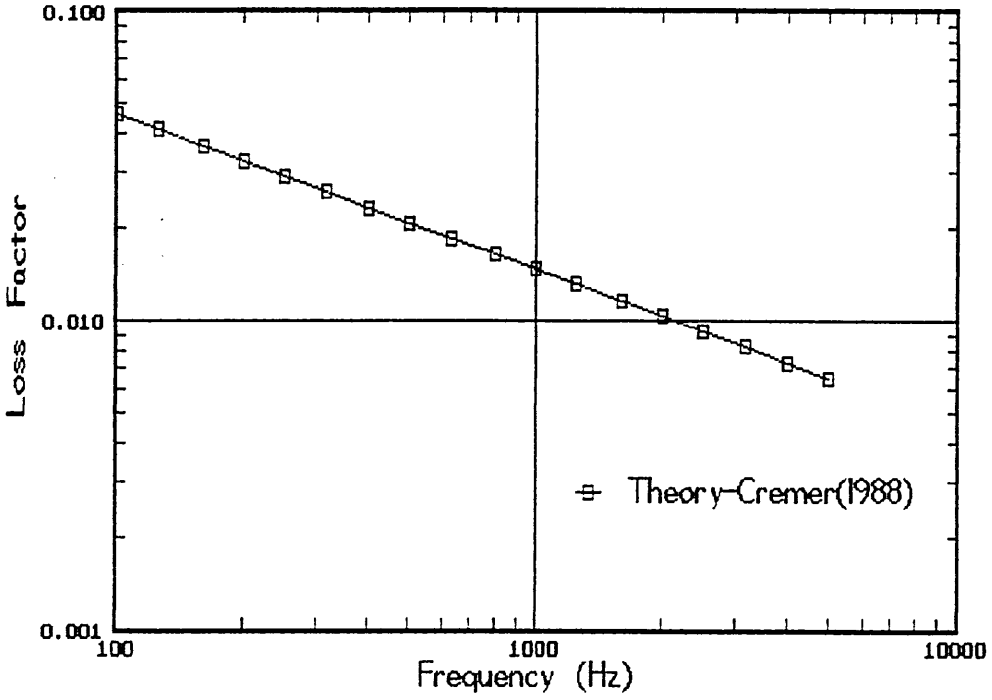

Fig. 6 Upper limit of loss factor for minimum sound radiation

2.7 Transmission of Structure-Borne Noise through Composites

Within a vehicle the vibrating panels radiate sound into the compartment. The application of treatments reduce the radiated noise components. It is therefore the radiated noise that needs to be

predicted for modelling purposes. It was mentioned above that the composite system can be modelled better when it is excited at a single point. It is further simplified if it is represented by a lumped parameter model. It is the performance of the composite that is to be assessed i.e. the foam + septum, and not the whole system (panel, foam and septum). This means that it is the insertion loss of the system that is to be calculated. This also enables comparisons to be made more readily with measured results due to the measurement procedure described in Chapter 3.

2.7.1 Insertion Loss

Insertion loss, L_{IL}, is the difference in sound levels (measured in dB) at a specified receiver position before and after a treatment is applied, or a barrier is inserted. This is illustrated in Fig. 7.

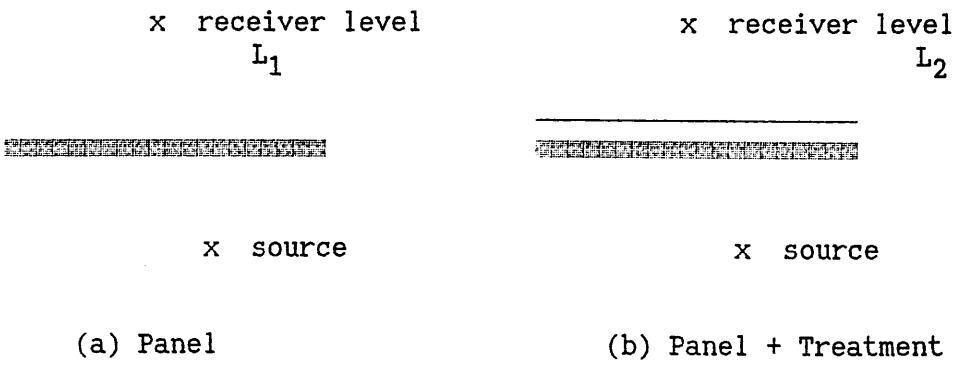

Fig. 7 Insertion Loss

The insertion loss is given by;

$$L_{IL} = L_1 - L_2 \quad \text{(dB)} \qquad \langle 27 \rangle$$

where, L_1 is transmitted level in the receiving room with the

base panel alone, and L_2 is the transmitted level with base panel + treatment.

2.7.2 Model Development

To predict the insertion loss of a system for structure-borne excitation we need to examine the panel vibration. In Section 2.5 it was stated that the noise radiated by a vibrating structure is proportional to the mean square surface velocity i.e. $I \propto v^2$. This is shown by rewriting Eqn. <17> knowing that power is related to the intensity by;

$$W = IS \qquad (W) \qquad \text{<28>}$$

where W is the power radiated (W)
and I is the intensity (Wm^{-2}) radiated through an area S (m^2).

The radiated intensity is given by;

$$I = \sigma_{rad} \rho_0 c_0 \langle v \rangle^2 \qquad \text{<29>}$$

This is the quantity that is therefore to be obtained. For the model it is assumed that the radiation efficiency is the same for the panel, and the panel+composite. If this assumption is made then the insertion loss of the composite can be obtained from the ratio of the velocities of the surfaces with and without the composite in place.

The model representation (a lumped parameter model) is illustrated

in Fig. 8. The mean square velocity of the driven panel without any additional layers is designated $\langle v_0 \rangle^2$. This panel velocity is reduced by the addition of the composite via the extra mass and damping. The panel vibration is now $\langle v_1 \rangle^2$. The vibration of the top surface is $\langle v_2 \rangle^2$. The ratio $\langle v_2 \rangle^2 / \langle v_0 \rangle^2$ gives the system insertion loss.

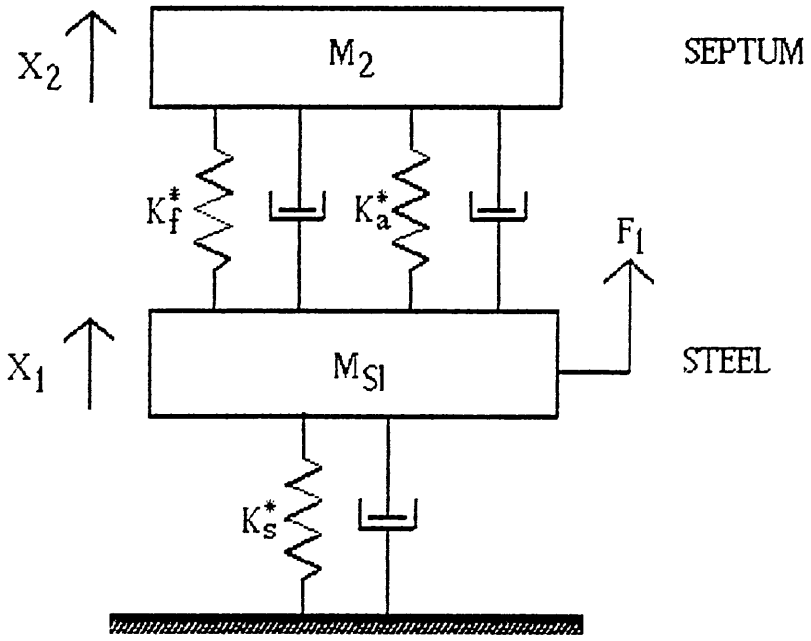

Fig. 8 Lumped parameter representation of composite system

For a broadband excitation force Cremer *et al* (1988) derived for a lumped parameter system a relationship between exciting force and panel vibration response;

$$v^2_{\Delta\omega} = \frac{F^2_{\Delta\omega} k_b^2}{8\omega^2 m^2_{s1} S\eta} \qquad \langle 30 \rangle$$

where $v^2_{\Delta\omega}$ is the mean square velocity in the frequency band $\Delta\omega$

The panel vibration v_0 can be obtained from the above expression.

This is then altered by the additional layers. If we limit ourselves to considering this as an increase in mass and damping we can obtain the velocity v_1 which can then be substituted in the equation for system transmission. The application of the above equation yields the following ratio of v_0 and v_1.

$$\frac{v_0^2}{v_1^2} = \frac{\eta_1 m_t^2}{\eta_0 m_{s1}^2} \qquad \langle 31 \rangle$$

where m_t is the total surface density of the system

η_0 is the loss factor of the panel

η_1 is the loss factor of the panel and foam composite.

An approximation for the ratio of loss factors η_1/η_0 can be obtained from the data of Plunt (1991) which was given in Fig. 4. Using data for the loss factor of the 0.8mm steel panel and the panel + foam + septum the graph in Fig. 9 is obtained. It is seen that the ratio decreases with increasing frequency, from approximately 10 at 100Hz to 0.1 at 2kHz. A regression analysis carried out on the data yields the expression:

$$\eta_1/\eta_0 = 3270.75 f^{-1.40704} \qquad \langle 32 \rangle$$

This empirical equation can be incorporated into eqn. <31> to give the velocity ratio v_0^2/v_1^2.

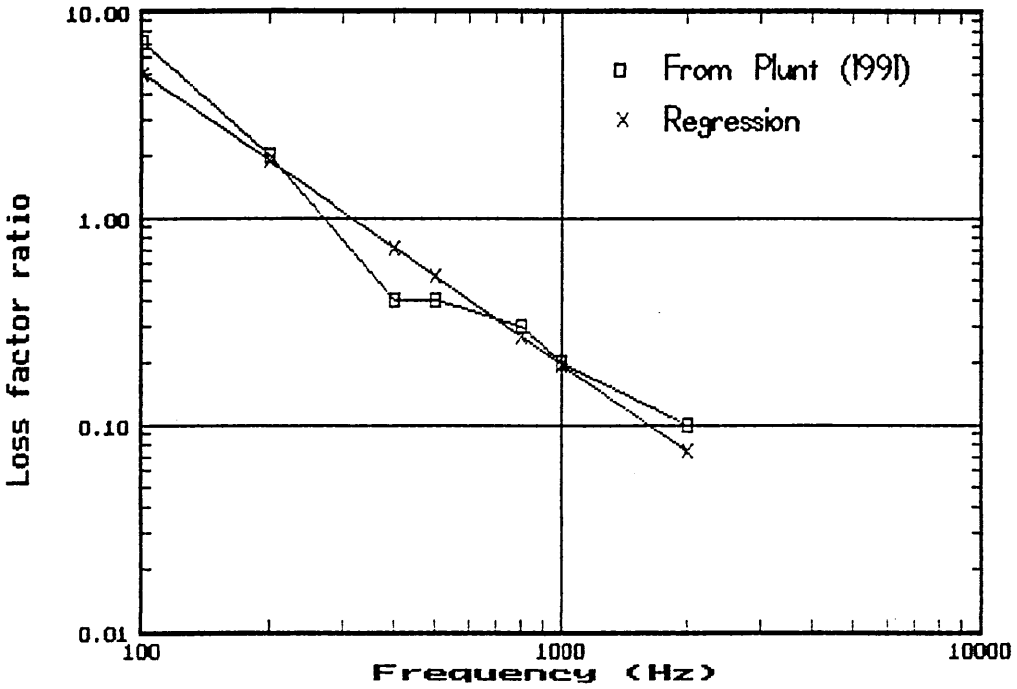

Figure 9 Ratio of loss factor for steel panel and composite

The relationship between v_1 and v_2 is obtained from the transmissibility of the system as;

$$\frac{v_1^2}{v_2^2} = \left[\frac{j\omega m_2 + K^*/j\omega}{K^*/j\omega}\right]^2 \qquad \langle 33 \rangle$$

where $K^*=(K'_{foam}+K'_{air})(1+j(\eta_{foam}+\eta_{air}))$, and K^* is the total modulus of the foam core and the enclosed air. The air loss factor η_{air} is small in comparison with that of the foam. The use of this combined stiffness is justified by the work of Bolton (1984) who observed that "..the air and frame move together, much as if the foam were a single homogeneous medium..". The sound and vibration that acts upon the foam causes vibration of the air within the pores. If no air flow through the material occurs because the boundaries are impervious, then there is a pressure increase inside the matrix. Free movement of this enclosed air would result in adiabatic compression and a rise in pressure of $(\rho c^2/Yd)x$, where x is the displacement of

air into the surrounding medium, Morse (1986). Polyurethane foams can possess a matrix of open and closed cells. If the matrix pores are small then the compressed air loses some of it's energy to the cell struts and the compression/expansion is isothermal. The increase in pressure would be $(\rho c^2/\gamma_c Yd)x$. The ratio of specific heats, γ_c = 1.4 . At low frequencies, f<100 Hz, the behaviour is predominantly isothermal, whilst at high frequencies, f>1 kHz, the behaviour is adiabatic. The isothermal value of K_{air} is approximately $1.1x10^5$Pa, whilst the adiabatic value is $1.4x10^5$Pa. As the frequency range of interest lies between these two extremes K_{air} was taken as $1.2x10^5$Pa. For a foam the bulk modulus, K_{air}, is related to the Young's modulus by $K^*_{foam}=E^*_{foam}/[3(1-2\nu)]$. In compression the Poisson's ratio, ν, of a polyurethane foam is approximately zero and in tension approximately 0.25, Hilyard *et al* (1990), so that $K^*_{foam}=E^*_{foam}/3$.

The ratio v_2^2/v_0^2 is obtained from the product of equations <31> and <33>. By taking logarithms of these equations then the ratio becomes an addition of terms. The intensity is proportional to the squared velocity, the intensity term is equal to $\log_{10}v^2$ plus a constant. So the intensities radiated by the panel, I_0 , and the composite, I_2 are given by

$$I_0 = 20\log(v_0) + K_0 \qquad \text{<34a>}$$

$$I_2 = 20\log(v_2) + K_2 \qquad \text{<34b>}$$

The constants K_0 and K_2 depend upon the radiation efficiency and are assumed to be equal. Thus the insertion loss is given by

$$VIBIL = I_0 - I_2$$

$$=20\log(v_0/v_1) + 20\log(v_1/v_2) \qquad \langle 35 \rangle$$

Substituting for the ratios v_0/v_1 and v_1/v_2 gives the vibration insertion loss as;

$$VIBIL = 10LOG_{10}[\eta_1 m_t^2/\eta_0 m_{s1}^2] + 10LOG_{10}\left[\frac{j\omega m_2 + K^*/j\omega}{K^*/j\omega}\right]^2 \quad dB \quad \langle 36 \rangle$$

2.8 Theoretical Predictions

The theoretical response equation given in Eqn. <36> above was implemented on an IBM compatible personal computer using the Turbo C programming language. The programme utilised complex number handling routines and is given in Appendix B. The computer model was used with the material property values shown in Table 4. The data was chosen as being representative of the properties of foams that can be manufactured commercially. The use of the data within the model enables the influence of the various parameters to be examined.

Data No.	Surface Density	Thick-ness	Storage Modulus	Loss Factor	Flow Resistivity
	kgm^{-2}	mm	$x10^5Pa$		$kNsm^{-4}$
1	2.0	20	1.1	0.5	50
2	1.6	20	1.1	0.5	50
3	1.2	20	1.1	0.5	50
4	0.8	20	1.1	0.5	50
5	0.8	10	1.1	0.5	50
6	1.6	20	1.1	0.8	50
7	1.6	20	1.1	0.2	50
8	1.6	20	0.5	0.5	50
9	1.6	20	1.8	0.5	50
10	1.6	20	1.1	0.5	20
11	1.6	20	1.1	0.5	100
12	1.6	20	1.1	0.5	130
13	2.4	30	1.1	0.5	50
14	2.4	30	1.1	0.2	50
15	0.8	10	1.1	0.2	50
16	1.6	20	0.2	0.5	50
17	1.6	20	0.2	0.2	50
18	1.6	20	0.5	0.2	50
19	1.6	20	1.8	0.2	50

Table 4 Material property values of test pieces used in the theoretical study

2.8.1 Material Parameters

(a) Foam Damping

The influence of damping was examined with property values for foams 7, 2, and 6 from Table 4. These have loss factors of η=0.2, 0.5 and 0.8 respectively, with other properties constant. The insertion loss predictions are shown in Fig. 10. We see that with increasing loss factor the insertion loss at the resonance trough increases. The insertion loss level for the whole frequency range is also slightly increased.

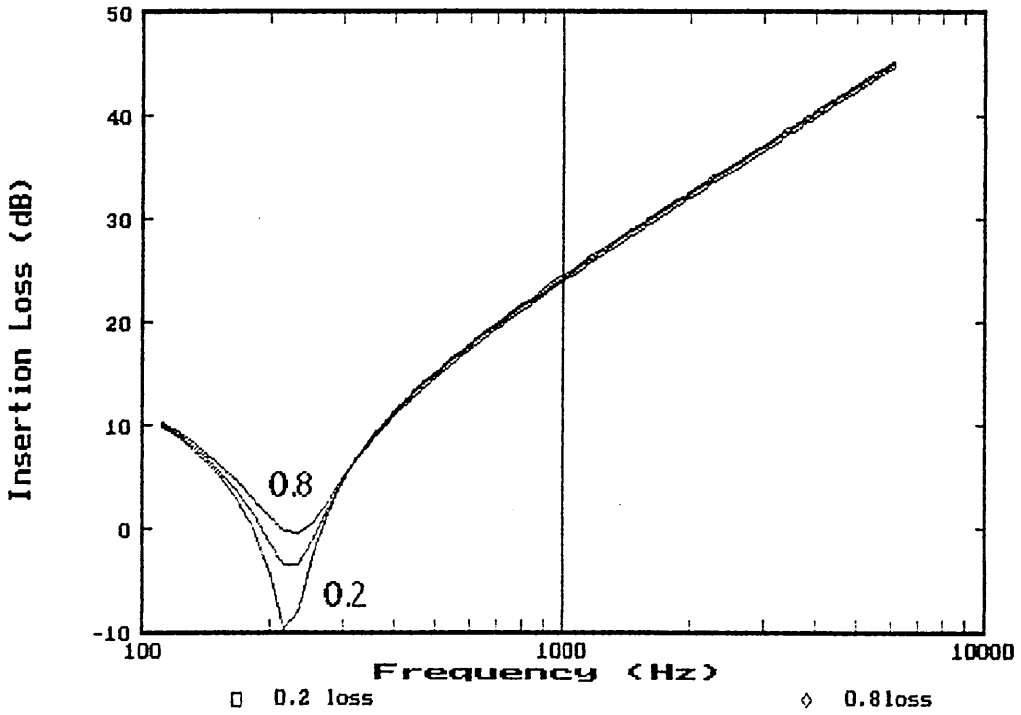

Fig. 10 Influence of foam damping upon insertion loss with modulus and density kept constant

(b) Foam Density

The influence of foam density was examined using property values for foams 1, 2, 3 and 4 from Table 4. These give a range of density from

20 to 80 kgm-3, with other material properties remaining constant. The predicted insertion losses are given below in Fig. 11. We can see that the predicted influence is that foam density has negligible effect upon insertion loss. The foam contributes approximately one sixth of the total composite mass, so any mass related effect will not be as marked as increasing the septum area density.

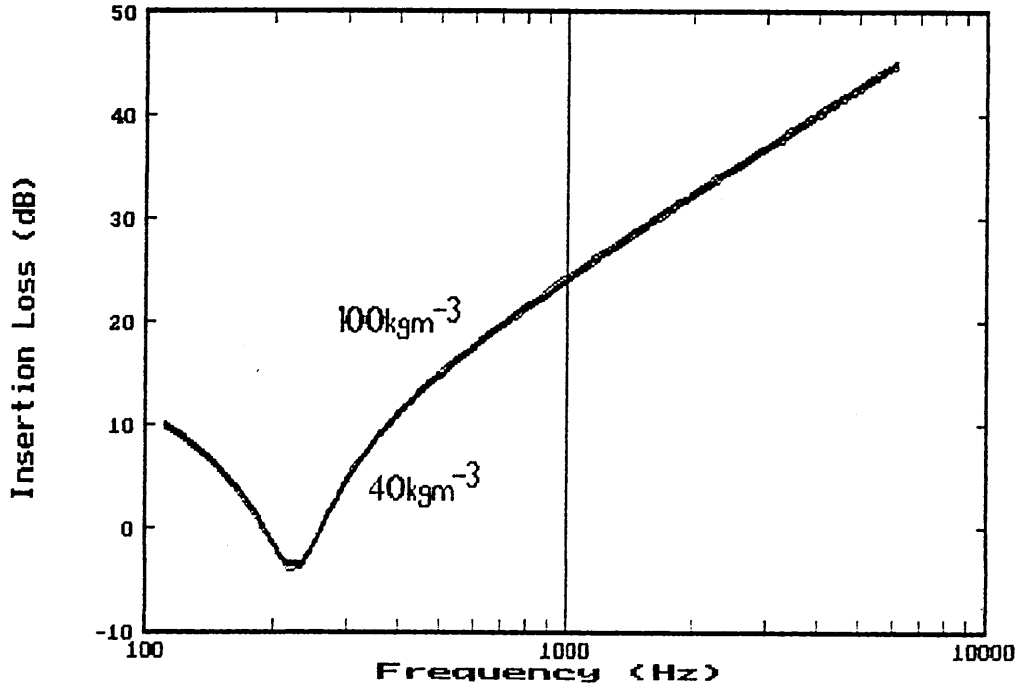

Fig. 11 Influence of foam density upon insertion loss with loss factor and modulus constant

(c) Foam Modulus

The influence of foam modulus upon the insertion loss was examined using the theoretical model with property values for foams 8, 2 and 9 in Table 4. These have moduli of 0.5×10^5, 1.1×10^5 and 1.8×10^5 Pa respectively with other material properties constant. The predicted IL is shown in Fig. 12. It can be seen that an increase in the foam modulus increases the frequency of the resonance minima. The increase of f_R means that the IL curve is shifted up the frequency

scale; thus the post-f_R level is reduced. There is a small decrease in the IL at resonance with decreasing modulus.

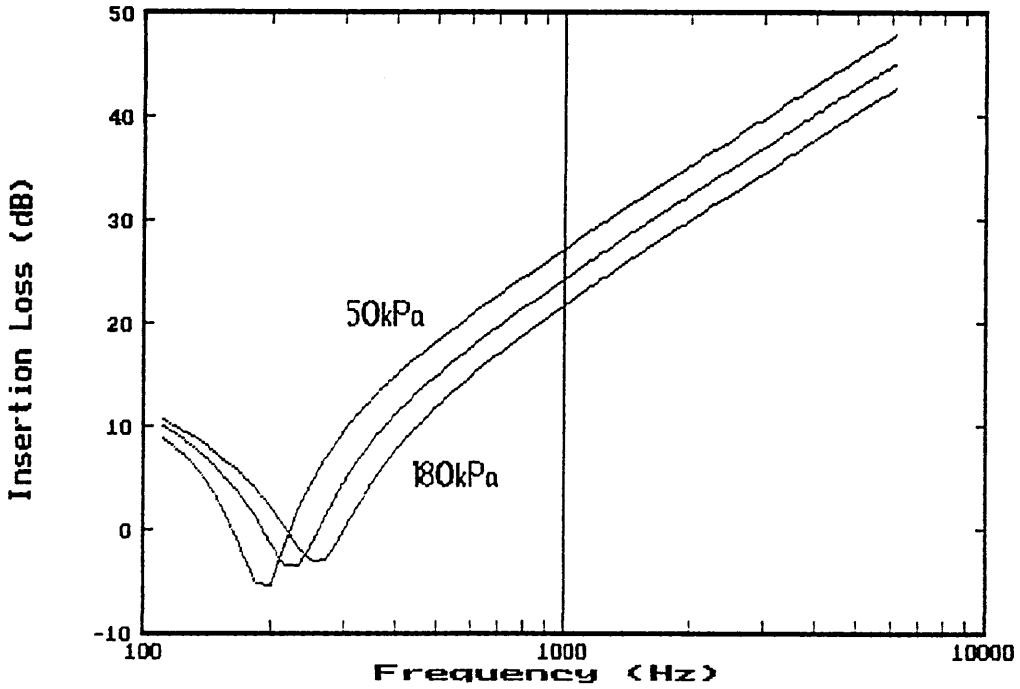

Fig. 12 Influence of foam modulus upon insertion loss with loss factor and density kept constant

2.8.2 System Parameters

(a) Foam Thickness

The influence of foam thickness was examined using property values for foams 5, 2 and 13 in Table 4. The thicknesses are 10, 20 and 30mm respectively, with other the material properties kept constant. A septum with area density of 5.9 kgm^{-2} was used. The predicted insertion loss is shown in Fig. 13 below. The IL increases with increasing thickness and frequency. This is because the frequency of the resonance dip, f_R, decreases with increasing thickness shifting

the IL curve down the frequency scale.

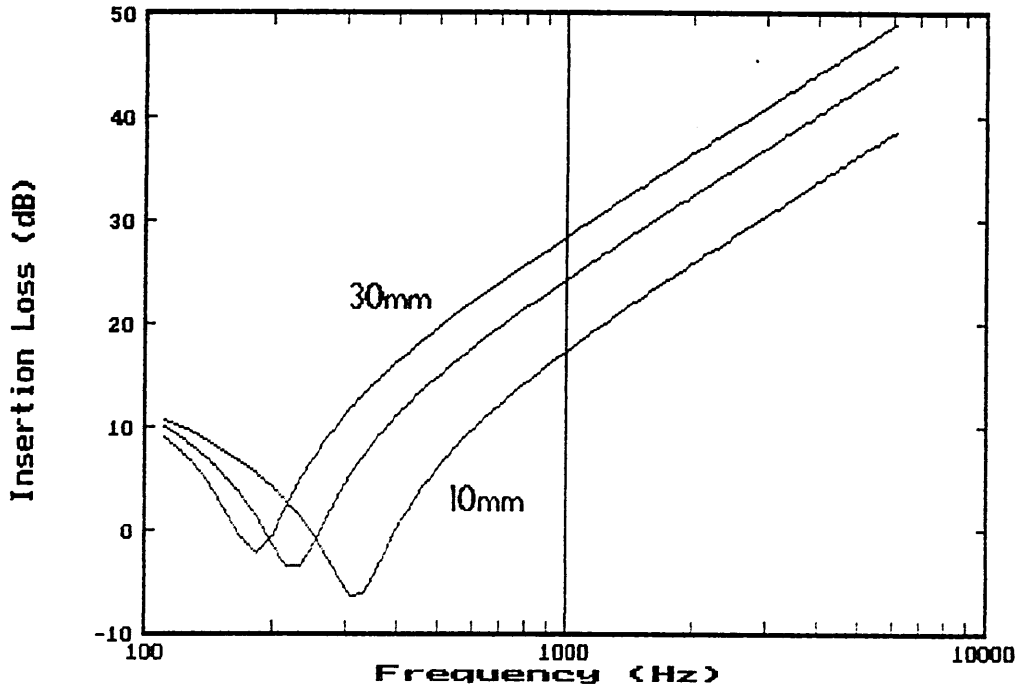

Fig. 13 Influence of thickness upon insertion loss with material properties constant

(b) Septum Area Density

The influence of the area density of the septum layer was examined using the property values for foam 2 from Table 4. Surface densities of 3.7, 5.9 and 8.7 kgm^{-2} were used. The prediction is shown in Fig. 14. The predicted resonance frequency decreases with increasing surface density. The predictions show that the IL of the composite increases with an increase in surface density. A decrease in IL at resonance is noticeable with decreasing septum surface density.

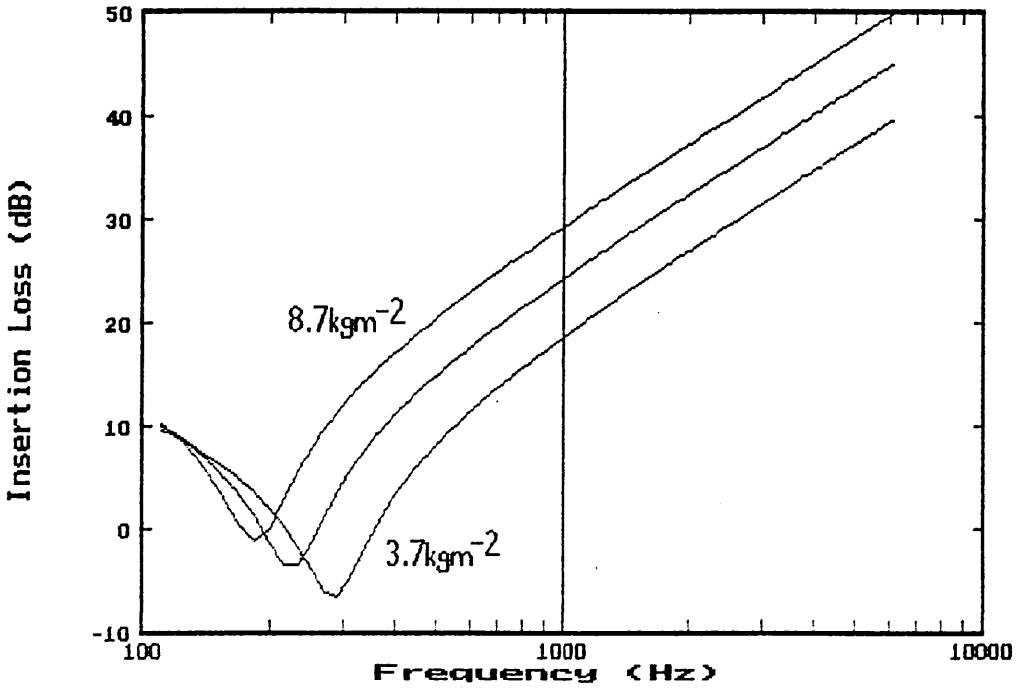

Fig. 14 Influence of septum area density upon insertion loss with other material properties constant

2.9 Transmission of Airborne Noise

A sound wave propagating through a medium will collide with boundaries and walls in its path. The wave energy is redistributed through reflection, absorption and transmission. The extent depends upon the properties of the various media, the angle of incidence, and the frequency of the sound wave. The multilayered system being considered consists of three non-bonded and distinct layers, as described in Chapter 1. This section discusses previous work, and the model that is developed to predict the insertion loss performance of multilayered composites.

2.9.1 Sound Reduction Index and Insertion Loss

Sound Reduction Index (SRI), also known as Transmission Loss (TL), quantifies the ability of a material to prevent, or reduce, the transfer of sound energy. The transmission coefficient is defined as the ratio of the transmitted intensity to the incident intensity;

$$\tau = I_t/I_i \qquad \langle 37 \rangle$$

where, I_i is the intensity on the incident side
and I_t is the intensity on the transmitted side

The sound reduction index, R, for free field plane waves on both sides of a panel is defined as

$$R = 10\ LOG_{10}\ 1/\tau = 10\ LOG_{10}\ I_i/I_t = 10\ LOG_{10}\ (p_i/p_t)^2 \qquad \langle 38 \rangle$$

where p_i and p_t are the incident and transmitted sound pressure levels respectively.

Normally, the intensities are calculated by creating diffuse sound fields on both sides of the partition. SPLs are then measured and the intensity is calculated. The diffuse field required for this calculation is the reason for the reverberant rooms in a transmission suite. Current instrumentation now allows direct measurement of sound intensity. This has a number of advantages. It is a vector quantity, and so background noise is less important. Also, as a direct measurement of intensity is being made, the receiving field does not need to be diffuse. A more detailed discussion of the comparison of conventional TL measurements with the intensity method

is given by Minten *et al* (1987) and Halliwell *et al* (1985). Halliwell *et al* (1985) suggest that TL measurements obtained using intensity are more accurate, as the technique makes fewer assumptions. The measurement of intensity and analysis of measurement errors are described in Chapter 3.

If the sound fields on either the incident and receiver sides are not diffuse, it is not possible to measure the transmission loss of a panel using pressure measurements. It is, however, possible to measure the intensity on the transmitted side of the material. This enables the insertion loss of a material to be evaluated.

The SRI of a panel or partition (in this case a steel sheet) is given from BS2750 as;

$$R_{steel} = L_i - L_1 + 10\ LOG_{10}\ (S/A) \qquad \langle 39 \rangle$$

where S is area of the sample under test, A is total equivalent absorption in the receiving room, L_i is the level in the source room and L_1 is the level in the receiving room

and for the foam composite as;

$$R_{composite} = L_i - L_2 + 10\ LOG_{10}\ (S/A) \qquad \langle 40 \rangle$$

By rearranging equations <39> and <40>;

$$L_1 = L_i + 10\ LOG_{10}\ (S/A) - R_{steel} \qquad \langle 41 \rangle$$

$$L_2 = L_i + 10\ LOG_{10}\ (S/A) - R_{composite} \qquad \langle 42 \rangle$$

Subtracting equations <41> and <42> to obtain the insertion loss from equation <27> gives;

$$L_{IL} = L_1 - L_2 = -\,(R_{steel} - R_{composite}) \qquad \langle 43 \rangle$$

The measurement of insertion loss gives an alternative means of quantifying the performance of acoustic materials. It is the parameter that is used in the reported work.

2.9.2 Transmission Through a Single Panel

The transmission of sound through a single panel has been analysed by Berger (1911). The panel is assumed to be without flexural rigidity. The 'mass-law' equation for the TL of this panel is given by;

$$R = 10LOG_{10}[1+(\frac{\omega m_{s1}\cos\theta}{2\rho_0 c_0})^2] \qquad dB \qquad \langle 44 \rangle$$

where the symbols are as previously defined and θ is the angle of incidence of the sound wave on the panel

When the flexural stiffness is introduced the TL becomes, Ver *et al* (1988);

$$R = 10LOG_{10}\{[1+\eta(\frac{\omega m_{s1}\cos\theta}{2\rho_0 c_0})^2(\frac{\omega^2 B}{\omega_0 c_0^4}\sin^4\theta)]^2 + [(\frac{\omega m_{s1}\cos\theta}{2\rho_0 c_0}\cos\theta)(1-\frac{\omega^2 B}{\omega_0 c_0^4}\sin^4\theta)]^2\} \qquad \langle 45 \rangle$$

where the symbols are as previously defined and η is the loss factor of the panel.

The mass law is illustrated in Fig. 15 for a 1mm steel panel for normal incidence.

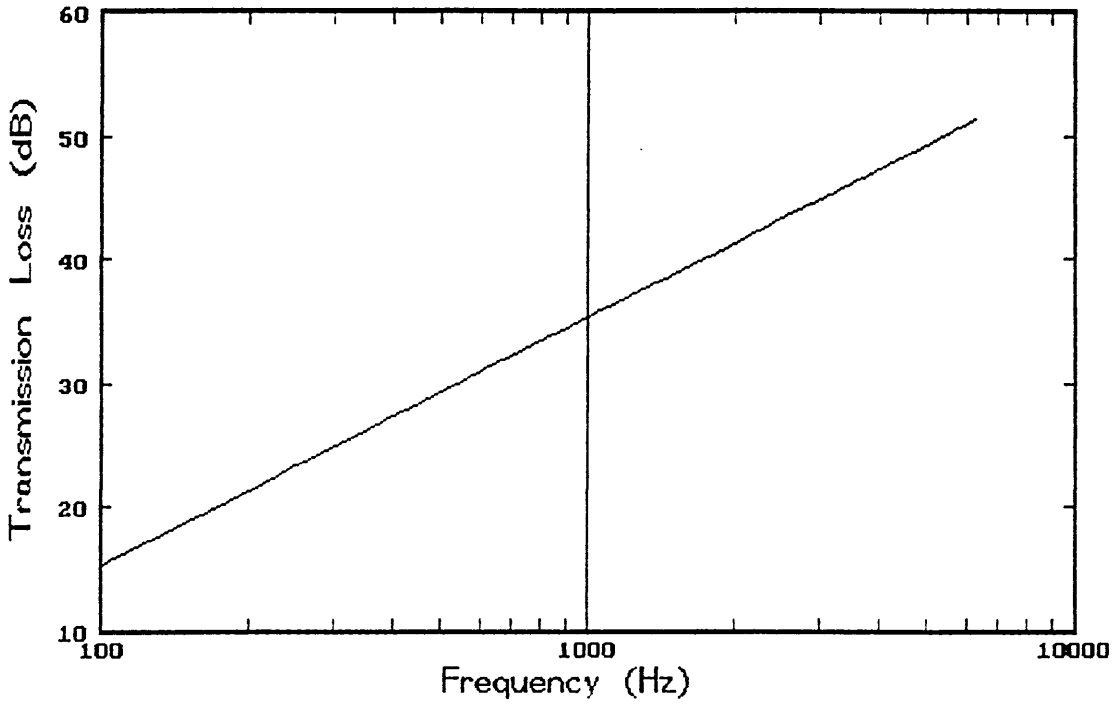

Fig. 15 Mass law for a 1mm steel panel

For a free wave propagating in a finite panel, the wave is reflected from the boundary discontinuities, and an interference pattern with maxima and minima is set up. If a sound wave incident upon a panel has the same wavelength as that of the propagated bending waves, then the phenomenon of coincidence is said to have occurred. The critical frequency is the upper limit of validity for the mass law. The effect is well documented, e.g. Cremer *et al* (1988), Heckl (1985). At and above this critical frequency, for a particular angle of incidence, this condition exists at every frequency. Practically this means that the TL can be substantially reduced as the incident and bending waves reinforce each other. The critical frequency for a

panel can be found by setting $C_B=c_0$ in Eqn. <1> above to give;

$$f_c = \frac{c_0^2}{2\pi} \cdot \left[\frac{m_s}{B}\right]^{\frac{1}{2}} \qquad \langle 46 \rangle$$

At this critical frequency the wavelengths only match if the wave hits the panel at grazing incidence. In this case little energy is given to the panel. The critical frequency is the crossover point where the panel vibration goes from being mass controlled to being resonance controlled. For the steel panel used in the test facility (see Chapter 3), the critical frequency from Eqn. <46> is f_c=12.4kHz, and the wavelength λ_c=27.8mm. Thus coincidence occurs above the frequency range of interest in this study (100-5000Hz).

At and above this frequency the panel is easily excited by the incident waves, having a detrimental effect on sound insulation. The critical frequency is designed to be above the frequency of interest in noise control applications. There is better coupling between a structure and air above coincidence, Kurtze *et al* (1959) i.e. the radiation efficiency is high. A wider frequency range is obtained, before coincidence has a deleterious effect. The concern about interior vehicle noise is at lower frequencies below 5kHz, so we need to ensure that coincidence is shifted above this value.

2.9.3 Transmission Through Multilayered Composites

Multilayered panels offer better transmission loss performance. The increase of mass explains some of the improvement, but even with the overall mass kept constant there is an increase in TL beyond that predicted by the mass law (Eqn. 44). This is because the layers introduce impedance mismatching. The majority of previous work has

been aimed at the aircraft industry for aircraft skin structures, Wallace *et al* (1946), Nichols *et al* (1947). The analysis by Beranek *et al* (1949) considers a variety of multiple layer structures. The approach requires knowledge of the complex impedance of the structure, which can be determined experimentally. Mangiarotty (1963) utilised Beranek's analytic technique to optimise the construction of aircraft fuselage constructions. His main conclusions were that optimum TL was obtained with structures where the impervious septa were of approximately equal mass, except at low frequencies where coincidence effects necessitated different masses to be used. These early authors considered only normal incidence TL. The analysis for partition walls by Kurtze *et al* (1959) stated that the low frequency double wall resonance that is introduced by a compressible core reduces the transmission loss of the partition. This may be alleviated by an increase in the core stiffness in the direction normal to the plate surface. Similar analysis has been done by Watters (1959), Trochidis *et al* and Price *et al* (1959). Analyses by Dym *et al* (1974,1975,1976) considered the optimal design of sandwich panels. These consisted of high stiffness skins ($4x10^{10}$ Pa) and cores ($6x10^{7}$ Pa). Their recommendations were that for construction purposes a core of high modulus and low density should be used; resulting in a panel that could be used for building purposes. No attempt was made to verify the theoretical analysis by experiment. Au *et al* (1987) in their application of impedance formulae to duct linings compare theoretical predictions with those determined experimentally by a test facility similar to that used in this work. The analysis is restricted to fibrous blankets. Analysis via an examination of the system equation of motion has subsequently been done by many authors Cremer *et al* (1981), Heckl (1981), and Fahy (1985). Hamada *et*

al (1985) used the analysis of a four-terminal network to obtain the general solutions. Their comparison with experimental work are relatively good. Trochidis *et al* (1986) presented a theoretical approach to the double partition with an absorptive cavity. The system is considered to be coupled, and utilises classical thin plate theory, the acoustic wave equations and standard boundary conditions. By producing a series of linear equations they obtain their solutions. These solutions show good agreement with experimental work. Recent developments in finite element modelling have been used for the problem by Lu *et al* (1979) and Ionnides *et al* (1979). Throughout the analysis the decoupling layer used was that of fibrous blankets.

The critical frequency for a three layered system will differ from that of a single panel, because the bending stiffness will be altered. Using the expression for composite bending stiffness the critical frequency for the composite can be calculated. For a typical foam used (no. 4) and a septum layer of surface mass 5.9 kgm^{-2} of modulus $10x10^5$ Pa, we find the bending stiffness, B=1.97 Nm and the coincidence frequency, f_c=52.4 kHz. This shows that the use of a sandwich type construction can increase the critical frequency by a factor of four. (This agrees with the analysis of Kurtze *et al* (1959)). This is well above the frequency of interest.

2.10 Model Development for Automotive Carpet Composites

The analytical approach to sound transmission through the three layer system is by the application of the media layer impedances, obtaining a system equation. The impedances are obtained from the

relationships between acoustic pressure and normal particle velocity in the layers. These can be obtained by consideration of Fig. 16.

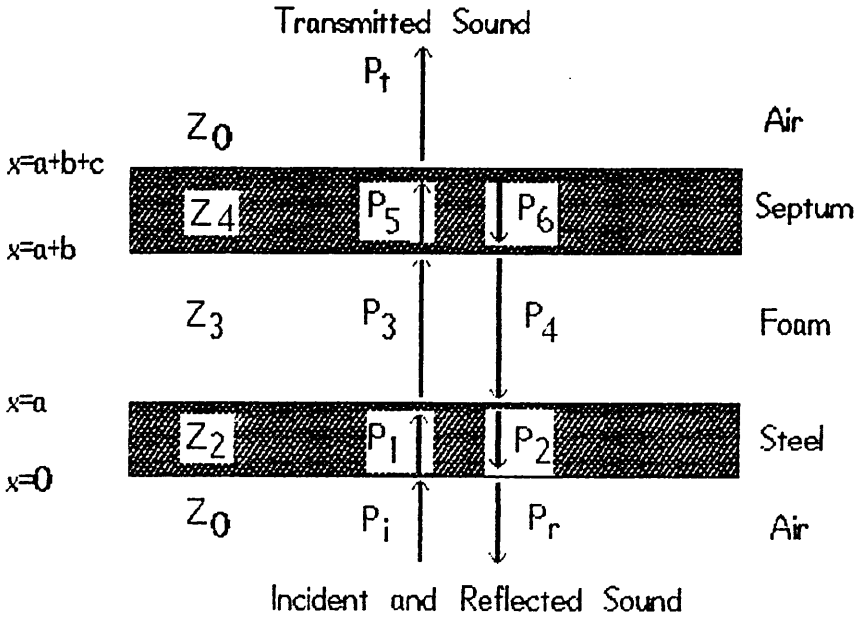

Fig. 16 The theoretical three layer system

The pressures p_i, p_r, p_t and p_1 to p_n are represented in the exponential form $p_n=Ae^{j(\omega t-knx)}$. The velocities are given by $u(x,t)_+=P_n(x,t)/z_n$ and $u(x,t)_-=-P_n(x,t)/z_n$, where the suffix + or - indicates a positive or negative going wave. The values of the complex wave numbers, k_n, are related to the wave frequency and the speed of sound within the medium by $k_n=\omega/c_n$. The layer impedance $z_n=\rho_n c_n$.

Now, there is continuity of pressure and velocity at the interface boundaries. Substitution of values in the continuity equations leads to the formulation of simultaneous equations. These equations can then be solved and an expression for the ratio of the transmit-

ted pressure wave amplitude, A_t, to the incident pressure wave amplitude, A_i, obtained. This is given in Eqn. <47>;

$$A_i/A_t = \frac{1}{2} \cdot \exp(jk_2a) \{ (1+z_1/z_3)\cos[k_4(c-b)] \exp(jk_3(b-a))$$

$$-j(z_3/z_4 + z_4/z_3)\sin[k_4(c-b)](\cosh[k_3(b-a)] + z_1/z_3 \sinh[k_3(b-a)])\} \qquad \text{<47>}$$

The ratio of the incident to transmitted wave amplitude is related to the transmission loss of the composite by the expression;

$$R_{composite} = 10LOG_{10} (A_i/A_t)^2 \qquad \text{<48>}$$

The medium on either side of the system is air so $z_1=z_5=415$ rayls at 20°C. The impedance of the two mass layers, z_2 and z_4 is given by Au *et al* (1987) as ;

$$z = z_T + j(\omega m - Dk_x^4/\omega) \qquad \text{<49>}$$

where z_T is the terminating impedance, and D is the flexural or bending stiffness of the layer. The value of z_T for layer 2 is z_3, the impedance of the polyurethane foam, and for layer 4 z_T is the characteristic impedance of air i.e. z_0.

The model used for this analysis is developed from that proposed by Beranek (1949) and is a simplification of the above expression for transmission loss. It employs a normal incidence technique for calculating the TL of multilayered systems. The decoupling layer used was a flexible fibrous blanket. Equations are provided for five general examples of structures. This method requires knowledge of the complex impedance and complex propagation constant of the core

material. These can be obtained for polyurethane foams from standing wave tube measurements, from design curves Beranek (1947), or from empirical relationships, Mechel (1976), Dunn *et al* (1986). The impervious layers are assumed to be without stiffness (as with the simple mass law equation). The porosity of the material, Y, is assumed to be such that Y>0.95. The ratio of the volume coefficients of elasticity of the enclosed air K'_{air} and of the material structure (i.e the framework), Q, is assumed to satisfy the inequality K'_{air}/Q >20. The fibrous blanket whilst being in contact with the base or septum layer offers minimal coupling of the system, with the attenuation being provided by the fluid flow within the core material. The inequality is not satisfied by the experimental materials, which typically give a value of K'_{air}/Q = 1.2. However, Bolton (1984) reported that for flexible foams that the air and frame motion are comparable so the inequality does not apply for the model developed here.

The analysis by Beranek (1949) gives a set of general equations, which when applied to the two layer system i.e. the steel panel and foam layer reduce to;

$$R = 10\ LOG_{10}\ [1 + \frac{j\omega m_{s1}}{z_1}]\cosh \Gamma d_1 + [\frac{z_3}{z_1} + \frac{j\omega m_{s1}}{z_3}]\sinh \Gamma d_1 \qquad \langle 50 \rangle$$

When the analysis is applied to the three layer system used for under carpet vehicle noise control the general equations reduce to;

$$R = 10\ LOG_{10}\ \{\ x_1 \cosh \Gamma d_1 + x_2 \sinh \Gamma d_1\ \} \qquad \langle 51 \rangle$$

where $x_1 = j(\omega m_{s1}/\rho c + \omega m_{s2}/\rho c)$ <52>

and $$x_2 = \frac{z_3}{\rho c} - \frac{\omega^2 m_{s1} m_{s2}}{z_3 \rho c} + \frac{j\omega m_{s1}}{z_3}$$ <53>

where m_{s1} and m_{s2} are the surface densities (area densities) of the foam and septum respectively in kgm^{-2}.

2.10.1 Propagation constant and characteristic impedance of polyurethane foam

The propagation constant of a wave through a porous material is given by Bies (1988);

$$\Gamma = j\omega \sqrt{(Y\rho'/K')}$$ <54>

and the characteristic impedance given by ;

$$z_3 = \sqrt{(\rho' K'/Y)}$$ <55>

The complex density, ρ' combines the density of porous structure and the enclosed air. It must include the effects due to viscous and inertial motion, which cause it to be complex. It's representation is;

$$\rho' = (\rho_{tot})(1 - \frac{jR_2}{\rho_{tot}\,\omega})$$ <56>

where $\rho_{tot} = \rho_3 + \rho_0$ the sum of the foam and air densities.

Between the limits of isothermal and adiabatic behaviour, described in Section 2.7, the thermal capacity of the PUR material due to the

compression/rarefaction of the gas requires a value of R_2 to be used. This takes into account this combination of isothermal and adiabatic compression/rarefaction of enclosed air, where $R_2 \approx 1.2R_1$.

As previously for structure-borne excitation the bulk compression modulus K^* is also represented as the combination of the foam modulus and the contained air modulus, i.e. $K^*_{tot}=(K'_{foam}+K'_{air})(1+j\eta_{tot})$ where $\eta_{tot}=\eta_{foam}+\eta_{air}$ The foam modulus is related to Young's modulus by $K^*_{foam}=E^*/[3(1-2\nu)]$. The loss factor of air, η_{air}, is small in comparison with the foam loss factor so is ignored in the subsequent analysis. In compression the Poisson's ratio, ν, of a Polyurethane foam is approximately zero and in tension approximately 0.25, Hilyard *et al* (1990), so that $K^*_{foam}=E^*_{foam}/3$.

The expression for transmission loss above can be split into the real and imaginary parts. This is aided by the simplification of $\cosh \Gamma d_1 = 1$ and $\sinh \Gamma d_1 = 0$. This is valid for $f<c/6d_1$. Thus for a thickness of 10mm the simplification is valid for f<5716 Hz and for a 30mm foam it is valid for f<1906 Hz.

$$\text{REAL [R]} = 1 - \frac{\omega^2 m_{s1} d_1}{K'_{tot}(1+\eta^2_{tot})} + \frac{\omega^3 m_{s1} m_{s2} d_1 \eta_{tot}}{\rho c K'_{tot}(1+\eta^2_{tot})} \qquad \langle 57 \rangle$$

$$\text{IMAGINARY [R]} = \frac{\omega(m_{s1}+m_{s2})}{\rho c} + \frac{\omega^2 m_{s1} d_1 \eta_{tot}}{K'_{tot}(1+\eta^2_{tot})} - \frac{\omega^3 m_{s1} m_{s2} d_1 \eta_{tot}}{\rho c K'_{tot}(1+\eta^2_{tot})} \qquad \langle 58 \rangle$$

For the computer modelling the expression in Eqn. <51>, was implemented along with the expression for the mass law of the steel panel in Eqn. <44>. As previously mentioned the mass law for the steel

panel is valid for the required frequency range, as the predicted critical frequency of a 1mm steel panel is 12.4kHz.

2.10.2 System Resonance Frequency

When a triple layered system is used, with the two outer layers separated by a compressible material, resonances are introduced into the system. The principle one is that arising from the mass-spring-mass system nature. This resonance frequency, f_R, can be obtained by setting the imaginary part of the transmission loss in Eqn. <58> to zero, to give;

$$f_R = \frac{1}{2\pi}\left[\left(\frac{K'_{tot}}{d}\right)\left(\frac{1}{m_{s1}} + \frac{1}{m_{s2}}\right)\right]^{1/2} \qquad \text{<59>}$$

This equation is important for under carpet vehicle noise composites as it identifies the parameters that affect the resonance frequency of the system. At the resonance the insertion loss goes through a minimum. The position of the resonance frequency is therefore important. The choice of the resonance frequency in vehicle composite design is discussed further in Chapter 6.

2.11 Airborne Noise Theoretical Predictions

The theoretical response equation <51> in the previous section was implemented on a IBM compatible personal computer using the Turbo C programming language. The programme utilised double precision complex number handling routines and is given in Appendix B. The computer model was used with the theoretical property values for foams in Table 4. The data enables the influence of the various parameters

to be examined whilst other parameters remain constant.

2.11.1 Material Parameters

(a) Foam Damping

The influence of damping was examined using property values for foams 2, 6, and 7 from Table 4. These gave loss factors of 0.2, 0.5 and 0.8 respectively with other material properties kept constant. The predictions are shown below in Fig. 17. It is seen that with increasing damping the depth of the resonance trough is reduced. This effect is also observed at the second resonance. At high damping values the second resonance disappears. The IL between the two resonances decreases slightly with increasing damping. This constitutes a 1dB difference between η=0.8 and η=0.5, and slightly less between η=0.5 and η=0.2.

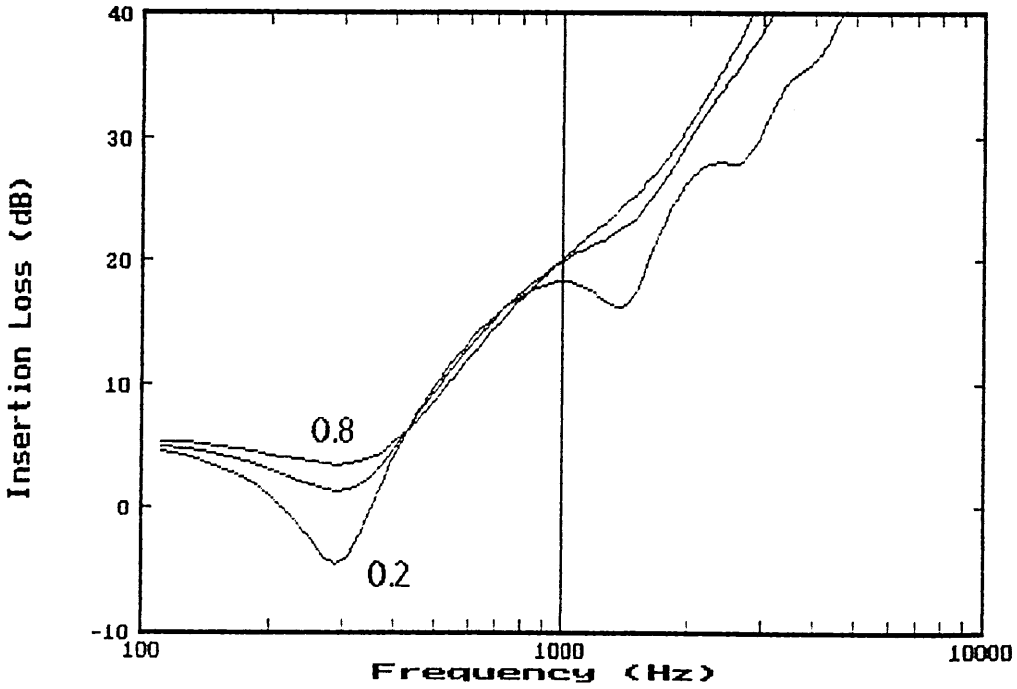

Fig. 17 Influence of loss factor (η=0.2, 0.5, 0.8) with other foam

properties constant

(b) Foam Density

We know from the mass law in Chapter 2 that a doubling in surface density of a panel increases the TL by 6 dB. The foam contributes approximately one sixth of the total composite mass. The effect of the foam will, therefore, not be as great as that of increasing the septum mass, as far as increasing system mass is concerned. Using foam property values for foams 1, 2, 3 and 4 from Table 4. This gives a density range from 20 to 100 kgm^{-3} with other material properties constant.

We can see from the prediction in Fig. 18 that increasing the foam density increases the IL at low frequencies slightly (~3dB from $20kgm^{-3}$ to $80kgm^{-3}$). But, at the higher frequencies (f>630 Hz) the lower density foams out perform the higher densities. Any shift in resonance frequency is unnoticeable.

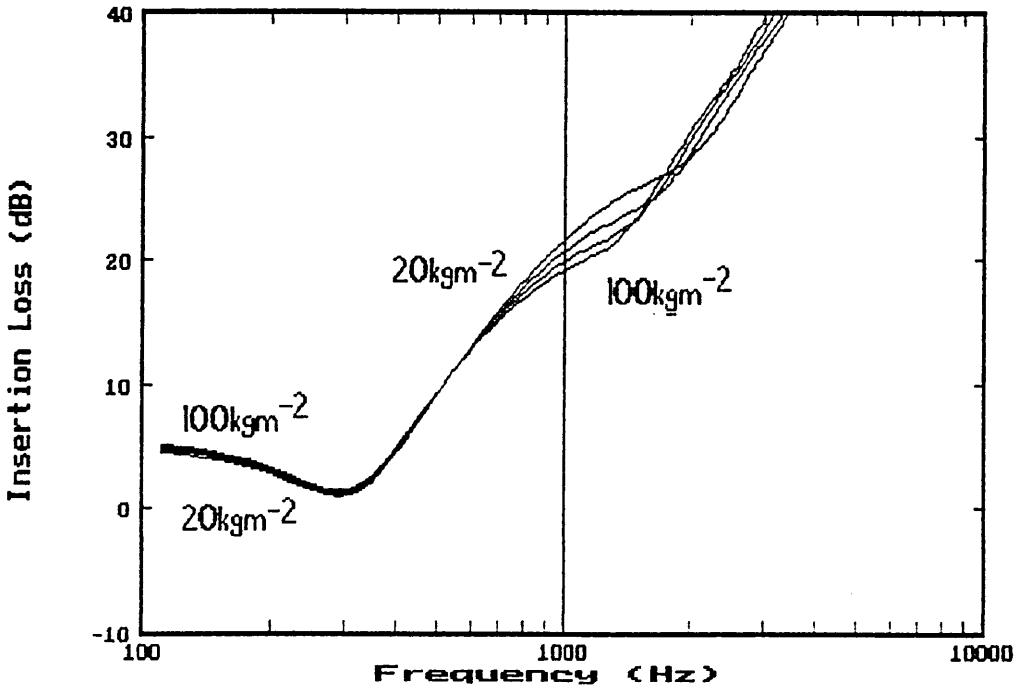

Fig. 18 Influence of foam density with other material properties kept constant

(c) Foam Modulus

The foam modulus, along with thickness, is influential in the design of the resonant frequency. By controlling the resonance the insertion loss can be increased in the frequency range required. The influence of the modulus of the foam layer was examined for foams with loss factors of η=0.2 and 0.5. Foams 17, 18, 7 and 19 for η=0.2, and 16, 8, 2 and 9 for η=0.5 from Table 4 were used. The predicted results are shown in Figs. 19 and 20.

The theoretical predictions show three phenomena. Firstly, an increase in foam modulus causes an increase in resonance frequency. This was expected from examination of the equation for resonant frequency (Equation <59>). Secondly, with decreasing modulus, the IL

level is increased (due to the decreasing resonance frequency shifting the IL curve down the frequency scale). This increases the post-f_R IL level, but decreases it below resonance. Thirdly, the IL at the resonance is predicted to be increased with increasing foam modulus.

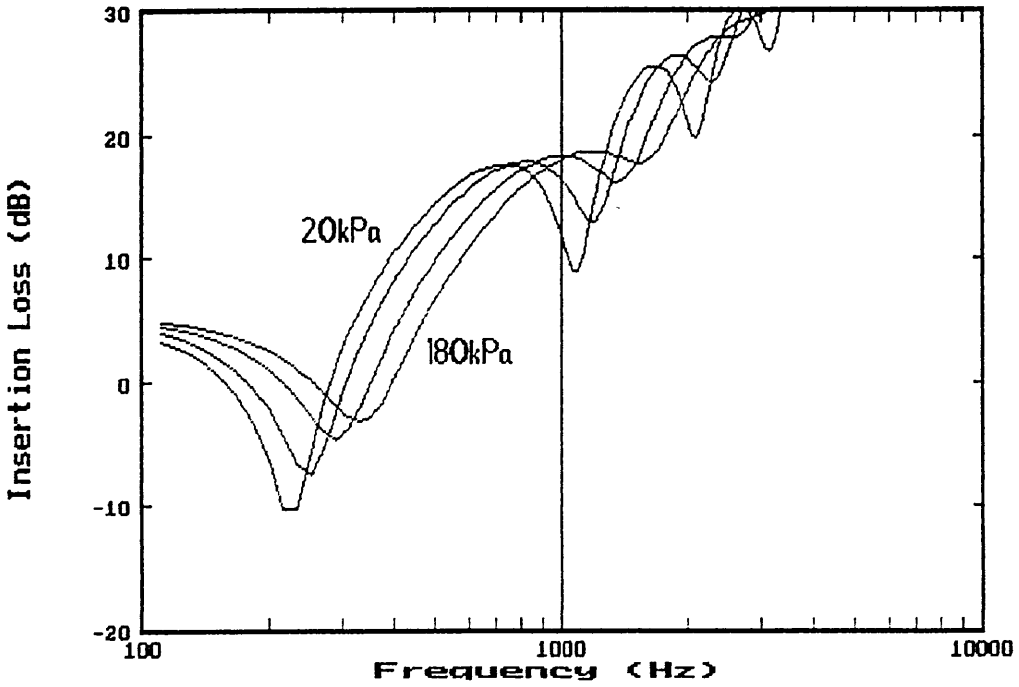

Fig. 19 Effect of foam modulus (η=0.2) with other material properties constant

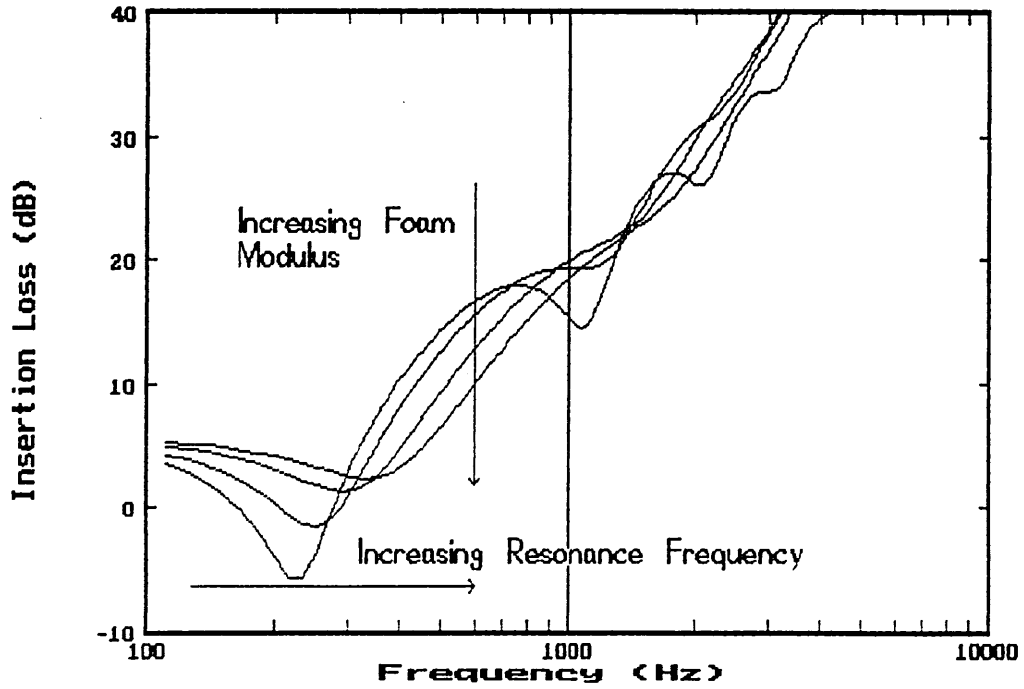

Fig. 20 Effect of foam modulus (η=0.5) with other material properties constant

(d) Foam Flow Resistance

We saw in Section 2.10 that the flow resistance affects the complex density of the PUR foam. This in turn also affects the propagation constant of sound in the foam. Using material data 2, 10 and 12 the influence of flow resistance was investigated with the computer model. The property values in Table 4 give a range of flow resistivity from 20000 to 130000 Rayls, with other material parameters kept constant. The predictions in Fig. 21, show that a low flow resistivity improves the IL.

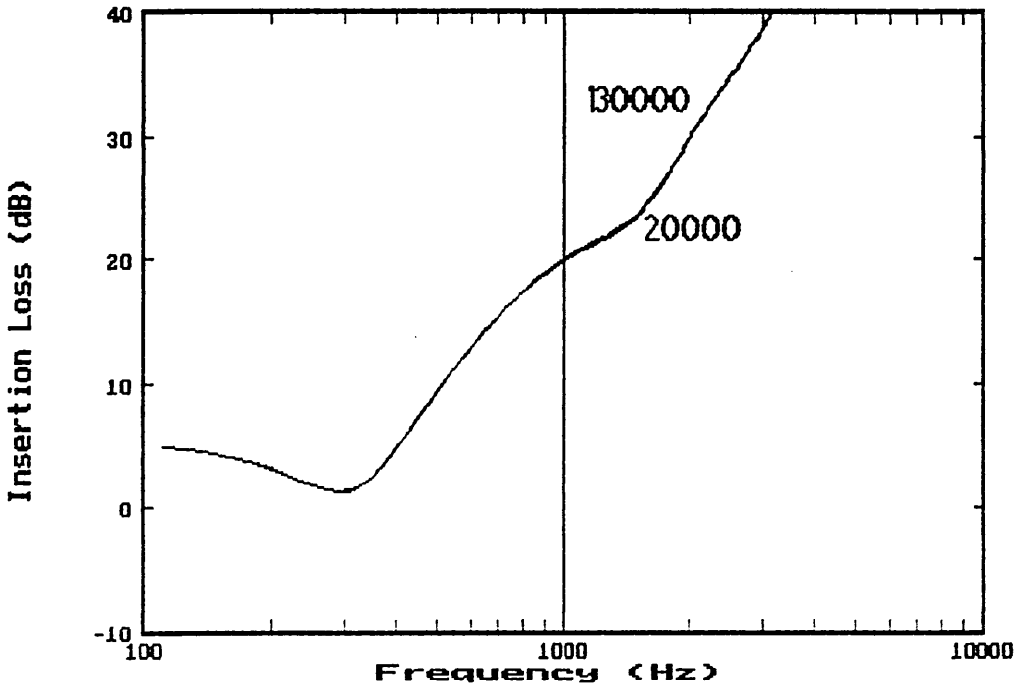

Fig. 21 Effect of flow resistivity with other material properties constant

2.11.1 System Parameters

(a) Influence of Foam Thickness

The theoretical analysis stated that the increase of thickness would result in a decrease in the first resonance dip. The property values for foams 5, 2 and 13 and 14, 15 and 7 from Table 4 were used to examine the influence of thickness for two different values of loss factor. Other material properties were kept constant as previously. A septum mass of $5.9 kgm^{-2}$ was used. The predicted IL is shown in Fig. 22 for a loss factor of 0.5 and in Fig. 23 for a loss factor of 0.2. As expected, the resonance frequency decreases with increasing thickness, and the post-f_R IL increases. Below the resonance fre-

quency it is possible to achieve better IL performance from a thinner foam. The IL for the higher damped (η=0.5) foam, between the first and second resonances, is improved by up to 7.5dB for a doubling of thickness , 11.2dB for tripling and up to 4.5 dB for an increase in thickness of 50%. If the loss factor is reduced (η=0.2) we see that the extent of the resonance dips increases. This gives us improved IL over the higher damped case. An IL of up to 11.3dB for doubling of thickness, 15.7dB for tripling, and up to 7dB improvement on a 50% increase in thickness. In both cases there is also a slight increase in IL at the resonance frequency with increased thickness.

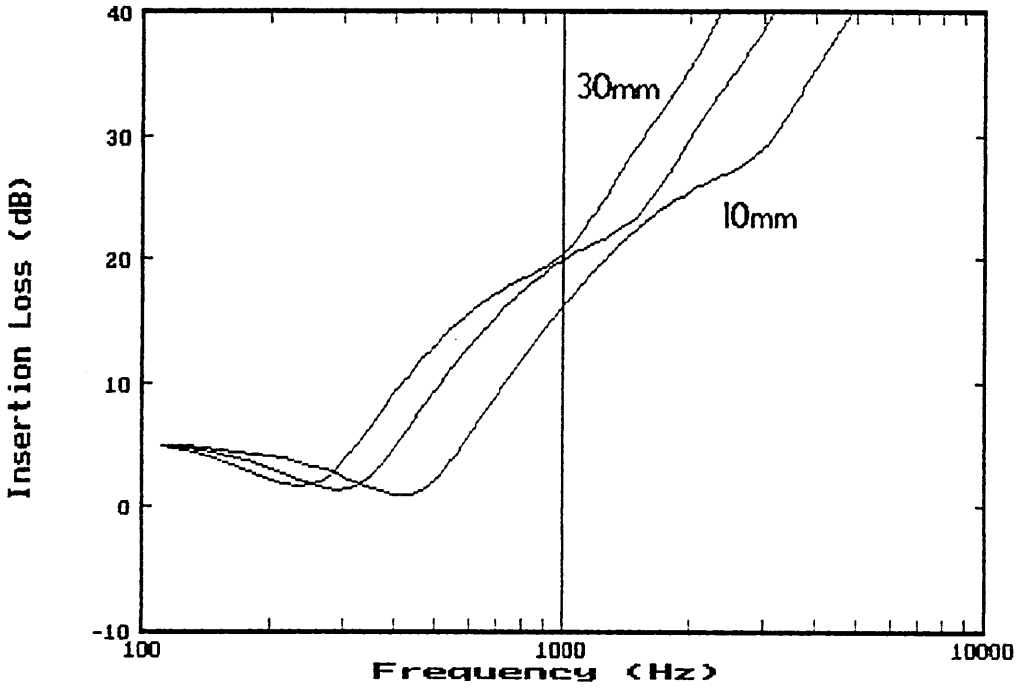

Fig. 22 Influence of foam thickness (η=0.5) with other material properties constant

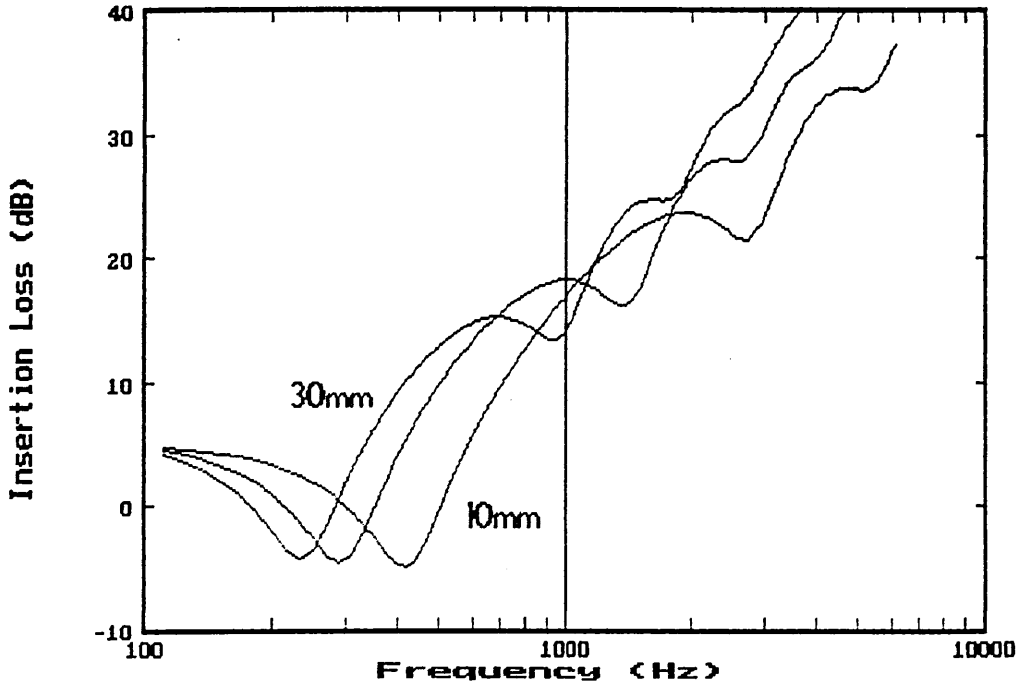

Fig. 23 Influence of foam thickness (η=0.2) with other material properties constant

(b) Septum Area Density

The equations developed for the theoretical analysis showed that increasing the area density of the septum (heavy) layer should result in a reduction of the resonance frequency and an increase in the level of the IL curve. Using the property values for foam 2, with septa of 1.5, 3.7, 5.9, 8.7 and 12 kgm^{-2}, the prediction is shown in Fig. 24. The predictions demonstrate that the increase in surface mass results in a decrease in the resonance frequency; the post-f_R IL of the composite increasing with increasing surface mass.

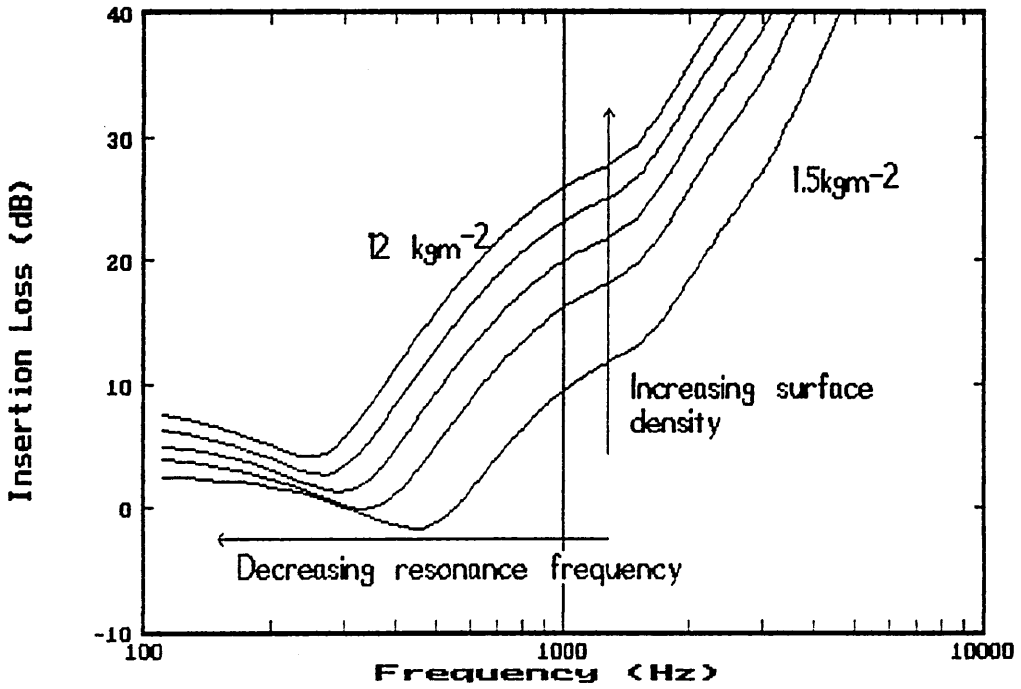

Fig. 24 Influence of septum surface density

2.12 Conclusions of Chapter 2

This chapter has described the response of multilayered panels when subjected to structure-borne or airborne noise excitation .

An analysis of panel vibration was introduced. It was shown that when the panel used in this study was excited many modes were predicted to be exhibited. It was shown that the noise radiated from a vibrating panel is proportional to its velocity. Reduction in the vibration level thus should reduce radiated noise. This can be achieved by applying damping layers. The theory of Oberst (1954) was cited for the prediction of the damping of constrained and free damping layers. Published data showed that the panel loss factor

decreased with increasing frequency from 0.002 to 0.0015 for a steel panel. The work of Plunt (1991) showed that for a typical vehicle carpet system loss factors from 1.0 at 100Hz to 0.01 at 2kHz were achievable in practice. The theory of Cremer (1988) for point excitation of panels gave an upper limit of loss factor, above which additional damping would have little effect on reducing radiated noise. This has implications on the type of foam that is to be used for noise control purposes i.e. viscoelastic (VE) foams potentially offering similar performance to that of higher damped high hysteresis foams (HHF). These latter types of foams are more complex and expensive to process.

The equations for point excitation of panels were combined with simple transmissibility theory to derive an equation to predict the insertion loss of the vehicle composite systems. Material test data with values typical of those that can be manufactured was used in the model to predict system insertion loss (IL). (The IL of the composites is shown in Chapter 3 to be more easily obtained experimentally than the transmission loss). The dependence of system IL performance upon a single parameter was investigated, whilst other properties were kept constant. The predicted response was one of decreasing IL until a resonance dip was reached. Above this resonance frequency the IL increased.

The predicted effect of increasing foam damping was to increase the IL. This was more pronounced in the resonance dip. Varying foam density had little effect upon IL. The predictions showed that increasing foam modulus increased the resonance frequency and slightly improved the insertion loss at resonance. However, a higher

resonance frequency shifts the response curve up the frequency range thus resulting in a lower IL level above resonance. Increasing foam thickness increased the IL and reduced the resonance frequency. The IL at resonance was also increased as the thickness increased. The septum area density had a similar effect to foam thickness except that the IL at resonance was slightly reduced.

The concepts and principles of transmission of airborne noise through panels was introduced. The relationship between transmission loss (TL) and IL was derived. The critical frequency of a typical foam composite system was shown to be 54kHz, compared with 12kHz for a 1mm steel panel. Thus this effect is exhibited well above the frequency range of interest in this study. This justified the use of the mass law for the steel panel in subsequent model development. Using the transmission line theory of Beranek (1949) and other workers a model was developed to predict the TL of multilayered under-carpet systems. This was related to the IL of the composite using the previously derived equations and the mass-law equation for a steel panel. An expression for the system resonance frequency (Equation <59>) showed that the resonance was dependent upon foam stiffness, foam thickness and the surface densities of the steel panel and septum.

The model predictions showed a characteristic shape. The IL decreased until a resonance dip was reached. Above this resonance frequency the IL increased. At higher frequencies (f>1.5kHz) secondary resonance dips were predicted. As with the structure-borne noise model above the materials test data was used to investigate the dependence of system IL performance upon material and system parame-

ters.

The predicted effect of increasing foam damping was to reduce the IL of the resonance dips. Increasing foam density had little effect upon IL. The resonance frequency increased with increasing foam modulus as predicted by the resonance frequency equation. An increase in the resonance frequency also shifts the response curve up the frequency scale, thus reducing the overall IL level above resonance. Foam flow resistance was predicted to have little effect upon IL. As expected from resonance frequency equation increasing the foam thickness reduced the resonance frequency. This shifted the IL response curve down the frequency scale, thus increasing the overall IL level. A slight increase in IL at resonance was predicted. Increasing foam surface density reduced the resonance frequency, shifting the response curve down the frequency scale, and increasing the overall IL level. The IL at resonance was also increased.

Both theoretical models demonstrated the influence of material and system parameters on insertion loss of multilayered composites. The theoretical models are used to predict composite performance in Chapter 5 and compared with experimental data. The theoretical predictions indicate that by varying the position of the resonance trough and material and system parameters allow the IL level to be altered.

3. EXPERIMENTAL PROCEDURES

3.1 Introduction

Procedures for the evaluation of the noise reduction composites can be divided into two categories (a) in-car tests, on the road and in the laboratory (e.g. Gahlau, 1987) and (b) large and small scale laboratory tests. The collaborating company has arranged the in-car field trial evaluation, whilst this project concentrates on the large and small scale laboratory tests. The techniques used (a) compare the functional performance of the composites and (b) create a routine testing procedure that can be used in industrial laboratories for the characterisation of the insertion loss of vehicle carpet systems.

Although large scale test facilities, such as the standard acoustic transmission suite (ISO 140, BS 2750), and its variants, were not used in this project brief comments on the techniques and their applicability to the investigation are given as they are used by some automotive manufacturers to evaluate their noise reduction systems.

The laboratory work concentrated on small scale test procedures for material characterisation and comparison of system performance. Since the experimental data are used for two purposes (a) to convey information to industrial/commercial organisations and (b) to provide scientific data for the evaluation of theoretical models, the procedures used combine Standard Tests (ISO/BS/ASTM), industrially accepted procedures (such as the BMW test for the evaluation of

dynamic stiffness and damping of automotive under carpet foams), and more fundamental techniques e.g. dynamic mechanical spectroscopy, which measures the dynamic stiffness and damping of foams over a range of frequencies.

The development of the test facility is described, and the use of intensity measurements to obtain insertion loss data is detailed. A description of the measurement of intensity is included, as well as an evaluation of the errors due to the technique.

3.2 In-Vehicle Testing

Field trials for evaluation of vehicle noise is carried out by manufacturers. This is both subjective and objective. However, due to the commercial sensitivity of this information, little is ever published in the open literature. Independent in-vehicle laboratory testing is carried out by several organisations e.g. Stankiewicz in Germany, and Teroson in the UK.

There are a number of techniques for measuring interior noise. (a) A microphone placed at the position of the driver or passenger head. The SPL is measured and a frequency spectrum of the noise made either from a recording of the noise, or *in situ* with a spectrum analyser. (b) An intensity probe, coupled with a spectrum analyser, is used to identify the noise sources and sinks within the vehicle compartment. The measurement of intensity allows the direction and magnitude of the noise to be identified. Based on this knowledge, targeted treatment can be used to control the noise sources. (c) A slightly different technique is to obtain a transfer function be-

tween two points on the vehicle. This can form the basis of a modal analysis. The trim, including carpets are removed from a vehicle to reduce attenuation. A calibrated hammer is used to provide a known force at a specific position, e.g. an engine mount, and the pressure response measured at driver head position using a microphone. A transfer function can then be calculated, and used to assess possible vibration problems.

A description of some laboratory tests was published by Gahlau (1987). He described the evaluation of four commercial cars with and without a variety of sound insulation packages. The cars were dissected with the front half being enclosed in a semi-anechoic chamber. The rear of this section being within a reverberant compartment. Treatments were applied to the vehicle floor-pan and bulkhead; and their comparative performance measured. The work is the first to present data for these systems. Whilst the methods used are of interest, the data presented is of little use for the theoretical predictions presented here; this is due to the limited information given regarding system and material parameters. (The method is also not easily repeatable due to the nature of the experiment).

The assessment of interior noise quality and annoyance is the final criteria for judging how good a vehicle noise control package is. The various techniques used are discussed in Chapter 6.

3.3 Large Scale Laboratory Tests - Transmission Loss Suite

This is the standard method for evaluating the random incidence transmission loss of materials and panels. It is detailed in ISO 140

and BS 2750. The facility is illustrated in Fig. 25. It consists of two isolated reverberant rooms, separated by the panel under test. The source room contains the noise source; normally broadband random noise. The sample is bonded onto a steel base panel and mounted vertically. A number of microphone positions are used to measure the SPLs in the two rooms, and the TL is then calculated from Eqn. <39>.

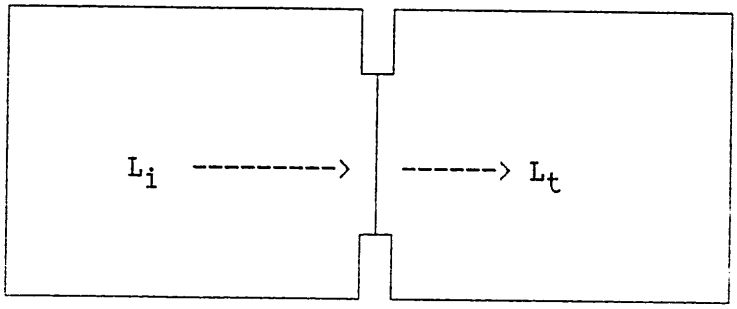

Fig. 25 Transmission loss suite

This equation takes into account the sample size and the absorption present within the receiving chamber.

$$R = L_i - L_t + 10LOG_{10}\ S/A \qquad \langle 39 \rangle$$

The diffuse sound fields on either side are not representative of the conditions inside a vehicle. The international standard aims to increase the reproducibility of the measurements, but it is found that results from different laboratories, for the same samples, show variations of up to 6 dB (Whatmore *et al*, 1973). This would thus appear to indicate that more economical TL facilities could be used, with measurement variability comparable to major test facilities. Discrepancies often arise if the samples are not sealed effectively. The available facilities are almost always for vertically bonded samples, whilst the trend in the automotive industry is towards

unbonded carpet systems. Horizontal or 45° configuration transmission suites are available at some companies which allow unbonded systems to be used, but these are comparatively rare.

3.4 Small Scale Laboratory Tests

The need for a small scale laboratory test facility, which satisfied the requirements of economical, but effective, evaluation of material attenuation properties has been an attractive proposition for many years. A number of small scale test facilities have been employed. The earliest appears to be that described by Wallace *et al* (1946), and Nichols *et al* (1947). This measured TL for small section (18" x 18") aircraft panels, and was later modified by Beranek *et al* (1949). It provided a measure of transmission loss for the materials under test. The test facility offered by GM is based upon this using an array of loudspeakers. More recently Bridgestone (Japan) and Papanikolaou *et al* (1985) have used a small facility for their transmission measurements. These involved a small test chamber placed within a reverberant chamber. These thus fail to meet the criteria of an economic facility. The two main facilities used are those of GM and Interkeller (Apamat II). These are detailed below.

(a) Apamat II

The Apamat facility is produced by Interkeller of Zurich. It is used to evaluate the insertion loss performance of materials, under both structure and airborne excitation. It is illustrated in Fig. 26. The structure-borne excitation is provided via the impact of 8mm steel balls against the steel base panel. The airborne noise is from broadband random noise. A measurement of SPL is made with and with-

out the sample in place, and the SPL insertion loss is evaluated from the difference. The manufacturer recommends that the steel panel is replaced every four tests - a practice that is rarely observed. The quoted frequency range is 100-100000 Hz, though they state that the equipment should not be used below 400 Hz.

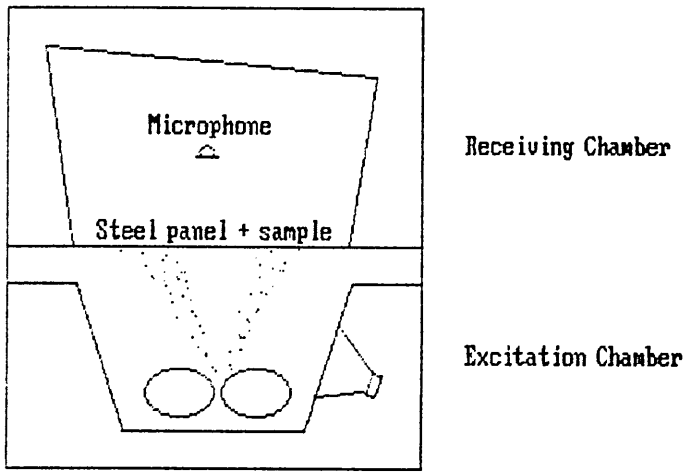

Fig. 26 Apamat test facility

(b) The GM Facility

This test facility measures the SPL insertion loss. It is based upon that described by Beranek *et al* (1949), and is illustrated in Fig. 27. The facility consists of two compartments. The walls are made of steel sections filled with sand. The source loudspeakers are mounted in a 3x3 array close to the test panel. The aim of this is to provide a uniform plane incident wave on the test panel. The close proximity also reduces lateral standing waves. The receiving chamber

is terminated by anechoic foam wedges to reduce reflections and standing waves. This compartment is removable via a supporting cable to allow for application of sample. A single microphone position is used to measure the SPLs. The recommended measurement procedure is extensive concerning the sample preparation and environmental conditions.

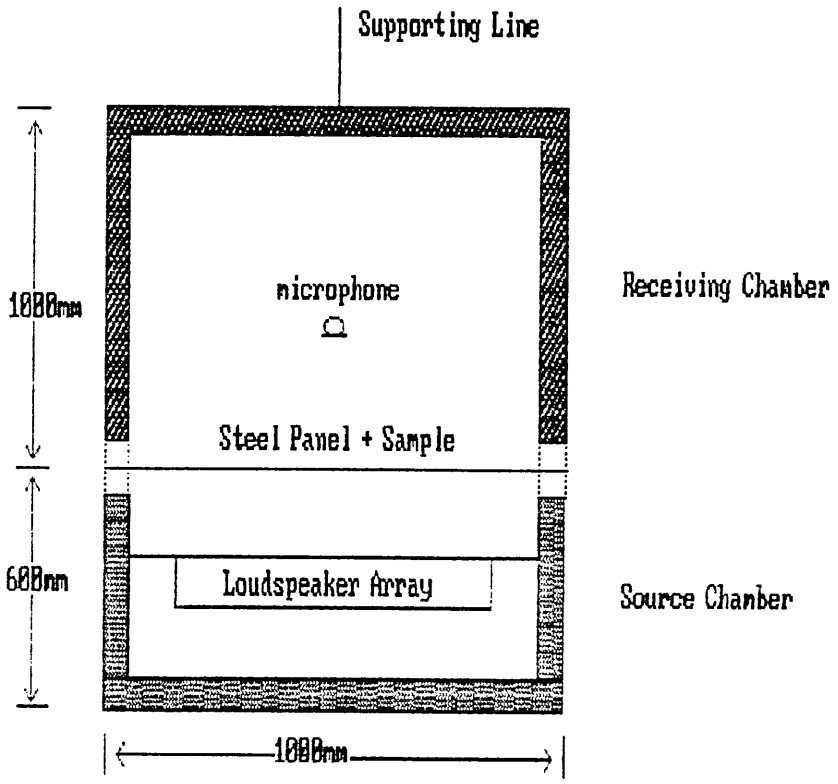

Fig. 27 The GM noise transmission method

3.5 Development of a Small Scale Laboratory Test Facility

A small scale test facility was required to investigate the behaviour of foam cored composite systems, when subjected to airborne and structure-borne noise sources. It was anticipated that experimental measurements would be compared with in-car tests and theoretical results. The requirement of a low-cost in-house test facility also needed to be considered. The facilities described previously were considered unsuitable so a test rig was constructed which would satisfy the above criteria. The initial prototype rig is described briefly below, followed by a description of the final test facility used for this study. A square panel was chosen for the experimental work (i) to conform with the majority of industry test methods (ii) because it was easily incorporated into the test rig, and (iii) it conformed with the shape and size of the experimental foam samples that could be manufactured by the collaborating company.

3.5.1 The Prototype Test Facility

The prototype test facility was similar to the type used by the Bridgestone Corporation and is illustrated in Figure 28 below. The design was chosen for its low cost and portability.

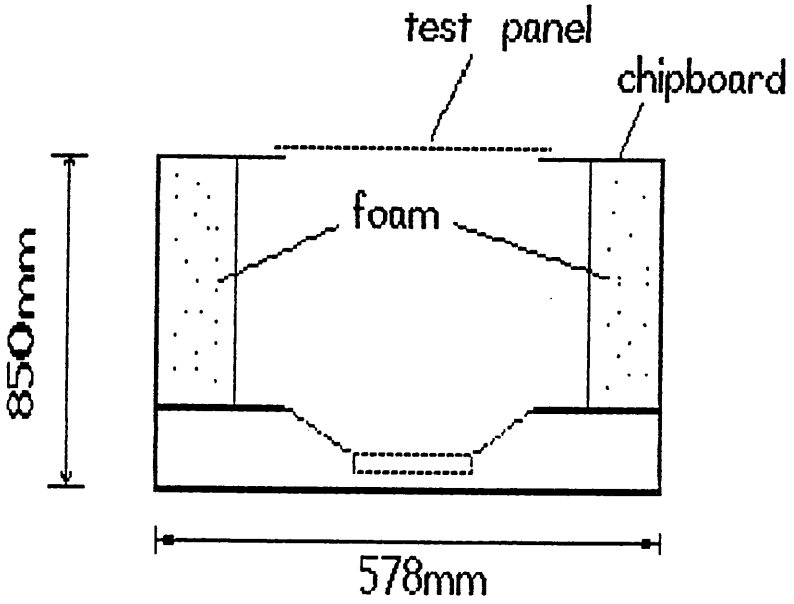

Fig. 28 Prototype Test Facility

It was constructed from single skinned 1/2" chipboard, with dimensions 850mmx578mmx578mm. The aperture in the top surface was 300mmx300mm, covered with a 0.8mm mild steel panel. This horizontal mounting enabled unbonded foam samples to be used. The panel was clamped in place using a one-piece chipboard frame, secured with nuts and bolts along its edges. Inside, the walls were lined with polyurethane foam to reduce lateral reflections. The loudspeaker, a 50W 8Ω Peerless base unit, was driven by a B&K sine/random generator (type 1024). A 1/2" microphone inside the box monitored the source level, via a B&K single channel narrow band real time analyser (RTA type 2033). The monitored level enabled the source level to be maintained at a constant level. The radiated level was measured using a 1/2" microphone, also connected to a B&K 2033 RTA. The SPL radiated from the top surface was measured with and without the foam in place. The difference of these levels giving an insertion loss value.

The prototype test facility did not give very satisfactory results for a number of reasons, principally;

(1) The measuring microphone outside the box was subjected to pressure variations dependent upon microphone to source distance. Differences of 10 dB over 0.4m were observed for a particular frequency. These variations are in the near field region of the source as described by Ver *et al* (1988).
(2) Radiation of noise from the sidewalls and panel surround was not negligible. This contribution thus influenced the measurement values.

It was considered that placing the test facility in an anechoic room or a reverberant chamber (as reported by Papanikolaou *et al* 1985) might enable measurements to be made. Whereas this would have overcome some of the above problems, it would result in costly facilities being used and not necessarily solve the problem of noise radiated through the sidewalls and panel surround. In addition the facility would no longer be small scale and inexpensive as originally required. To overcome these problems, a larger free-standing test facility was proposed. This is detailed below.

3.5.2 The Test Facility

The shortcomings of the original prototype test facility were described above. The new test rig was designed to overcome these problems in conjunction with a different measurement technique utilising intensity measurements. The test facility construction is

described in this section whilst the intensity technique is described later in this chapter.

In addition to making the test rig more massive than its predecessor (to reduce unwanted transmission through the walls) a larger aperture was also incorporated. This was to enable larger foam samples to be tested more typical of the surface areas used within a vehicle. This larger foam area also reduces the influence of localised moulding variations (see for instance Rodwell *et al* 1989). The test rig is illustrated in Fig. 29, and in Plates 1 and 2. It has approximate external dimensions of $1m^3$. The walls were made from sand/lime brick and mortar construction, upon a reinforced concrete base. The base rests upon four TICO anti-vibration mounts. The top was also of reinforced concrete, with an aperture of 870x870mm cut out. At a distance of 300mm above the base a 2.5cm thick chipboard baffle was inserted, with a small array of loudspeakers. These consisted of a 100W woofer (Celestion, type G12H-100T3597 CE 8Ω) with a frequency response from 50 Hz to 3.5 kHz, and two piezo tweeters with a frequency response from 2.2 kHz to 33 kHz. A 1mm steel sheet was placed over the aperture, and secured with a 4mm angle iron framework and toggle clamps. These enable quick access to be made to the source chamber. The edges of the steel panel had a thin self-adhesive foam layer attached to ensure good sealing from acoustic leakage when clamped. The 1mm thick mild steel panel was used as being representative of that used in vehicle panels. Access holes were built in the sides to allow cabling to be routed. These could be sealed to prevent leakage during measurements.

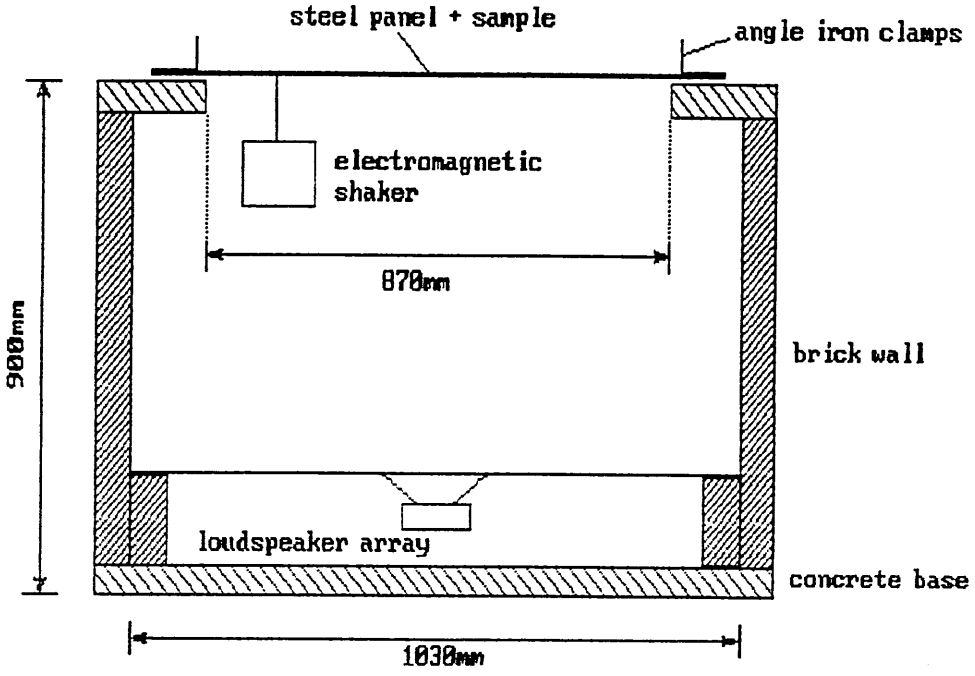

Fig. 29 Test facility

The steel panel was divided into a matrix to aid the vibration and intensity measurements to be made. The grid points were marked with a separation of 0.1m, giving a total of 81 points in a 9x9 configuration. The grid is shown below in Fig. 30.

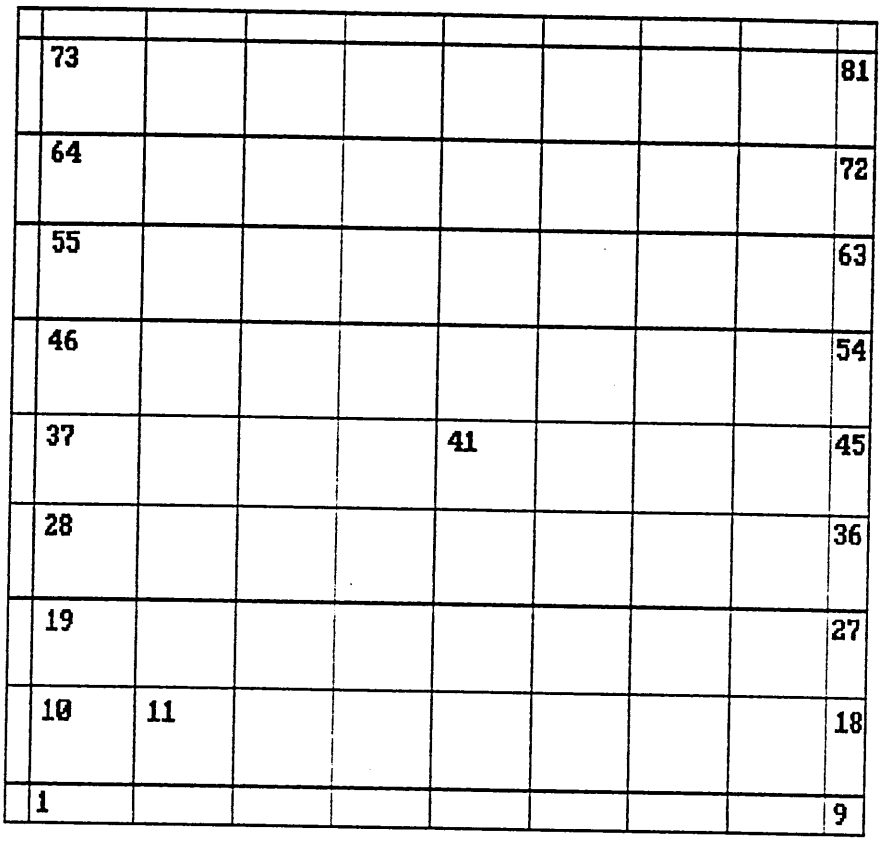

Fig. 30 Measurement positions on steel panel

Broadband excitation was provided via a B&K 1024 Sine/Random generator, shaped by a Sony graphic equaliser, and amplified by a Sony power amplifier (type TA-1130). For structure-borne noise the broadband noise was fed to a Ling Dynamic Systems (LDS) power amplifier (type TPO300) and electromagnetic shaker. The shaker was loosely connected to the panel by a steel shaft and a rubber coupling. This was at position No.11, a distance (0.15,0.15m) from the side of the panel. This point was chosen in order that a fundamental panel mode was not excited. The radiated intensity was measured using a Norsonic AS real time analyser (type 830) with intensity probe (type 216).

The test-rig was located in a laboratory which has a rever-

beration time of approximately half a second. The sound field on either side of the test panel is not diffuse, so transmission loss measurements are not possible. Within the source chamber the brick and concrete walls provide reflective surfaces, and thus standing waves are set up laterally and longitudinally.

Because a measure of the carpet system acoustic performance was required, and ordinary sound pressure measurements were not suitable due to the large variation in SPL over small distances, another procedure needed to be adopted. It was mentioned in Chapter 2 that intensity measurements can be used in transmission loss measurements on the receiving side to obtain the sound intensity radiated through a panel. The receiving room does not then need to be reverberant. This corresponds with the acoustic field within the laboratory. The natural extension of this method was thus to measure the intensity on the receiving side with and without the carpet system. The difference between the intensity values being the insertion loss of the PUR carpet system. This can then be related to the transmission loss of the material if required as described in Eqn. 43 in Chapter 2.

3.6 Intensity Measurements

Intensity is the rate of acoustic energy flowing through a unit area, normal to the direction of propagation. It is a vector quantity, possessing both magnitude and direction. It is defined as

$$I = 1/T \cdot \int^{S} p.\bar{u}\, dt \qquad (Wm^{-2}) \qquad \langle 60 \rangle$$

where p is the instantaneous pressure, $\bar{u}$ is the instantaneous parti-

cle velocity, s is the surface area, and T is the averaging time. For a comprehensive description of the theory and practice of acoustic intensity the text by Fahy (1989) is recommended. There are two methods of measuring sound intensity. Both methods measure intensity in one direction e.g. x-direction only. (1) The indirect method. This uses two closely spaced pressure microphones (hence the terminology of p-p probe). The particle velocity is obtained from a finite approximation using the two pressure signals, whilst the sound pressure at the coincident point is calculated from the two pressure signals. The intensity is then the product of the two values. The frequency response of the probe is restricted by the separation of the two microphones. This is due to the finite difference approximation. Hence for a complete frequency range two different microphone separations may need to be used. The B&K analyser (type 4433) and probe (type 3520) is typical of equipment that uses this method. (2) The direct method. As its name suggests this method obtains the sound intensity via direct measurement of the particle velocity and sound pressure (hence the terminology of p-u probe). The particle velocity is measured using a pair of ultrasonic transceivers. A sound wave impinging on the ultrasound beam causes a phase change in the received signal which is proportional to the particle velocity. The pressure signal is obtained from a pressure microphone close to the geometric centre of the ultrasonic beam. The intensity is the product of these two signals given in Eqn. 61.

$$I = \tfrac{1}{2}PU \cos(\phi_f \pm \phi_s) \qquad \langle 61 \rangle$$

where ϕ_s is the equipment phase mismatch between the two RTA channels, and ϕ_f is the field phase angle between the particle velocity

and the pressure. Small p-u phase angles correspond to high intensities and large phase angles to small intensities.

Because of the finite path length (typically 28mm) of the ultrasonic beam and the pressure measurement being slightly offset from the point at which particle velocity is measured the intensity value will be slightly inaccurate compared with the p-p method. However, as described later, this is small for the frequency range of interest. A windshield is used over the probe to shield the ultrasound beam from hydrodynamic fields and to suppress stray ultrasonic wave reflections in the vicinity. Hydrodynamic effects occur in the acoustic near field where pressure and particle velocity are in quadrature (Cremer *et al* 1988). The Norsonic AS analyser (type 830) and p-u probe (type 216) is typical of equipment that uses this method. It is this equipment that is used in this study.

3.6.1 Errors in p-u Acoustic Intensity Measurements

(1) Analyser and Probe Phase Mismatch

The normalised random error $\epsilon(I)$ in the intensity I due to phase mismatch is given by Fahy (1989) as;

$$\epsilon_{\phi}(I) = \phi_s \tan \phi_f \qquad \langle 62 \rangle$$

From this and the previous equation the importance of phase mismatch can be seen. The term residual intensity is used to quantify the apparent flow of acoustic energy due to phase mismatch in p-p and p-u probes. It is measured by subjecting the two transducers to iden-

tical signals. The difference between the measured pressure level and the detected residual intensity is the residual pressure-intensity index, δ_{pIO}. For a p-u probe this is related to the phase angle error by;

$$\delta_{pIO} = 10\log[\sec(\phi_s)] \text{ dB} \qquad \langle 63 \rangle$$

The p-u probe transducers are calibrated at the manufacturers factory to compensate for differences in phase responses of the transducers. According to the manufacturers the 830 analyser and probe have a value of $\delta_{pIO} > 30$dB for f<10kHz. This corresponds to a phase angle $\phi_s < 0.1°$ for 10Hz<f<5kHz.

(2) Finite Ultrasound Beam Length

The frequency range of operation due to finite ultrasound path length has been shown by Fahy (1989) to be limited to kd<1.2 for an error of 0.5dB, where k is the wavenumber ($k=2\pi f/c$) and d is the transceiver separation. For the Norsonic 216 probe, with a separation of 28mm, the maximum frequency is 2339 Hz. For an error of 1.5 dB a maximum frequency of 4 kHz is usable.

(3) Temperature Variation

The sensitivity of the velocity sensors in the p-u probe is directly proportional to temperature. A change in the mean absolute temperature T_0 of δT_o results in a change in sensitivity of $(1-2\delta T_0/T_0)$. Thus for a change in temperature of 1° in 20° C the resultant change in sensitivity is a factor of 0.9.

(4) Averaging Time

The normalised random error due to measurement averaging time is given by Fahy (1989) as;

$$\epsilon(I) = (\delta f T_{av})^{-\frac{1}{2}} \qquad \langle 64 \rangle$$

where δf is the bandwidth and T_{av} is the averaging time. Fahy (1989) does however mention that it is difficult to estimate averaging errors.

3.6.2 Field Indicators

There are a number of field indicators which gauge the validity of a measurement. These are well documented in the literature (e.g. Fahy 1989, ISO 9614 1990 and Jacobsen 1990). The most widely used one is the pressure-intensity (p-I index) or reactivity index (L_k) where the local index δ_{pI} is given by;

$$\delta_{pI} = L_p - L_{Ii} \qquad \langle 65 \rangle$$

The global pressure-intensity index, (this is also known as the negative partial power indicator) Δ_{pI} (or F_3) is given by;

$$\begin{aligned} \Delta_{pI} = F_3 &= L_p - 10\log[1/N \, \Sigma_{i=1}^{N} I_{ni}/I_0] \\ &= L_p - L_I \end{aligned} \qquad \langle 66 \rangle$$

where I_{ni} is a sample normal intensity, L_p is the sample average mean square sound pressure level, L_I is the sample mean sound intensity level, I_0 is the reference intensity level (10^{-12} Wm^{-2}) and N is

the number of samples.

Another field indicator that is used is the surface pressure-intensity indicator F_2 where

$$F_2 = \Delta_{p|I|} = \bar{L}_p - 10\log[1/N \Sigma_{i=1}^{N} |I_{ni}|/I_0] \qquad \langle 67 \rangle$$

The choice of which to use is not definite, in that Fahy (1989) recommends F_2 whilst Jacobsen (1991) recommends the use of F_3 because it includes the sign of the intensity, whereas F_2 uses only the magnitude. The use of F_2 can cause the evaluation of the phase mis-match error to be under-estimated. Ideally both indicators should be evaluated, though this is not always possible if scanned measurements are made with some equipment e.g. the Norsonics 830 analyser. If the difference between F_2 and F_3 is large it indicates that there is a large quantity of energy flowing into the measurement volume i.e. if $\bar{L}_I$ is negative due to energy flow into the measurement volume then the difference F_2-F_3 is also negative.

The accuracy of an intensity measurement can be assessed by the dynamic capability index, L_d (ISO 9614, 1990);

$$L_d = \delta_{pOIO} - K \qquad \langle 68 \rangle$$

where the error factor K depends upon the desired grade of accuracy. For an accuracy of 1 dB the p-I index must be 7dB less than the residual p-I index (B&K, 1986) i.e. K=7dB and

$$\delta_{pIO} - \Delta_{pI} > 7 \text{ dB} \qquad \langle 69 \rangle$$

3.6.3 Calibration of the p-u Probe

The pressure microphone is calibrated with a standard pistonphone calibrator. It is coupled to the calibrator using an adapter which avoids damage to the ultrasound transducers. A correction factor of +1.2 dB @ 1kHz is necessary due to the adapter. The sensitivity on the 830 analyser is then adjusted via the front control panel. As previously mentioned, calibration of the sound velocity transducer is carried out by the manufacturer at regular intervals. A check can be made on the electronic circuitry via the TEST button on the probe handle. A reading of between 90 and 100 dB @ 500 Hz indicates the equipment is functioning correctly.

3.6.4 Measurement of Insertion Loss using Sound Intensity

It was mentioned above that the PUR composites were to be evaluated by their insertion loss measured using sound intensity. The insertion loss of the composite is obtained using the following method. First the radiated intensity from the steel panel is measured, to give a value I_1. With the composite in place a second intensity level measurement, I_2 is made. The insertion loss, IL, is the difference of these two measurements;

$$IL = I_1 - I_2 \qquad \langle 70 \rangle$$

The intensity can be measured either by sweeping the probe close to the surface, or by using a number of fixed positions to obtain an average. A swept measurement gives a single value spatial average

intensity. Obviously care needs to be taken to sweep the probe at a constant rate, and to cover the surface equally. This ensures that a good average of radiated sound intensity is obtained. Swept measurements were used in this work as they give a better approximation of the space integral, B&K (1986) and McGary (1986). ANSI S12.21 recommends that scan speeds should be preferably in the range $0.1ms^{-1}$ and $0.5ms^{-1}$ with a maximum of $3ms^{-1}$. The draft standard also recommends a surface to probe distance of between 0.1m and 0.2m, with a scan area of less than $1m^2$. All these requirements are easily achievable in practice.

3.6.5 Errors due to Background Noise in Insertion Loss Measurements

In the measurement of sound power of a radiating object the sound power is given by Gauss's equation;

$$W = \int_S I \, d\bar{S} \qquad \langle 71 \rangle$$

where I is the intensity normal to the surface area $d\bar{S}$

Because the integral is an average over the whole surface area any extraneous noise source will contribute an intensity component that is measured as negative when entering the volume and positive on exiting. Thus the net effect is zero. This is not the case in insertion loss measurements because the sound intensity is not measured over the surface of an enclosed volume. However if the external noise environment is stationary over the insertion loss measurements, it can be shown that the net contribution to the insertion

loss is nil. I.e. if the first intensity measurement in the presence of an external noise source is I_1' which is related to the actual intensity value I_1 by

$$I_1 = I_1' + I_e \qquad \langle 72 \rangle$$

where I_e is the intensity due to the extraneous stationary sound source, and if the intensity with the composite in place is given by;

$$I_2 = I_2' + I_e \qquad \langle 73 \rangle$$

then the insertion loss is given by;

$$IL = I_1' - I'_2 \qquad \langle 74 \rangle$$

which is of the form in Eqn. 43 above.

3.7 Insertion Loss Measurement Procedure

The measurement of insertion loss was carried out as described above, and is illustrated below in Plates 1 and 2.

The radiated intensity for both structure-borne and airborne generated noise was measured using scanned measurements at a distance of approximately 0.1m from the sample surface, and an average scan speed of $0.4ms^{-2}$. A fifteen second average was used. This value was chosen on the basis of radiated intensity being measured over a range of averaging times from 5 to 90 seconds. It was found that a

measurement time of 15 seconds gave both a repeatable intensity value and agreed with the 90 second averaged value to less than 0.5 dB. This agrees with the findings of Fothergill (1984). This averaging time from Section 3.6.1 gives a predicted error of $\epsilon(r)=0.054$ (0.23dB) for the 100Hz third octave band, and $\epsilon(r)=8.52\text{x}10^{-3}$ (0.04dB) for the 4kHz band.

Assuming the errors due to probe and equipment phase mismatch is ϵ_1=1.0dB, the error due to finite ultrasound beam length ϵ_2=0.5 (f<2339Hz), and that due to averaging time ϵ_3=0.5dB then the total error, ϵ_{tot}, is given by (Bockhoff *et al* 1988) as $\epsilon_{tot} = [\epsilon_1 + \epsilon_2 + \epsilon_3]^{\frac{1}{2}}$. This gives an error of 1.2dB in the intensity value. If the probe is to be used up to 4kHz the error increases to 1.7dB. With the quoted residual pressure-intensity of at least 30dB over the frequency range of interest, the dynamic capability index, L_d, is 23dB. If the field indicator F_2<10 dB then the measurement meets engineering grade (Fahy, 1989).

The measured data was stored onto floppy disc by the Norsonic analyser. This data was then transferred to a PC into ASCII format, and manipulated using a spreadsheet to obtain the system insertion loss.

The measurements were carried out in an environment with a stable temperature. Over 9 hours the temperature was found to be typically 19° ± 1°C. This would change the probe sensitivity by a factor of 0.9. However, for similar reasons to those for eliminating background noise the effect can be neglected i.e. over a short measurement time the change in temperature will be so small that it does not change the sensitivity by a quantifiable amount.

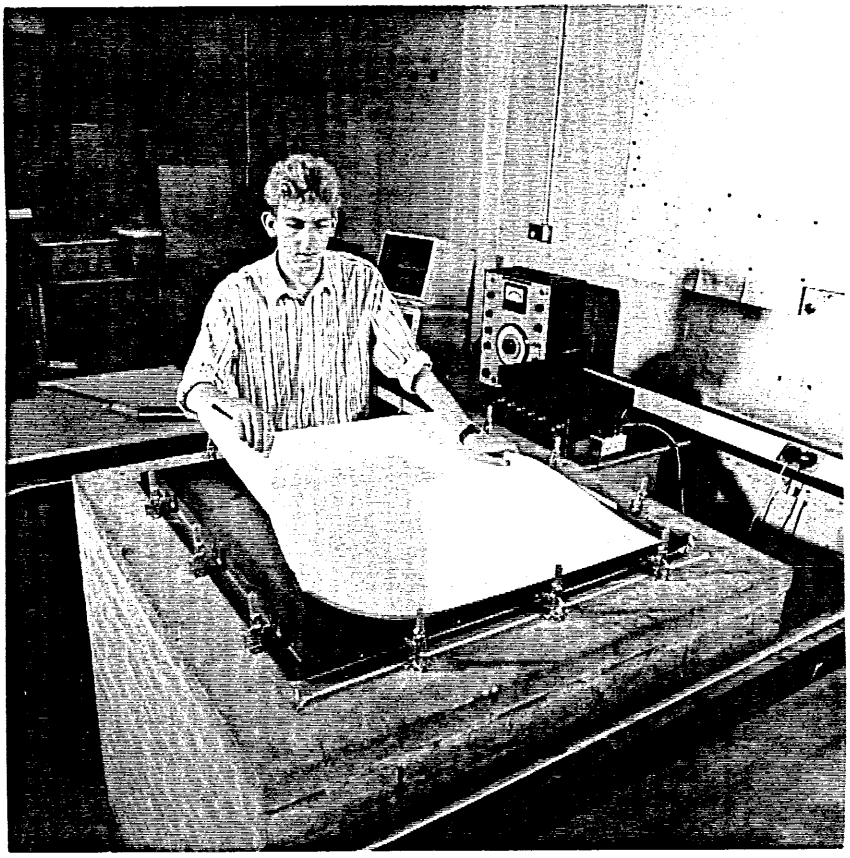

Plate 1 Installation of foam sample on experimental test facility

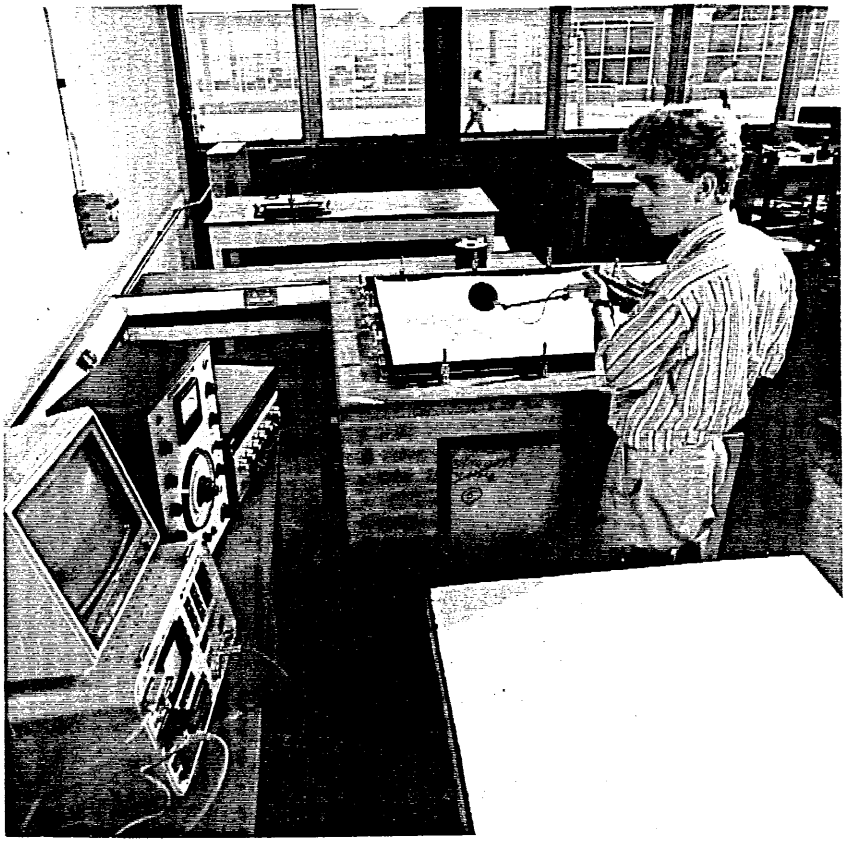

Plate 2 Measurement of radiated intensity

3.7.1 Insertion Loss for Airborne Noise

The noise source was from the internal loudspeaker array driven by random noise via an amplifier and spectrum equaliser as described above. The experimental set-up for the measurement of radiated airborne intensity is shown in Fig. 31. A typical spectrum of radiated intensity is shown in Fig. 32.

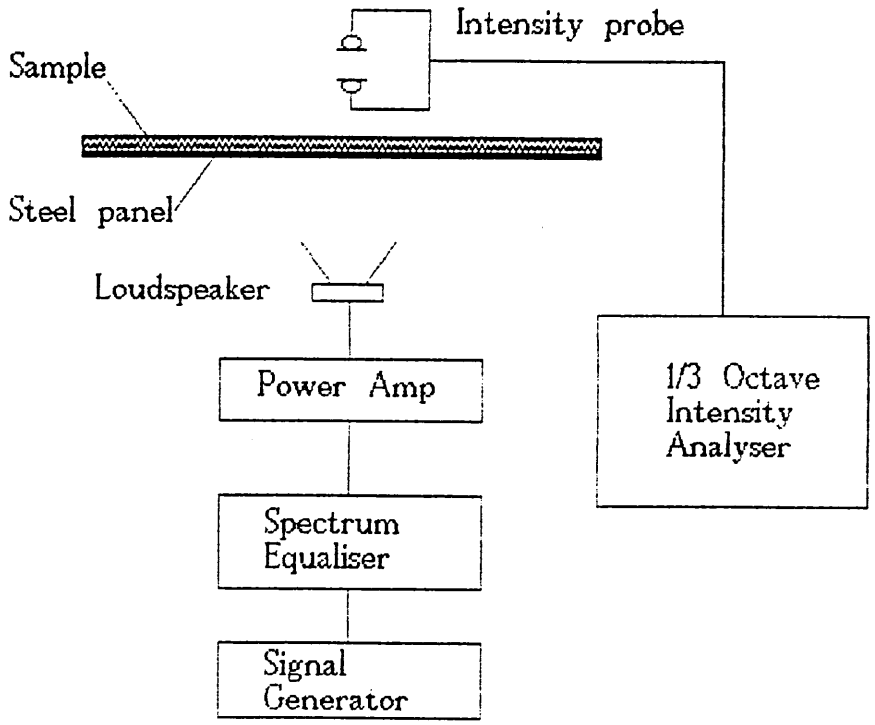

Fig. 31 Experimental configuration for insertion loss airborne generated radiated noise

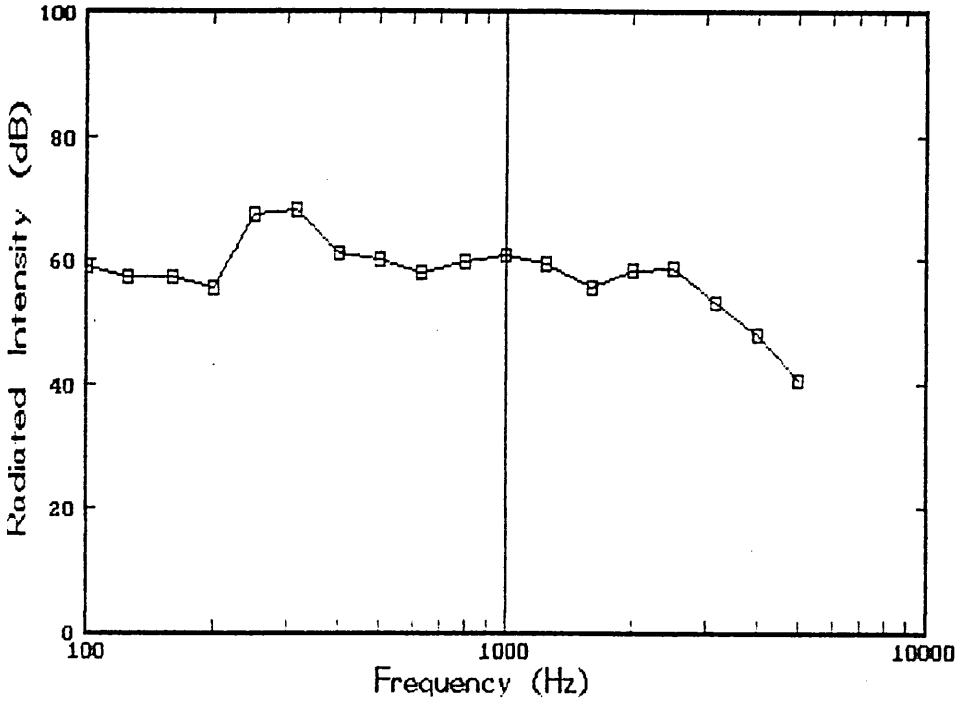

Fig. 32 Typical radiated intensity spectrum from steel panel

3.7.2 Insertion Loss for Structure Borne Noise

The noise source used was a broadband random noise generator supplied to the system via the electromagnetic shaker at a point 21.1cm from a corner along the diagonal (position No. 11). The radiated intensity was measured as described above. The experimental setup used is shown in Fig. 33. A typical spectrum of radiated intensity for structure-borne noise is shown in Fig. 34.

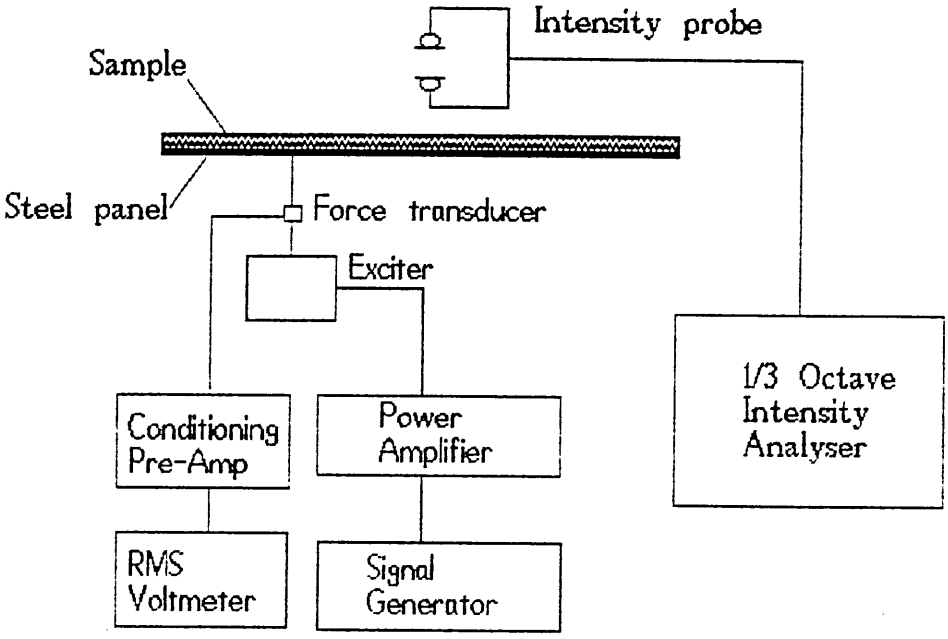

Fig. 33 Measurement of insertion loss for structure-borne noise

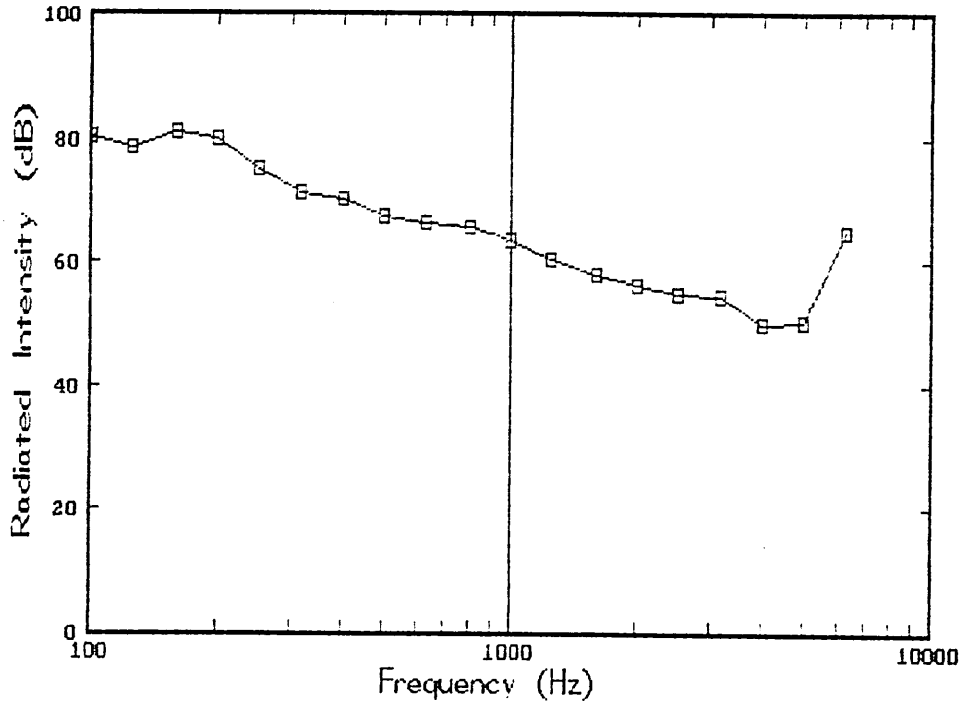

Fig. 34 Typical radiated intensity spectrum from steel panel

3.8 Panel Vibration and Panel Damping

Lack of published data on multilayered unbonded systems means that the investigation of panel vibration is important to the understanding of the mechanisms that affect panel vibration and damping. The theory in Chapter 2 showed that the sound radiated by a panel is proportional to the its velocity. Reducing panel vibration is therefore an important part of reducing radiated noise.

3.8.1 Panel Vibration

Panel vibration was investigated using the equipment in Fig. 35. A constant amplitude (force, displacement, velocity or acceleration) signal controlled the excitation. The compression/feedback loop was monitored using a transducer (force or accelerometer) at the excitation point. The signal generator was a LDS sine generator (type SCO200). The response to this excitation was measured at a number of positions on the plate surface by an accelerometer. The measurement positions were those of the grid in Fig. 30. The accelerometer signal, once conditioned, was measured using one channel of a Gould 1604 storage oscilloscope. A voltage proportional to frequency was applied to the second oscilloscope channel from the sine generator. With the oscilloscope set to 'roll' mode a frequency response similar to that obtained using a chart recorder could be obtained, but with greater accuracy. The frequency range used was from 100 to 1000Hz. Once the frequency sweep was completed, the data was transferred to a PC using the DADISP software across the IEEE interface

bus. This software allows easy manipulation of the data, whilst maintaining a signal image on screen. The data was thus calibrated before being exported as an ASCII format data file. This data was then imported into a spreadsheet programme for plotting.

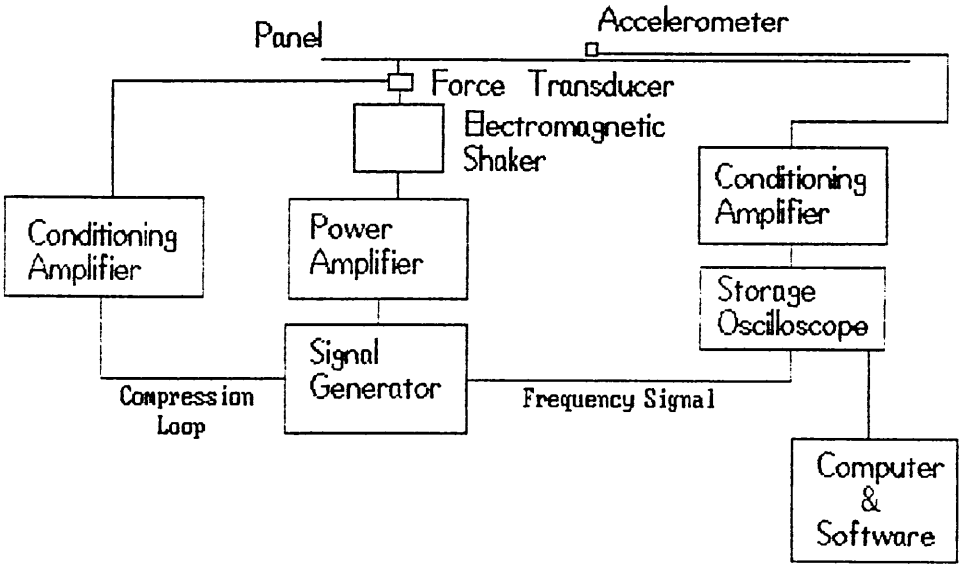

Fig. 35 Measurement of panel vibration

3.8.2 Panel Damping

A number of methods exist to measure the damping of panels, Plunkett (1959), Clarkson *et al* (1981), and Ranky *et al* (1984). The main ones are the measurement of the Q-factor of resonant modes, the decay of random excitation and decay of an impulsive excitation and power injection method (Bies *et al*, 1980). Measurement of the Q-factor requires modes which have a separation greater than a half bandwidth. The panel under test was found to possess a high number of modes, some of which were overlapping. This causes modal coupling. The Q-factor technique could thus not be applied with a high

level of accuracy. Measurement of the decay of random noise is dependent upon a high excitation level with a rapid decay rate. This was not available so the method was not adopted. The power injection method applies a signal to a structure. The input force, acceleration and respective phases are measured. The response to the input is measured at various positions. By using power balance equations (Lyon, 1984) the *in situ* loss factors can be obtained. However, the test method has two drawbacks. Firstly that the power balance equations rely on statistically independent modes. This might not be the case in practice. Secondly, the method is more complex to carry out due to the instrumentation required. As mentioned in Section 2.3 above the method gives loss factors which are consistently higher than those obtained with the reverberant decay method (Bies *et al* 1980).

The panel damping was thus obtained by measuring the reverberant decay of free vibrations, Plunkett (1959) and Ungar (1988). This is similar to the measurement of reverberation time, and absorption in rooms. The reverberation time of free vibrations was measured in third octaves. The excitation was provided by a short impulse using a 3½ oz hammer. The Norwegian Electronic 830 1/3 octave analyser, was used in transient mode to measure the decay. The analyser also carries out the evaluation of the reverberation time using internal software. The loss factor is then obtained from;

$$\eta = \frac{2.2}{f_n T_{60}} \qquad \langle 75 \rangle$$

where f_n = band centre frequency (Hz)
T_{60} = reverberation time (s)

3.9 Conclusions of Chapter 3

This chapter has discussed the test methods used to evaluate composites destined for use in vehicles as interior noise reduction treatments. Various commercial test facilities and techniques have been described. It was concluded that large scale facilities, such as a transmission suite did not meet the needs of this project, principally those of non-bonded horizontally mounted composites, low cost and ease of implementation in an industrial laboratory. For this reason a purpose designed test facility was constructed. The basic design concepts e.g. shape and size are similar to those of other industry based apparatus. The detailed design was adopted to comply with available laboratory accommodation. The design was massive to reduce flanking transmission.

The measurement of sound intensity and the associated errors has been described. The intensity method was applied to the measurement of insertion loss of composites, and the experimental procedure explained. The method eliminates both temperature effects and the influence of extraneous stationary noise sources, with an error of less than 1.5dB on the measured intensity values. Finally, the measurement of vibrational characteristics and system damping using the decay technique was discussed.

4 POLYURETHANE FOAM EXPERIMENTAL MATERIALS

4.1 Introduction

This chapter discusses the polyurethane foam materials used in the experimental work. A brief introduction to foam chemistry is given and the manufacturing process described. The foam characterisation techniques are described, and material properties are presented.

4.2 Foam Chemistry

A polyurethane foam is made by the reaction of a polyol and a polyisocyanate and a blowing agent. The reaction is described by Eqn. <76>.

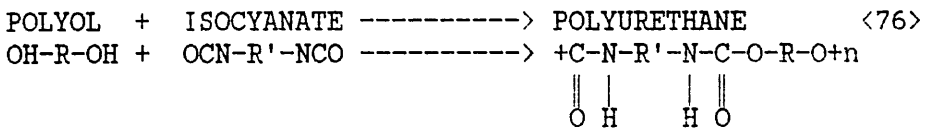

The blowing agent is vaporised by the exothermic reaction. The water reacts with the polyisocyanate to release carbon dioxide gas. This gas expands the foam and forms the cellular structure. Foam properties can be varied by changing the polyol/blowing agent/filler blend ratios. For instance the use of a filler such as Barium Sulphate ($BaSO_4$) increases the foam damping and density (Woods, 1987). The rigidity of a foam is determined by the cross-linking of the polymer chains. The greater the cross-linking the more rigid the foam.

Two isocyanates are used in commercial manufacture. The first is toluene diisocyanate (TDI) and the second is diphenylmethane-4-4-

diisocyanate (MDI). Both of these are hazardous to health. MDI is is preferred because it is less volatile, though TDI has superior processability.

The mechanical properties of thermoplastic polymers are very dependent upon temperature. The two extremes are the glassy state and the rubbery state. The glassy state is where the polymer is hard and brittle. This occurs at low temperatures. The rubbery state is where the polymer exhibits elastic or viscoelastic behaviour. This occurs at higher temperature. The transition from glassy to rubbery states occurs at the glass transition temperature T_g. In the region above T_g the polymer is highly viscoelastic and exhibits behaviour of elastic solid and viscous materials. The majority of the foams in this study are water-blown, wholly MDI based polyurethane foams.

4.3 Foam Manufacture

The experimental foams were made by the Technical Section of ICI Polyurethanes Ltd. using a Kraussmaffei 8/16 foaming machine. This is coupled to an L-shaped mixing head, and injected into the mould via a linear entry gate. The chemicals are mixed at a temperature of approximately 20°C and at a pressure of 180-200 atmospheres (1 atmosphere=1.013×10^5 Pa). The metal mould is a two part mould of external dimensions 1mx1m, and internal dimensions 0.87mx0.87m. Mould height depends upon the foam thickness required. The mould temperature is 40°C. The cure time of the PUR foam is short giving demould times of four to five minutes. Because the PUR acts as a bonding agent a wax dispersion releasing agent is used to coat the mould prior to the chemicals being injected.

4.4 Vehicle Under Carpet Systems

The manufacture of the complete vehicle carpet system is by a process similar to that described above. The mould is a metal two piece mould, into which is placed the heavy septum layer. This is made of filled EVA, rubber or polyurethane elastomer. The polyurethane foam components are poured directly onto the mass layer and the mould closed. Demould times are of the order of five minutes. By the use of suitable mould the system can be manufactured for a specific vehicle with different thickness profiles. A close fitting single unit carpet system is thus produced.

4.5 Foam Characterisation

The material properties of the foam isolating layer which are of importance are (a) the dynamic stiffness and damping and (b) air flow resistivity. The following sections detail the experimental procedures used to characterise the materials. Although dynamic thermal analysis and dynamic mechanical spectroscopy were not used in this study their descriptions are included because they are widely used in the chemical and automotive industries to characterise foam behaviour.

4.5.1 Dynamic Mechanical Properties using the BMW Test Method

The BMW test method was used to obtain mechanical properties (foam modulus and loss factor) for the experimental materials. Other methods exist for material characterisation e.g. dynamic mechanical

thermal analysis (DMTA) and dynamic mechanical spectroscopy (DMS), but were not used in this work. This is because their frequency range of operation is restricted to low frequencies (f<80Hz), and are outside the range of interest (f>100Hz).

The BMW test is a resonance method of obtaining values for dynamic stiffness and damping, based upon a BMW standard test method (BMW Informationspause, 1984). The technique produces a value of stiffness and damping for one frequency. This frequency is dependent upon the stiffness of the foam, and the area mass of the plate. The system is excited via signal generator providing a constant acceleration excitation on the base plate. The signal is a swept sinusoid. The acceleration response of the upper surface is plotted on a chart recorder against frequency. From this response curve the resonance frequency, f_0, and the 3dB down frequencies, f_1 and f_2, are obtained. The frequency dependence of the loss factor and storage modulus can be investigated by varying the surface mass, m_1.

The loss factor of the system is given by;

$$\eta = \frac{f_2 - f_1}{f_0} = \frac{1}{Q} \qquad \langle 77 \rangle$$

where Q is the quality factor.

The in phase storage modulus, E', is obtained from;

$$E' = \frac{4\pi^2 f_0^2 m_{tot} h}{A} \qquad \text{(Pa)} \qquad \langle 78 \rangle$$

where m_{tot} is the combined mass of plate, accelerometer and foam
A is the surface area
h is the sample thickness

4.5.2 Air Flow Resistivity

Air flow resistance measures the resistance that a material offers to the flow of air through it. The equipment used to measure air flow resistance is described by Collier (1985). The flow resistance was measured for the foams with and without the surface skin. It was this second value which was used in the theoretical modelling, as this value represents the bulk property of the foam.

4.5.3 Cellular Structure

Cellular structure can be examined using scanning electron microscopy (SEM) techniques. A beam of electrons is scanned across the surface of the sample. The quantity of reflected electrons depend upon the surface morphology, and it is from these that the image is built up. Cell size can thus be obtained and the open/closed cell ratios evaluated. In Plates 3 to 6 below, SEM pictures are shown for a number of the PUR experimental foams. All are for magnifications of approximately 65. Plate 3 is for foam 1, taken at an edge. It demonstrates clearly a skin that occurs due to the moulding process. Although only thin it can alter the flow resisistance measurements significantly. The extent to which the skin occurs varies from foam to foam. This is illustrated in Plate 4 for foam 10. it can be seen that there is no skin visible after demould. Plates 5 and 6 are SEM pictures for foams 3 and 22 respectively. The plates illustrate the variation in cell size that can occur in the PUR foams. Foam 22 in Plate 6 has the smallest windows in the cells and foam 1 in Plate 3 the smallest. The flow resistivity values in Tables 6 to 8 show that

foam 22 has a higher flow resistivity than foam 1.

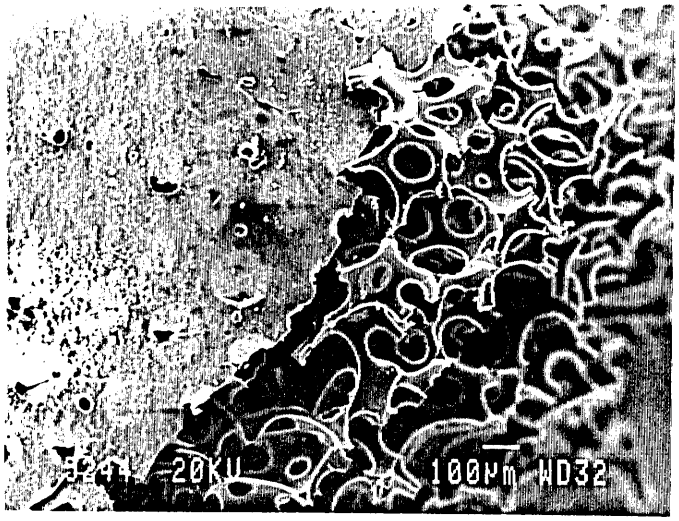

Plate 3 SEM micrograph of foam 6 at corner of sample

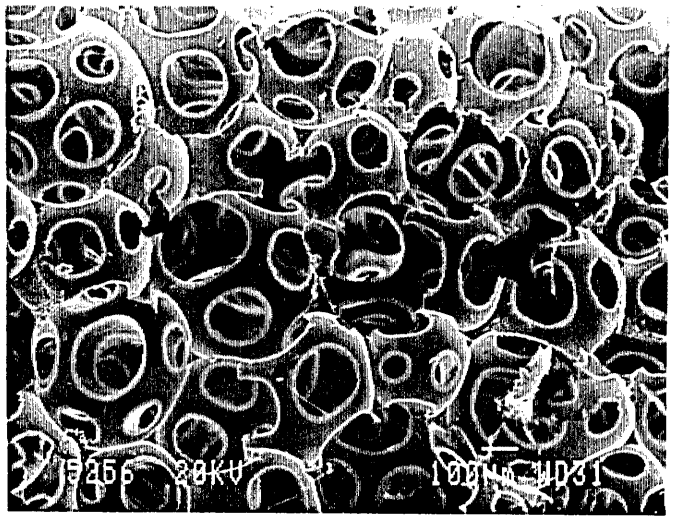

Plate 4 SEM micrograph of foam 10 (with skin)

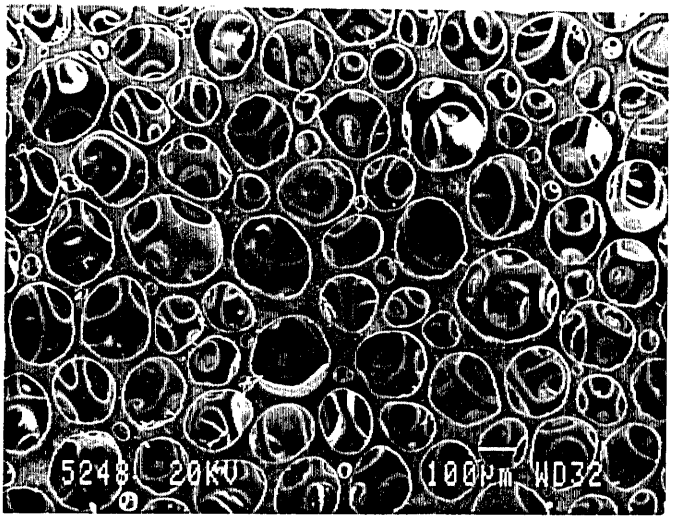

Plate 5 SEM micrograph of foam 3 (without skin)

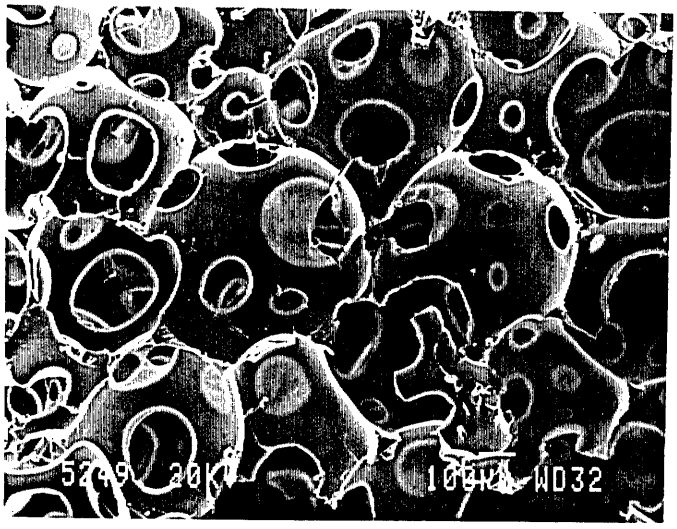

Plate 6 SEM micrograph of foam 22 (no skin)

4.6 Material Properties

A series of twenty-nine polyurethane foams were provided by ICI Ltd. These foams and a felt underlay, typical of that used in under-carpet treatments, were used in the experimental work. The materials were characterised using the above methods. The material properties are presented in Tables 6 to 8 below. (These are also reproduced inside the back cover for reference purposes). The resonance frequencies in the tables are for the three surface masses used in the BMW test. Two flow resistance values are given. The foams were supplied with a thin surface skin, due to the manufacturing process. As the interest is in the bulk properties of the foam core, the flow resistance was also measured without the surface skin. The first value, designated 1, is for the foam with the surface skin in place. The second value, designated 2, is for the foam without the surface skin. The second value is the one used for theoretical predictions. Foams 24 to 28 were slabstock foam bought through a commercial supplier and did not possess an integral skin.

Foam	Surface Density	Density	Thick-ness	Storage Modulus	Loss Factor	Freq	Flow Resistivity	
	kgm^{-2}	kgm^{-3}	mm	$x10^5Pa$		Hz	$kNsm^{-4}$	
							1	2
1	1.65	84.8	19.5	0.63 0.47 0.32	0.16 0.16 0.24	122 94 64	31	50
2	0.93	86.0	10.8	0.36 0.36 0.35	0.18 0.15 0.21	123 103 76	85	107
3	1.52	77.9	19.5	1.25 1.24 0.44	0.42 0.39 0.43	155 130 58	39	28
4	1.73	88.5	19.5	1.17 1.17 1.08	0.41 0.35 0.44	153 125 90	40	36
5	1.67	85.6	19.5	0.47 0.41 0.33	0.46 0.43 0.44	95 75 50	29	26
6	1.58	80.8	19.5	4.21 3.72 4.25	0.25 0.27 0.31	285 225 180	84	74
7	1.56	80.2	19.5	1.87 1.88 1.59	0.40 0.38 0.37	190 160 110	56	44
8	0.89	89.6	9.9	2.35 1.87 1.57	0.40 0.43 0.44	315 235 160	215	56
9	2.00	102.7	19.5	1.27 1.07 0.89	0.42 0.48 0.44	155 120 82	43	47
10	2.01	103.1	19.5	0.89 0.90 0.69	0.45 0.41 0.47	130 110 72	43	44
11	1.24	63.6	19.5	2.36 2.48 2.55	0.30 0.35 0.32	215 185 140	312	122

Table 6 Material properties

Foam	Surface Density	Density	Thick-ness	Storage Modulus	Loss Factor	Freq	Flow Resistivity	
	kgm^{-2}	kgm^{-3}	mm	$x10^5Pa$		Hz	$kNsm^{-4}$	
							1	2
12	1.26	64.6	19.5	0.84 0.63 0.46	0.44 0.62 0.50	128 93 60	20	182
13	1.99	101.8	19.5	0.82 0.63 0.61	0.22 0.28 0.31	125 92 68	403	378
14	1.65	85.7	19.2	1.00 0.99 1.00	0.18 0.11 0.14	137 115 87	137	61
15	2.00	101.2	19.8	1.90 1.80 1.60	0.14 0.17 0.11	185 150 108	268	115
16	2.45	83.2	29.4	0.89 0.80 0.83	0.16 0.12 0.14	102 82 63	99	63
17	0.88	87.7	10.0	1.10 1.40 1.20	0.23 0.21 0.19	200 192 135	272	88
18	1.32	69.2	19.0	0.87 0.92 1.10	0.15 0.18 0.14	130 112 90	348	59
19	1.66	86.0	19.3	0.90 0.95 0.90	0.49 0.42 0.51	130 112 82	113	50
20	1.60	84.8	18.9	0.88 0.67 0.61	0.50 0.56 0.47	130 95 68	78	53
21	1.60	84.8	18.9	0.21 0.17 0.21	0.22 0.21 0.20	64 48 40	31	29

Table 7 Material properties

Foam	Surface Density	Density	Thick-ness	Storage Modulus	Loss Factor	Freq	Flow Resistivity	
	kgm^{-2}	kgm^{-3}	mm	$x10^5Pa$		Hz	$kNsm^{-4}$	
							1	2
22	1.65	103.3	19.4	0.38 0.33 0.21	0.92 0.80 0.76	85 67 40	35	35
23	1.31	69.5	18.9	0.45 0.38 0.31	0.41 0.41 0.43	94 72 49	235	77
FELT	1.41	76.2	18.5	0.04 0.05 0.06	0.24 0.35 0.53	29 26 22	17	
24	0.40	29.6	14.0	2.20	0.18	200		1.5
25	0.78	31.2	25.0	1.90	0.15	200		4.5
26	1.12	29.5	38.0	1.90	0.14	200		10.5
27	2.49	85.9	29.0	1.50	0.21	200		27
28	2.44	84.1	29.0	2.50	0.65	200		110

Table 8 Material properties

4.7 Conclusions of Chapter 4

This chapter introduced the chemistry and manufacture of polyurethane foams. Methods used for material characterisation were described. Scanning electron micrographs for a number of the experimental foams were shown. These demonstrated the skin that forms on foams due to the manufacturing process. In general the flow resistivity of the test pieces was reduced by the removal of the surface layers. With the surface layer intact the range was 20 to 403 $kNsm^{-4}$. The flow resistivity of the foam samples was 1.5 to 378 $kNsm^{-4}$ without the surface layers. The felt had a value of 17 $kNsm^{-4}$. It is seen that the elastic modulus ranged from 0.2 to 4.2 $x10^5$ Pa for the

foams and 0.04 to 0.06 $x10^5$ Pa for the felt. These compare with an air modulus of approximately 1.1 $x10^5$ Pa. It can be seen that this value is at the centre of the measured modulus range for the foams. Loss factors for the foams varied from 0.1 to 0.9 and the felt had a value of 0.2 to 0.5. Chapter 5 uses the measured material properties in the prediction models developed in Chapter 2 to predict the insertion loss of composite systems. The test samples allowed the systematic study of the influence of material parameters upon composite design when other properties remained approximately constant.

5 RESULTS AND ANALYSIS

5.1 Introduction

This chapter presents the experimental results for the test materials described in Chapter 4. The influence of the foam materials on panel vibration is reported. The effect of the foam on system (composite) damping is measured. Results for the effective system loss factor are obtained using the decay method described in Chapter 3. Measured data are compared with those predicted by the theory of Oberst (1954) for bonded treatments.

Results are presented for the system insertion loss when the composite is subjected to point excited structure-borne noise. These are measured using the test facility and intensity method described in Chapter 3. The measured data are compared with predictions from the insertion loss model developed in Chapter 2, using the material property data in Chapter 4. (The material property data can also be found inside the rear cover of the thesis for reference purposes).

Data is also presented for the system insertion loss when the composite is subjected to excitation by airborne noise. This is also measured using the test facility and intensity technique. The measured insertion loss data are compared with those predicted by the airborne noise model developed in Chapter 2, using the material data from Chapter 4.

5.2 Panel Dynamics

Results are presented for the vibrational response of a clamped (C-C-C-C) mild steel panel. The effect of foam layers upon system response an system damping is also examined. Lack of published data on multilayered unbonded systems means that these results are important to the understanding of the mechanisms that affect panel vibration and damping. This is important because the sound radiated by a panel is proportional to the its velocity (see Chapter 2). Reducing panel vibration is therefore an important part of reducing radiated noise.

5.2.1 Panel Modal Response

The panel response was examined using the method described in Chapter 3 above. A constant acceleration excitation level of 5g was used at position 11. The response accelerometer was situated in the centre of the panel (position No.41). Response curves are presented for the steel panel, panel with foam, and panel with foam and septum layer. This enables the influence of thickness, material damping and surface density to be examined. Response curves are only presented for the frequency range 10 to 1000Hz. Above this frequency the compression loop was unable to maintain a constant acceleration at the shaker position.

The panel response in Figs. 36 and 37 show that the vibration consists of a large number of resonances. There are more resonances than predicted by the theory in Chapter 2, although in the frequency range 100 to 1000Hz there is good agreement between the predicted mode frequencies and the major resonances e.g. mode (4,3) with a

predicted value of 250Hz and a measured value of 243Hz. These are labelled on the graph. The extra modes observed are attributed to the influence of shaker position, the cavity internal modes and the boundary conditions.

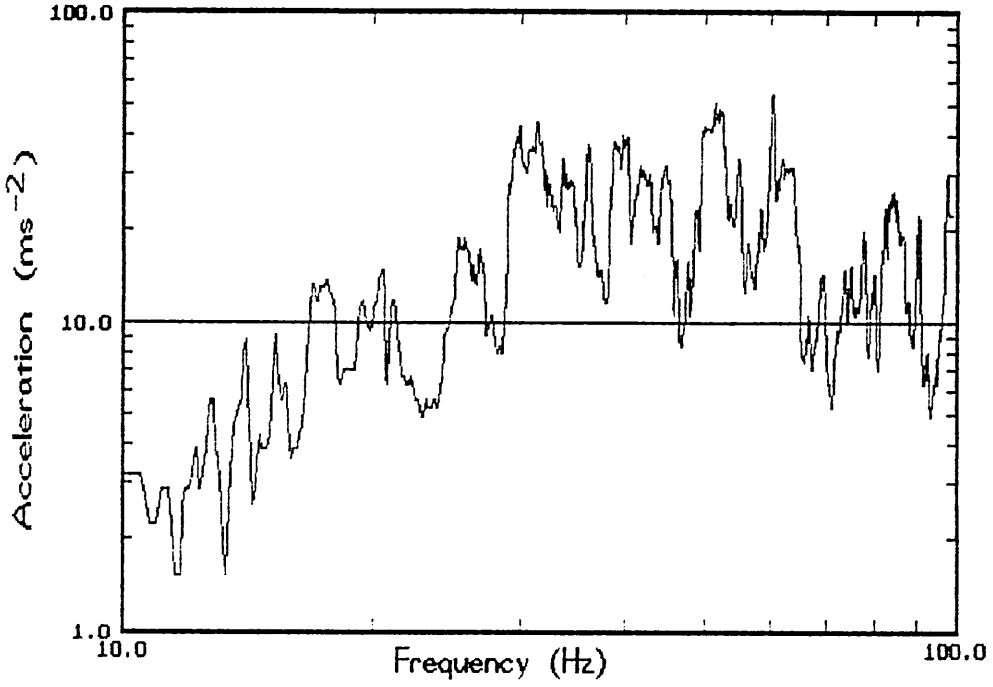

Fig. 36 Response of 1mm clamped steel panel (10-100Hz)

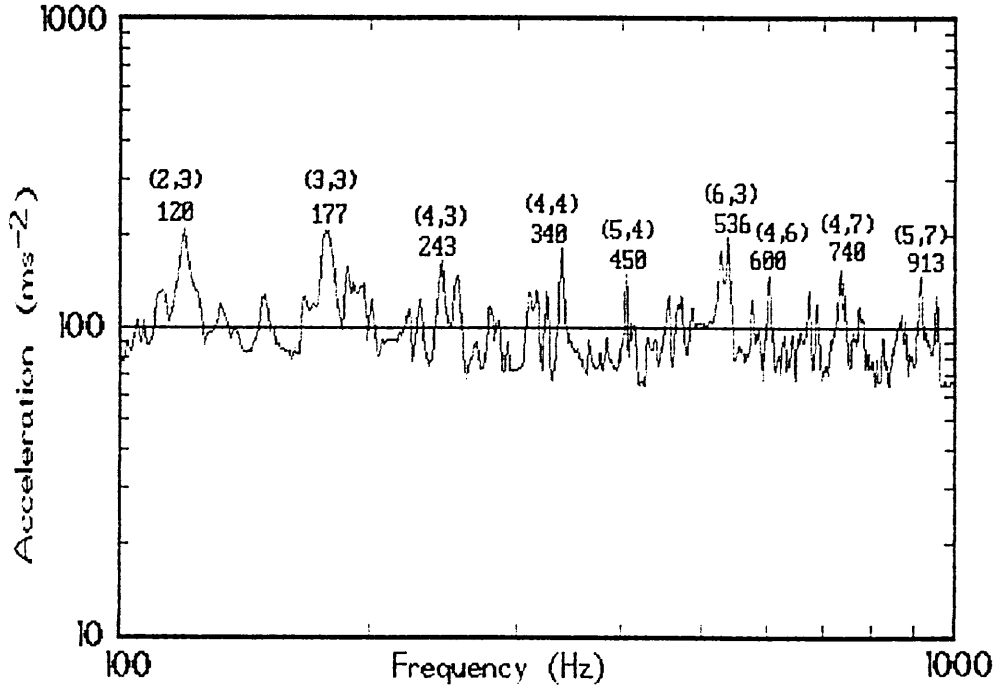

Fig. 37 Response of 1mm clamped steel panel (100-1000Hz)

The complex panel response does not enable modal loss factors to be obtained from mode bandwidth measurements (i.e. using the Q-factor). This is because the peaks are not discrete, merging into one another. This modal coupling would invalidate the values, as mentioned in Chapter 3. Above 1 kHz the modal density of the panel was too high to measure the response accurately.

It was mentioned above that reduction in system vibration is important in the reduction of radiated noise. Figure 38 shows the response for the steel panel and panel with foams 24, 25and 26 with area densities 0.40, 0.78 and 1.12 kgm^{-2} respectively and approximately the same modulus and loss factor (see Table 8). The vertical scales are acceleration in dB. The addition of the foams to the panel has the effect of reducing the amplitude of the resonances e.g. by about 8-10dB for the (2,3) mode. Thus the foam layer damps the panel vibration. However, comparing the response of the different foams shows that surface density has little effect on the panel vibration.

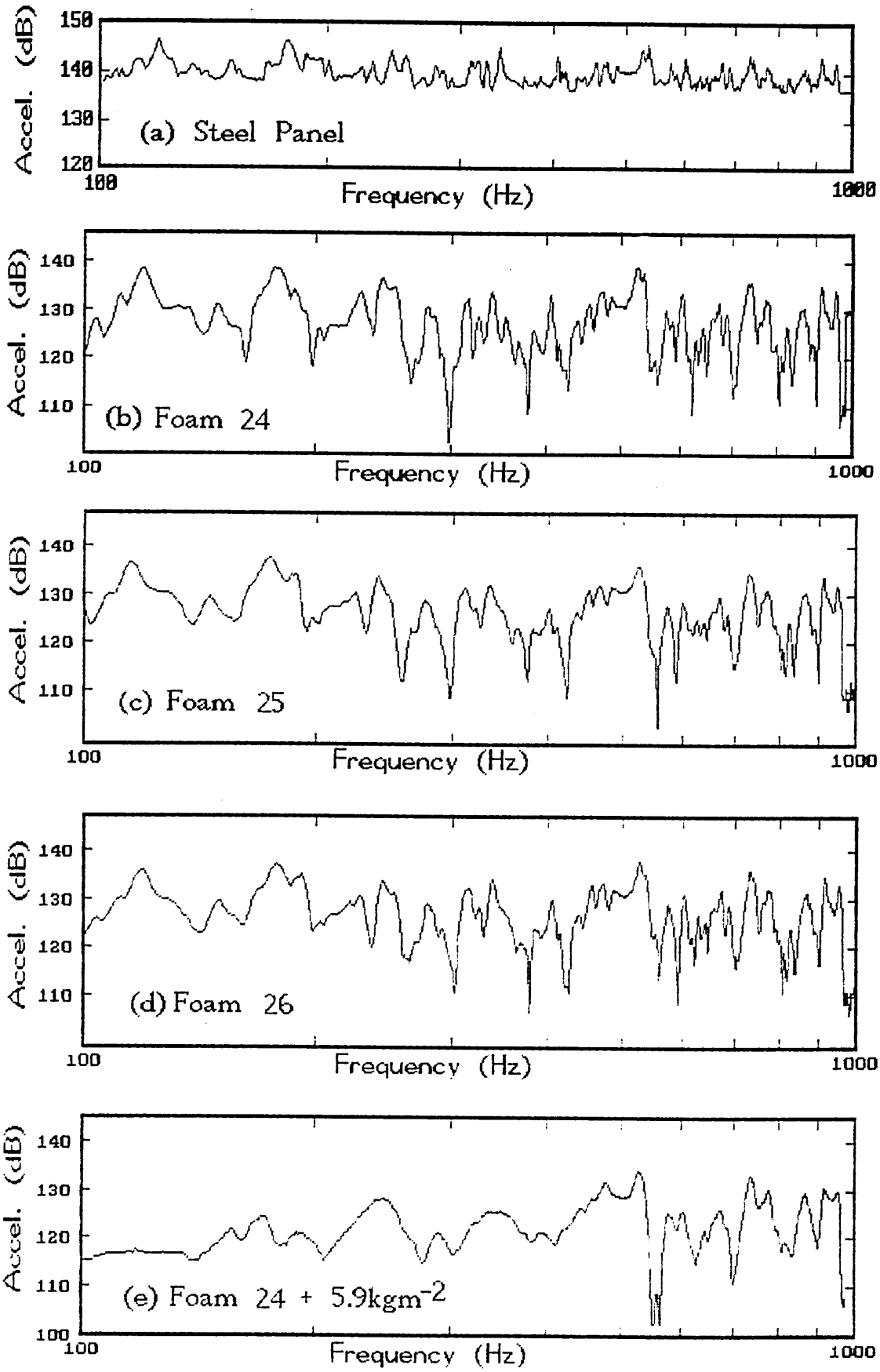

Fig. 38 Response of (a) steel panel and (b) foam 24 (c) foam 25 (d) foam 26 (e) foam 24 + 5.9 kgm^{-2} (dB re. 1e-5 ms^{-2})

This is probably because the additional mass is small compared with the panel surface density. The addition of foam 24 represents an increase of 5% in panel surface mass and an increase of 14.5% for foam 26. Indeed, this is demonstrated in practice; e.g. Fig. 38 (e) which is for foam 24 with a septum mass of 5.9 kgm^{-2}. The addition of the foam and septum increases the system surface mass from 7.7 to 14.0 kgm^{-2}; an increase in surface mass of 82%.

The addition of the septum layer smooths the panel vibration response, by reducing resonance amplitudes and broadening the peaks. Modal damping is thus increased. A marked reduction in the low frequency response (f<250Hz) is observed. A number of mechanisms are thought to be responsible for the reduction in response. Firstly, the reverberant vibration field is affected more than the direct field by the additional mass. Secondly, the septum mass increases the duration of the contact between the foam and panel. Thus, when the panel deflects and the foam core undergoes shear, energy is lost. The energy losses would be due to a combination of constrained layer (shear) damping and frictional damping.

The influence of material damping can be explored by examining the response curves for foams 25, 27, and 28 in Fig. 39. These foams have the same thickness, approximately the same dynamic modulus (150-250kPa) and loss factors of 0.15, 0.21, 0.65 respectively. It is seen that the modal response is reduced and hence the modal damping is enhanced. However in some limited frequency ranges the response with the higher damped foam is largely greater than that of the lower damping foam even though the overall response is reduced. This is attributed to the fact that the foams influence the mode frequencies.

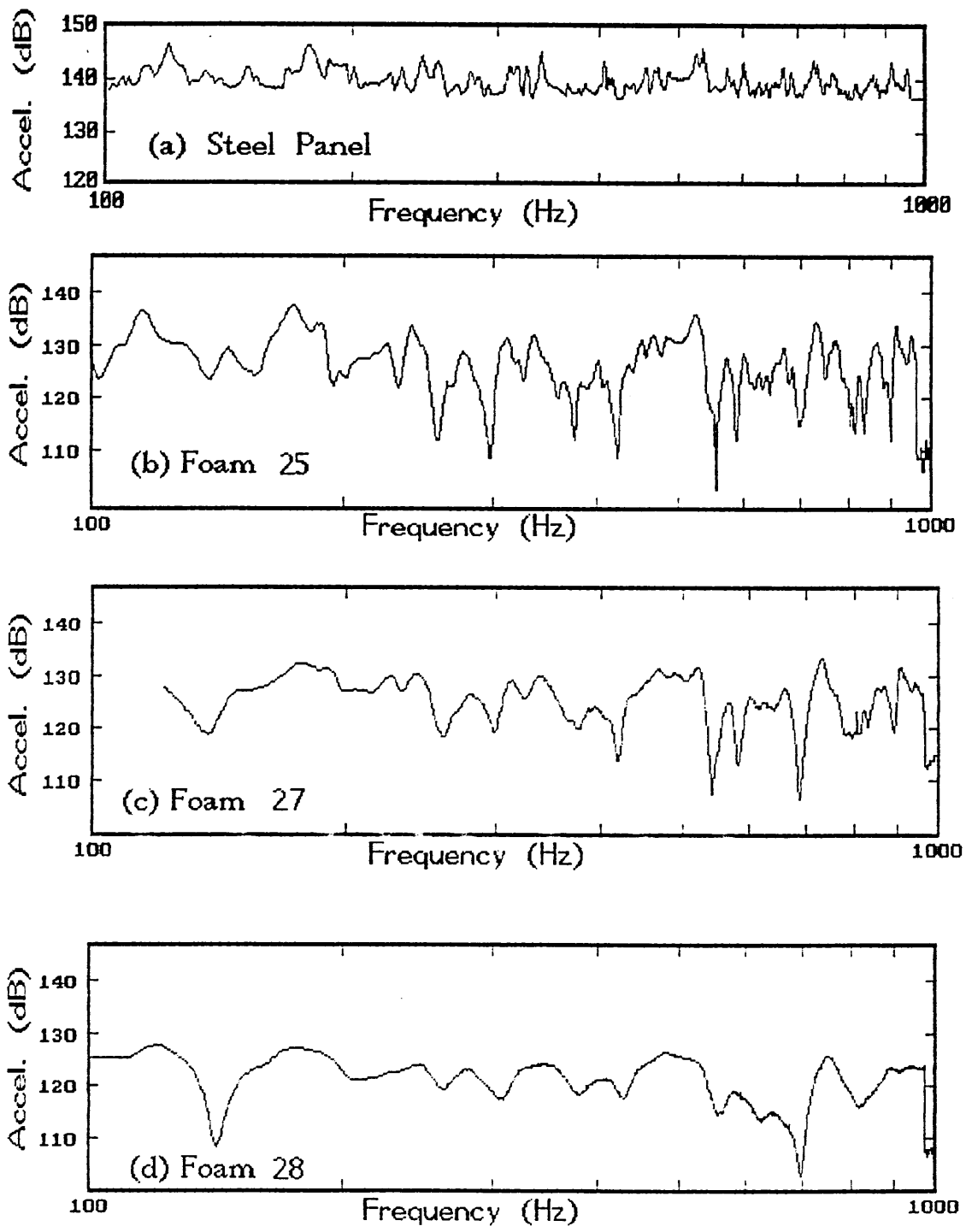

Fig. 39 Constant acceleration response of (a) steel panel with (b) foam 25 (c) foam 27 and (d) foam 28 (dB re. 1e-5 ms^{-2})

5.2.2 Effective Panel Loss Factor

The previous section demonstrated that the addition of a foam or foam + septum influences the panel vibration. Over most of the frequency range investigated the vibration was reduced. In order to quantify this qualitative observation the effective panel loss factor was measured.

Loss factors were obtained using the reverberant decay method, described in Chapter 3. The damping was obtained for the panel + foam and panel + foam +septum. The results are presented in detail in Appendix E.

The BMW test in Chapter 4 provided data for the foam loss factor over a limited frequency range up to approximately 200Hz. These foam loss factors are used in the theory of Oberst (1954) from Chapter 2 to calculate the system effective loss factors. This section compares measured and predicted loss factors for the system.

The problem with obtaining loss factor measurements using the decay method is the excitation of the panel. A sharp impulse is necessary to maximise the number of panel modes excited. This is difficult when the septum is in place. If the resulting decay curves are not exponential the loss factors cannot be calculated. Consequently, loss values for some third octave frequencies do not appear on some of the graphs e.g. below 250Hz for foam 11. This is due to measurement uncertainty.

The effective loss factor for the clamped steel panel is shown in Fig. 40. This shows a trend of decreasing loss factor with increas-

ing frequency. Measured values were 0.008 at 100Hz and 0.0003 in the 6300Hz 1/3 octave band. These values lie between those of Plunt and Tarnoczy in Fig. 4.

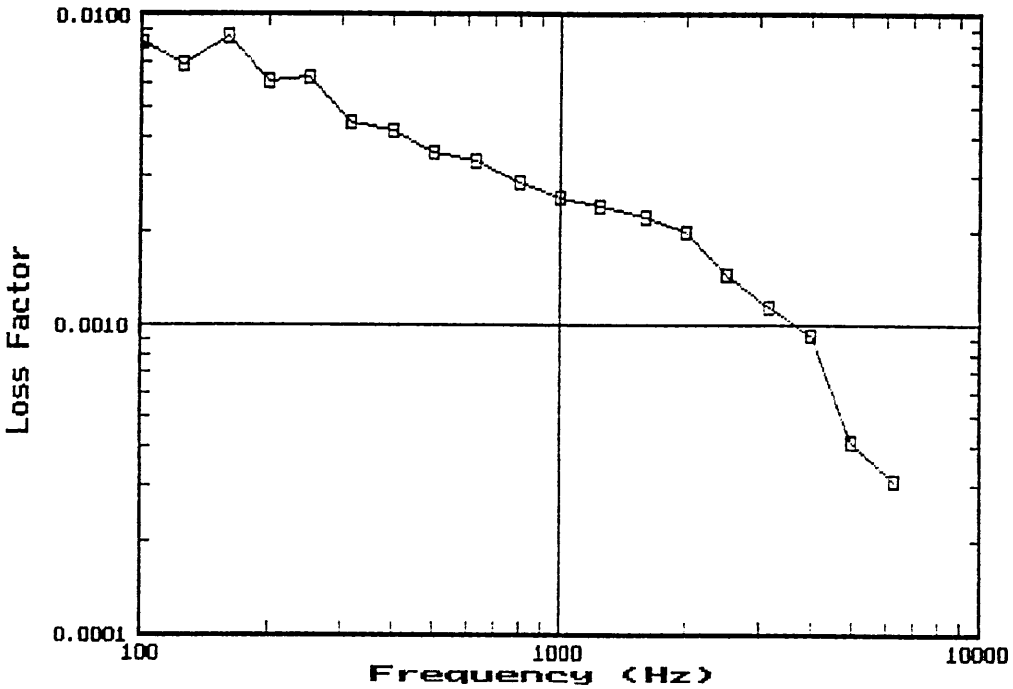

Fig. 40 *In Situ* loss factor for 1mm steel panel

The addition of a foam layer to the steel panel introduces extra damping to the system. Tarnoczy reported an increasing loss factor with frequency, when a 5mm bonded damping layer was applied, whereas Plunt (1991) reported a decreasing loss factor with increasing frequency for carpet systems (see Section 2.4). The vibration responses given in the previous section showed that the vibration was reduced by the addition of a foam layer, and reduced further with an added septum. An increase in system damping with added foam and foam + septum should therefore be expected.

Measured data for the unbonded PUR foams, in Figures 41 to 43, show that the loss factor decreases with increasing frequency and that the system loss factor is increased by the addition of a foam as expected from Section 5.2.1. This improvement continues up to approximately 2kHz. Above this frequency the measured system loss factor is similar to the panel alone. The addition of the foam layer also has the effect of smoothing the damping decay curve. On comparison of system loss factors, with different foams, it is found that the influence of foam loss factor is small, the main differences being noticeable at low frequencies.

Chapter 2 presented the mechanism of extensional damping. Equations were given for the prediction of the loss factor of a panel with an attached extensional layer according to Oberst (1954). Using equation <9> in Chapter 2, with values for material modulus and loss factor from Tables 6 to 8 system loss factors were predicted. The theory assumes that the foam and panel were bonded. It can be seen in Figs. 41 to 43, comparing the predicted loss factors with measured values, that the predictions are consistently lower than the measured values.

Only a limited number of theoretical damping predictions could be made, because the modulus and loss factor information of the foams was only known for a few frequency values (usually three). Ideally characterisation of the foams is needed over the whole range of acoustic frequencies in order to obtain a more complete understanding of system damping. Unfortunately, the BMW test which was used to obtain the material damping and modulus operates over a limited range. This is due to the resonance frequency of the test being

inversely proportional to surface density. Thus a septum with a low area density is required to obtain material values at high frequencies. However there comes a point where the mass of the foam contributes more than the surface density, and an upper limiting frequency is reached. Thus predicted values for system damping can only be obtained over a limited frequency range.

The poor agreement between the predicted and measured loss factors is perhaps not unexpected. The theory was derived for panels with bonded treatments. It was expected that for an unbonded damping treatment that there would be energy losses due to the frictional forces at the panel/foam interface (i.e. slip-stick damping). Indeed, Harris (1957) suggested that using an unbonded treatment would increase the energy losses of a vibrating panel due to frictional losses. No data was presented to support this argument. The fact that the damping was greater than that due to extensional damping alone indicates that the increase in system damping might well be attributable to frictional damping.

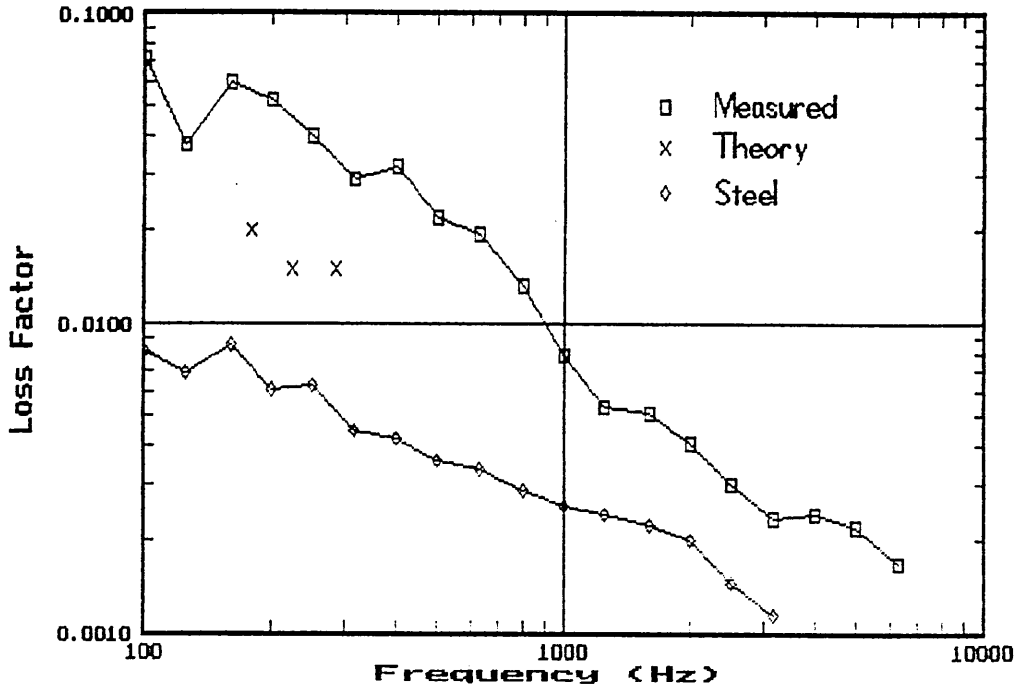

Fig. 41 Comparison of theoretical and measured values of loss factors for foam 6

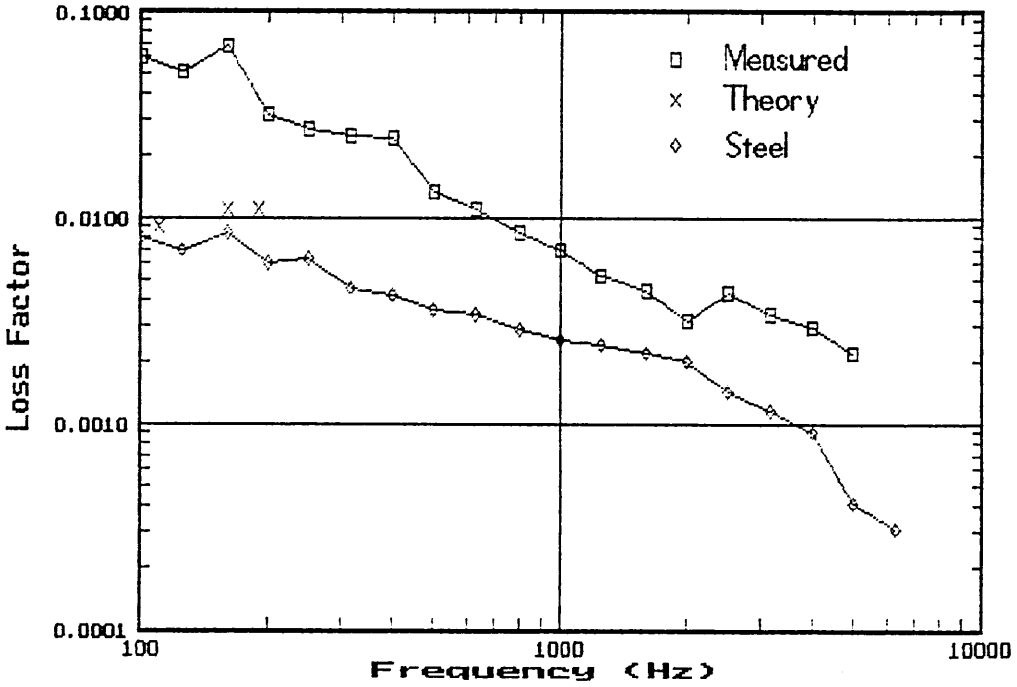

Fig. 42 Comparison of theoretical and measured values of loss factors for foam 7

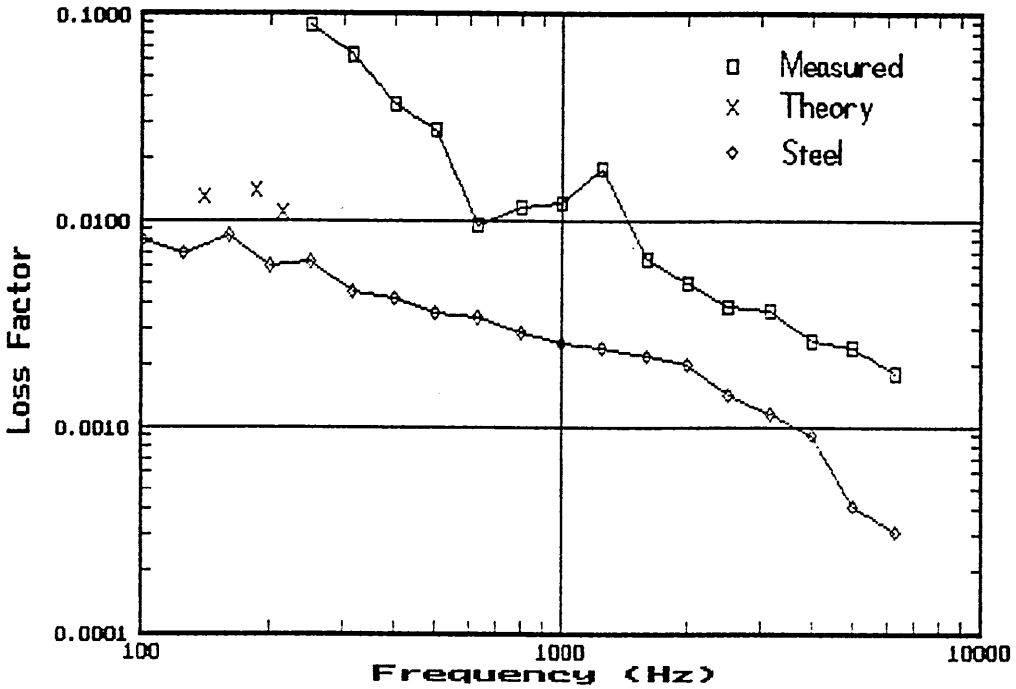

Fig. 43 Comparison of theoretical and measured values of loss factors for foam 11

The addition of a septum layer has a small effect upon the measured system loss factor, contrary to the modal damping observed above. This is shown below, in Figs. 44 and 45, for foam 22 and 3. With increasing septa surface density the system loss factor is increased. The loss factor for the steel panel is also shown. The measured damping for the foam and septum is higher than the panel alone.

Predictions for loss factor of the composite (panel + foam + septum) using Oberst's constrained damping equations were not made. This was, as mentioned, because of experimental difficulties in measuring loss factors. This is principally a problem at low frequencies where the material properties were known.

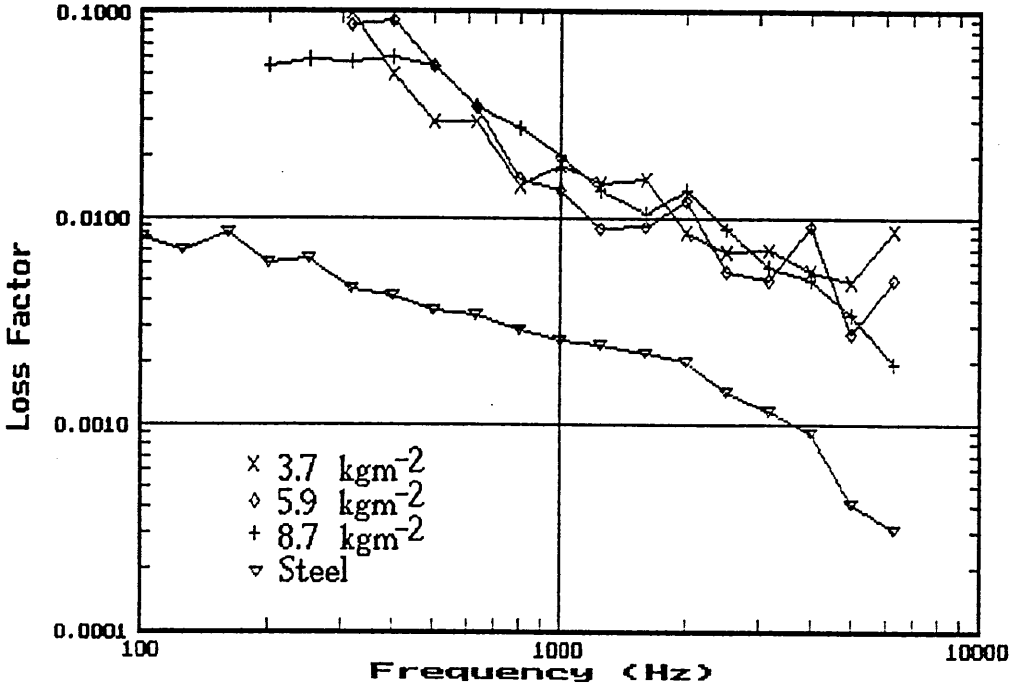

Fig. 44 Influence of septum surface density on *in situ* system loss factor for foam 22

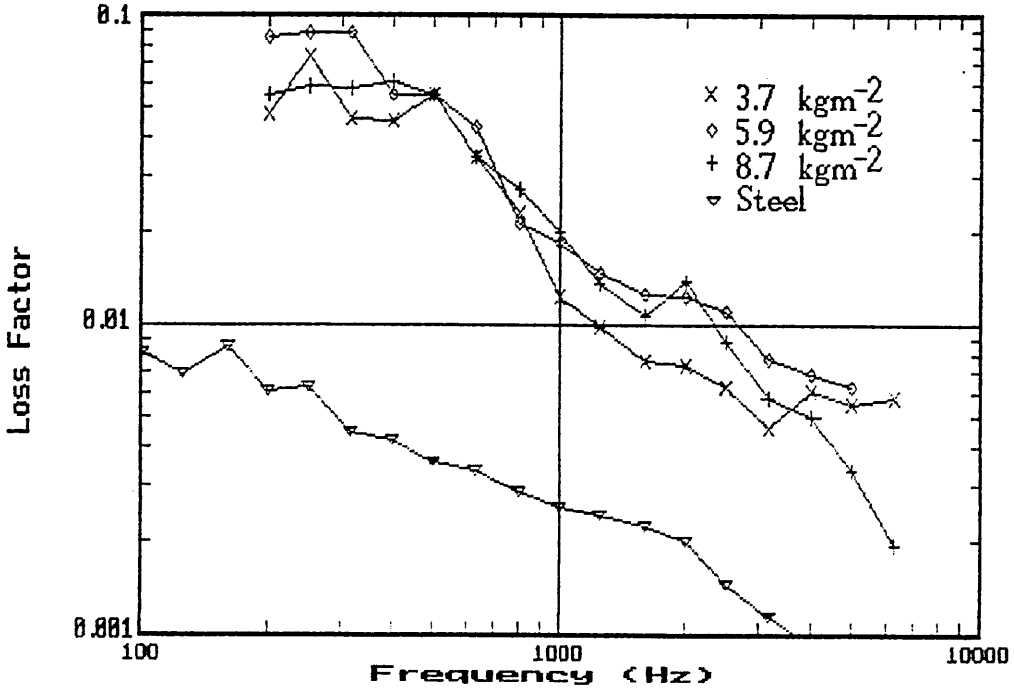

Fig. 45 Influence of septum surface density on *in situ* system loss factor for foam 3

5.3 Vibration Insertion Loss of Composites

The results presented in this section were obtained using structure-borne excitation and the intensity method as described in Chapter 3. Unless otherwise stated the septum had a surface density of 5.9 kgm^{-2}. A full set of vibration insertion loss data for the experimental foams is presented in Appendix **C**.

5.3.1 Measurement Reproducibility

To investigate the repeatability of measurements for structure-borne insertion loss a number of the measurements were repeated. The results for foams 4, 5 and 6 are shown in Figs. 46 and 47. Figs. 48 and 49 are for the same foams with a 3.7kgm^{-2} septum. The time interval between the measurements was five months. It can be seen from the graphs that there is a problem with measurement reproducibility. Between separate runs, on different days it was found that there was variation between the measured data. This was due to the coupling between the exciter shaft and panel. A loose rubber coupling was used to minimise the effect of the shaker on the panel response, but this would appear to have been insufficient. The results thus emphasise the need for a better coupling method to be made; one that minimises the wear on the rubber coupling. However, despite the differences between sets of data, the trends observed here were consistent. This establishes the validity of the test for qualitative purposes, though casts doubt on the accuracy of the quantitative values obtained.

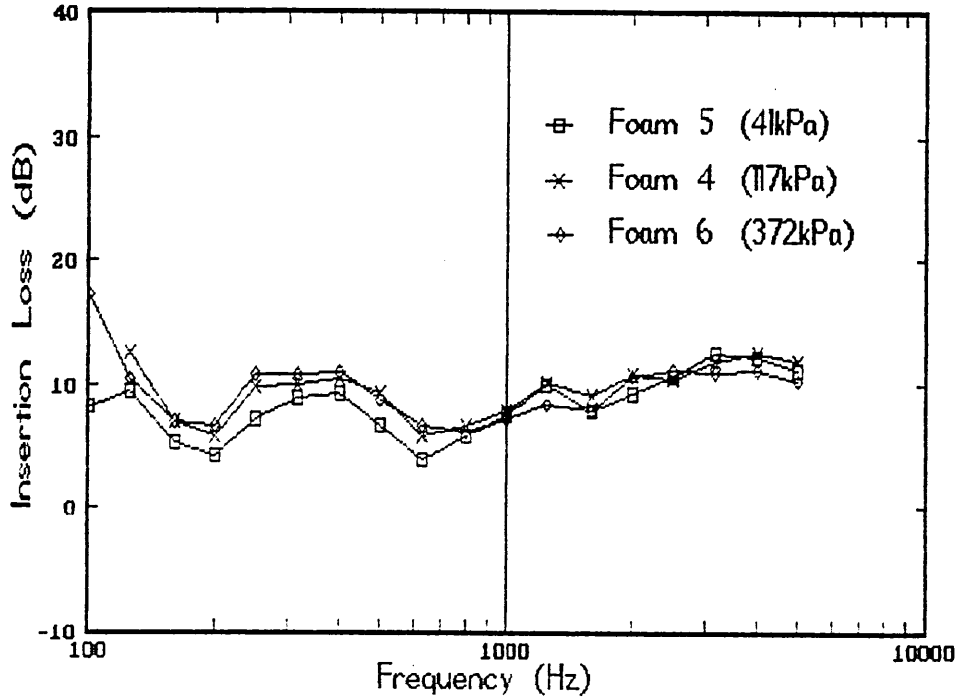

Fig. 46 Insertion Loss for Foams 4, 5 and 6 (First Measurement)

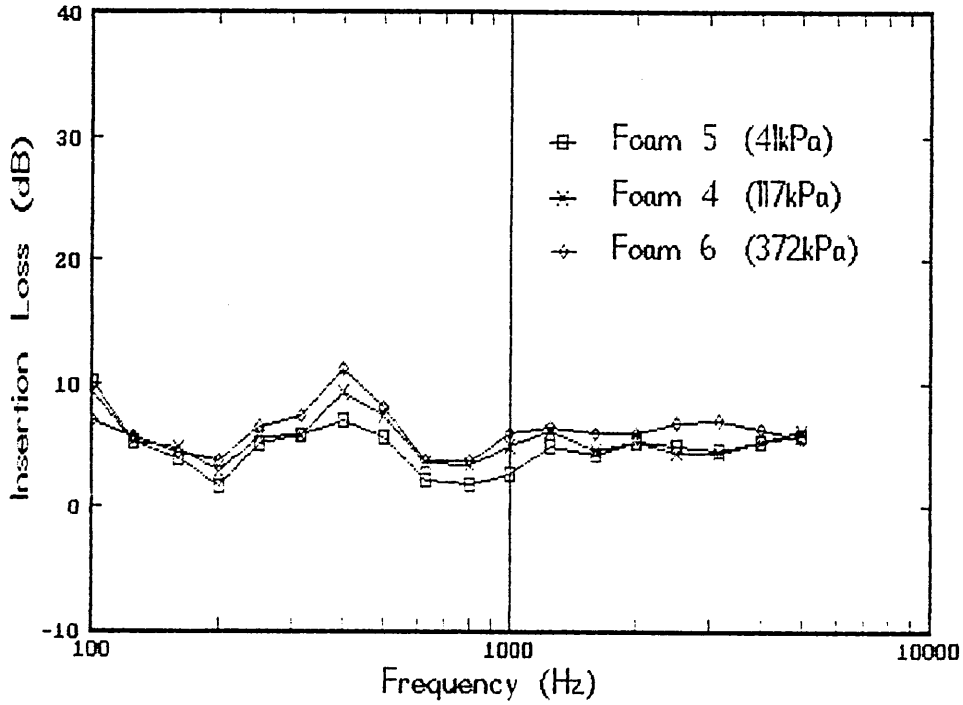

Fig. 47 Insertion Loss for Foams 4, 5 and 6 (Second Measurement)

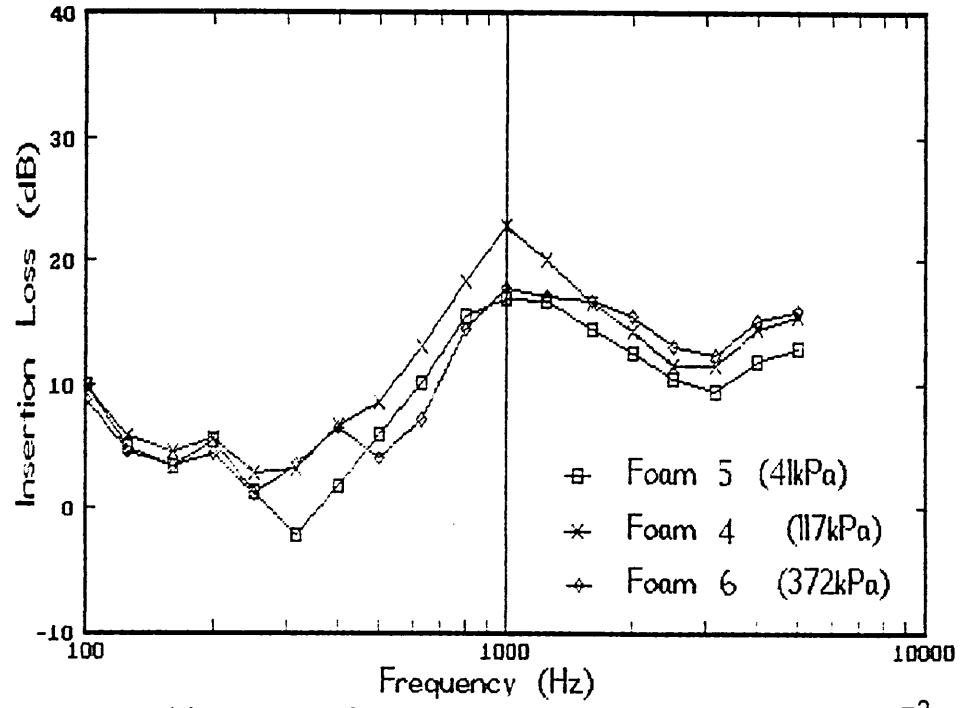

Fig. 48 Insertion Loss for Foams 4, 5 and 6 with 3.7kgm^{-2} Septum (First Measurement)

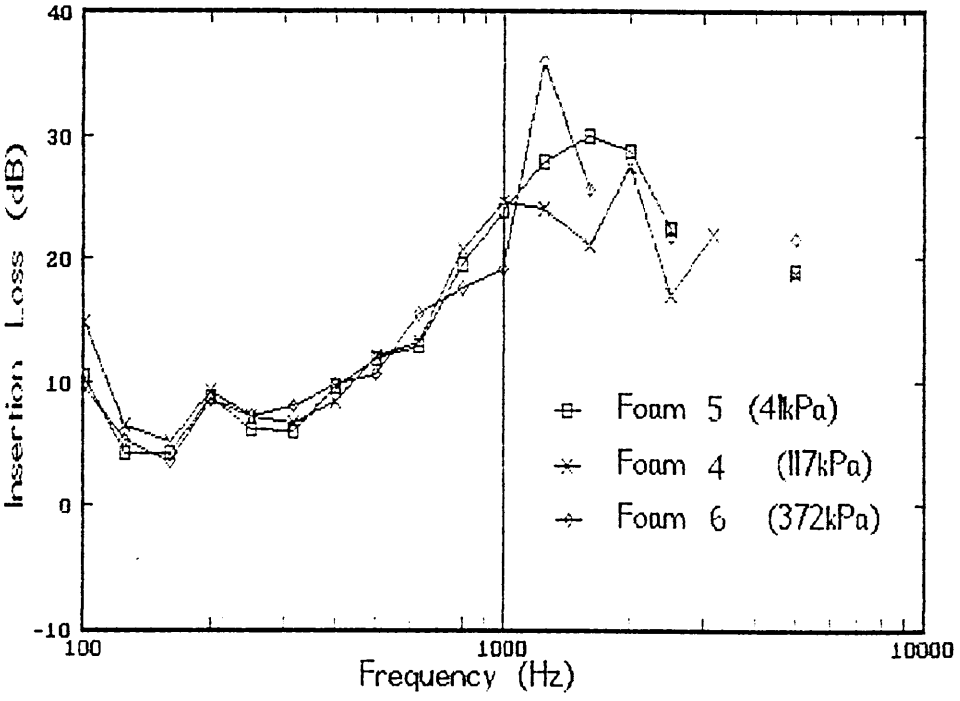

Fig. 49 Insertion Loss for Foams 4, 5 and 6 with 3.7kgm^{-2} Septum (Second Measurement)

5.3.2 P-I Index

The pressure-intensity (p-I) index was used to assess the validity of an intensity measurement. The criteria of F_2<20 dB from Eqn. <69> assuming the manufacturers value for δ_{pIO}, if satisfied, shows that the measurement is to precision and engineering grade accuracy. In practice this value indicates the diffuseness of the sound field i.e. a p-I index of zero indicates the measurement was carried out in free-field conditions. The field indicator F_3 is measured by the Norsonics 830 analyser and was used to establish the validity of intensity values. Its difference to F_2 is in using the signed value of intensity to calculate the index rather than the unsigned (modulus) value. Low excitation forces resulted in a large p-I index being measured. To maintain a high radiated sound level from the steel panel and composite a force of magnitude 25N was used during the measurements. The criteria of low p-I index was easily met for the intensity measurements with structure-borne noise when this force was used. Examples of typical p-I values are shown in Figs. 50 and 51 for foams 3 and 6. The p-I (F_3) values are consistently low (typically 5-6dB) except at high frequency when a foam or foam + septum are added. In that region values are ≈12dB.

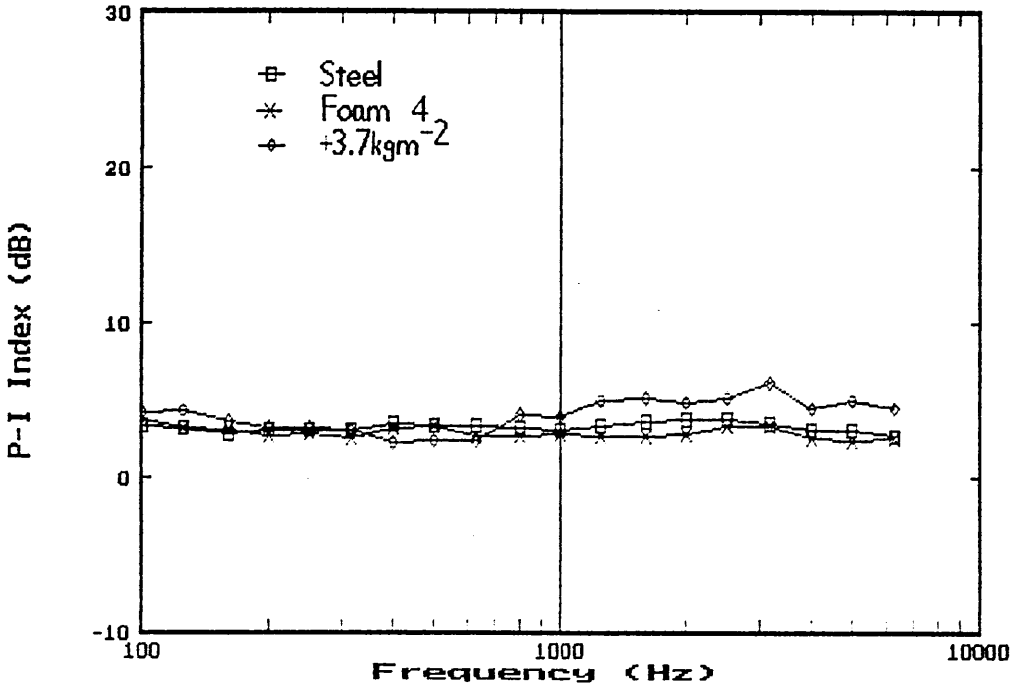

Fig. 50 P-I Index for Foam 3

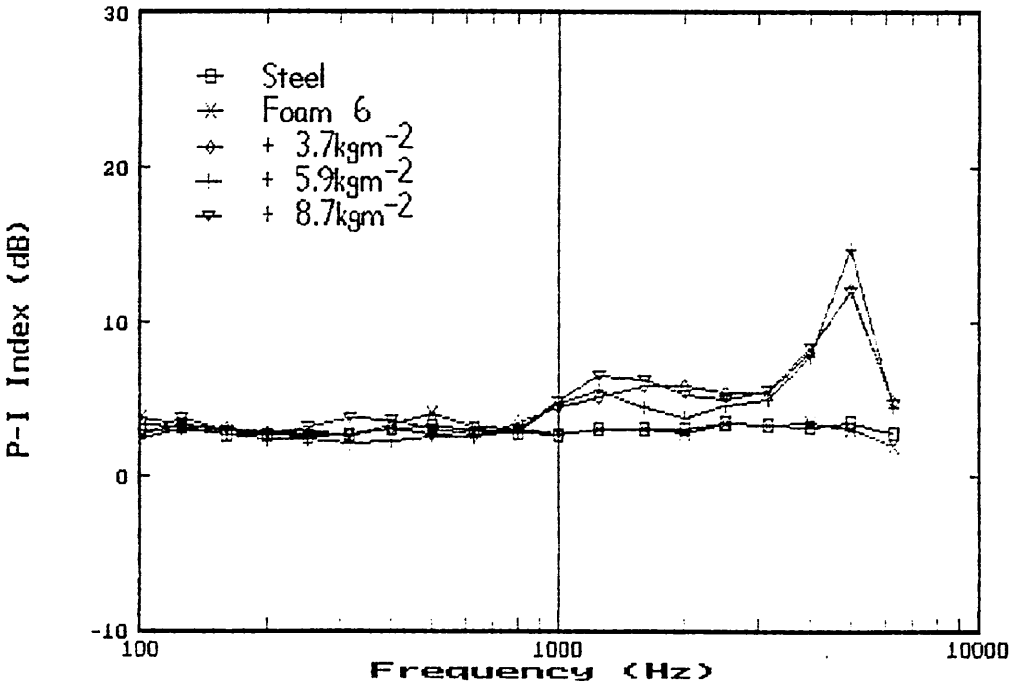

Fig. 51 P-I index for Foam 6

5.3.3 Model Predictions and Measured IL

The problems highlighted above regarding measurement repeatability mean that any comparisons between measured and predicted data should be made tentatively. It is for this reason that predictions are made for only two composite systems. It should also be noted that the model predictions are for discrete frequencies (approximately 150), whereas measurements are carried out in 1/3 octave bands. As 1/3 octave values are the summation of the sound energy within the bandwidth, the measured values will be slightly higher than for discrete frequencies.

Two comparisons between predicted and measured data, for foams 3 and 6, are shown in Fig. 52 and 53 below. It is seen at frequencies below 1 kHz the IL curves show fairly good agreement. The position of the first resonance is predicted reasonably well, although the predicted level at resonance is lower than measured.

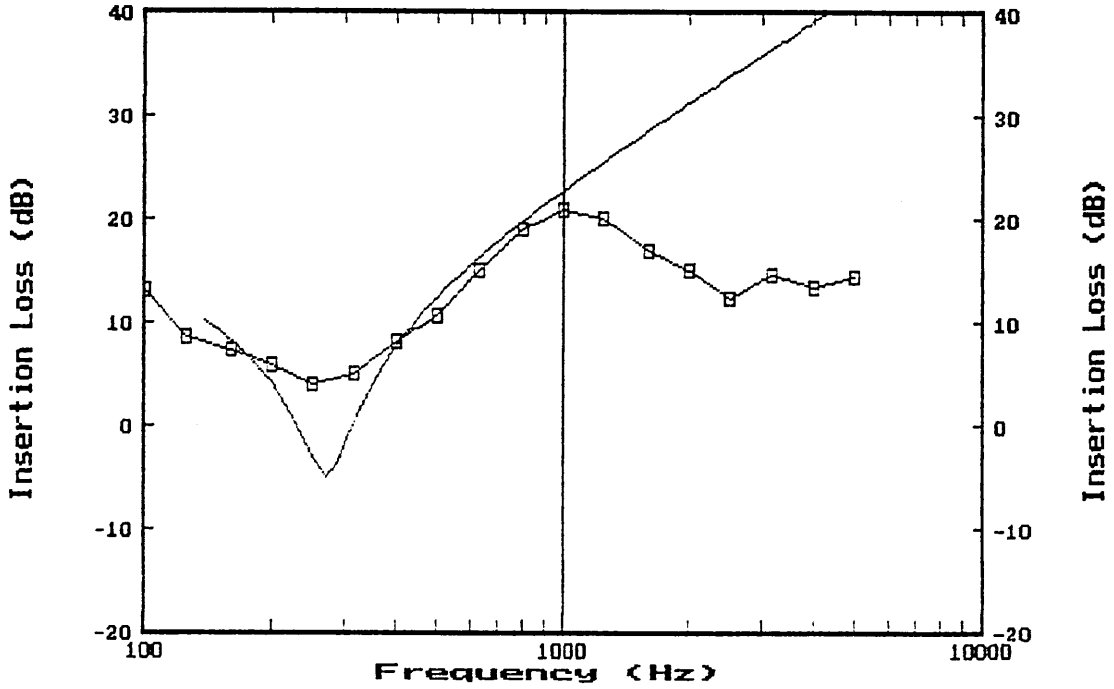

Fig. 52 Comparison between predicted and measured IL for foam 3

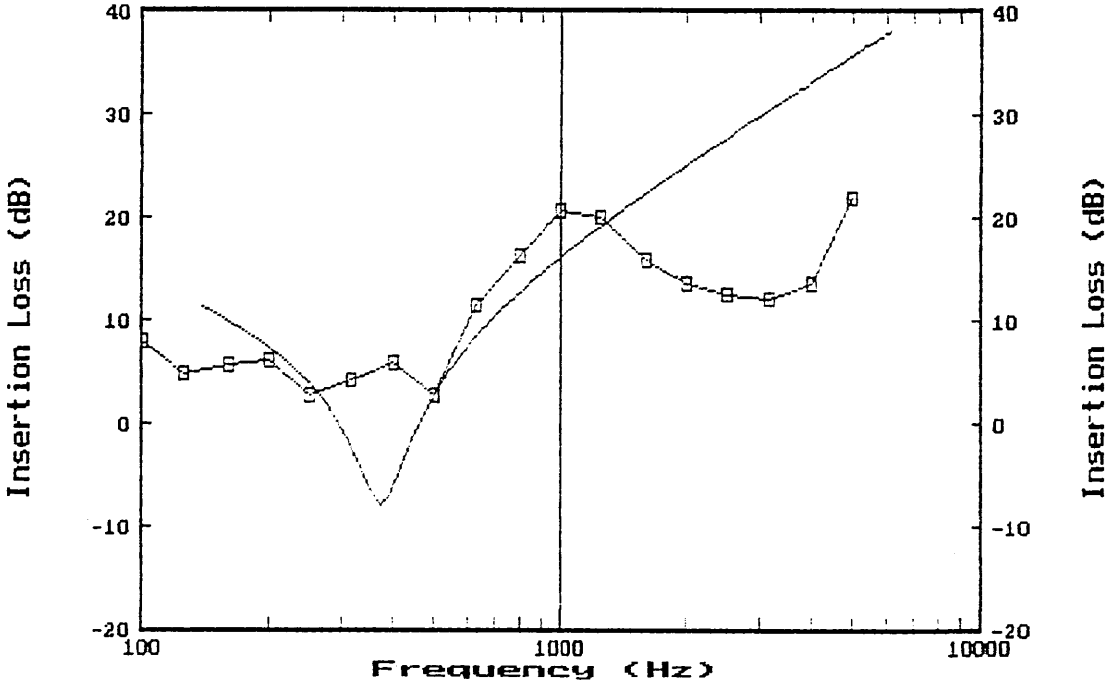

Fig. 53 Comparison between predicted and measured IL for foam 6

The theoretical predictions in Chapter 2 demonstrated that the principal effect of increasing the foam damping was to increase the IL at resonance. Thus it could be that the empirical model used for

the ratio of system to steel panel loss factors, i.e. η_1/η_0 in equation 31, is not a good representation of the behaviour at resonance. The ratio of loss factors may be obtained using the measured data given in Section 5.2.2. These are presented below for foams 3 and 22 in Figures 54 and 55. The empirical values for the ratio, from the regression analysis of Plunt's data, are also plotted for comparison. The measured data is higher than that for the empirical equation, derived from Plunt's data (1991), used in the model. It is also observed that the measured data does not display a linear (or logarithmic) behaviour. This means that a linear regression can not be carried out on the data to obtain a different empirical equation for substitution into the model. Examination of the first term of equation <36> shows that the contribution of the damping ratio to the system IL is $10\text{Log}_{10}(\eta_1/\eta_0)$. The difference between the two damping ratios given in the graphs show that for the experimental system the value is higher by a factor of approximately 10. This would result in an increase in IL of 10dB. Unfortunately, this would shift the predicted IL curve up above the measured values; although the IL at resonance would be predicted more accurately. It is speculated that when the system is excited by the shaker the foam remains in contact for a greater percentage of time and the dominant damping mechanism is extensional not frictional damping.

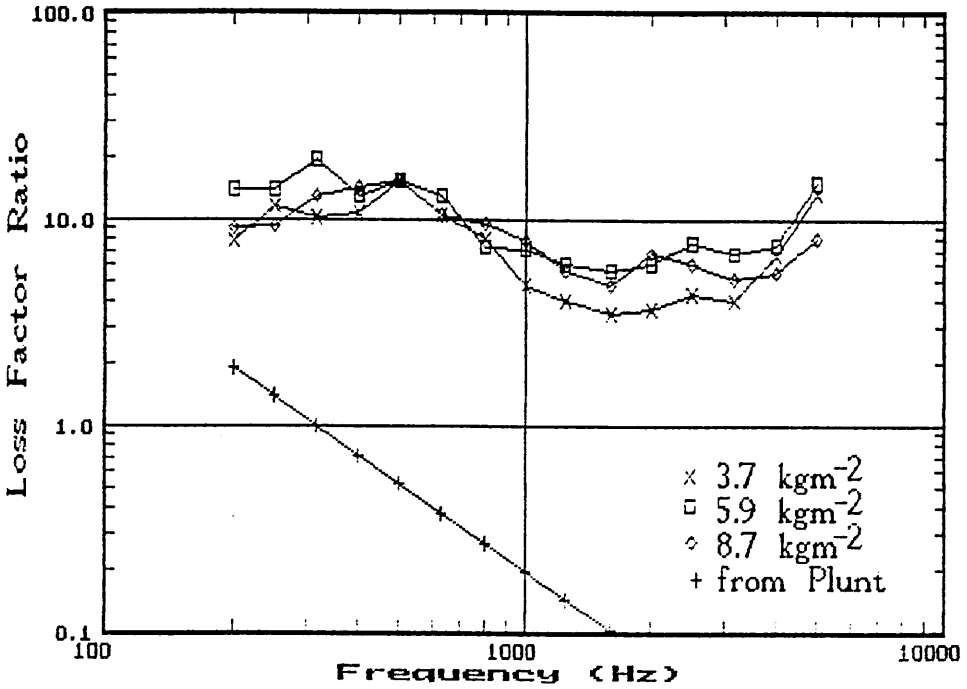

Fig. 54 Comparison of measured and predicted ratios of loss factors for foam system and the steel panel for foam 3

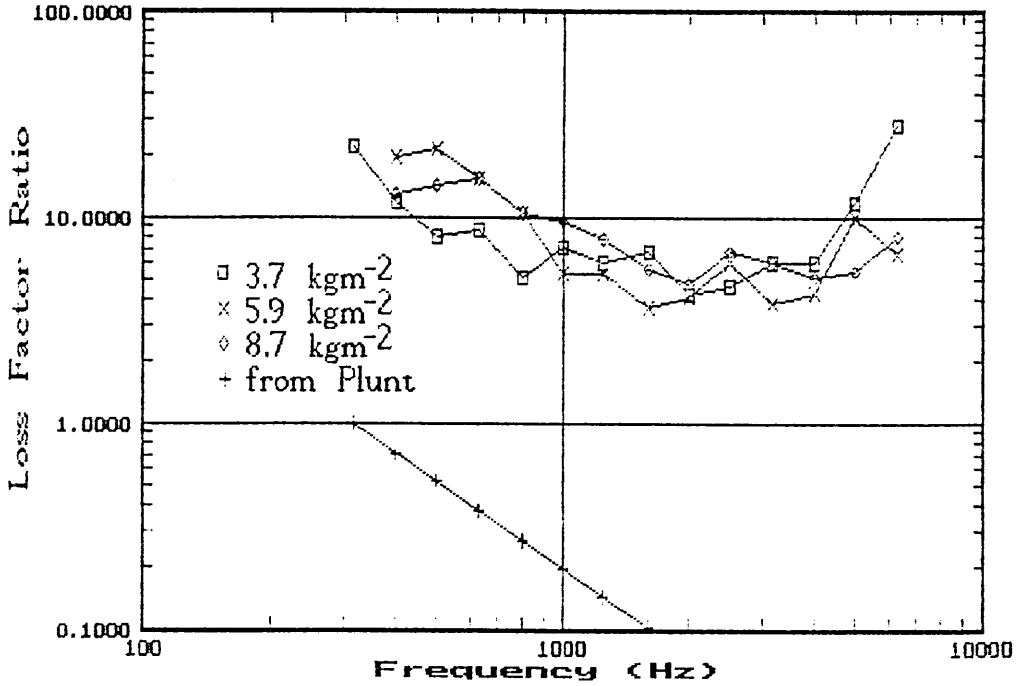

Fig. 55 Comparison of measured and predicted ratios of loss factors for foam system and the steel panel for foam 22

The large differences between measured and predicted values above 1 kHz also have to be explained. The theoretical model is a simple one and assumptions were made.

(i) It was assumed that the system can be modelled using a lumped parameter model. At the higher frequencies wave propagation mechanisms might influence the response i.e. resonances within the foam composite. This phenomena is seen in foam materials in other situations (e.g. the acoustic absorption response and the airborne noise insertion loss response).

(ii) The damping ratio of foam composite to steel panel was represented using empirical formulae derived from Plunt's data (1991). It was shown earlier in this chapter that the lower damping ratio obtained from Plunt's data was lower than that measured.

(iii) The radiation efficiency of the panel is assumed to be the same as that of the steel + foam + septum combination. No data has been published in the literature for the radiation efficiency of foam composites.

(iv) Some of the parameters used, e.g. foam modulus and damping, are frequency dependent. Single values obtained at low frequencies were incorporated into the model.

Measured data is presented below for two configurations: (i) the steel panel + foam layer, and (ii) the steel panel + foam + septum composite. (Although the first configuration is not that of a carpet composite it was investigated in order that more knowledge of PUR foam backed systems could be obtained). It was found that the addition of a foam to a vibrating panel increased the insertion loss.

The behaviour displays a characteristic shape which is seen repeatedly. It is one of two maxima and minima. These minima appear in the region of 200 Hz and 1 kHz. Apart from the thinnest foams (10mm), the insertion loss is always greater or equal to 0 dB. If the performance is compared with the airborne insertion losses described in the following section, it is seen that for vibration generated excitation the foams offer a greater insertion loss than for airborne noise excitation i.e. the noise insulation for structure-borne noise is greater than that for airborne noise.

The addition of a septum to the panel and foam was expected to introduce a mass-spring-mass resonance, as predicted by the theory in Chapter 2 similar to that seen for airborne excitation. In practice this resonance was not as distinct as for airborne noise, and in some cases was not visible at all. The IL increases from low frequencies to a maximum at approximately 1-2kHz. It then drops, only to subsequently increase once more at higher frequencies.

5.3.4 Material Parameters

(a) The Effect of Damping

The influence of foam damping was examined with foams 19, 14 and 22. These had loss factors of 0.4, 0.1 and 0.8 respectively. The vibration IL for the panel and foam is shown in Fig. 56 below. At low frequencies (f<500Hz) foam 14 with the lowest damping gave the worst IL, whilst the two other foams performed comparably. This would indicate that for this system configuration that a very high damping material does not offer any benefits to IL. This is contrary to the

trends shown in Chapter 2. However, above 500Hz, it is seen that foam 22, with a loss factor of 0.8, gives the best performance. The remaining two foams show similar insertion losses below that of foam 22. Thus it can be concluded that at high frequencies there are benefits in higher damped foams.

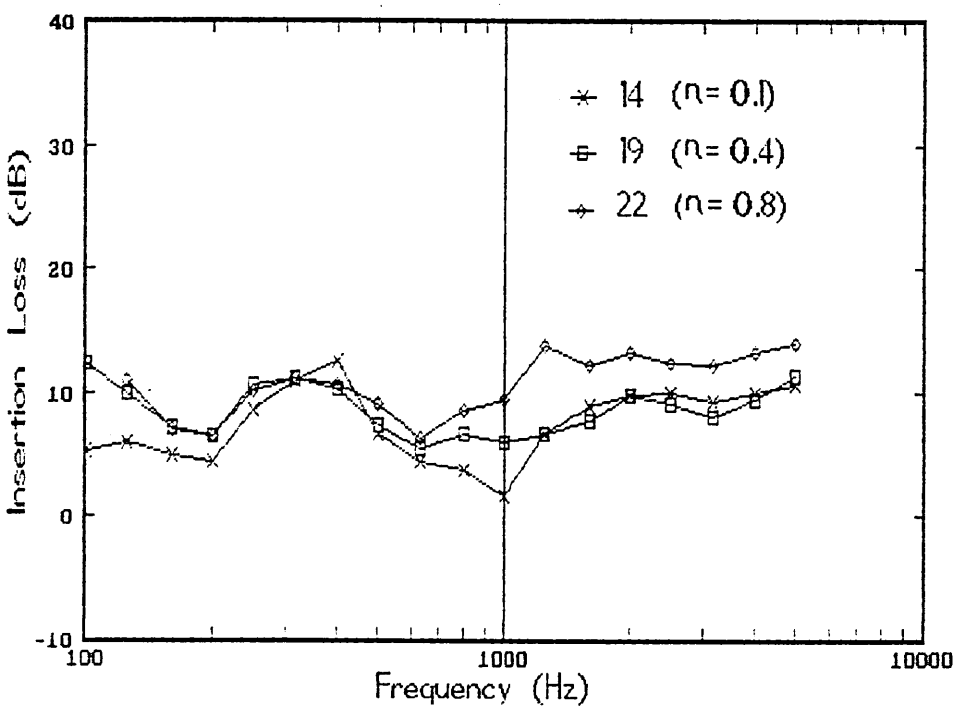

Fig. 56 Influence of foam loss factor on vibration IL (no septum)

When a septum is added to the panel and foam the IL is greater than for the panel and foam, as expected. The behaviour for septa of 5.9 and 8.7 kgm^{-2} is shown in Figs. 57 and 58 below. At low frequencies ($f<250Hz$) the performance of the three foams is comparable. In the mid-frequency range ($250<f<1250Hz$), the medium damped foam (19) gives the worst IL for a septum of 3.7 and 8.7 kgm^{-2} and the lowest damped foam offers the worst for a septum surface density of 5.9

kgm^{-2}. The highest damped foam (22) provides the best IL. At high frequencies (f>1250Hz) the highest damped foam gives the best IL and the lowest damped foam the worst. The conclusions from this behaviour is that a highly damped foam is preferable at medium and high frequencies to maximise system vibration IL, but at low frequencies the material damping has little influence on system IL performance.

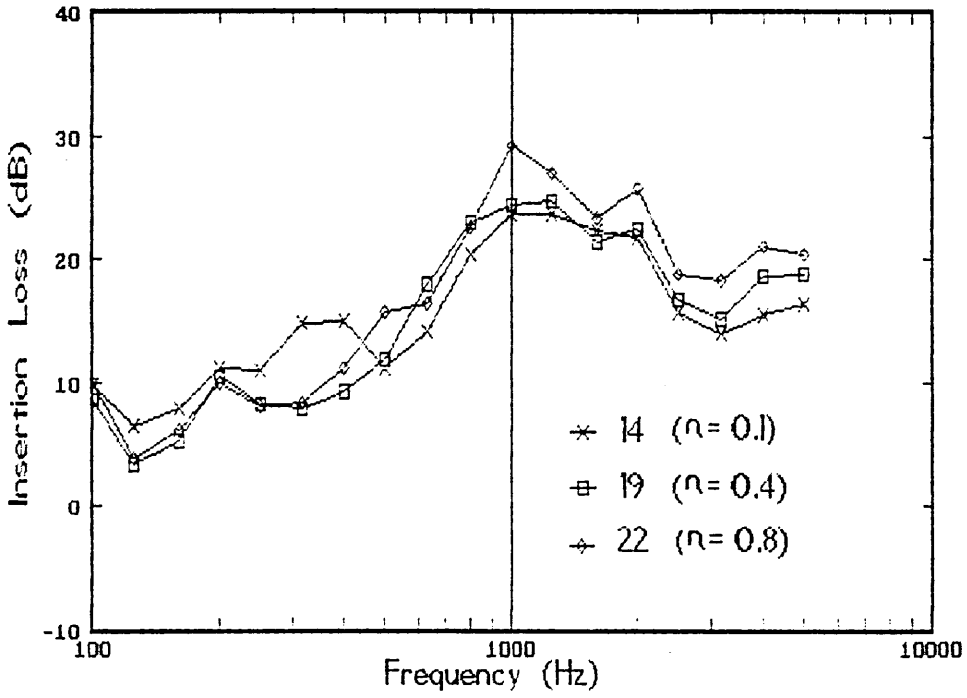

Fig. 57 Influence of foam loss factor on vibration IL (septum = $5.9kgm^{-2}$)

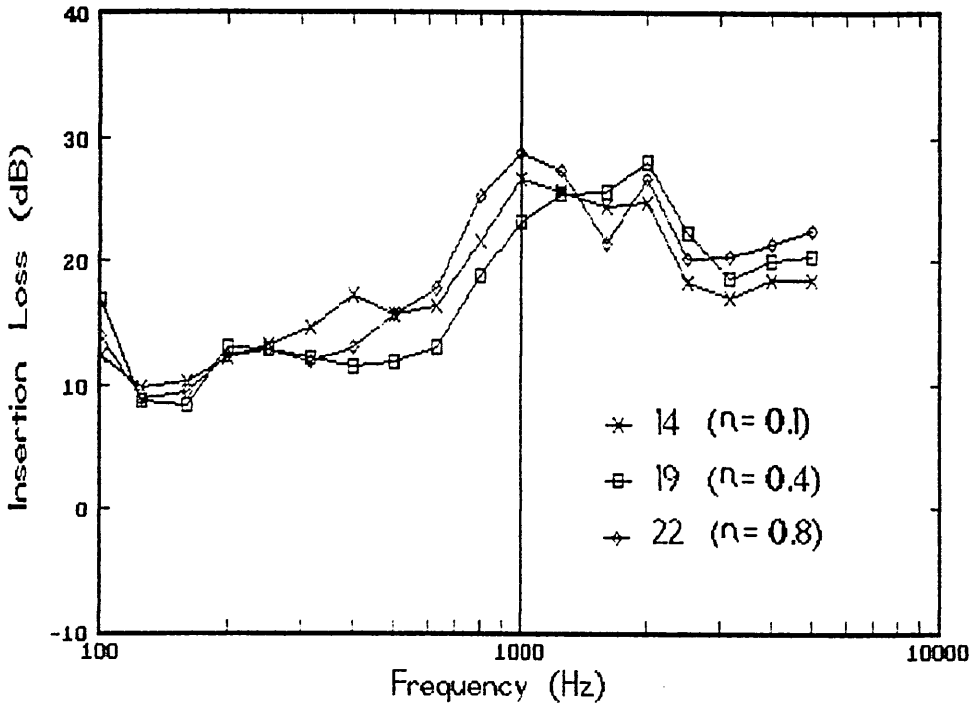

Fig. 58 Influence of foam loss factor on vibration IL (8.7kgm^{-2} septum)

(b) The Effect of Density

The influence of foam density upon vibration insertion loss was examined using foams 6, 4 and 9, with unit densities 1.69, 1.84 and 2.09kgm^{-2} respectively. Fig. 59 shows the IL of these three foams. There is little difference between the performance of the three foams.

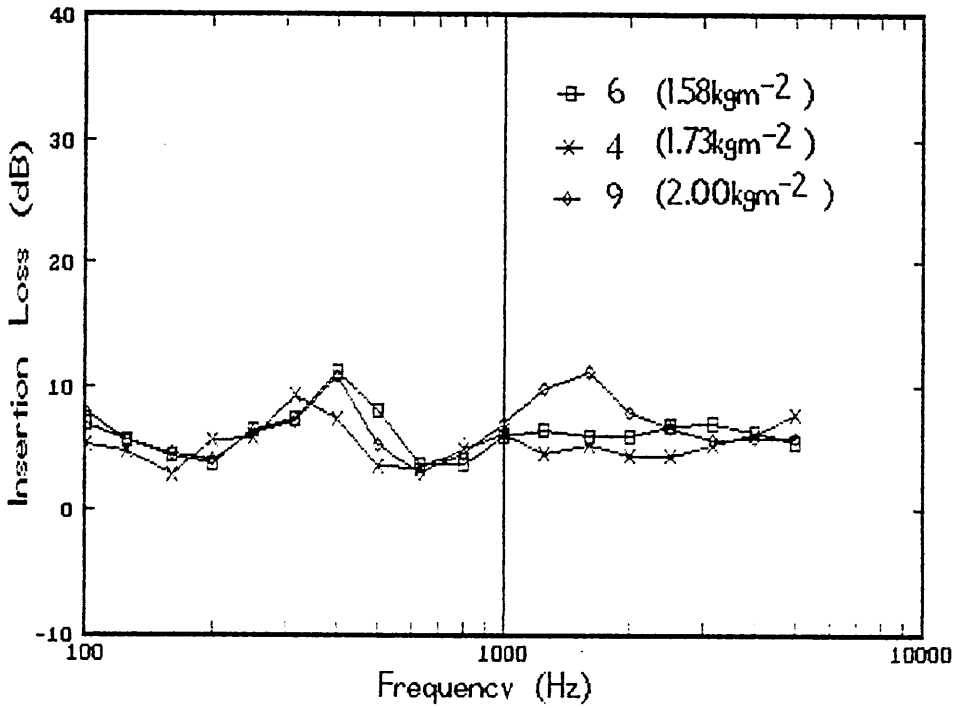

Fig. 59 Influence of foam density upon vibration IL (No Septum)

The vibration IL behaviour with a septum of 5.9kgm^{-2} is shown in Fig. 60. Below 300Hz the performance of the foams is comparable. Between 300 and 1000Hz foam 4 (medium surface density) offers the best performance, with the highest density foam (9) next best. This would appear to be due to the IL peak of foam 4 occurring at a lower frequency than the other two foams. As a consequence of the curve being shifted down the frequency scale, above 1kHz, ($1.0<f<2.5$kHz), the best performance is given by foam 9. Above 2.5kHz foam 4 again gives the best IL.

The conclusion is that for best vibration IL, especially at mid-frequencies, a foam of surface density 1.8kgm^{-2} should be used. However, the problem of manufacturing foams with one property varied whilst other remain constant could explain the above behaviour. If the material property values are considered it is seen that foam 6

has a modulus of three times that of the other two foams. Chapter 2 predicted that this would increase the resonance frequency and shift the IL curve up the frequency range. this could explain why the IL for foam 6 is lower (300-1000Hz) than the other two foams.

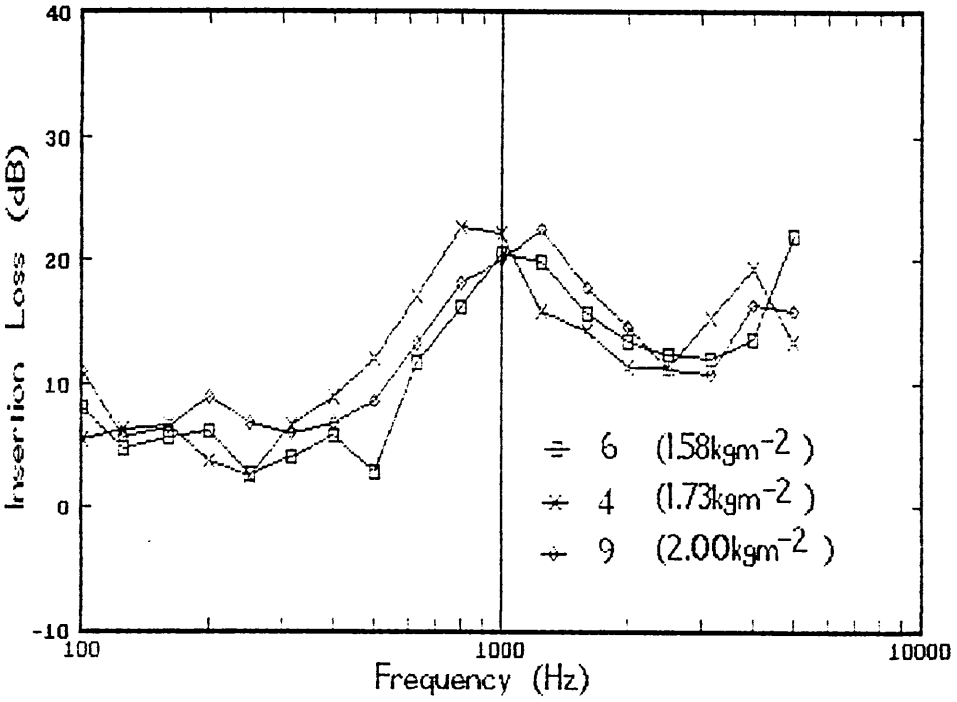

Fig. 60 Influence of foam density upon vibration IL

(Septum=5.9kgm^{-2})

(c) The Effect of Modulus

The influence of foam modulus was examined using foams 5, 4 and 6. These had moduli of 41, 4 and 122 kPa respectively. The insertion loss for the panel + foam is in Fig. 61. Differences in performance are noticeable at low frequencies (f<1000 Hz). It is seen that the IL increases with increasing modulus. Above this frequency the behaviour of the foams is comparable.

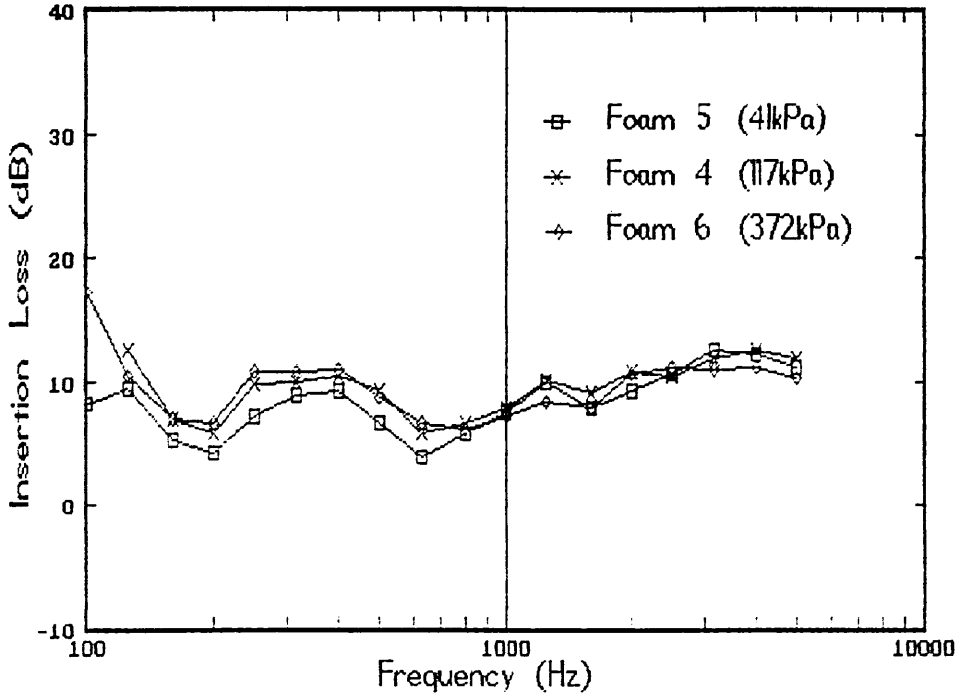

Fig. 61 Influence of foam modulus on vibration IL (no septum)

The IL for the composite system of steel + foam + septum is shown in Fig. 62. It can be seen that there is little difference between the three foams, and the conclusion is made that modulus does not appear to affect the system response. This is contrary to the behaviour of the theoretical predictions in Chapter 2 where increasing the foam modulus increased the resonance frequency and increased the composite damping at resonance.

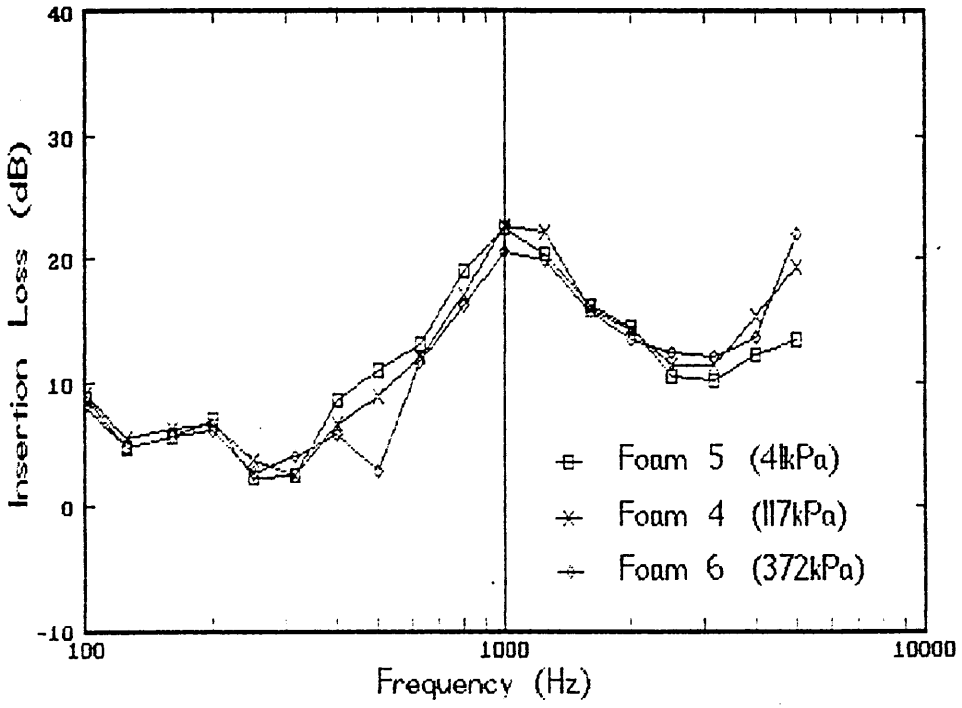

Fig. 62 Influence of foam modulus on vibration IL (5.9kgm^{-2} septum)

5.3.5 System Parameters

(a) The Effect of Foam Thickness

This was investigated with foams 17, 14 and 16. These had nominal thicknesses of 10, 20 and 30mm respectively. For the panel and foam we see from Fig. 63 that the response shape of the three foams is similar and that the highest IL is given by the thickest foam. This behaviour would appear to be contrary to that of Section 5.2.1 and 5.3.4 (b), where an increase in surface density (thickness) had little effect upon the vibration response. The reasons for this are unknown.

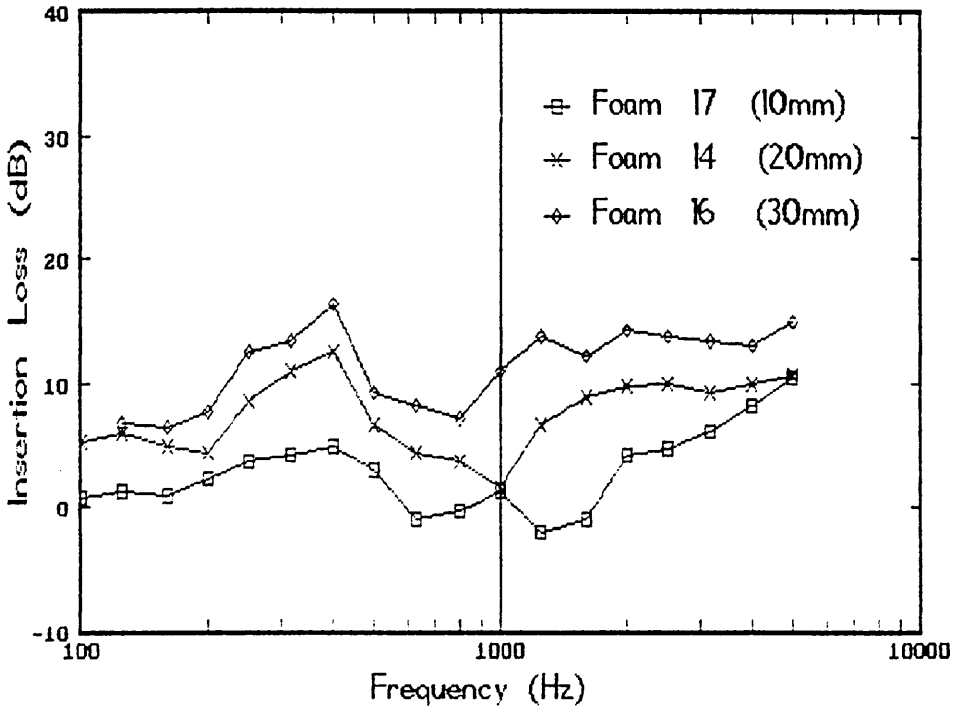

Fig. 63 Effect of thickness on insertion loss (10, 20, 30mm - no septum)

The addition of the septum layer is demonstrated in Fig. 64. At low frequencies the highest IL is obtained using the thickest foam. This is because the characteristic shape of the IL response produces a maxima in this frequency range. For the mid-frequencies (400<f<1250Hz), the performance is in order of thickness; with the 30mm foam producing the highest IL and the 10mm foam the lowest. At high frequencies (f>1250Hz), it is the 30mm foam that offers the highest IL, whilst the two thinner foams perform comparably. It should also be noted that the maxima to minima value of insertion loss also decreases with thickness. If surface density was the only difference between the foams then Section 5.4.4 indicated that a surface density of 1.8kgm^{-2} would give the best performance i.e. the 20mm foam should give the best IL. This is not the case with ob-

served behaviour. The change in thickness thus also causes a change in system response. This is most likely to be due to system resonances being changed with differing thicknesses.

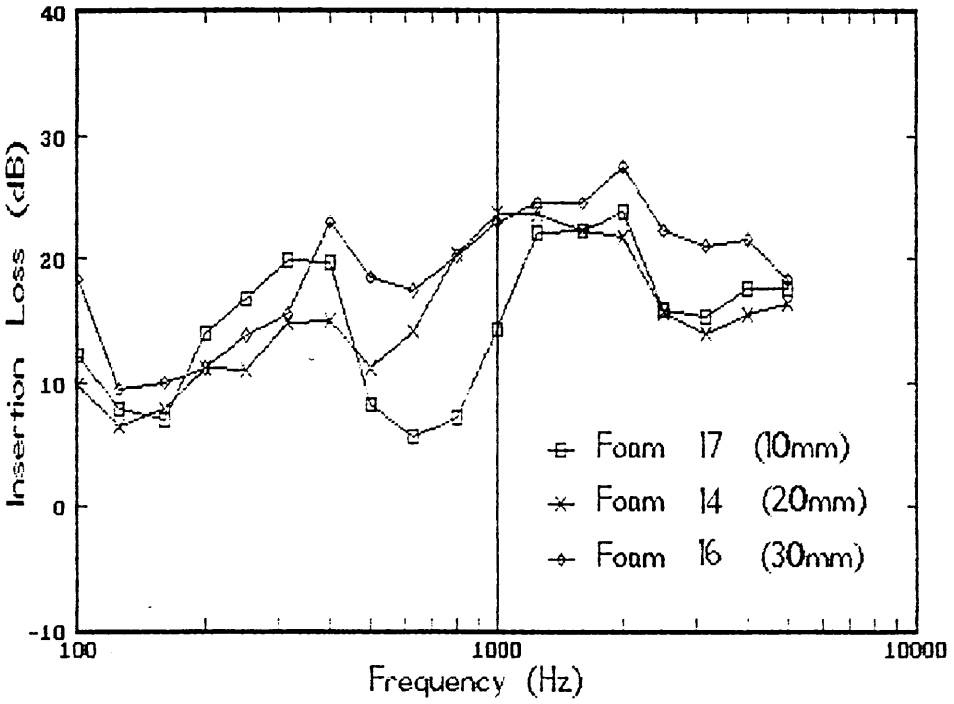

Fig. 64 Effect of foam thickness on vibration insertion loss (septum=5.9kgm^{-2})

(b) The Effect of Septum Layer

The measured data indicate that with increasing septum surface density, the vibration IL increases. This is illustrated below in Figs. 65 to 68. However, the behaviour of some foams differed in the mid-frequency range (approximately 800Hz depending on the foam). For these foams (examples shown are those of 10 and 1) the behaviour in this frequency band is similar. This is in contrast with the IL of foam 14, for example, where a large difference is observed in the IL

for the three septa as expected from the theoretical prediction in Chapter 2. There appears, at this stage, no explanation for the differences in observed behaviour. The phenomena does not appear to be related to measured material properties.

The theoretical prediction also indicated that an increase in septum surface density would result in a decrease of resonance frequency. Maxima and minima are visible for foam 17. These minimum-maximum values are larger for the thinner foams (cf. foam 14).

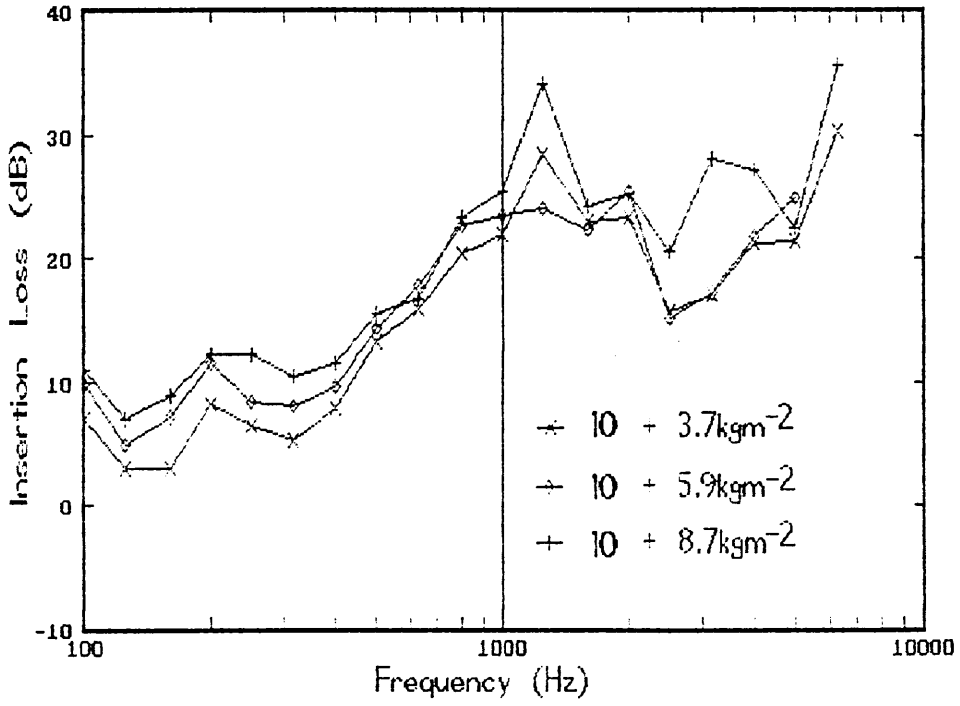

Fig. 65 Influence of septum surface density on vibration IL

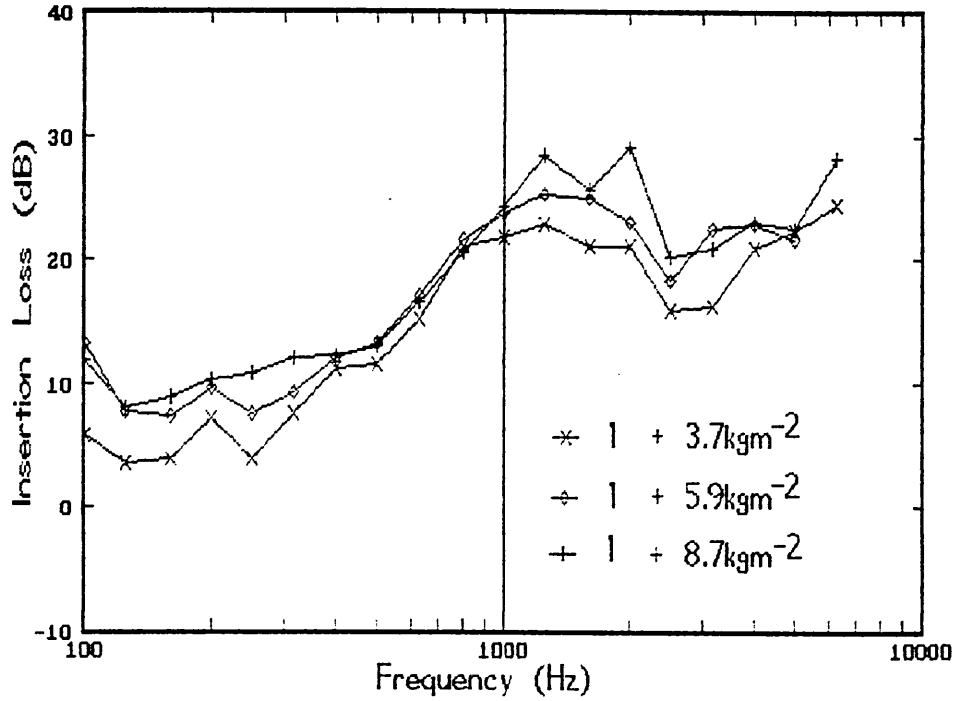

Fig. 66 Influence of septum surface density on vibration IL

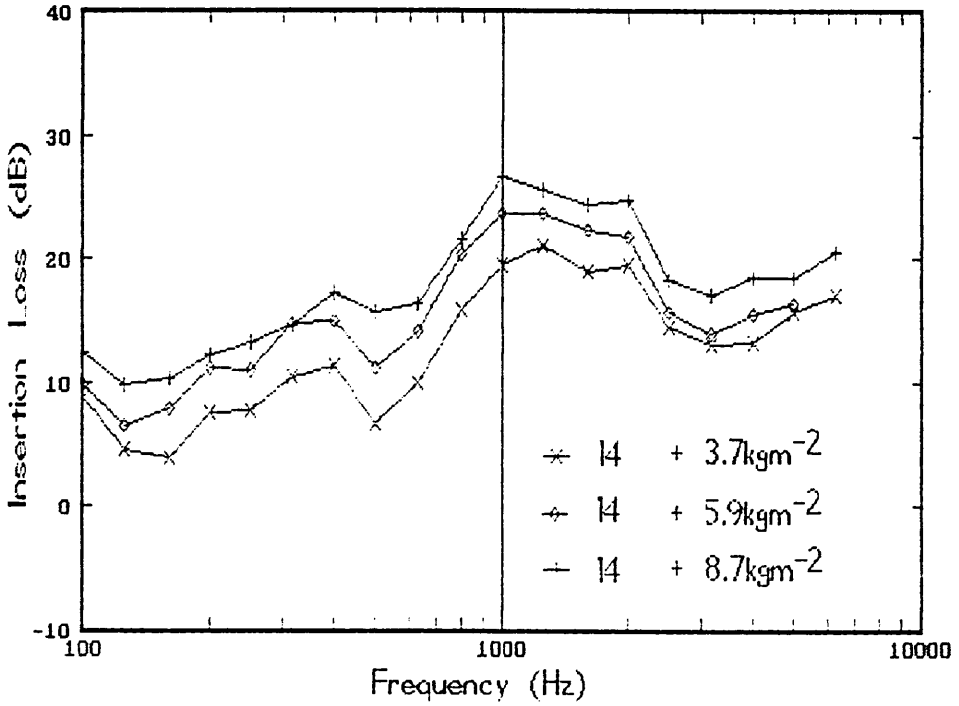

Fig. 67 Influence of septum surface density on vibration IL

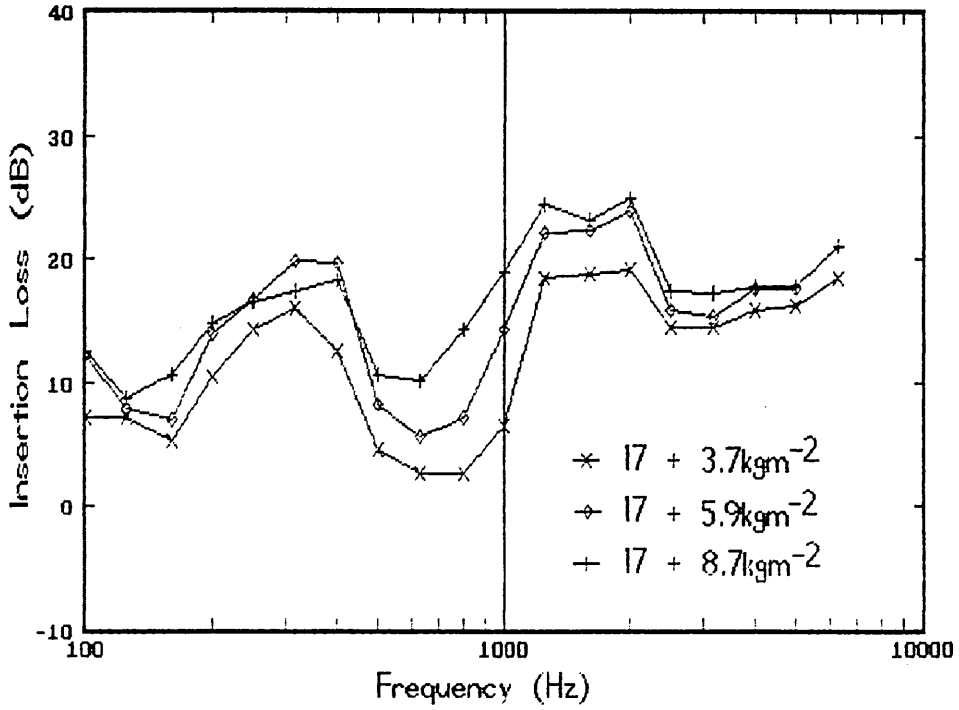

Fig. 68 Influence of septum surface density on vibration IL

5.4 Airborne Insertion Loss

The insertion loss test facility described in Chapter 3 was used to measure the airborne insertion loss of the experimental foams. Material and system parameters from Chapter 4 are used in the computer model of Chapter 2 to predict the theoretical insertion loss. Unless otherwise stated the septum layer used had a surface density of 5.9 kgm^{-2}. A full set of airborne insertion loss data for the experimental foams is presented in Appendix **D**.

5.4.1 Measurement Reproducibility

To investigate measurement reproducibility the measurement procedure was repeated several times for a number of foam composites. The

results are shown in Figs. 69 to 71. These graphs are for foam 3, with three different septum area densities (3.7, 5.9 and 8.7 kgm^{-2}). It can be seen that the difference in IL between the two data sets is of the order of 1.5dB, except at high frequencies (f>2kHz). This reproducibility of measurements was observed both on a day-to-day and month-to-month basis. The differences can be attributed to the errors in measurement and small differences in installation of the composite in the test facility. Larger variations observed on some occasions could be attributed to leakages of sound on the composite perimeter i.e. poor sealing, or sudden extraneous noises. In both these cases the measurement could be repeated when the identified problem was remedied. The high level of reproducibility shows that the test facility constructed in our laboratories and procedure can be used in the long-term to compare and assess the airborne noise insulation performance of under-carpet composites without degradation in measurement accuracy beyond that of experimental error.

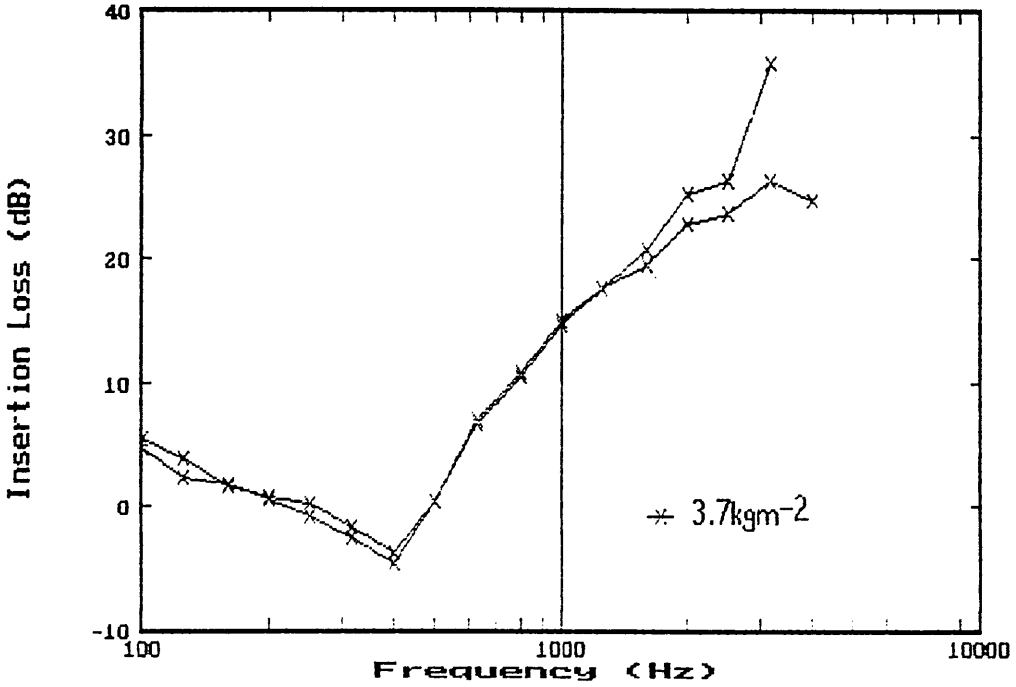

Fig. 69 Repeatability of Insertion Loss Measurements (Foam 3 + 3.7 kgm^{-2} Septum)

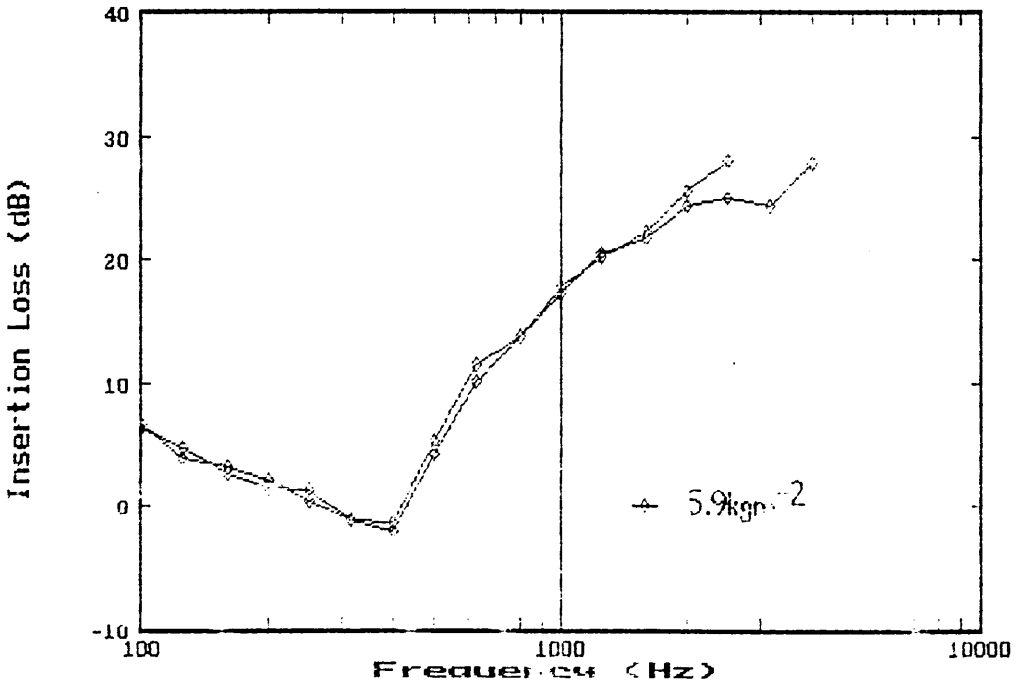

Fig. 70 Repeatability of Insertion Loss Measurements (Foam 3 + 5.9 kgm^{-2} Septum)

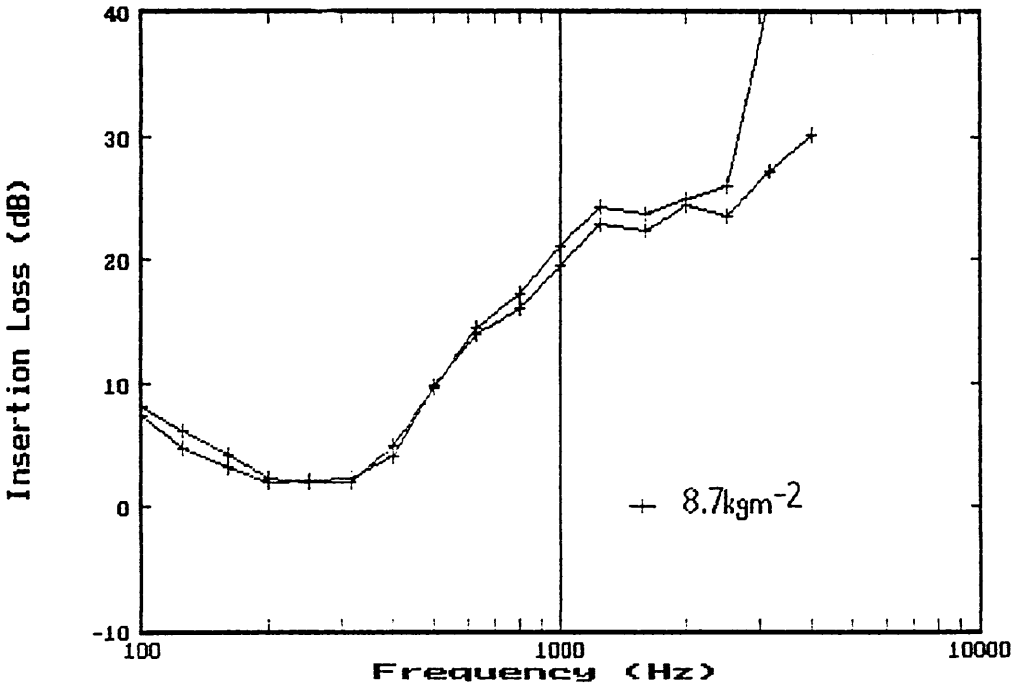

Fig. 71 Repeatability of Insertion Loss Measurements (Foam 3 + 8.7 kgm^{-2} Septum)

5.4.2 P-I Index

The pressure-intensity index was used to assess the validity of the acoustic measurement as with the vibration insertion loss measurements described in Section 5.3 above. The criteria of a low p-I (low F_3) index was easily met in the intensity measurements. This is shown in Fig. 72 for foam 3. The p-I values are for one set of the measurements given in Section 5.4.1. For the conditions of steel panel and steel panel plus foam the index is low, 4-6dB. With the addition of septa the index increases at higher frequencies but still remains less than 20 dB (f<4kHz). This is well within the specification set by Eqn. <69> and thus meets both precision and engineering grade requirements.

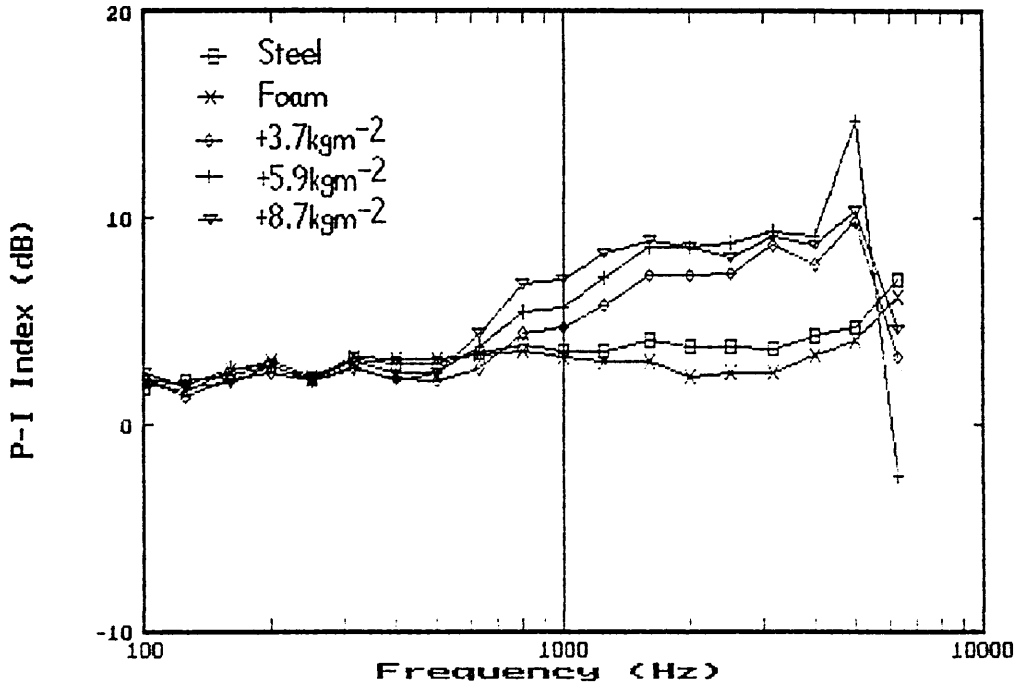

Fig. 72 Typical Pressure-Intensity Index Values

5.4.3 Initial Predictions and Model Modification

The model predictions are again for discrete frequencies (approximately 150), whereas the measurements are carried out in 1/3 octaves. Thus the measured values will be slightly higher than for discrete frequencies.

The initial model predictions were not encouraging when compared with experimental results. Fig. 73 below shows comparisons of measured and predicted behaviour for foams 12 and 17, with septum surface densities of 5.9kgm^{-2}. The predictions underestimate the resonance frequency of the system. It was found that the resonance frequency, f_R, was underestimated by a factor of 1.7 using the foam modulus. The reason for this was attributed to the propagation

constant and foam impedance. Both of these calculated values used formulae derived for semi-rigid and fibrous materials not flexible polyurethanes. This empirical form-factor was thus introduced into the programme for model predictions i.e. $K^{*'}_{tot} = 1.7K^{*}_{tot}$, where $K^{*'}_{tot}$ is the modified combined foam and air modulus. Other authors (e.g. Craggs, 1986) have also reported the need for empirical values in calculations with PUR materials. Rewriting equation <59> gives

$$f_R = \frac{1}{2\pi}\left[\left(\frac{K'_{tot}}{d}\right)\left(\frac{1}{m_{s1}} + \frac{1}{m_{s2}}\right)\right]^{1/2} \qquad \langle 79 \rangle$$

where the modulus K'_{tot} is the modified value $1.7K'_{tot}$.

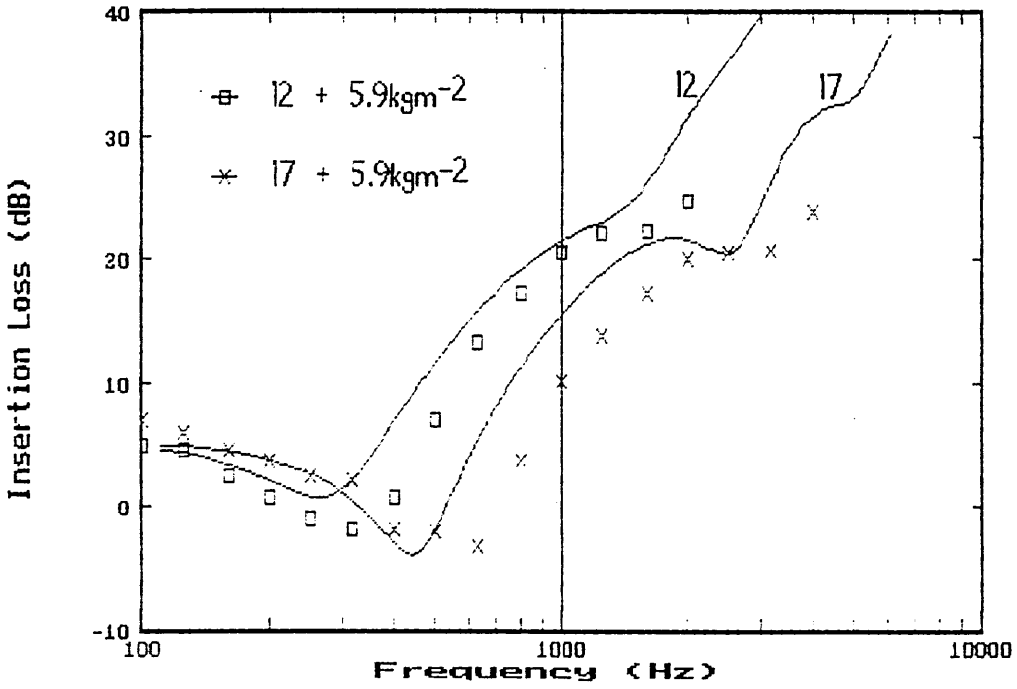

Fig. 73 Comparison of Model Predictions with Experiment

With the modified programme the predictions are much improved. These are shown in Figs. 74 and 75. The IL predictions given in the remainder of this chapter use the modified modulus to calculate the

system transmission loss. Figure 76 compares the resonance frequency from the measured data with the values predicted by equations <59> and <79>. The solid lines represent the upper and lower third octave frequency limits. It is seen that for the unmodified equation <59> few measured resonance frequencies fall within the band limits, whereas with the modified resonance equation fairly good correlation is obtained between measured and predicted resonance frequencies.

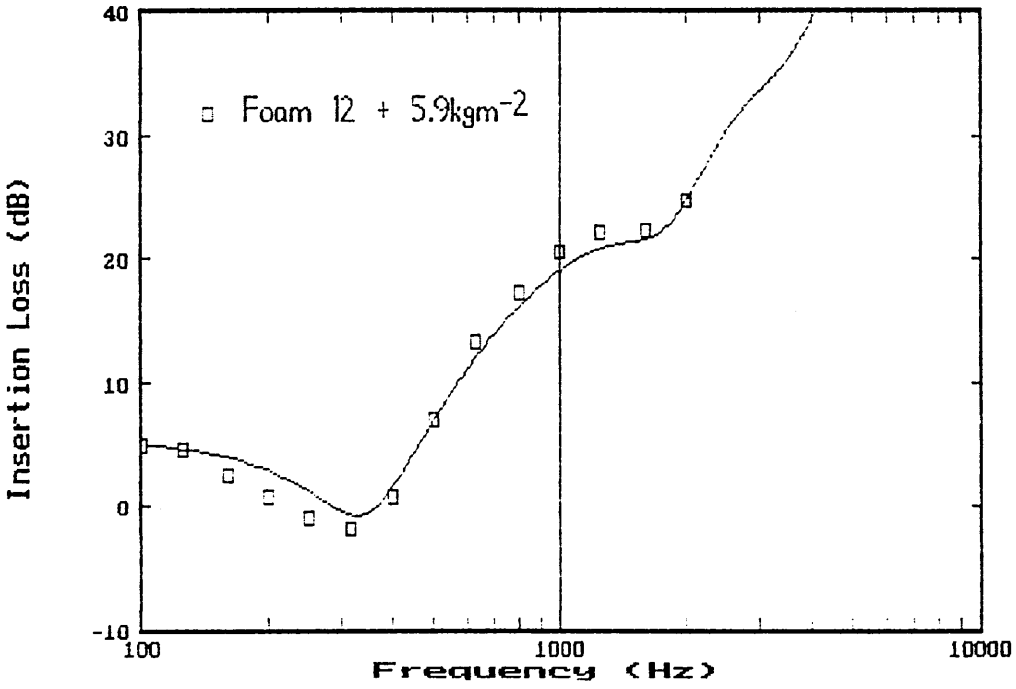

Fig. 74 Comparison of Modified Prediction with Experiment

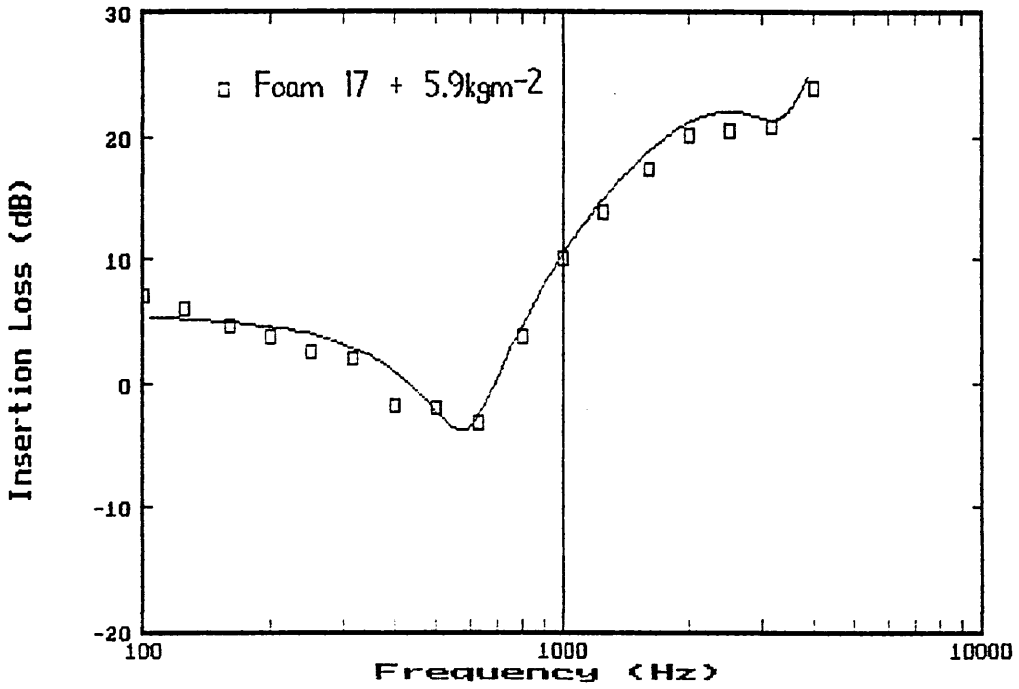

Fig. 75 Comparison of Modified Prediction with Experiment

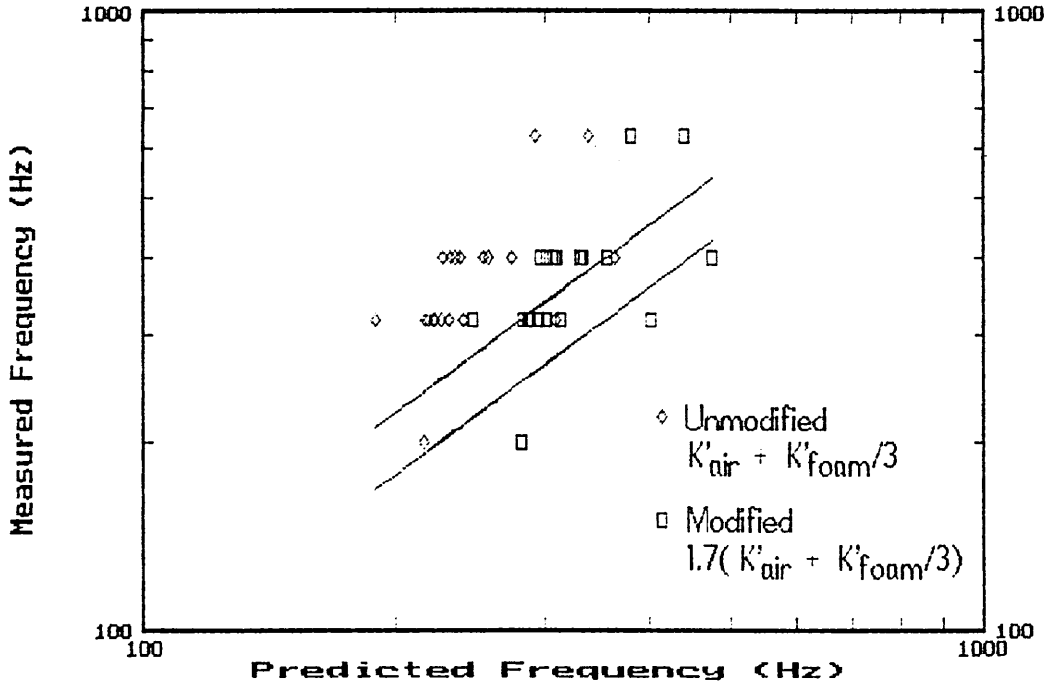

Fig. 76 Comparison of predicted resonance frequency with measured resonance frequency.

5.4.4 Material Parameters

(a) Foam Damping

It was shown in Section 2.11.1 that the predicted effect of increasing foam damping is to increase the IL at and around the resonance trough.

Experimental data for foams 19, 14, and 22 are used to examine the experimental influence of damping. Measured values of loss factor were η=0.47, 0.14 and 0.83 respectively. The measured IL are shown in Fig. 77 and the predicted IL in Fig. 78. It was expected from the theoretical analysis that the foams would show a difference in IL, principally at resonance. However, we observe that the IL for 19 and 14 is about the same at resonance. The higher damped foam (22) manifests no second resonance at f>1kHz, as expected. The result for the foam 22 is slightly misleading as the modulus is low. This causes a shift down the frequency scale of the overall IL curve due to the lower resonance frequency. The IL is therefore superior to the other two foams at f>300Hz because of this low modulus and also because of the increased IL at resonance. The predicted curves below for the foams show that the model is not so good for predicting the IL performance for the lowest damping foam 14. For the higher damped foams there is good correlation between the measured data and predicted response.

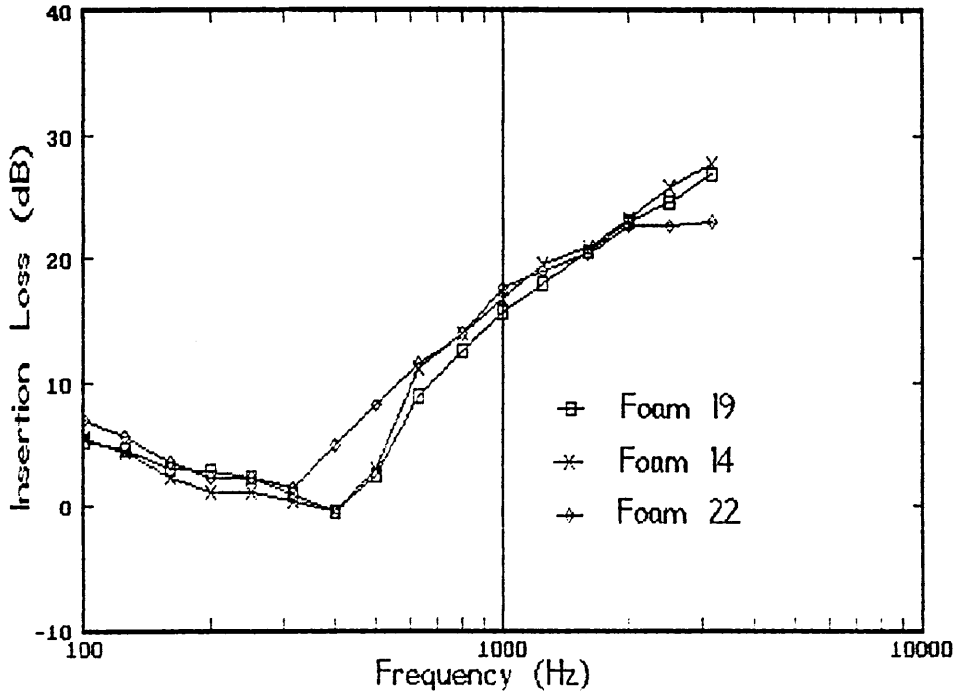

Fig. 77 Experimental influence of loss factor

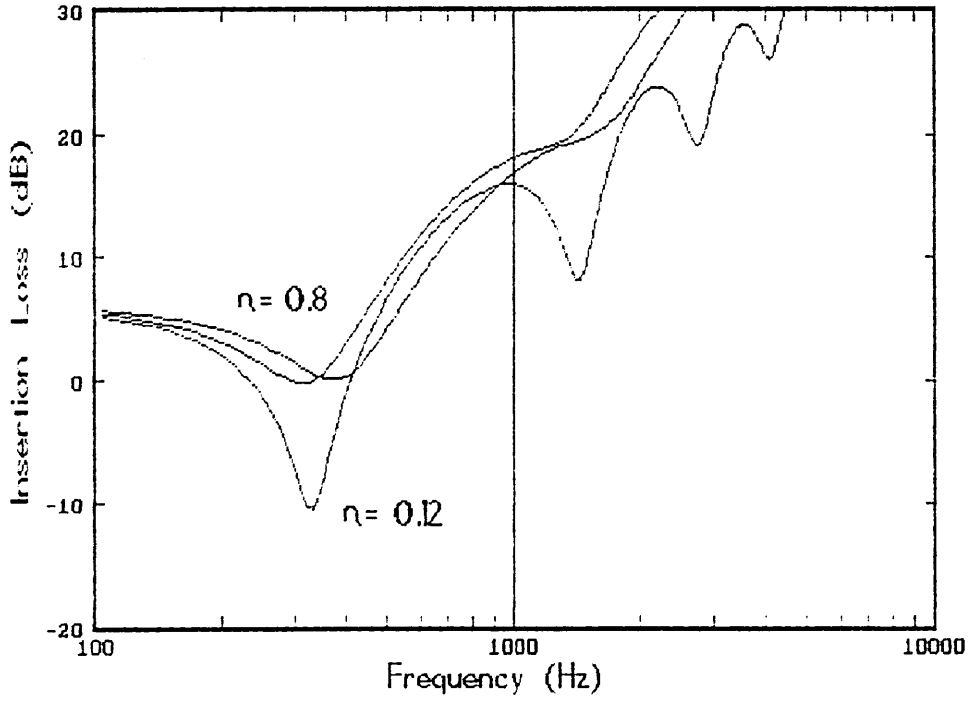

Fig. 78 Predicted IL for foams 14, 19, and 22

(b) Foam Surface Density

The three graphs below in Figs. 79 to 81 with three different septa (surface densities 3.7, 5.9 and 8.7 kgm^{-2}) are for foams 12, 4, 9 with surface densities 1.26, 1.73 and 2.00 kgm^{-2} respectively. They give the expected insertion loss characteristic shape, with a prominent minimum at the resonance frequency. Below 400Hz the best IL is achieved by the foam with the highest unit area mass (9). Above this frequency best performance is given by the medium density foam (4). As the surface density increases, it is found that the resonance frequency increases, and also that the IL of the lowest area density foam (12) approaches that of the medium area density foam (4). This is attributed to the fact that the foam surface density is small compared with the septum surface density, and thus the septum becomes the dominating contributor to system surface density. As with the data for structure-borne insertion loss the practical difficulty of producing materials with constant physical properties is seen. Based upon the predictions given in Chapter 2 the slightly lower modulus of foam 12 should reduce the resonant frequency of the composite. If this is the case then it could explain why the medium density foam, 4, ($1.73kgm^{-2}$) gives the best IL performance in the post-f_R region. These data, like most others in this investigation show that the overall airborne noise IL response is controlled in the main by the resonance, or trough, frequency.

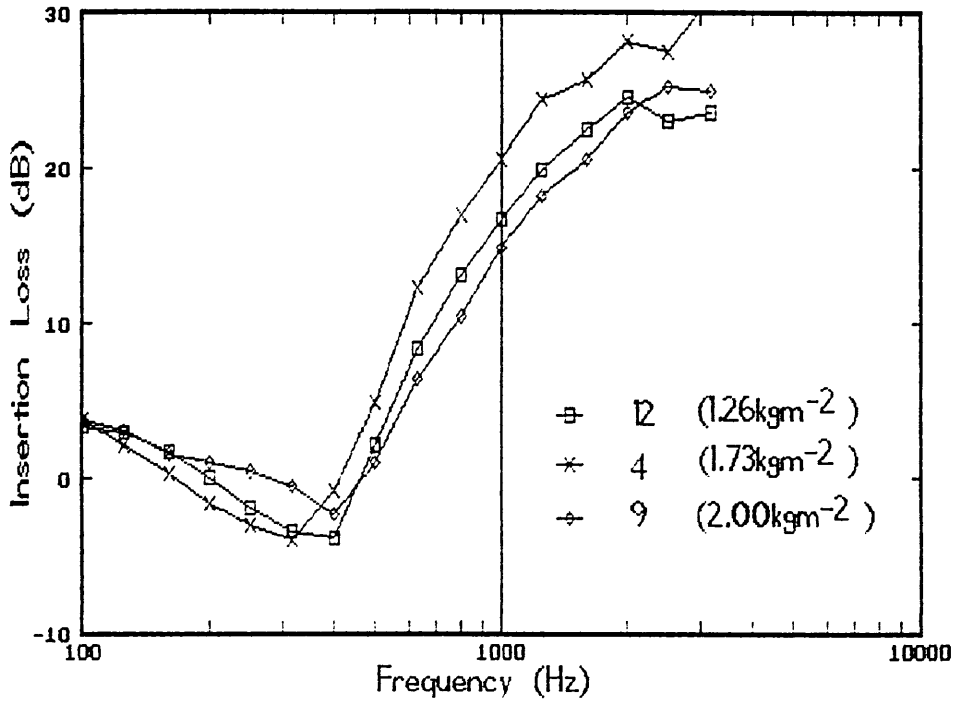

Fig. 79 Effect of foam surface density (3.7kgm^{-2} septum)

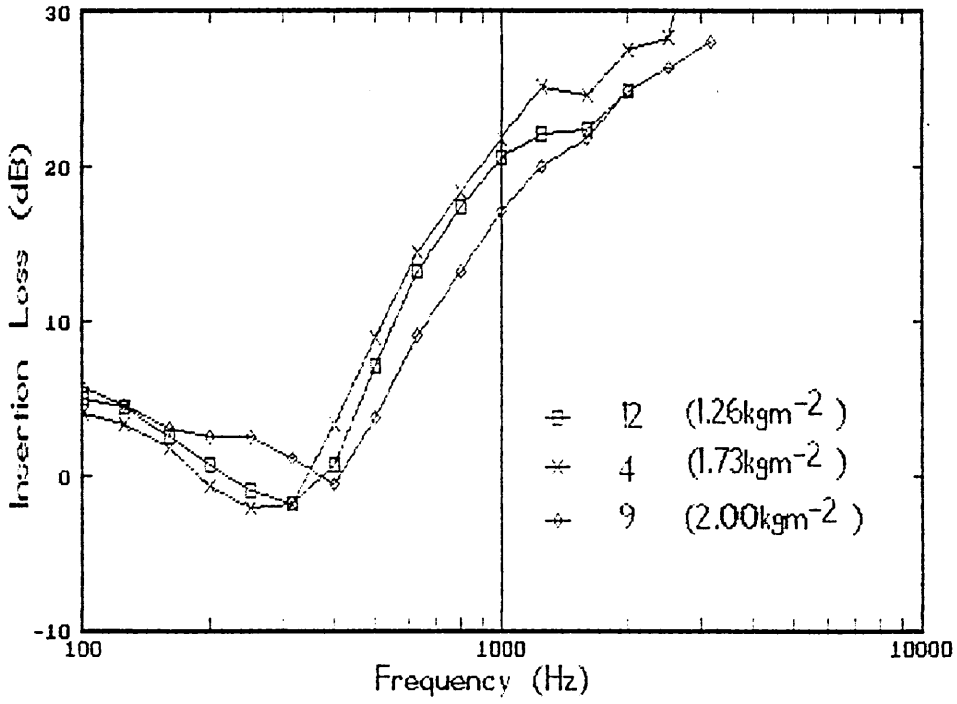

Fig. 80 Influence of foam surface density (5.9kgm^{-2} septum)

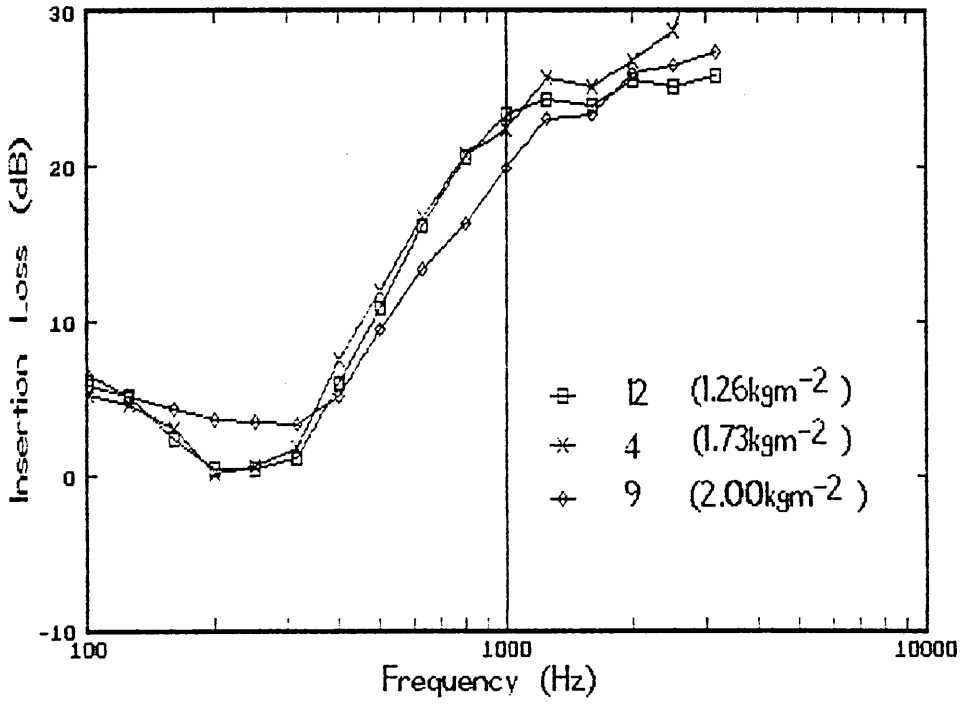

Fig. 81 Effect of foam surface density (8.7kgm^{-2} septum)

(c) Foam Modulus

The theoretical predictions of the model in Chapter 2 indicate that an increasing modulus should increase the resonance frequency, f_R, and shift the IL response curve up the frequency spectrum.

IL measurements for foams 5, 4 and 6 are used to demonstrate the effect experimentally, and are shown in Fig. 82. The foams had moduli of 0.41×10^5, 1.17×10^5 and 3.72×10^5 Pa respectively.

The experimental IL behaviour for the foams differ in some respect from the theoretical analysis in Section 2.11 above. It is observed that the positions of the lower two foams is reversed, with the f_R for foam 4 occurring a third octave lower than for foam 5. The corre-

sponding IL curves are also opposite to that expected. If we examine the predicted IL values for foams 5 and 4 in Fig. 83 it is seen that the resonances occurs close together. The measured behaviour of foam 6 in Fig. 82 is as expected from the prediction; i.e. a high resonance frequency and lower values for the post f_R IL.

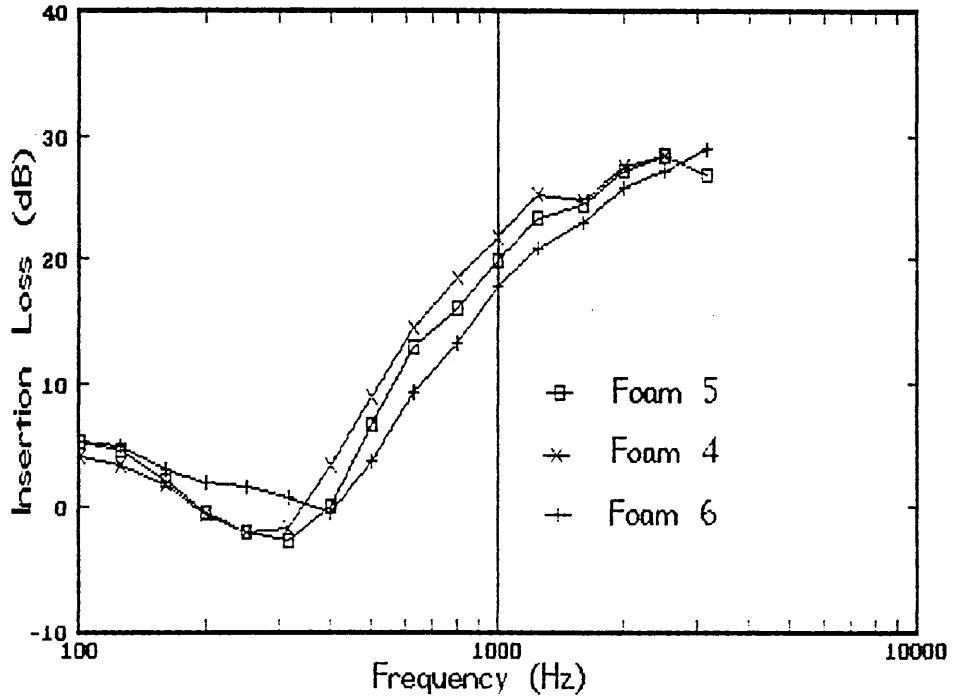

Fig. 82 Effect on measured IL of foam modulus

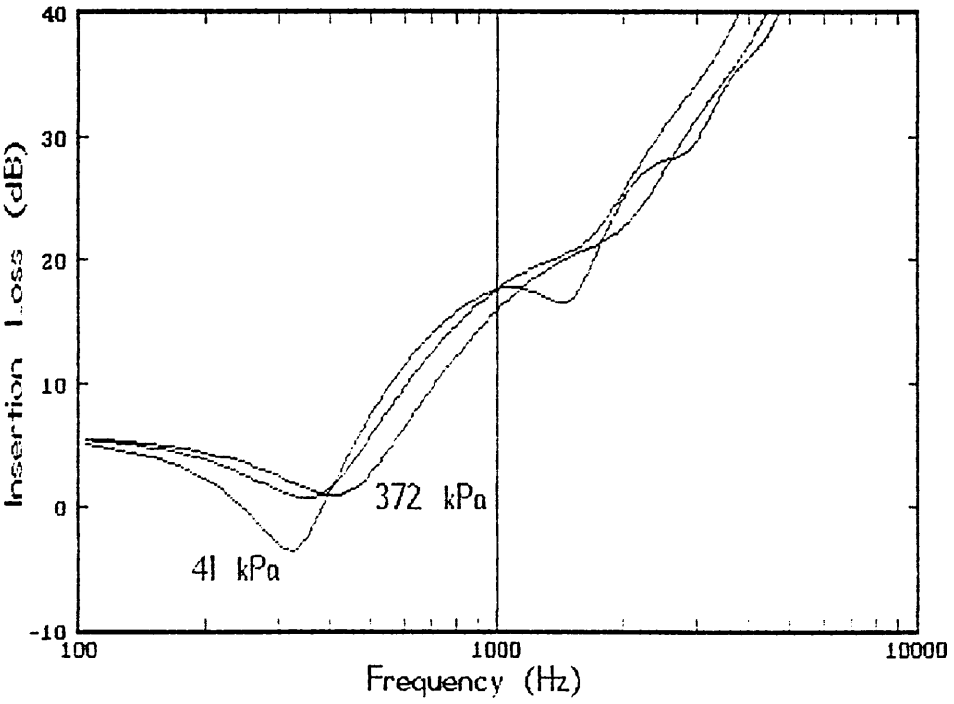

Fig. 83 Predicted IL for foams 5, 4 and 6

5.4.5 System Parameters

(a) Foam Thickness

Theoretical predictions from Chapter 2 indicate that the airborne IL is highly dependent upon foam thickness. Increasing the foam thickness reduces the resonance trough and increases the post-f_R IL level. This influence of foam thickness was examined experimentally with foams 17, 14, 16 and 8, 3, 8+3. Experimental data is shown in Figs. 84 and 86. These foams had nominal thicknesses of 10, 20 and 30mm respectively. The experimental data show a decrease in resonance frequency with increasing thickness as predicted in the model (e.g. in Figure 86). The insertion loss performance of the 20mm and 30mm foams is comparable above resonance, which is contrary to the predicted behaviour shown in Fig. 86. The predicted IL shows a larger difference between the foams than observed experimentally. The prediction is very good for foam 16 (10mm), but for the other two foams the IL at the resonance is larger than measured. However, the predictions do offer a reason for the similarity in the IL of the 20mm and the 30mm foams. The second resonance whilst being apparent for the measured IL of foam 16 (30mm), does not manifest itself on the IL measured for foam 14 (20mm). The lack of second resonance might be caused by a change in loss factor at higher frequencies.

In Fig. 86 the IL for 8, 3 and 8+3 is shown (thicknesses 10, 20 and 30mm respectively). It is seen that the measured behaviour agrees with the theoretical prediction. An increase in thickness reduces the resonance frequency and also the IL level above resonance. Below

the resonance, the measured data is comparable. For these foams the loss factor is higher (approximately 0.43) compared with 0.1 to 0.2 for foams (17, 14 and 16). The model appears able to predict the insertion loss better for foams of moderate to high damping than low damping foams. It is likely that this is due to the dependence in practice of foam loss factor upon frequency. This was demonstrated in Section 5.2.

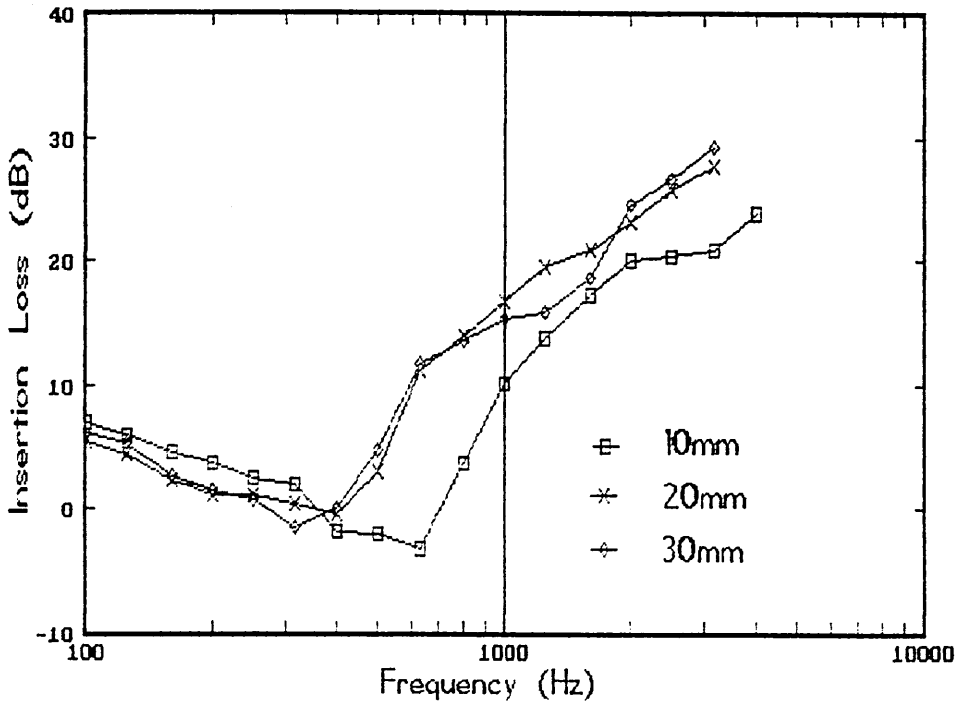

Fig. 84 Measured insertion loss - foams 17, 14, 16

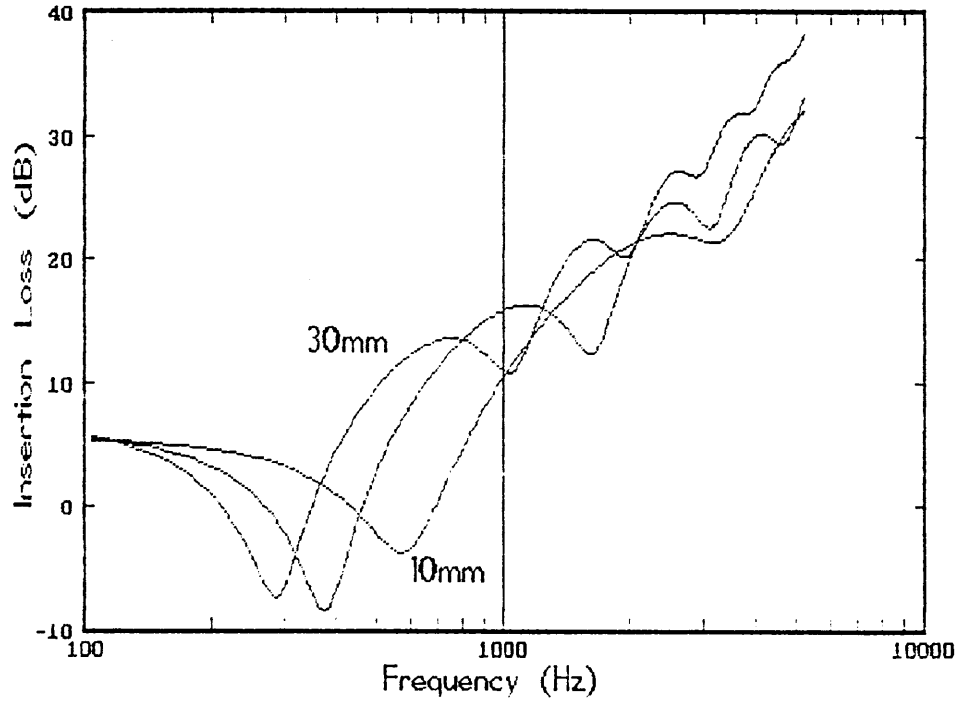

Fig. 85 Predicted insertion loss foams 17, 14, 16

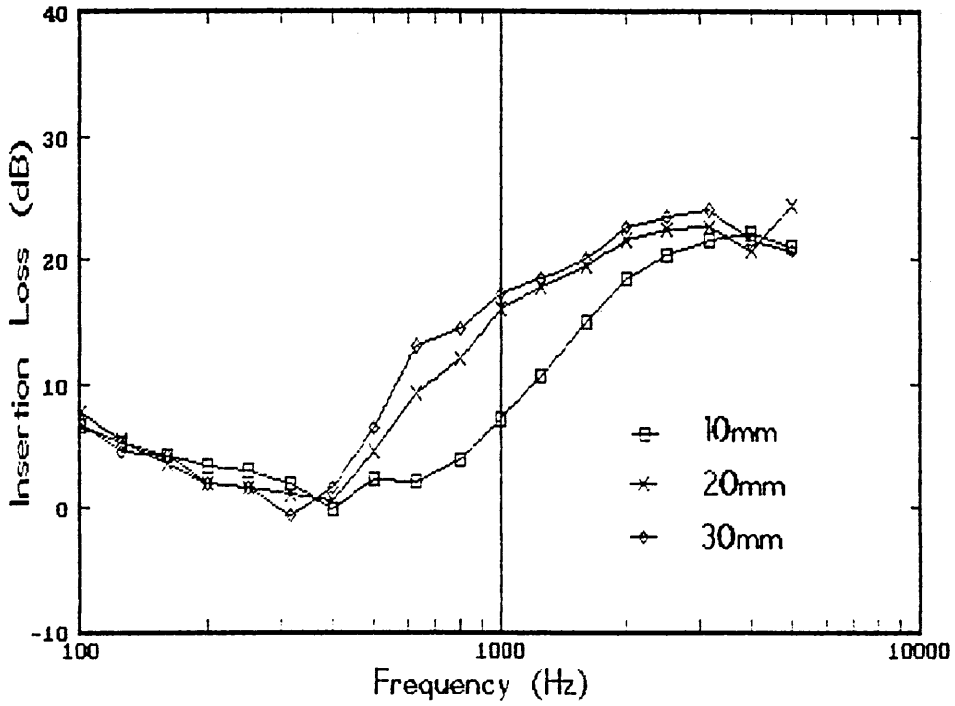

Fig. 86 Influence of thickness upon IL for foams 8, 3 and 8+3, with 5.9kgm^{-2} septum

(b) Septum Layer

The experimental data agrees with the trend predicted by the theoretical model in Chapter 2, i.e. with increasing septum area density the resonance frequency decreases and the post-f_R IL level.

If we examine the IL for foam 12 in Fig. 87 we see that the predicted behaviour is observed. The model predictions in Fig. 88 agree well with theoretical performance. The predicted resonant frequencies are slightly higher than those observed in practice. The influence of septum area density was examined experimentally for foam 12 and 4 in Figs. 84 and 86.

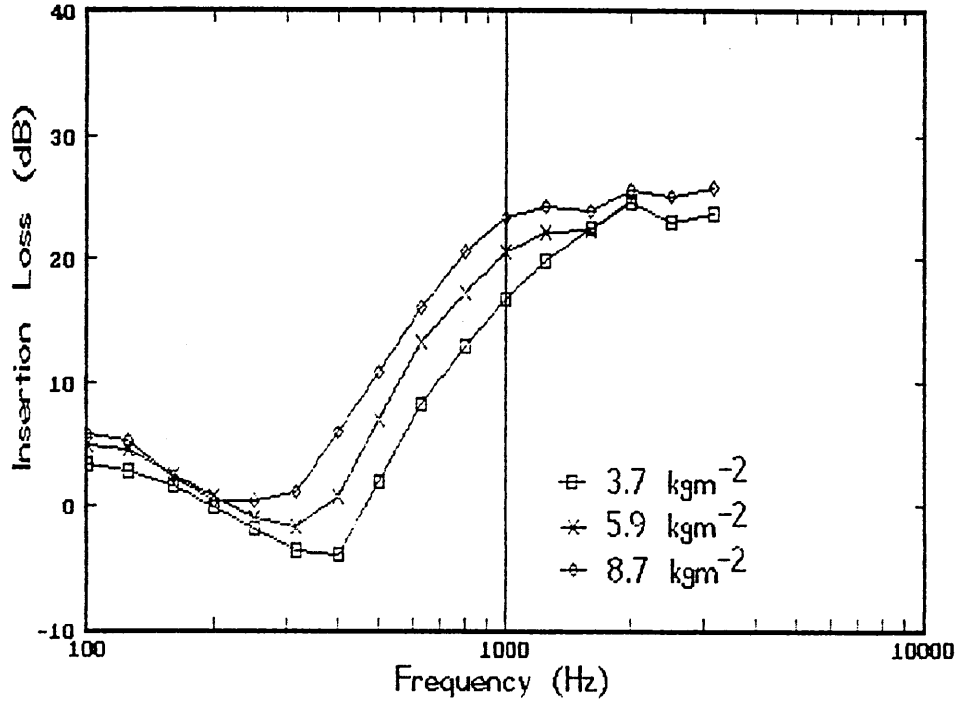

Fig. 87 Measured influence of septum surface density - 3.7, 5.9, 8.7kgm^{-2} (foam 12)

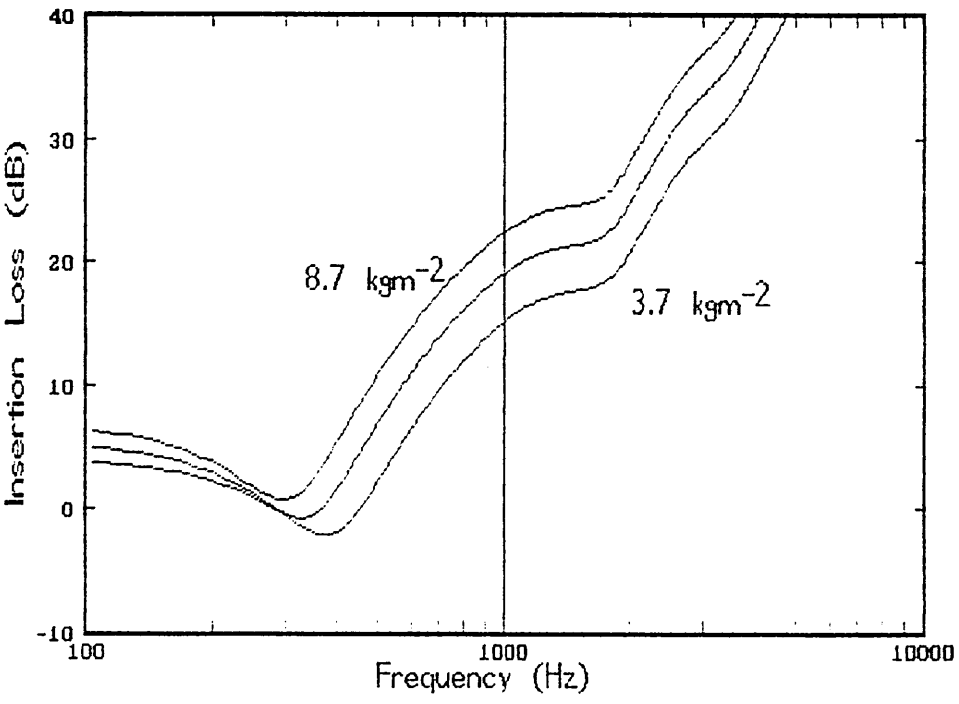

Fig. 88 Predicted influence of septum surface density - 3.7, 5.9, 8.7kgm^{-2} (foam 12)

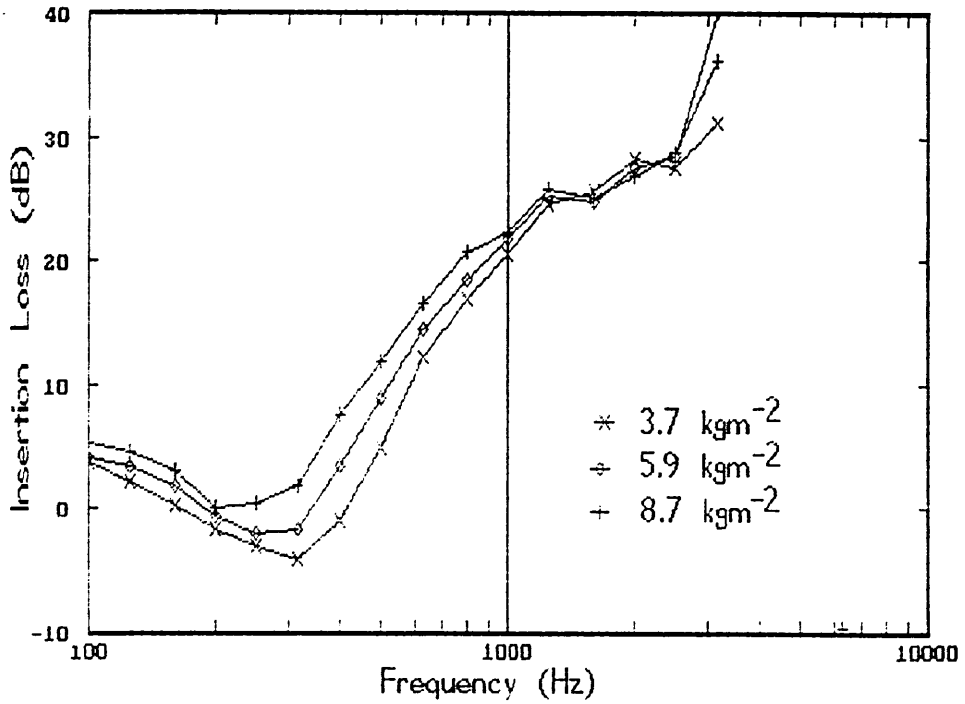

Fig. 89 Measured influence of septum surface density - 3.7, 5.9, 8.7kgm^{-2} (foam 4)

Conventional automotive carpet systems have made use of a fibrous felt instead of the PUR foam. The measured IL for a typical felt with area density of 1.41 kgm^{-2} is shown in Fig. 90. It can be seen for the three septa that the resonance trough occurs at approximately 200 Hz. Below this frequency the behaviour is comparable. Above resonance the rate of increase in IL is similar to that with PUR foams. The trend is as for the PUR foams, i.e. with increasing septa surface density the IL increases. However, above 1 kHz the behaviour is again comparable. In the resonance region it is observed that the IL is well below 0 dB, performing worse than the foams. This is attributed to the very low storage modulus (0.05x10^5 Pa at 26 Hz).

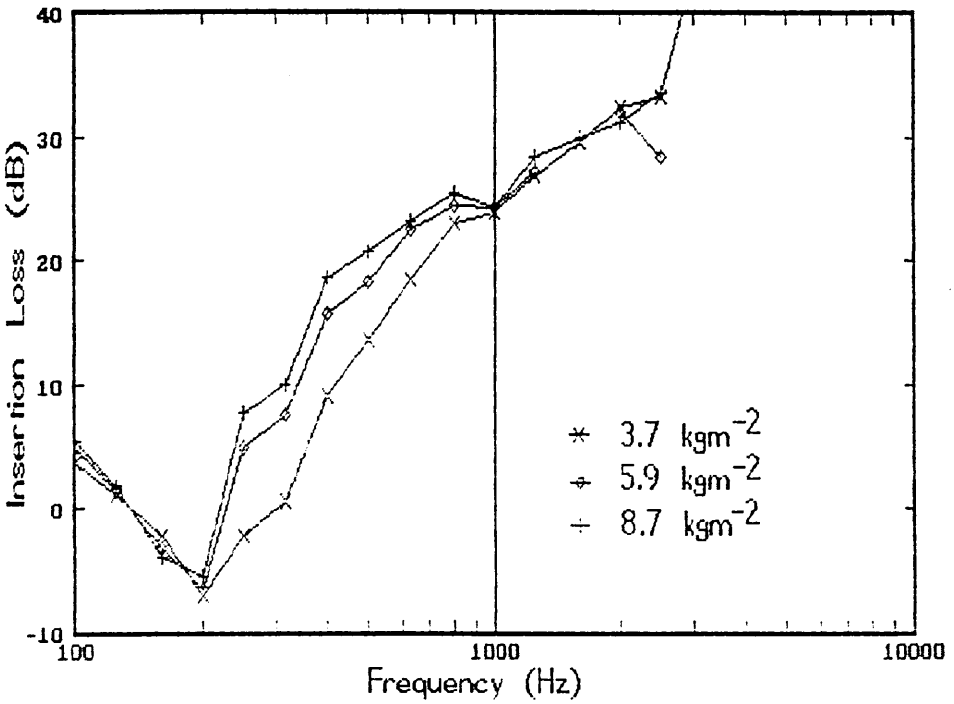

Fig. 90 Influence of septum surface density upon IL for Felt

If the experimental IL is compared for a 3.2 kgm^{-2} rubber septum and a 3.7 kgm^{-2} EVA septum it is seen that even though the EVA septum has a higher stiffness than the rubber septum the behaviour is similar. This shows that septa stiffness does not contribute greatly to the insertion loss. This is shown for foams 10 and 11 in Figs. 91 and 92.

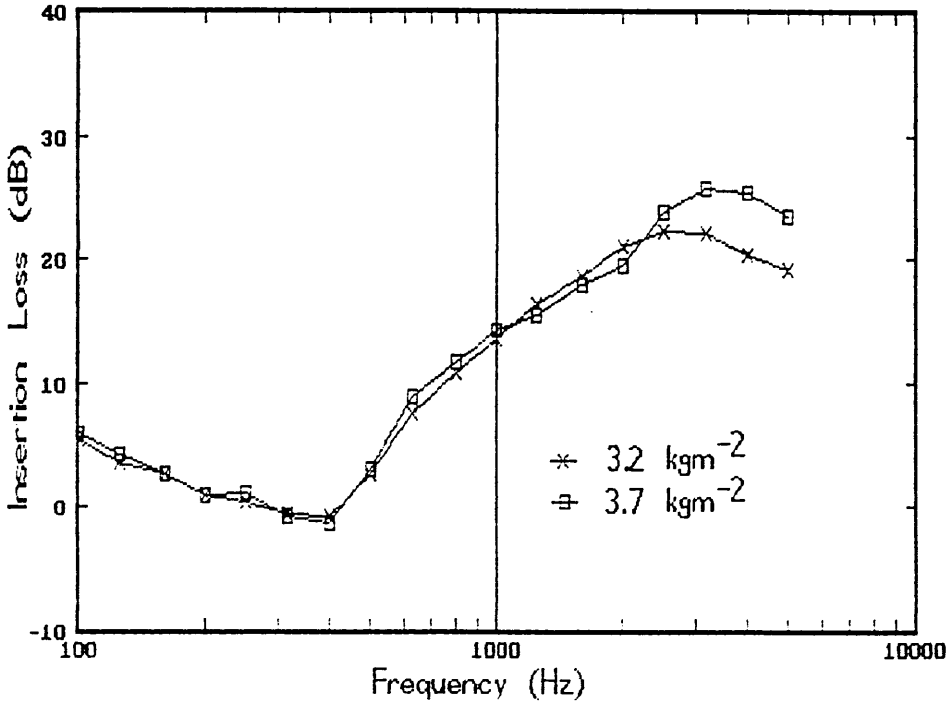

Fig. 91 IL of EVA and rubber septa for foam 10

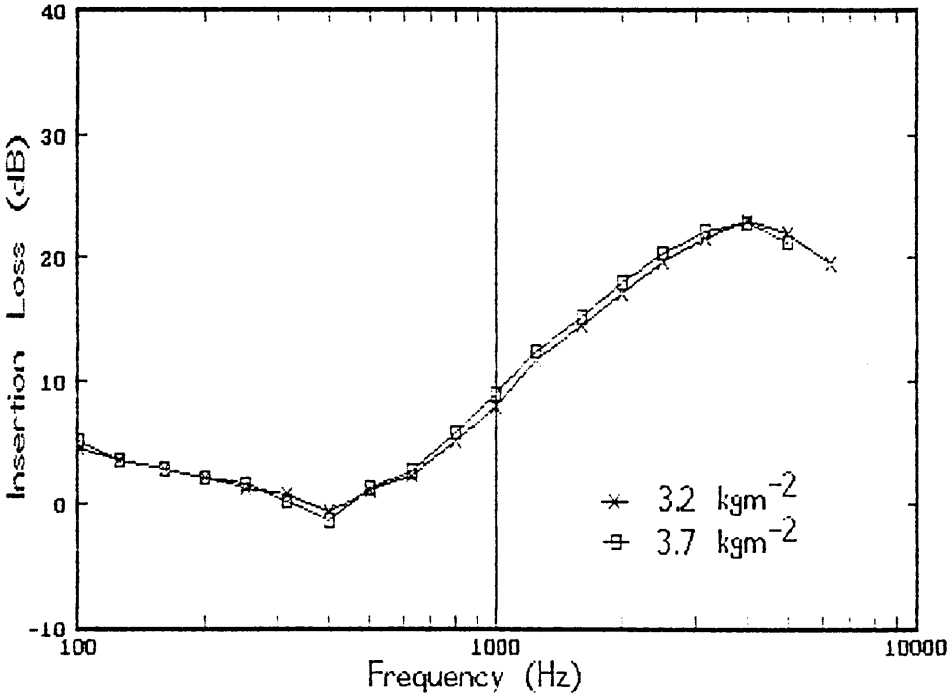

Fig. 92 IL of EVA and rubber septa for foam 11

The IL for the steel panel and septa is shown in Fig. 93. It is seen that the IL level increases with increasing surface density. At approximately 2 kHz there is a resonance which causes the IL to approach or be less than 0 dB. Above this resonance the insertion loss increases steeply. The resonance is caused by a combination of the trapped air beneath the septum, and the septum stiffness and surface density.

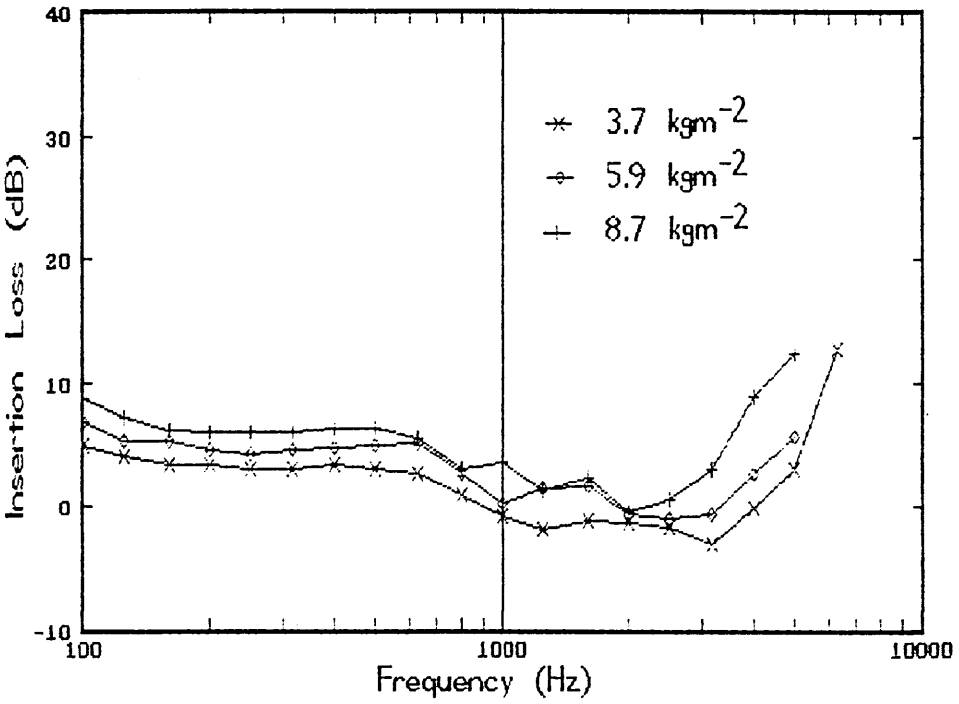

Fig. 93 Insertion loss of steel panel and septum

(c) Carpet

A carpet, typical of that used for automotive purposes, was added to the foam and septum. The carpet had a surface density of 0.99 kgm^{-2}, with a nominal thickness of 0.01m.

The measured IL is shown for foams 4 and 10 in Figs. 94 and 95 with 3.7 kgm^{-2} and 5.9 kgm^{-2} septa respectively. It can be seen that the addition of the carpet degrades the IL at high frequencies. This is more clearly demonstrated by examining the additional IL that the carpet provides to the system for a range of septa mass. This is illustrated in Figs. 96 and 97 for foams 4 and 10. The curves show a dip in IL in the region of 1-2 kHz. This is due to the stiffness of the carpet and enclosed air causing a second resonance, thus causing the curves to be similar to those obtained for steel panel and septa in Section (b) above.

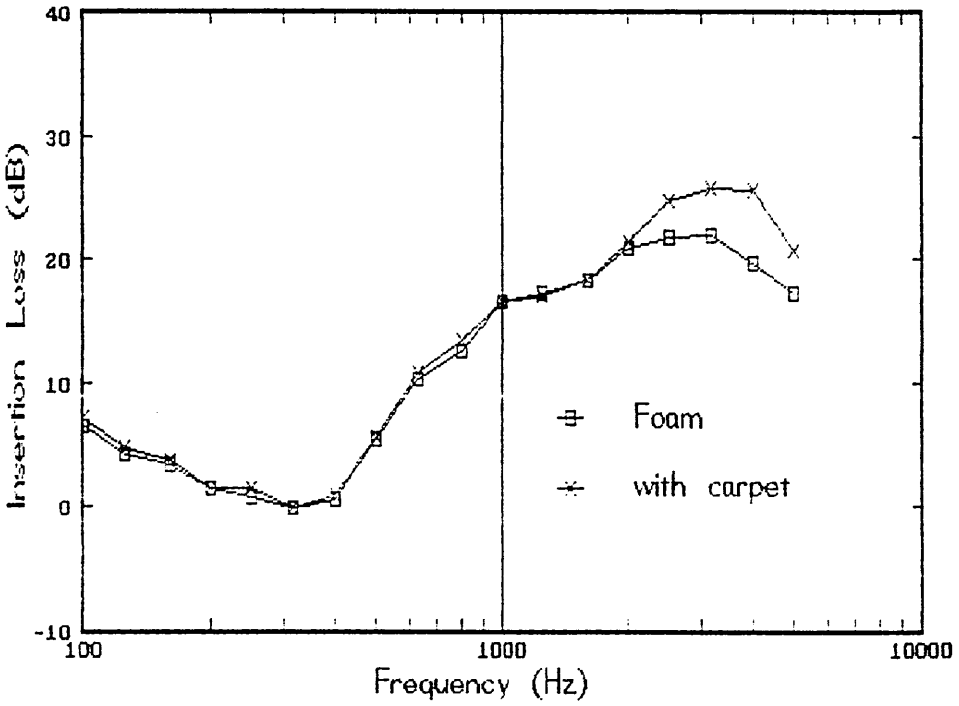

Fig. 94 Influence of the addition of carpet on IL for foam 4 with 3.7 kgm^{-2} septum

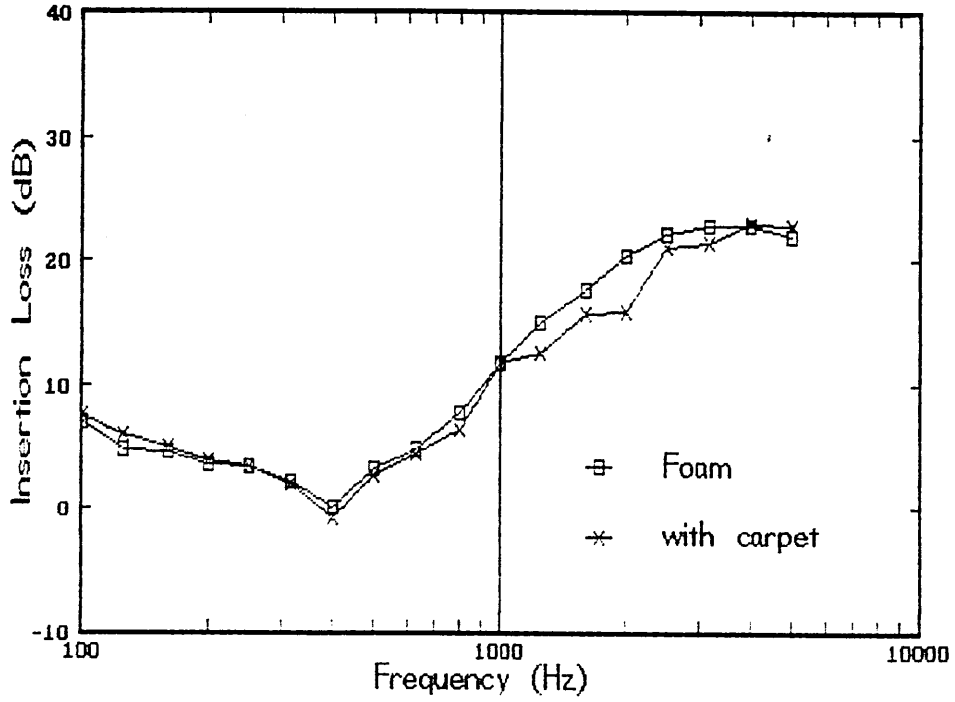

Fig. 95 Influence of the addition of carpet on IL for foam 11 with 5.9 kgm^{-2} septum

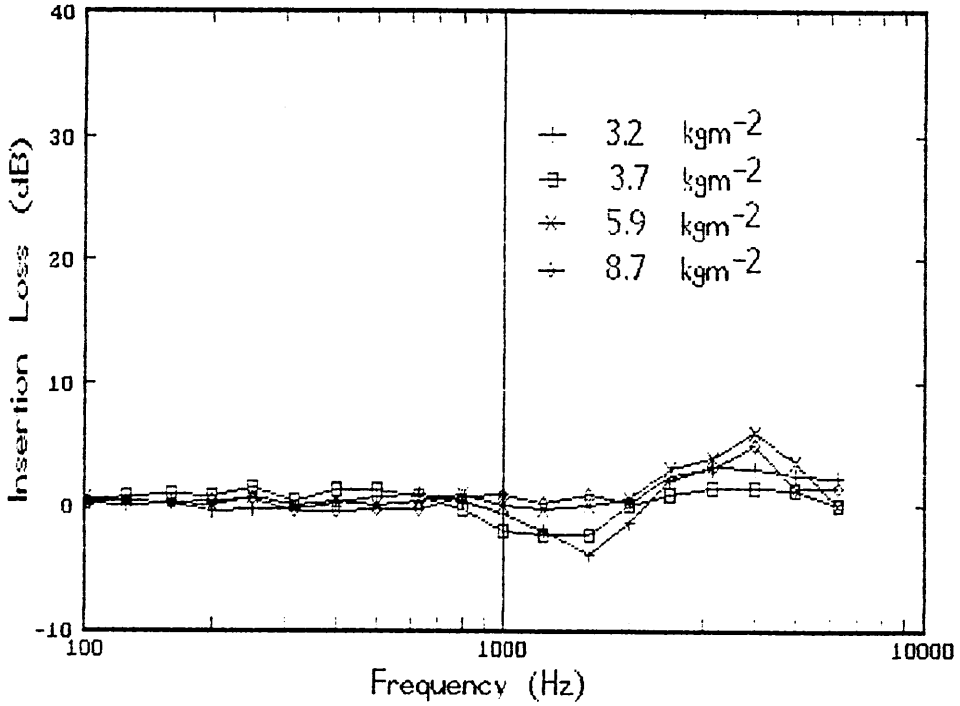

Fig. 96 Influence of the addition of carpet on IL for foam 4 with 3.2, 3.7, 5.9, and 8.7 kgm^{-2} septa

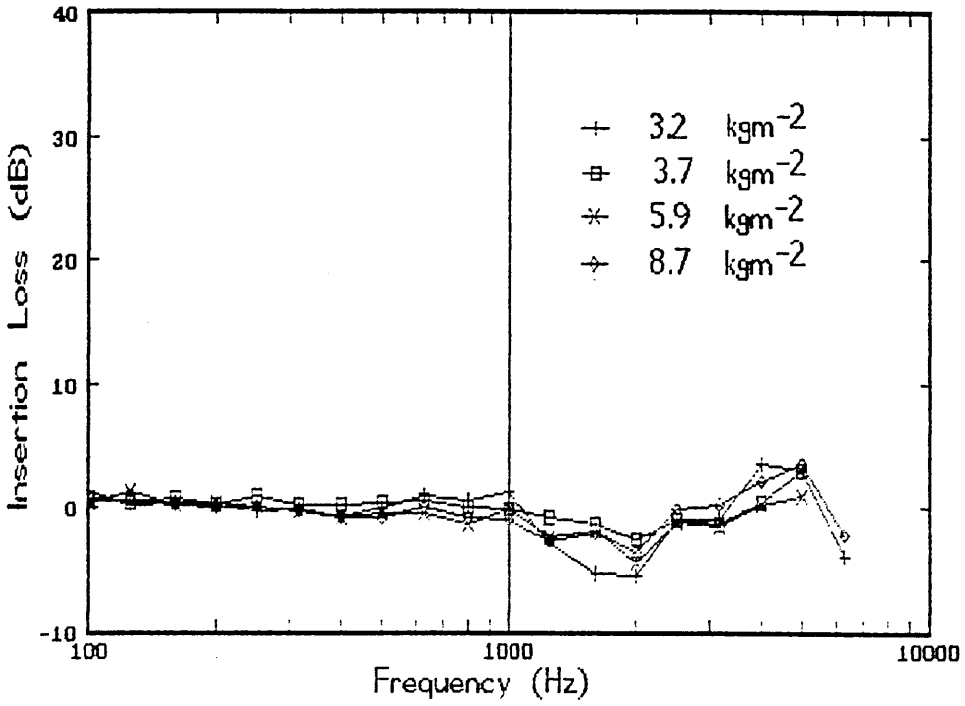

Fig. 97 Influence of the addition of carpet on IL for foam 10 with 3.2, 3.7, 5.9, and 8.7 kgm^{-2} septa

5.5 Conclusions of Chapter 5

This chapter has presented experimental data for polyurethane foam cored composites, as used in vehicle applications. Where possible predicted behaviour was compared with experimental data.

More panel resonances were observed in practice than were predicted by the theory. In the frequency range 100-1000Hz there was good agreement between the measured and predicted frequencies for the principle modes. Vibration response curves showed that the addition a foam layer to a vibrating panel reduced the modal response. This was further reduced by the addition of a septum layer. Increasing the surface density of the foam had little observed effect on modal

response. Increasing the foam damping reduced the modal response as would be expected.

Effective loss factors were obtained for the panel and composite. Loss factors were found to decrease with increasing frequency, in agreement with other published data for vehicle composite systems (Plunt, 1991). For the 1mm steel panel effective loss factors ranging from 0.008 at 100Hz to 0.0003 in the 6300Hz 1/3 octave band were measured. Little change was observed with the addition of a septum. Comparisons were also made between predicted and measured loss factors. Predicted damping values were much lower than measured data. This increase in system damping was attributed to frictional damping.

Results were presented for structure-borne insertion loss, using the intensity technique described in Chapter 3. The pressure-intensity (p-I) index was generally <10dB, and satisfied the requirements for precision and engineering grade measurements. Measurement reproducibility was found to be poor due to the coupling of the shaker to the panel. However trends in behaviour were comparable. Experimental data demonstrated the importance of system and material parameters. Variation in modulus had little effect upon the composite insertion loss. A foam density of $1.8kgm^{-2}$ gave the best IL, though this could be attributed to other material properties changing. Above 400Hz the thickest foam (30mm) gave highest IL levels. Increasing the septum surface density increased the IL. Systematic variation in the first resonance frequency as predicted by the theoretical model were not observed in practice. Comparison between predicted and measured data was poor, though the general position of the resonance frequency and

level of IL was predicted reasonably well.

Airborne insertion loss data was also presented for the foam composite systems. Measurement reproducibility was good (~1.5dB for f<2kHz~). Larger differences were attributed to measurement errors and variability in sample installation. The p-I index was generally less than 10dB and satisfied the requirements for precision and engineering grades of measurement accuracy.

Initial model predictions did not compare particularly well with measured IL behaviour. An empirical fitting constant for the effective modulus of the foam core was incorporated into the model. Values of resonance frequencies predicted using this modification were shown to be in good agreement with measured values. The model predicted system insertion loss better for moderate to highly damped foams than for low damped foams. The data demonstrated the relative importance of system and material parameters. Foam damping was shown to have little effect upon insertion loss. As with structure-borne excitation a medium density foam ($1.73kgm^{-2}$) was shown to give best IL performance. Generally predicted behaviour agreed with the experimental data. Increasing foam modulus increased the resonant frequency, shifting the IL curve up the frequency scale. With increasing foam core thickness the f_R decreased, increasing the post-f_R IL level. Increasing the septum surface density also decreased the resonant frequency. Septum stiffness had little observed effect, whilst the addition of a carpet layer reduced the IL at frequencies greater than 2kHz.

The data demonstrated that the overall airborne insertion loss

response is controlled by the resonance frequency. Increasing the resonant frequency, f_R, shifts the IL curve up the frequency scale reducing the high frequency IL level.

A major difficulty associated with the interpretation of data presented in this chapter is the variation in the physical and mechanical properties of the moulded test materials e.g. density, modulus, damping and airflow resistivity. Only in one test regime was it possible to examine the influence of a single design variable whilst all others remained constant. That was when examining the influence of septum surface density with the same foam test piece. For the airborne insertion loss the effect of changing septum density was highly reproducible and the observed changes in response conformed well with the predictions of the theoretical model. This is also true, to some extent, for the vibration-borne insertion loss but the reproducibility was not so good. Thus a systematic investigation of the parameters that influence the noise insulation and isolation behaviour of foam cored composites is constrained by the ability to manufacture large test area test pieces in which only one physical characteristic is altered at a time.

6 CONCLUSIONS AND RECOMMENDATIONS

6.1 Introduction

The purpose of this work was to examine the airborne and structure-borne behaviour of multi-layered polyurethane foam cored composites and to identify ways of optimising their design. These systems are used by the automotive industry as under-carpet treatments to reduce vehicle interior noise. To isolate the parameters that affect the response of these composites to noise and vibration a systematic theoretical and experimental study was carried out. The system essentially consists of a steel panel (vehicle floorpan), an isolating core (PUR foam) and a septum layer (EVA and carpet). Theoretical models of the system were developed in Chapter 2 to predict the effective loss factor of the system and the acoustic insertion loss behaviour of a model system, for either structure-borne or airborne noise. To establish the validity of these theoretical predictions experimental studies were made of the system acoustic insertion loss performance using a laboratory scale test facility with an intensimetry technique.

6.2 Laboratory Test Facility

Large scale test facilities, such as the ISO 140 transmission suite, were not considered suitable for this industry related project so a smaller scale test facility was built. It was designed to enable the testing of horizontal unbonded materials and systems. The facility was developed from a simple industrial design which initially proved to be unsuitable. The final form was of a brick and concrete con-

struction, with dimensions of 900 x 900 x 1030 mm. An 870x870mm aperture in the top was covered by a steel panel typical of that used in the automotive industry. Excitation was provided by either an electromagnetic shaker connected to the panel or by an array of loudspeakers within the cavity. The essential design configuration was based upon accepted industrial testing facilities for automotive carpet systems.

6.3 Panel Dynamic Behaviour

6.3.1 Modal Response

The theory of panel vibration and radiation identified the importance of panel response in the radiation of sound. The vibration response of the test panel to a constant acceleration excitation was measured for a number of system configurations *in situ* on the test facility i.e. C-C-C-C. The clamped panel exhibited a large number of resonant modes and a high modal density. The modal frequencies predicted by the theory of Warburton (1954) and Leissa (1969) have been compared with measured data. At low frequencies (f<100 Hz), modes additional to those predicted were introduced into the system by the system constraints which made comparisons difficult. However, in the frequency range of interest (f>100 Hz), the magnitude of the additional modes was lower, and good agreement was seen between predicted and measured data. It was thus shown that for the test system the panel mode frequency equation <7> was a good representation of system behaviour in the frequency range investigated.

The theoretical analysis showed that radiated noise from a panel was

related to its velocity. Reduction in the panel velocity would thus reduce radiated noise. This can be achieved by increasing panel damping by the addition of damping materials. This was previously demonstrated by Oberst (1954) in the form of unconstrained and constrained damping layers attached to a panel. The reduction of panel vibration response was observed experimentally by the addition of PUR foam layers. Reductions of the order of 10 dB were observed for some resonances. The addition of a septum layer to the panel and foam decreased the vibration level further, typically by an additional 8 dB. This reduction was more noticeable at low frequencies ($f<250Hz$). Modal frequencies were observed to be shifted, for some modes by as much as 6 Hz, due to the added foam layer. Panel response was also affected by material damping. Increasing the material damping reduced the mode amplitude. This resulted in the response curves appearing to be smoothed.

The addition of a foam, or foam and septum layer can thus be used to reduce panel vibration. Reduction in panel vibration can be further enhanced by increasing the material damping.

6.3.2 Effective Panel Loss Factor

To examine the influence of the foam layers on panel damping, the effective loss factor of the panel, i.e. the loss factor of the clamped panel *in situ*, was measured using a decay method. The measurements were for third octaves bands. This technique was chosen in preference to other methods for a number of reasons; primarily because modal bandwidth measurements were not possible due to the close spacing of resonant modes and also because instrumentation was

not available for implementation of the steady state and power injection methods. Loss factors measured using the decay method are reported to give a systematically lower values than the power injection method (Bies *et al*, 1980, Plunt, 1991). The measured data showed that the loss factor of the panel without damping treatments decreased with increasing frequency from 0.008 at 100Hz to 0.0003 at 6300Hz. This behaviour was between that reported by Plunt (1991) and Tarnoczy (1970). The addition of a PUR foam layer increased the effective loss factor by a factor of approximately ten at low frequencies. At high frequencies the *in situ* loss factor was similar to that of the steel panel alone. The increase in effective loss factor by the addition of a septum layer to the panel and foam was small. Increasing the septum mass increased the measured loss factor. Plunt (1991) reported similar behaviour for vehicle carpet systems using the power injection method.

Theoretical predictions of the panel loss factor using the Oberst (1954) model in Equation <9> for bonded unconstrained layers gave systematically lower loss factors than those measured experimentally over the range of frequencies that could be compared. This implies, that extensional damping is not the only damping mechanism present. The additional damping was attributed to frictional damping due to the stick/slip of the panel and foam.

6.4 Insertion Loss Measurement

A technique, using sound intensity, was described in Chapter 3 to measure the insertion loss of composites. The method involved the measurement of radiated intensity from the steel panel with and

without the composite in place. The insertion loss is obtained by the subtraction of the two measurements.

The errors involved were examined and it was estimated that the measurement accuracy was 1.7dB below 4kHz and 1.2dB below 2.2kHz. The influence of extraneous stationary noise sources and temperature variation was shown to be insignificant due to the short time interval over which measurements were made.

6.5 Transmission of Structure-Borne Noise Through Composites

No models were found in the literature for the prediction of the insertion loss of a three layer composite subject to structure-borne excitation. A simple theoretical model was developed based upon a lumped parameter representation of the system, and the theory of Cremer *et al* (1988). The ratio of the damping of the system to the steel panel was calculated using an empirical relationship obtained from the data of Plunt (1991). The predicted IL demonstrated a resonance trough at low frequency, and a rapidly increasing IL with increasing frequency. The model predicted that the main system parameters were foam core thickness, septum surface density and foam modulus. The variation of these parameters affected the position of the resonance trough and the IL level over the remaining frequency range;

(1) Foam damping affected the level of the IL in the resonance trough; the level being reduced with increasing foam loss factor.

(2) Increasing foam core thickness reduced the resonance frequency and shifted the IL curve down the frequency scale.

(3) Increasing the septum surface density reduced the frequency of

the resonance trough, shifting the IL curve down the frequency scale.

(4) The model predicted that increasing the foam modulus would increase the resonance frequency and consequently shift the IL curve up the frequency scale.

Experimental data was obtained using intensity equipment and the method described in Chapter 3. Measurement repeatability was shown to be poor. This was due to the poor coupling between the shaker and the panel. However, trends observed in the experimental data were consistent between repeated measurements. The measured insertion loss were positive over the whole measured frequency range. A characteristic shape was decreasing IL with increasing frequency to a first resonance, then increasing IL to a second resonance trough at higher frequency. The p-I index used to assess the validity of intensity measurements was within specified limits, and satisfied the requirements for both precision and engineering grade measurements. Some difficulty was encountered in investigating the influence of a single material parameter due to variation of other material property values resulting from the manufacturing process of the polyurethane foam test pieces.

The structure-borne insertion loss of the composite was predicted using the measured material property data in Tables 6 to 8. The theoretical model was moderately successful in predicting system response at frequencies below 1kHz. The position of the first resonance trough was predicted well though the predicted IL levels at resonance were below measured values. Detailed comparison of predicted and measured IL response was not possible due to the poor

reproducibility of the measured data. The use of measured data values to obtain an expression for the ratio of composite to steel panel damping gave a higher value than used in the model. The effect of this upon the IL was shown to be an increase in IL level of approximately 10dB. This resulted in the overall level being predicted incorrectly except at the resonance where agreement was now achieved. It was postulated that the system damping was overestimated due to the damping measurement technique. A number of mechanisms were considered as causes for the model to unsatisfactorily predict the system response at high frequencies. Firstly the influence of wave effects at high frequencies. Secondly the damping ratio being predicted too high. Thirdly the radiation efficiency was assumed identical for the steel panel and the composite system. This might not be a valid assumption. Fourthly, the parameters used in the model were single frequency values whereas in practice the properties are frequency dependent.

No theoretical models were found in the literature to predict the response of vibration excited unbonded multilayered composites. The model developed here, despite its drawbacks, therefore provides a reasonably accurate prediction of system response below 1kHz, and as such provides a useful prediction tool for the development engineer.

The experimental structure-borne insertion loss results demonstrated the influence of system and material parameters. These were:

(1) Increasing material damping improved the IL at frequencies greater than 250Hz.

(2) A foam of surface density of 1.8kgm^{-2} gave the best IL for the

frequency range 300<f<1000Hz.

(3) Foam modulus did not significantly influence the measured IL.

(4) A thick foam (30mm) gave the best IL at low and high frequencies, whilst the thinnest foam (10mm) provided the best IL at mid-frequencies.

(5) Increasing septum surface density resulted in increased IL. The predicted decrease in resonance frequency was not observed.

6.6 Transmission of Air-Borne Noise Through Composites

A theoretical analysis of the transmission loss of three layered PUR foam cored panels was developed using a transmission line approach, similar to that used by Beranek (1949). The impedances of the individual elements are used to obtain overall system transmission loss. The mass law transmission loss was then used to calculate the transmission loss of the steel panel. Subtraction of these two theoretical predictions gives the composite IL which was used to compare with experimental data.

The predicted airborne insertion loss curves had a characteristic shape of a resonance trough at low frequency, then increasing with frequency. Secondary resonance troughs were predicted at higher frequencies.

The theoretical model predicted the influence of material and system parameters. The principle parameters were foam modulus, core thickness and septum surface density. The predictions showed that the effect of varying these parameters was;

(1) Increasing foam modulus increased the resonance frequency and shifted the IL curve up the frequency scale.

(2) Increasing the foam core thickness reduced the resonance frequency, and thus the post-f_R IL was increased.

(3) Increasing the septum surface density also reduced the resonance frequency and shifted the IL curve down the frequency scale.

(4) Foam damping reduced the IL at the resonance troughs.

Experimental data was obtained using the intensimetry technique described in Chapter 4. The characteristic shape predicted by the model was seen experimentally, though secondary resonances were not always observed. Measurement repeatability was shown to be good. Differences of 1.5dB between sets of data were observed below 2kHz. The p-I index was used to assess the validity of intensity measurements and found to be within specified limits, satisfying the requirements for precision and engineering grades of measurement.

The insertion losses of the composite systems were predicted from the model representation given in Chapter 2 and measured values of material properties. Initially the predictions did not agree particularly well with measured behaviour, the predicted resonance frequency being less than that observed experimentally. However, when a fitting constant parameter was introduced better agreement was obtained. The need for this fitting constant can be attributed to (i) the value of the air enclosed by foam matrix being closer to the adiabatic value (1.4×10^5Pa) rather than the isothermal value (1.1×10^5Pa) indicated in Chapter 2, and (ii) the frequency dependence of the mechanical properties of the foam. Comparison of predicted and measured resonant frequencies showed that with the modi-

fied modulus the resonance frequency was reasonably well predicted by Equation <79>;

$$f_R = \frac{1}{2\pi}\left[\left(\frac{K'_{tot}}{d}\right)\left(\frac{1}{m_{s1}} + \frac{1}{m_{s2}}\right)\right]^{1/2} \qquad <79>$$

where the modulus K'_{tot} is the modified value, $1.7K_{tot}$, from Chapter 5.

The experimental and theoretical data demonstrated the following influence of system and material parameters upon insertion loss:

(1) Foam damping principally affected the IL around the primary and secondary resonances; increasing material damping increased system insertion loss.

(2) Foam surface density affected both the resonance frequency and the overall IL. Increasing surface density increased the resonance frequency.

(3) Foam modulus strongly determined the resonance frequency. Increasing the foam modulus caused an increase in resonance frequency and a decrease in the overall IL level.

(4) An increase in foam thickness was shown to reduce the resonance frequency. Above resonance the thickest foam tested (30mm) gave the highest IL. Below resonance the highest IL was given by the thinnest foam (10mm).

(5) An increase in septum surface density reduced the resonance frequency. Highest septum surface density gave the highest IL at all frequencies.

(6) Septum stiffness was shown not to be influential upon system insertion loss.

(7) The addition of a carpet layer to the composite was shown to only significantly affect high frequencies (f>2kHz).

As previously mentioned initial comparisons of predictions with measured data indicated that a fitting constant was required. Once this was incorporated the theoretical model was used successfully to predict the system performance. The need for a fitting constant was attributed to the approximation of the propagation constant. A more accurate value of propagation constant, and thus foam impedance is required to eliminate the need for the fitting constant. The use of the theory of Biot (1956) which has been developed by Bolton (1984) is suggested to predict the impedance and propagation constant of foam materials. However, this would make calculation of insertion loss much more complex and thus computationally slow. Biot's theory also requires detailed knowledge of the foam macrostructure which is not always available, thus where possible the use of empirical values developed for PUR foams is preferable.

This work has shown that there is good agreement between the predicted and measured behaviour of PUR cored composites for airborne excitation. The model predicts the IL better for medium to highly damped foams than lower damped foams.

The data demonstrates that the overall airborne insertion loss is controlled, in the most part, by the primary resonance frequency.

6.7.1 Vibration Noise Insertion Loss

Experimental data for vibration insertion loss of composites is not sufficiently reproducible to discuss optimisation in detail. However, the importance of optimisation in terms of damping performance and processability was discussed in Section 2.1. Figures 98 and 99 below compare measured data for the panel alone, and the panel with foam and septum, with the theoretical optimum damping predicted by Equation <26> for foams 3 and 22. The line for optimum damping is the value above which additional damping will have little effect on reducing the sound radiation of the panel.

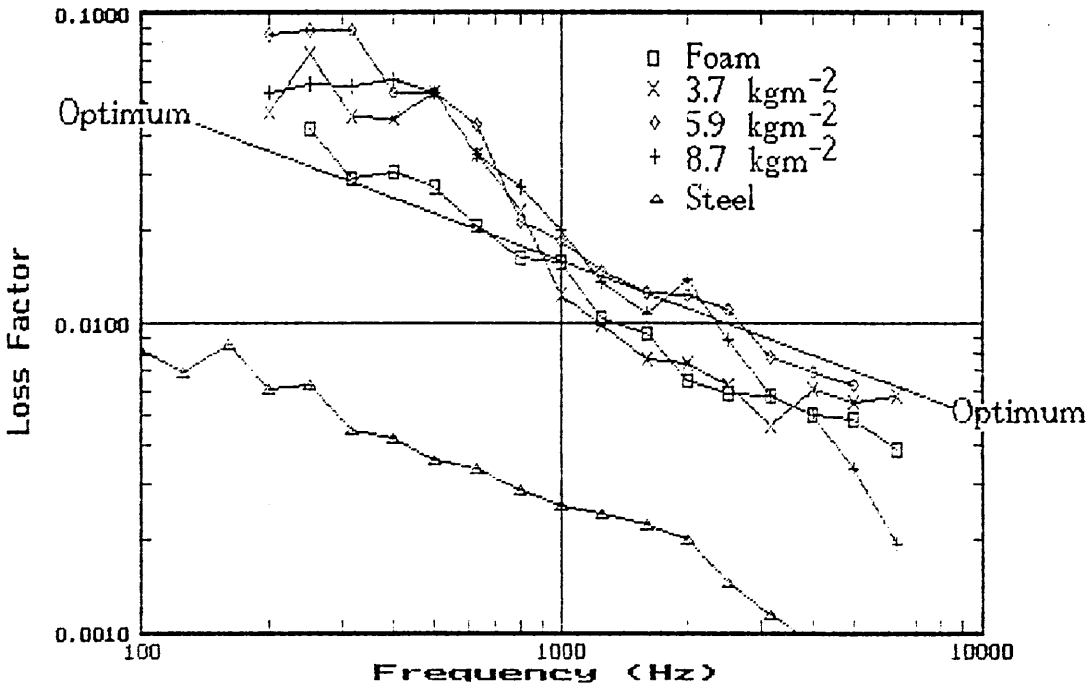

Figure 98 Comparison of system damping with theoretical optimum damping for foam 3 (η=0.2)

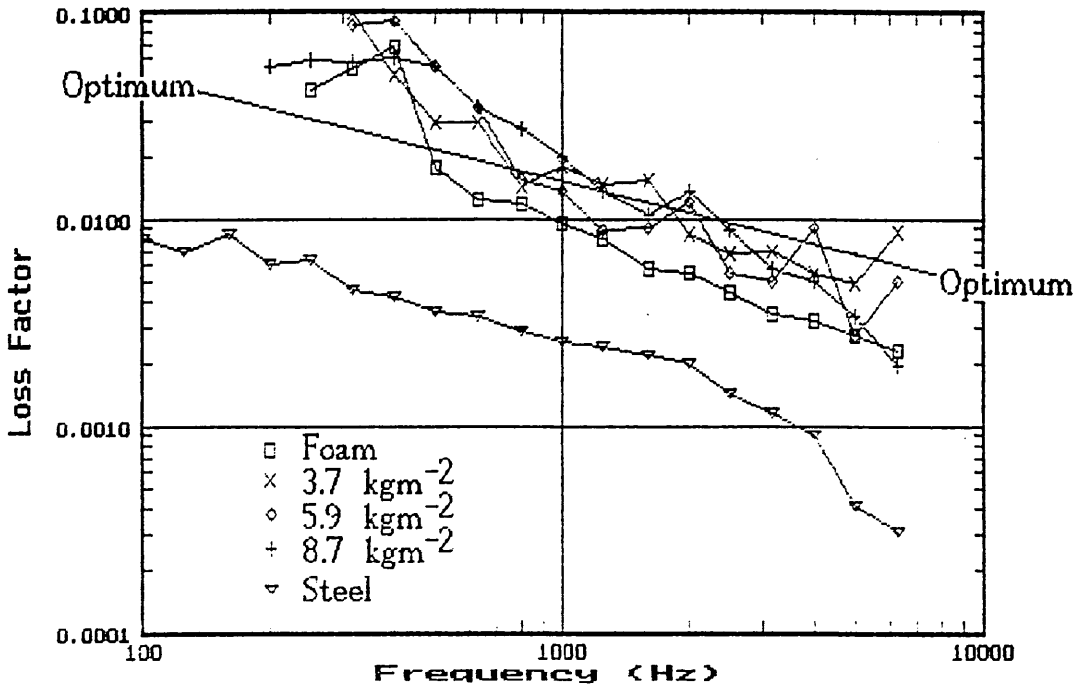

Figure 99 Comparison of system damping with theoretical optimum damping for foam 22 (η=0.8)

The damping of the panel + foam composite is seen from the above graphs to be of the same order as that of the optimum for minimum noise radiation. At frequencies below 1kHz the measured damping exceeds the optimum. Above 1kHz the measured damping is slightly below the optimum. In addition increasing the foam damping does not appear to give large improvements over that of the lower damped foam (η=0.8 for foam 22, η=0.2 for foam 3). The implication for the manufacturer is that although a highly damped system is desirable to reduce sound radiation the use of a higher damped foam (HHF) offers only a marginal advantage over the lower damped foams (VE). The processability of HHF foams is more complex than VE foams resulting in on-line cost advantages to the manufacturer if VE foams can be

used.

6.7.2 Airborne Noise Insertion Loss

The performance optimisation of the PUR composites used in this work is a complex issue. The aim is to obtain the best performance from the carpet composite by correct choice of the material and system parameters. The influence of these parameters has already been discussed, but no criteria has yet been made for their selection. The following section aims to discuss the optimisation and suggest procedures that can aid this process. Optimisation requires consideration of a number of factors. Firstly, knowledge of the noise source spectrum is necessary to assess the frequency content and noise level. Secondly, cognizance of attenuation of the noise as it travels from the source to receiver i.e. the insertion loss of the foam cored composite (the noise path). Finally, the response of the receiver i.e. vehicle occupants is essential as it enables the effectiveness of a complete noise control treatment to be assessed. In addition to the noise performance the manufacturer needs to take into consideration other factors which affect the choice of materials e.g. cost, durability.

6.7.2.1 Internal Noise Spectrum

Chapter 1 discussed the sources which contribute to the internal noise in a vehicle. The noise spectrum consists of essentially two different frequency components. (1) Discrete. These are caused by the engine combustion process. The frequency of the noise is proportional to the engine speed and number of cylinders. This noise is

principally at low frequencies (f<400Hz). (2) Broadband. These are caused by aerodynamic effects and the interaction between the tyres and road surface. The noise is broadband and occurs principally at higher frequencies (f>400Hz). A typical interior noise spectrum was shown in Fig. 2, whilst Fig. 100 gives a typical spectrum in front of an engine power unit. A peak sound pressure level of approximately 78 dB can be seen in the 160Hz 1/3 octave band. This corresponds to the firing frequency at this engine speed (4500 r.p.m.). Above 250Hz the spectrum increases smoothly with frequency to a maximum level of approximately 80dB in the 3150Hz 1/3 octave band. Noise with discrete tones is more annoying than broadband noise, whilst broadband noise affects the intelligibility of speech. This is discussed in the next section.

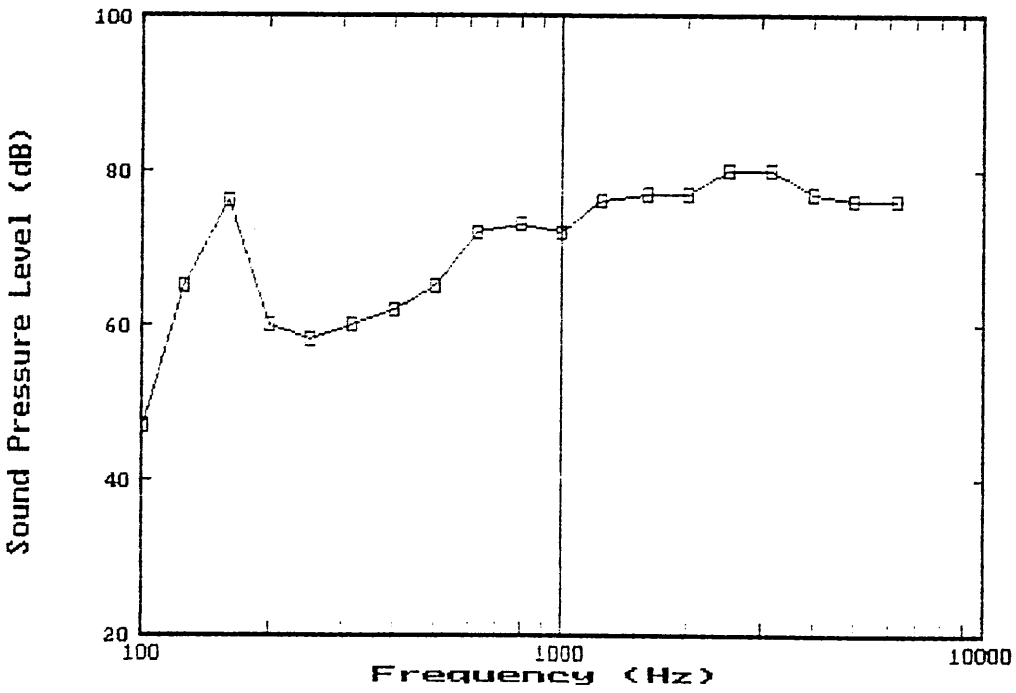

Figure 100 Typical vehicle noise spectrum (after Gahlau, 1987)

6.7.2.2 Noise Path Attenuation

The attenuation of the vehicle noise by PUR foam cored composites has been discussed previously in this work. It is characterised by the insertion loss of the composite. The shape of a typical insertion loss curve is illustrated in Fig. 101. The curve exhibits a resonance dip in the region of approximately 200-400Hz with an IL level of approximately 0dB. At this resonance the composite is a poor attenuator of sound. The position of the resonance is controlled by the foam stiffness and thickness and the septum and panel surface density. Above the resonance the insertion loss increases rapidly with frequency to a value of approximately 30dB.

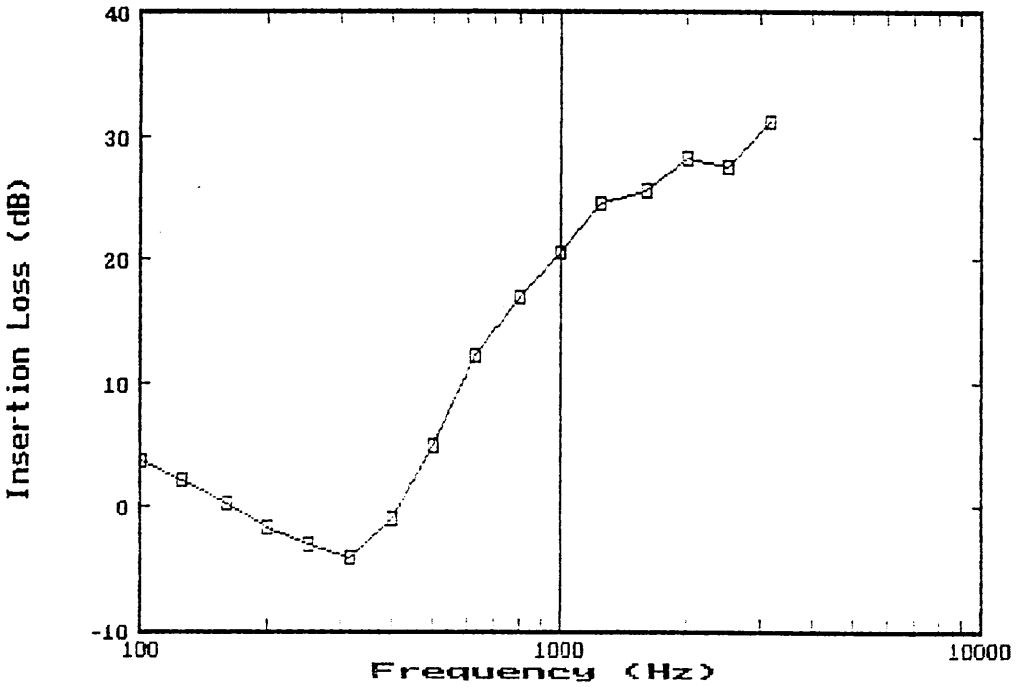

Figure 101 Typical insertion loss for a PUR foam cored composite

6.7.2.3 Criteria for Assessment of Interior Noise

Assessment of interior vehicle noise is difficult. Final judgment on interior noise quality is carried out by a subjective appraisal by the automotive manufacturer. However it is of value to use an appro-

priate rating method to quantify the performance of noise control packages so that a performance ranking can be made. The problem lies with finding a criteria that enables the evaluation of the factors that affect the noise comfort of the vehicle occupants. The two main factors are annoyance and speech interference.

Annoyance of a noise source is controlled by its loudness and noisiness. Loudness is related to the occupants impression of noise strength and intensity, whilst noisiness is related to its physical characteristics e.g. spectral content, impulsiveness. Annoyance is thus a measure of the 'unwantedness' of noise due to both the psychological response or perception of the noise, and the physical nature of the noise.

Many attempts have been made to rate noise annoyance. These are well documented in the literature (Kinsler *et al* 1982, Beranek 1988). The principle one is the A-weighting which gives a single number rating of a noise spectrum. The A-weighting method simply applies a weighting curve to the noise spectrum in 1/3 or 1/1 octave bands. The band levels are then summed to give the A-weighted level (dBA). The weighting curve is derived from the 40 Phon equal loudness contour, obtained from measurements on subjective response of the human ear to pure tones (Robinson *et al*, 1957). Inside the vehicle discrete frequencies occur at lower frequencies due to the engine firing frequency (f<400Hz). These occur at low frequencies where the sensitivity of the rating methods decreases due to the reduction in sensitivity of the human ear. However discrete frequencies are perceived as noisier than broadband levels. Thus corrections are often applied to rating methods if discrete frequencies

are present e.g. a correction of +5dB to the A-weighted value (Kinsler *et al*, 1982).

The assessment of the effect of noise on speech interference has also resulted in a number of rating methods. The important range for speech intelligibility is 400 to 6000Hz. Two main methods exist for speech intelligibility evaluation. The first is the Articulation Index (AI) (French *et al* 1947, ANSI S3.5). This is calculated from the relative sound level of speech and noise within 1/3 octave bands. The second method is the Speech Interference Level (SIL). this is obtained from the unweighted average of sound pressure level of a noise in the 500, 1000, 2000 and 4000Hz octave levels (Beranek, 1988).

Preferred Noise Criterion (PNC) curves were developed for use in buildings to assess noise and speech intelligibility (Beranek, 1988). A set of curves based upon the earlier Noise Criteria (NC) curves are used. The noise spectrum is superimposed onto the PNC curves and the maximum PNC value that coincides with the noise spectrum is taken as the single number rating.

A more recent assessment technique applied to vehicles was reported by Morris-Kirby *et al* (1990). The criteria that they use is that "good quality noise is that which displays a frequency spectra with smooth inter-1/3 octave changes." In addition to this requirement, they specify that the spectrum should have a negative gradient of greater than 2.5. This can be measured using a linear regression of the interior noise spectrum. The analysis is easy to carry out, and

emphasises the importance of discrete frequencies in interior noise comfort.

The choice of which of the above rating methods to use is uncertain. Fields *et al* 1987 reported that for speech levels the A-weighted, SIL and AI rating methods all give a reasonable prediction of speech interference.

6.7.2.4 Procedure for Rating Composite Systems

The application of the concepts discussed above to the conventional noise control model of source, path and receiver can be combined to give a procedure for the noise performance rating of the foam composite inside the laboratory. This is illustrated in Fig. 102 below. A typical vehicle noise spectrum (source) is acted upon by the PUR composite (path) to give a resultant noise spectrum. This is then assessed using a noise annoyance and speech intelligibility criteria (receiver).

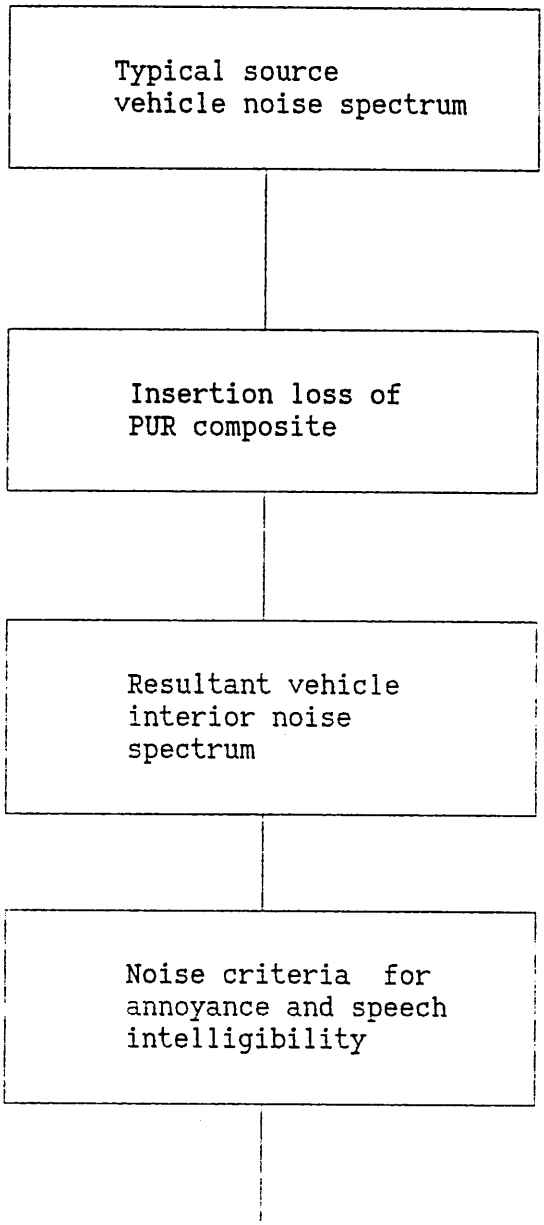

Figure 102 Generalised Rating Model for Vehicle Noise Control Composites

The generalised model can be used with the criteria discussed in Section 6.7.3.2. Hilyard *et al* reported using this model for carpet composites. The quality criterion used was Noise Criteria (NC) curves to give a single number rating. The procedure used by Teroson (Morris-Kirby *et al*, 1990) can also be applied to laboratory evaluation if a typical vehicle noise spectrum is used.

The model is useful for the ranking of PUR foam cored noise control composites. This facilitates the evaluation of the systems in the laboratory before expensive road trials are carried out.

However, there are two drawbacks to the model. Firstly the result is dependent upon the spectral content and sound level of the typical source spectrum. The vehicle noise spectrum is in practice constantly changing with engine speed, road speed and other driving conditions. The use of number of source spectra representative of a variety of conditions could be used to obtain a rating. This does reduce the value of single figure ratings. Secondly, the criterion used may not satisfactorily reflect the annoyance caused by discrete frequency components in the noise spectrum or speech interference due to broadband noise. It would thus appear a criterion should also incorporate an algorithm to detect a smooth internal noise spectrum which is desirable for noise quality.

6.7.2.5 Optimisation Procedure

An optimisation procedure must take into account the factors in Section 6.7.2.1 to 6.7.2.3. The use of the generalised model discussed above might also be a useful tool. Using the principles of the assessment model yields Figure 103 below. The graphical representation of the system will be used to discuss the difficulties of system optimisation, and suggest the possible control parameters. The graph superimposes a typical source spectrum (Figure 100) and composite insertion loss spectrum (Figure 101). The noise quality criteria is incorporated by dividing the frequency scale into two

ranges based on the discussion in Section 6.7.2.3. (The negative gradient line is the criteria placed upon good quality interior noise by Morris-Kirby *et al*, 1990). Below 400Hz noise quality is primarily controlled by the annoyance caused by the discrete frequency nature of the vehicle noise. This is designated the 'annoyance zone'. Above 400Hz the noise quality is controlled by the noise level that causes speech intelligibility problems. This is designated the 'speech interference zone'.

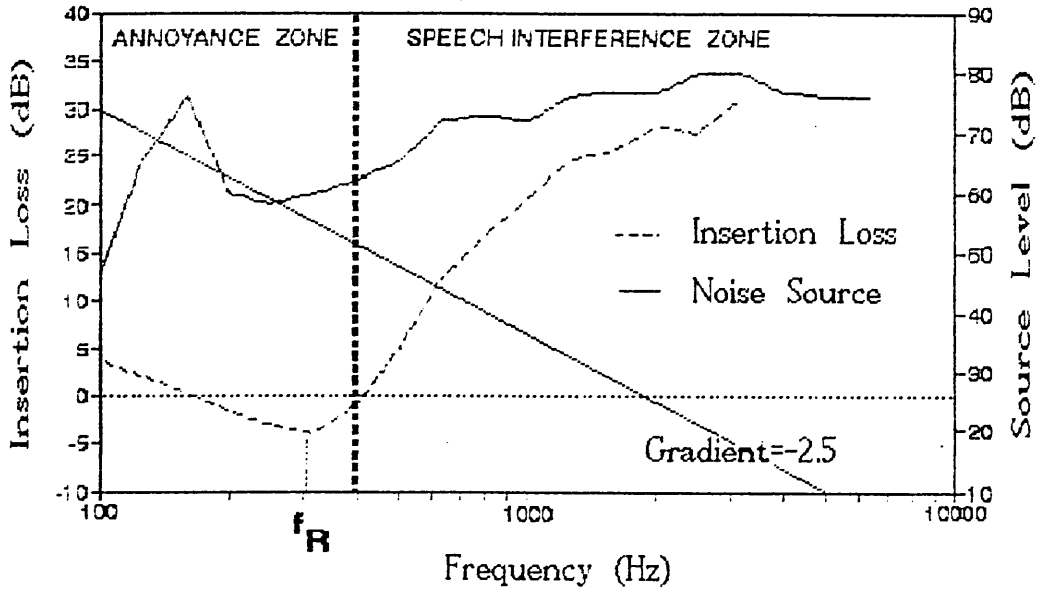

Figure 103 Design graph for system optimisation

The graph demonstrates the importance of the position of the resonance dip, where noise will be transmitted readily, and of the source level which will also affect the final internal noise spectrum. The principle method of controlling the insertion loss level is through design of the composite resonance. The position of this minimum has been shown in Chapter 5 to be predicted by Equation <59> in its modified form of Equation <79>.

The equation predicts that the resonance frequency can be varied by choice of material and system parameters. This was verified by the experimental work in Chapter 5. The problem is in the choice of position of the resonance in order to design the composite. This difficulty can be understood by referring to Figure 103. If the resonance frequency, f_R is reduced then the IL resonance dip coincides with the peak in the noise source. Breakthrough of the discrete frequency components will occur and thus the annoyance level will be high. However, at high frequencies the insertion loss level is high reducing the part of the spectrum thus speech intelligibility would be high. Conversely, if f_R is designed to occur at a higher frequency, the insertion loss improves at lower frequencies and the annoyance is low. Unfortunately, the insertion loss level is now reduced at higher frequencies and speech intelligibility is reduced.

A number of options therefore exist:

(1) f_R is designed to a very high frequency. This moves the resonance dip away from both the quality zones. This could be achieved by appropriate selection of system parameters. The behaviour of the composite system with a high resonance frequency is not known, and it is possible that the IL level is reduced by this technique.

(2) f_R is designed to occur at a very low frequency. The resonance minimum would thus occur below the quality zones. The post-f_R IL would be high in both the annoyance and speech interference zones, and thus the comfort of the vehicle occupant would be high.

(3) f_R is designed to be in the range of 200 to 400Hz. For this resonance frequency the IL minimum is midway between the annoyance and speech interference zones. Thus the combined effect is mini-

0742 532114
0742 532125

Please supply returning form with item reporting within 3 months if unavailable.

hor LING, M.K.

e Structural design optimisation of composites for noise suppression in vehicles

tion Publisher

e of publication Price per copy

l of new ies reqd. Course

of students whom reqd. LLO

ommended for student purchase Yes/No

n requested by

ool

e

ou wish the item to be reserved for you please enter r Library Ticket No.

FOR LIBRARY STAFF

Total cost

ISBN

Librarian | Class No TH 620.23 LIQ

New copies: Loan Type	No reqd	Already in stock	Already on order	In Process
Reference TH	1			
Normal Loan				
Short Loan				
Pt tm Loan				
Wk Loan				

mised. This position can be achieved by correct selection of composite. Any breakthrough of discrete frequency components which occur in the annoyance zone could be reduced using active noise control methods (see Chapter 1); as these are principally caused by the harmonic components.

All these options contain an element of compromise, and depend upon the criteria set by the automotive manufacturer. In practice certain design parameters are also determined by manufacturing processes. These are discussed in the next section.

6.7.2.6 Design Optimisation Restraints

The above section discussed the various design options that exist to maximise or optimise the comfort of the vehicle occupant. The restraints that are placed upon the composite design by either the vehicle manufacturer or by the processability of materials with certain properties affect which of the options are easily obtainable in practice. The restrictions are best considered with respect to the theoretical resonance frequency equation.

The parameters that control the resonance are foam modulus (K'_{tot}), foam thickness (d) surface density of the panel (m_{s1}) and of septum (m_{s2}). (Foam surface density has a limited effect because of its small magnitude compared with that of the panel and septum). The principle effect of foam damping (η_{foam}) was shown in Chapter 5 to be to reduce the IL at resonance. Of these parameters m_{s1} and m_{s2} are normally specified by the manufacturer. Thus the primary design variables are foam modulus and foam thickness. The foam modulus is

made up of the modulus of the foam material (K_{foam}) and the modulus of the air contained within the matrix (K_{air}). Foam thickness is usually restricted to the range 10 to 30mm. Figure 104 below shows the range of resonance frequencies that are predicted using Equation <79> for a septum surface density of 6.0kgm^{-2}, a panel surface density of 7.7kgm^{-2}, and a typical modulus of K_{air} of 1.1x10^{5}Pa.

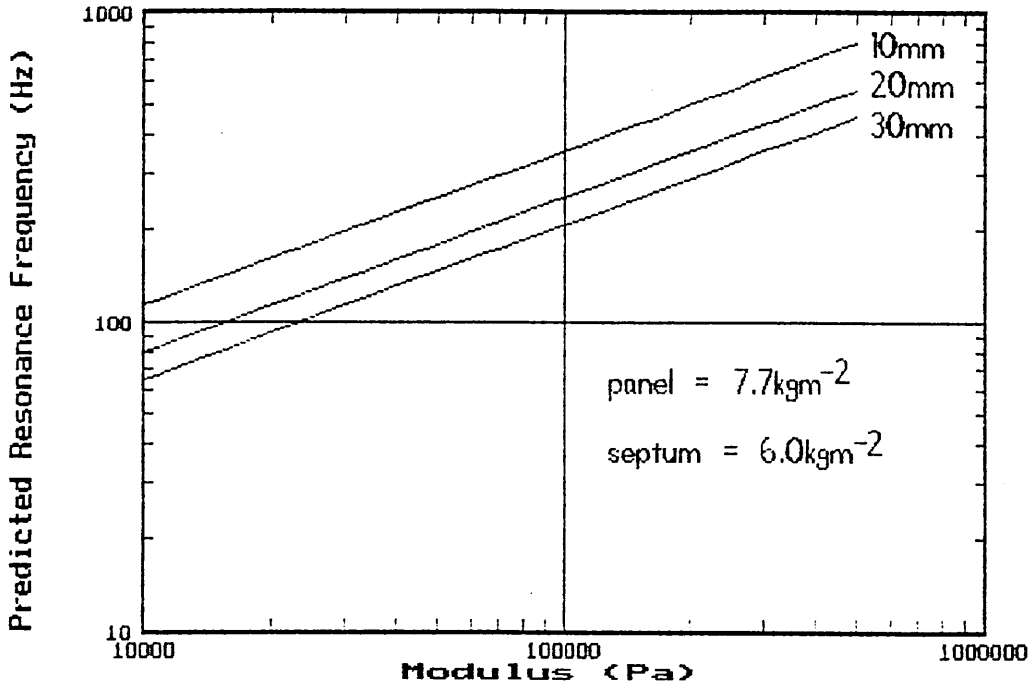

Figure 104 Variation of resonance frequency with modulus

If option (1) is chosen, then examination of the measured data values show that the maximum foam modulus measured was 4.2x10^{5} Pa for foam 6. This gives a maximum design frequency of 475 Hz for the above septum surface density. This assumes that this foam modulus value is the maximum achievable by the foam processor (a reasonable assumption). This frequency is too low for option (1) to be feasible in practice. In theory the septum and panel surface densities can be varied to extend the frequency range. But the theoretical and exper-

imental data demonstrated that reducing the septum surface density would also reduce the overall IL level. The choice of surface density of the floor pan is principally controlled by the structural rôle that it plays in the vehicle design and therefore cannot be modified.

If option (2) is chosen then a low f_R is required. The combined air and foam modulus controls the minimum frequency. The minimum theoretical value that the modulus K_{tot} can have is approximately $1.1x10^5$ Pa which gives a minimum design frequency of 216 Hz. The lowest measured foam modulus from Tables 6 to 8 was $0.17x10^5$ Pa for foam 21. This gives a lowest design f_R of 223 Hz. Increasing the septum surface density would reduce f_R, but to obtain a sufficiently low enough value would result in an unacceptable weight increase to the vehicle manufacturer. This means that option (2) is unachievable.

If option (3) is chosen it is seen from the measured data that this is easily achievable in practice. A combined modulus of $2x10^5$Pa and a foam thickness of 30mm would give a resonance frequency of approximately 300Hz. Of the three options discussed the third one is the only viable design solution.

6.7.2.7 Optimal Composite Selection using Design Curves

The analysis in the previous section demonstrated that, due to system design restraints, the optimum system resonance frequency is in the range of 250 to 400Hz. If a design frequency of f_R=300Hz is chosen then a set of design curves can be constructed. These are

shown in Fig. 105 below. For the convenience of the design engineer, the vertical axis is labelled in terms of effective surface density where, m_{seff} is given by:

$$\frac{1}{m_{seff}} = \frac{1}{m_{s1}} + \frac{1}{m_{s2}} \qquad \langle 80 \rangle$$

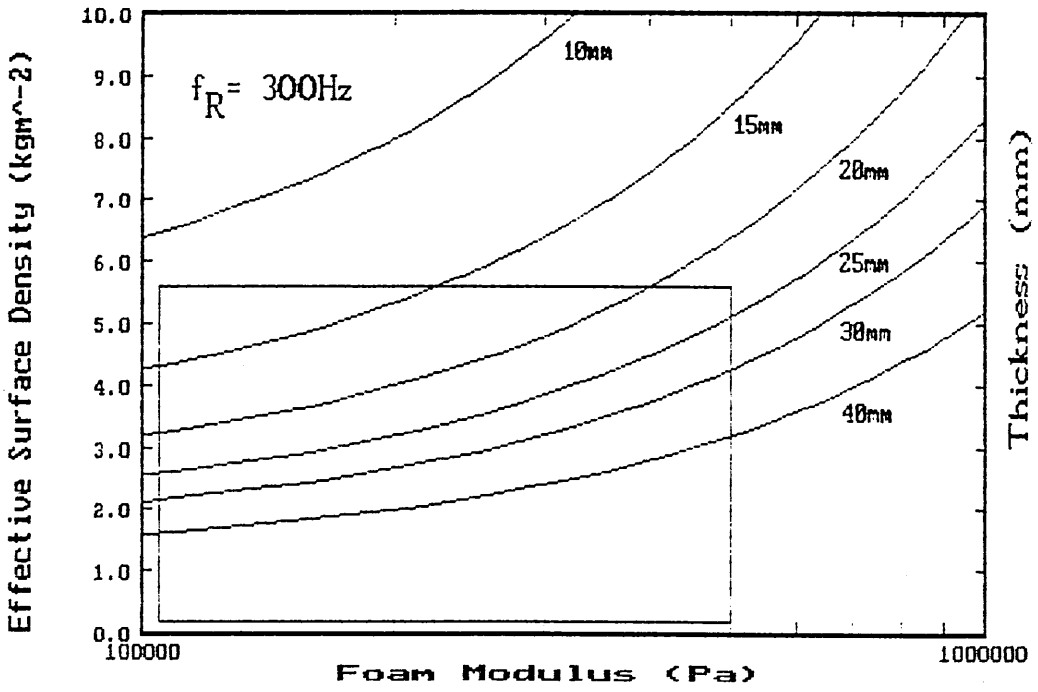

Fig. 105 Optimisation Design Curves

The curves show the interdependence of foam modulus, foam thickness and system surface density. Superimposed upon the graph is a rectangle. The material properties within this box represent those supplied by the collaborating company and so might be regarded as the range suitable for manufacturing this product.

The curves can be used to select the material properties required,

to tailor a carpet composite to a particular application. However, the data presented in Chapter 2 and 5 demonstrated the dependence of IL upon material and system parameters, and these factors must also be considered. For example, if a 40mm foam is to be used then a foam with modulus of $5.0x10^5$ and an effective system surface density of $3.3kgm^{-2}$. If the manufacturer then decides that a 40mm foam would not be suitable, and changes the selection to 25mm then the design curve for this thickness can be used. Thus a number of effective surface density and foam modulus combinations exist. However, the effect of varying the parameters on the IL response must be considered.

If only the foam modulus could be varied then the modulus would have to be set to $2x10^5Pa$. The reduction of foam thickness was shown theoretically and experimentally to slightly reduce the IL at resonance, and to increase the resonance frequency, thus reducing the post-f_R IL due to the response curve being shifted up the frequency scale. Reducing the foam modulus was shown to reduce the IL at resonance, but to increase the post-f_R level because of the reduction in f_R. Thus the combined effect of reducing foam modulus and thickness upon system performance needs to considered. In this case the net effect would be to reduce the IL at f_R, the other effects cancelling one another out.

If only the surface density of the system is a design variable, then using the design curves it is found that a value of approximately $5.0kgm^{-2}$ would be required. If the foam thickness was reduced to 25mm then the IL would be slightly reduced at resonance, and the resonance frequency increased, thus reducing the post-f_R IL due to

the response curve being shifted up the frequency scale. The experimental and theoretical data in Chapters 2 and 5 showed that increasing the surface density reduced f_R, and also increased the IL at f_R. In addition the change of resonance also shifted the IL curve down the frequency scale increasing the post-f_R level. In this case the change in design parameters would result in a net effect of the overall IL remaining approximately the same but with a slight increase in the IL at resonance.

6.7.2.8 Conclusions of Design Optimisation for Airborne Noise

This section has discussed the problem of design optimisation of composite carpet systems when subjected to airborne noise. By considering the vehicle noise spectrum, the noise path and the subjective response of the passenger a generalised design optimisation model was developed. Using this model, with the constraints upon system parameters, it was found that the optimum frequency for the system resonance was in the region of 250 to 400 Hz. Based upon a design value of 300Hz a set of design curves were created. These enable a design engineer to examine the interdependence of design variables for a composite. An example of system design was given, and using the theoretical and experimental data obtained in the previous chapters, the influence on overall IL behaviour was considered. The design example highlighted the fact that changing system parameters could have a detrimental effect on system IL performance.

6.8 Recommendations and Further Work

6.8.1 Modification of the test facility

Whilst the experimental results obtained using the test facility have proved to be of value, showing good correlation with theoretical predictions for airborne excitation, a number of modifications are suggested to further the understanding of the behaviour of the composites.

To examine the influence of specific excitation modes the distance from the loudspeaker baffle to the steel panel should be reduced. A larger array of loudspeakers each connected to its own control circuitry would enable specific airborne patterns to be investigated. It would also mean that to a spatially uniform sound field on the steel panel could be more easily obtained. However the drawbacks of this configuration are that separate amplifiers and phase matching circuits would be required. Also the smaller panel-baffle distance would prevent a shaker being used.

The data presented for vibration generated sound did not display a high degree of reproducibility. This was attributed to the shaker/panel coupling. A loose coupling was used in order that the shaker did not influence the panel vibrations. The use of a more robust coupling is therefore recommended; investigating the influence of a bolted shaker on the vibration results and the reproducibility of the vibration insertion loss measurements.

6.8.2 Vibration Insertion Loss Model

The model developed to predict insertion loss for vibration excitation was quite successful in predicting system response below approximately 1kHz. There was reasonable agreement in the position of the first resonance trough, although the predicted levels at resonance were lower than those measured. Precise comparisons could not be undertaken due to the poor repeatability of the vibration excited insertion loss measurements. The differences in radiation efficiency between the steel panel and the composite could explain some of the model inadequacies (this was assumed to be the same for the purposes of this study). The intensity method can be used to measure radiation efficiency (Forssen *et al* 1983, Loyan 1990) as the particle velocity is approximately the same as the panel velocity. The intensity is measured in the manner described. Alternatively a non-contacting transducer could be used to measure the surface velocity, and the radiated intensity using the intensity probe. A non-contacting sensor is recommended to eliminate the mass loading of the sensor on the composite. The radiation efficiency is then calculated from Eqn. 29. The study of a number of different composites and configurations should yield empirical expressions which can be incorporated into the model.

The model in general used single value material data values in its calculations e.g. modulus. In practice these properties are frequency dependent (Woods,1987). To improve the model's accuracy, properties which are frequency dependent need to be used.

The fitting constant in the present model is a large drawback as precise formulae are preferable. The need for this was attributed to the propagation constants and impedance values used. The use of a different propagation constants and foam impedance is recommended using the theory of Biot (1956) and Bolton (1984). Alternatively empirical relationships could be used, which do not rely on knowledge of foam macrostructure. An empirical relationship developed for evaluation of PUR foam impedance was reported by Ling (1991). The measurements were obtained using the foams in this study. The real and imaginary parts of the impedance, Z=R+jX were found to be related to flow resistivity and frequency by;

$$R/z_0 = 0.00148(f/R_1)^{-0.2402} \qquad \langle 81 \rangle$$

$$X/z_0 = -0.0001(f/R_1)^{-0.97} \qquad \langle 82 \rangle$$

The model used (as did the structure-borne model) single value material data values. The use of frequency dependent values should be used to increase the model accuracy. This should improve accuracy at high frequencies, as data values used were obtained at low frequencies.

An alternative approach to the modelling of the multilayered composite that could be used is that of Statistical Energy Analysis (SEA) (Price *et al* 1969, Crocker *et al* 1969, Lyon 1984 and Ver *et al* 1988). This method describes a system in terms of the energy of the system and the flow of the energy in its constituent subsystems. The subsystem energy is characterised by the modal energy and modal

density whilst energy loss and energy flow are characterised via loss factors.

6.8.4 Experimental Studies

The airborne insertion loss for composites should be measured for an extended range of experimental materials. The choice of experimental materials could be improved by the use of a statistical analysis for multivariate processes (Dillon *et al* 1984, Taguchi 1989). Such an analysis technique would minimise the number of different tests that needed to be carried out. Other areas of further experimental study are;

(1) The system core could consist of a combination of foam layers e.g. two 10mm foam layers of different mechanical properties used in place of a 20mm layer.

(2) The composite system should be tested with a filled polyurethane foam instead of the septum layer. The manufacture of filled foam (using for example $BaSO_4$ as a filler) is achievable with multi-hardness foaming equipment, and is attractive for foam manufacturers, as it would result in increased demand for polyurethanes.

(3) This work has been solely concerned with the performance of composites with unbonded layers. The behaviour of bonded layers should be examined. This would help the understanding of transmission of noise and vibration through PUR composites.

(4) The performance of composites with more than 3 layers should be investigated. It is possible that these would give enhanced noise insulation performance. The models described in this work could be readily extended to incorporate four or five layered carpet composite systems.

6.8.5 Combined Airborne and Structure-borne Noise

Once a better understanding of structure-borne excitation is obtained combined airborne and structure-borne inputs can be used. Combined inputs are a better representation of the vehicle noise and vibration environment. McGary (1985) reported on aircraft structures subjected to combined excitation. He demonstrated that the surface velocity of a panel undergoing simultaneous airborne and structure-borne vibration is given by Eqn. <80>.

$$\langle v^2 \rangle = \langle v_s^2 \rangle + \langle v_a^2 \rangle + \langle v_{sxa}^2 \rangle \qquad \langle 83 \rangle$$

The last term, $\langle v_{sxa}^2 \rangle$, accounts for the interaction between the structure-borne and airborne inputs. When the two inputs are uncorrelated the panel response, $\langle v^2 \rangle$, due to the combined inputs is exactly equal to the response due to the inputs acting individually. Obviously care needs to be taken to ensure that the excitation levels used are representative of those found in vehicles. This data is rarely found in the published data, so collaboration is recommended with an automotive manufacturer.

7. REFERENCES

ANSI S12.21 Engineering Method for the Determination of Sound Power Levels of Noise Sources using Sound Intensity

ANSI S3.5 American National Standard Methods for Calculation of Articulation Index

AU A.C.K., BYRNE K.P., 1987, J. Acoust. Soc. Am., 82(4), 1325-1333

BERANEK L.L., 1947, J. Acoust. Soc. Am., 19(4), 556-568

BERANEK L.L., WORK G.A., 1949, J. Acoust. Soc. Am., 21(4), 419-428

BERANEK L.L., 1988, Noise and Vibration Control, Edited by L.L. Beranek, Institute of Noise Control Engineering

BERGER R., 1911, Dissertation th Munchen, Uber die Schalldurchlassigkeit

BIES D.A., HAMID S., 1980, J. Sound and Vibration, 70(2), 187-204

BIES D.A., 1988, Acoustical Properties of Porous Materials, Chapter 10, Noise and Vibration Control, Edited by L.L. Beranek, Institute of Noise Control Engineering

BIJL L.A., 1977, CONCAWE Rep. No. 8/77, The Oil Companies International Study Group for Conservation of Clean Air and Water in Europe, Den Haag, Netherlands, Measurement of Vibrations Complementary to Sound Measurements

BIOT M.A., 1956, J. Acoust. Soc. Am., Part I and II, 28(2), 168-191

BMW INFORMATIONSPAUSE, 1984, Drawing No. 1 933 613

BOCKHOFF M., TAILLIFET D., 1988, Proc. Internoise 88, 1125-1128

BOLTON J.S., 1984, PhD Dissertation, Institute of Sound and Vibration, Southampton, Cepstral Techniques in the Measurement of Acoustic Reflection Coefficients, with Applications to the Determination of Acoustic properties of Elastic Porous Materials

BRIDGESTONE Co. (Japan), Technical Report

BRUEL & KJAER, 1986, Sound Intensity, DK 2850 Nærum, Denmark

CLARKSON B.L., POPE R.J., 1981, 77(4), 535-549

COLLIER P., 1985, PhD Dissertation, Sheffield City Polytechnic, The Design and Performance of Non-linear Vibration Isolating Materials,

CRAGGS A., 1972, Enclosures, J. Sound and Vibration, 23(3), 331-339

CRAGGS A., 1986, J. Sound and Vibration, 108(2), 327-337

CRAGGS A., BUMA C.J., 1989, Applied Acoustics, 28, 229-239

CREMER L., 1942, Akustische Zeitschrift, 7, 81-104

CREMER L., HECKL M., UNGAR E.E., 1988, Structure-Borne Sound, 2nd Edition, Springer-Verlag

CROCKER M.J., PRICE A.J., 1969, J. Sound and Vibration, 9(3), 469-486

DELANY M.E., BAZLEY E.N., 1969, Nat. Phys. Lab. Aerodyn. Div. Rept., NPL AERO REPORT AC37

DELANY M.E., BAZLEY E.N., 1970, Applied Acoustics, 3, 105-116

DILLON W.R., GOLDSTEIN M., 1984, Multivariate Analysis - Methods and Applications, J. Wiley and Sons

DUNN I.P., DAVERN W.A., 1986, Applied Acoustics, 19, 321-334

DYM C.L., LANG M.A., 1974, J. Acoust. Soc. Am., 56(5), 1523-1532

DYM C.L., LANG M.A., 1975, Optimal Design of Sandwich Panels, J. Acoust. Soc. Am., 57(6), 1481-1487

DYM C.L., LANG M.A., 1976, J. Acoust. Soc. Am., 59(2), 364-367

ELLIOTT S.J., JOSEPH P., BULLMORE A.J., NELSON P.A., 1988, J. Sound and Vibration, 120(1), 183-189

FAHY F., 1984, Structural Acoustic Coupling, Chapter 12, An Advanced Course in Noise and Vibration, Institute of Sound and Vibration Research, Univ. of Southampton

FAHY F., 1985, Sound And Structural Vibration - Radiation, Transmission, and Response, Academic Press

FAHY F., 1989, Sound Intensity, Elsevier Applied Science

FIELDS J.M., HALL F.L., 1987, Community Effects of Noise, Chapter 3, Transportation Noise Reference Book, Edited P.M. Nelson, Butterworths London

FOAG W., 1989, Proc. Instn. Mech. Engrs, 203, 221-230

FORSSEN B., CROCKER M.J., 1983, J. Acoust. Soc. Am., 73(3), 1047-1053

FOTHERGILL L.C., 1984, Internal Note N75/84, Building Research Est.

FRENCH N.R., STEINBERG J.C., 1947, J. Acoust. Soc. Am., 19(1), 90-119

FRENCH C.C.J., 1989, Proc. Instn. Mech. Engrs, 203, 169-183

FUKUHARA H., 1988, Applied Acoustics, **24**, 169-191

GAHLAU *et al*, 1987, US Patent no. 4655496, April 7, Motor Vehicle Noise Insulation, 712-726

GAHLAU H.K. ,1987, (Dr. Alois Stankievicz GMBH), Proc. Polyurethanes World Congress

GAHLIN M.P., On the Transverse Vibration of Plates, Prikl. Mat. Mekl.

GME 60 313, 1978, General Motors Test Procedure

GOODMAN L.E., 1959, ASME Colloquium on Damping, December, (Ed. RU ZICKA J.E.), Pergamon Press 1960

GREENE D.C., 1961, J. Acoust. Soc. Am., **33(10)**, 1315-1320

HALLIWELL R.E., WARNOCK A.C.C., 1985, J. Acoust. Soc. Am., **77(6)**, 2094-2103

HAMADA Y., TACHIBANA H., 1985, Proc. Inter-Noise, 693-6

HARRIS C.M., 1957, Handbook of Noise Control, McGraw-Hill Book Co.

HECKL M. J., 1981, J. Sound and Vibration, 77(2), 165-189

HEMINGWAY N.G., 1986, Proc. Instn. Mech. Engrs, **200(D2)**, 125-134

HILYARD N.C., ELLIOT A.M., CUNNINGHAM A., MACFARLAND D., 1990, Proc. 33rd Annual Polyurethane Technical/Marketing Conference, Sept.30-Oct.3, 631-637

HILYARD N.C., CUNNINGHAM A., 1991, Proc. 1991 SAE Noise and Vibration Conference, No. 911087, 435-441

HUSSAIN M., GöLLES J., RONACHER A., SCHIFFBÄNKER H., 1991, Proc. 1991 SAE Noise and Vibration Conference, No. 911080, 359-367

IOANNIDES E., GROOTENHUIS P., 1979, J. Sound and Vibration, **67(2)**, 203-218

ISO 9614-1, 1990, Acoustics-Determination of Sound Power Levels of Noise Sources using Sound Intensity-Part 1:Measurement at Discrete Points

JACOBSEN F., 1990, Noise Control Engineering Journal, 35, 37-46

JACOBSEN F., 1991, Applied Acoustics, 33, 165-180

JHA J.K., 1976, J. Sound and Vibration, **47(4)**, 543-558

JUNGER M.C., FEIT D., 1986, Sound Structures and their Interaction, The MIT Press, 2nd Edition

KERWIN E.M., ROSS D., 1959, Proc. 3rd Int. Cong. of Acoustics, Stuttgart, W. Germany

KINSLER L.E., FREY A.R., COPPENS A.B., SANDERS J.V., 1982, Fundamentals of Acoustics, 3rd Edition, John Wiley & Sons

KRISHNAPPA G., MC DOUGALL J.M., 1989, J. Vibration, Acoustics, Stress and Reliability in Design, 111, 465-471

KURTZE G., WATTERS B.G., 1959, J. Acoust. Soc. Am., 31(6), 739-748

LANG M.A., 1974, Investigation of Sound Transmission Characteristics of Sandwich Panels, PhD Thesis, Carnegie Institute of Technology

LEISSA A.W., 1969, Vibration of Plates, NASA SP-160

LEISSA A.W., 1973, J. of Sound and Vibration, 31(3), 257-293

LEISSA A.W., 1977, Shock Vib. Digest, 9(10), 13-24

LING M.K., HILYARD N.C., HENG R.B.W., 1990, Proc. Inst. of Acoustics, Southampton, March 27-30, 12(1), 243-492

LING M.K., 1991, Applied Acoustics, 34(3), 221-224

LONDON A., 1950, J. Acoust. Soc. Am., 22(2)

LOVE A.E.H., 1927, Mathematical Theory of Elasticity, 4th Edition, Cambridge University Press

LOYAN T., 1990, Proc. Inter-Noise 90, 1053-1056

LU Y.P., KILLIAN J.W., EVERSTINE G.C., 1979, J. Sound and Vibration, 64(1), 63-71

LU Y.P, EVERSTINE G.C., 1980, J. Sound and Vibration, 69(2), 199-205

LYON R.H., 1984, Statistical Energy Analysis of Dynamical Systems: Theory and Application, MIT Press

MECHEL F.P., 1976, Acustica, 35, 210-213

MANGIAROTTY R.A.,1963, J. Acoust. Soc. Am., 35(7), 1023-1029

de MEY A., Guy R.W., 1987, Applied Acoustics, 30, 219-236

MCGARY M.C., 1986, PhD Dissertation, Dept. Aeronautics and Astronautics Stanford University, Separation of Airborne and Structure-borne Noise Radiated by Plates Constructed of Conventional and Composite Materials with Applications for the Prediction of Interior Noise Paths in Propeller Driven Aircraft

MINDLIN R.D., SCHACKNOW A., DERESIEWICZ H., 1956, Journal of Applied Mechanics, 430-436

MINTEN M., COPS A., WIJNANTS F., 1987, Applied Acoustics, 22, 281-295

MORRIS-KIRBY R., MCMICHAEL N., 1990, Proc. 22nd ISATA Conference, Italy

MORSE P.M., 1986, Vibration and Sound, ISBN 0-88318-287-4, Acoustical Society of America

NAKRA B.C., 1976, Shock and Vibration Digest, 8, 3-12

NAKRA B.C., 1981, Shock and Vibration Digegest, 13, 17-20

NAKRA B.C., 1984, Shock and Vibration Digest, 16, 17-22,

NELSON P.A., CURTIS A.R.D., ELLIOTT S.J., BULLMORE A.J., 1987, J. Sound and Vibration, 117(1), 1-58

NICHOLS R.H., SLEEPER H.P., WALLACE R.L., ERICSON H.L., 1947, J. Acoust. Soc. Am., 19(3), 428-443

NILSSON A.C., 1990, J. Sound and Vibration, 138, 73-94

NISHIDA K., KUBOTA Y., HAYASHI S., 1990, J. Sound and Vibration, 138(1), 1-15

OBERST H., 1954, Acustica (Beihefte), 4, 181-194

PAN J., HANSEN C.H., BIES D.A., 1990, J. Acoust. Soc. Am., 87(5), 2098-2108

PAPANIKOLAOU G., TROCHIDES A., 1985, Applied Acoustics, 18, 315-323

PERSONEN K., UOSUKAINEN S., 1984, Proc. Inter-Noise, December 3-5, 1125-1128

PLUNKETT R., 1959, ASME Colloquium on Damping, December 1959, (Ed. RUZICKA J.E.), Pergamon Press 1960

PLUNT J., 1991, Proc. 1991 SAE Noise & Vibration Conference, No. 911085, 417-425

PRICE A.J., CROCKER M.J., 1969, J. Acoust. Soc. Am., 3(1), 683-693

PRIEDE T., JHA S.K., 1970, Journal of Automotive Engineering, 1(5), 17-21

PRIEDE T., 1971, J. Sound and Vibration, 15(1), 61-73

PRIEDE T., 1985, Proc. Instn. Mech. Engrs, 198(D7), 95-106

RAFF J.A., PERRY R.D.H., 1973, J. Sound and Vibration, 28(3), 433-470

RANKY M.F., CLARKSON B.L., 1983, J. Sound and Vibration, 89(3), 309-323

RHODES D.M., PHILLIPS A.V., 1988, Proc. IMechE, C28/88, 147-157

RICHMOND J.W., PARKER D.A., 1987, Proc. Instn. Mech. Engrs.,201(D4), 235-244

ROBINSON D.W., DADSON R.S., 1957, J. Acoust. Soc. Am., 29, 1284-1288

RODWELL G., ROGERS C.G., 1989, Proc. Inst. Acoustics '89, Oxford

ROSS D., UNGAR E.E., KERWIN E.M., 1959, ASME Colloquium on Damping, Pergamon Press 1960

SATTER M.A., AHMADI G., 1977, Applied Acoustics, 10, 113-120

SCHIFFBÄNKER H., BRANDL F.K., THIEN G.E., 1991, Proc. 1991 SAE Noise and Vibration Conference, No. 911081, 369-379

SERVOTEST, 1988, Ride Vibrations: An Active-Suspension Test Rig, Automotive Engineer, April/May, 47

SMITH P.W., LYON R.H., 1965, Sound and Structural Vibration, NASA CR-160

TAGUCHI G., 1989, Introduction to Quality Engineering-Designing Quality into Products, APO (Asian Productivity Organisation)

TALBOT C.R.S., TIDBURY G.H., JHA S.K., 1975, American Soc. of Mech. Engrs., Paper 75 DET 115

TARNOCZY T., 1970, J. Sound and Vibration, 11(3), 229-307

TROCHIDIS A., KALAROUTIS A., 1986, J. Sound and Vibration, 107(2), 321-327

TYLER J.W., 1990, Visit to Lotus Engineering, Institute of Acoustics, Acoustics Bulletin, 15(2), 39-40

UNGAR E. E., 1988, Damping of Panels, Chapter 14, Noise and Vibration Control, Edited by L.L. Beranek, Institute of Noise Control Engineering

UTLEY W.A., POPE C.N., 1973, Applied Acoustics, 6, 143-149

VACAARI, 1979, Product Engineering, February, 47-51

VDI 3727

VER I.L., HOLMER C.I., 1988, Interaction of Sound Waves with Solid Structures, Chapter 11, Noise and Vibration Control, Edited by L.L. Beranek, Institute of Noise Control Engineering

VOIGT W., 1893, Nachr. Ges. Wiss. (Gottingen), 6, 225-230

WALLACE R.L., DIENEL H.F., BERANEK L.L., 1946, Thirty-first Meeting of Acoustical Society of America, J.Acoust. Soc. Am., **18**, 246

WALSH S.J., STIMPSON G., LALOR N., 1990, Proc. Inter-Noise 90, 969-972

WARBURTON G.B., 1954, Proc. Inst. Mech. Eng.
Ser. A, **168(12)**, 371-384

WATTERS B.G., 1959, J. Acoust. Soc. Am., **31(7)**, 898-911

WHATMORE A.R., LOWSON M.V., 1973, Applied Acoustics, 6, 293-300

WOODS G., 1987, Flexible Polyurethane Foams: Chemistry & Technology, Wiley

YOUNG D., 1950, J. Applied Mechanics, **47(4)**, 448-453

ZHU G.H., CROCKER M.J., RAO M.D., 1989, J. Acoust. Soc. Am., **85(1)**, 171-177

ZWINSELMAN J.J., BACHMANN W.D., 1987, Proc. Polyurethanes World Congress, 727-730

APPENDIX A PUBLICATIONS

1 Proceedings of Institute of Acoustics, Southampton, 12(1), 243-492

Performance of Polyurethane Cored Carpet Composites for Vehicle Interior Noise Control

M.K. Ling, N.C. Hilyard, R.B.W. Heng

Sheffield City Polytechnic

1. Introduction

Moulded foam backed carpet composites are now widely established in the UK motor industry as noise control components. There has been little information published on the measurement and evaluation of their performance. This paper reports on the initial findings of a study of the behaviour of polyurethane foam cored systems. Data is presented for the system insertion loss and the system frequency response for a number of PUR foams.

The transmission loss of multiple element constructions is well documented by many authors (Beranek and Work [2], Mangiarotty [8], Au and Byrne [1]. Their theoretical analysis is based upon the impedance of the component layers. The core isolating layer being a fibreglass blanket. Other authors have used viscoelastic materials for vibration damping purposes (Oberst [3]) and in multiple element systems (Reddy et al [6]). Their experimental and theoretical treatment of the subject used bonded systems. Despite the trend towards unbonded carpet systems within vehicles, the only published work known to the authors is that of Satter and Ahmadi[5]. They presented data for the radiation and response of a circular plate with unbonded PUR foam layers to structure borne vibration.

2. Theoretical Treatment

A low density material when applied to a vibrating surface moves with a motion very similar to that of the surface, at low frequencies. This renders the contribution of the applied layer to the insertion loss approaching zero. The crossover frequency, above which the wavelength of the radiated sound and layer thickness are more comparable is given by Schultz[9];

$$f_s = c_0/(10*h) \qquad \langle 1 \rangle$$

Schultz also gives the expressions for IL as

$$IL = 0 \qquad f<f_s \qquad \langle 2a \rangle$$

$$= 8.69\alpha h \qquad f>f_s \qquad dB \qquad \langle 2b \rangle$$

The attenuation constant for porous foams is a modified version of that given by Qunli [11] as;

$$\alpha = 0.163(0.25*1.21*f/R_1)^{-0.592} \qquad \langle 3 \rangle$$

The three layer system used for vehicle carpet treatments consists of a steel floorpan, covered with a PUR foam, on top of which is a heavy or septum layer. The Transmission loss of this three layer foam cored composite can be derived, [2], from equations <4> to <8> .

$$1/T = \{ x_1 \cosh(bd) + x_2 \sinh(bd) \}^2 \qquad \langle 4 \rangle$$

where $x_1 = 1 + jw(m_{s1}+m_{s2})/z_0$ <5>

$x_2 = Z_1/z_0 - w^2 m_{s1} m_{s2}/(Z_1 z_0)$ <6>

and Transmission Loss, $R = 10LOG(1/T)$ <7>

Substituting <4> and <5> into <3>;

$$(1/T)^{1/2} = [\, 1+jw(m_{s1}+m_{s2})/z_0] \cosh(bd) + [Z_1/z_0 + jwm_{s1}(1+jwm_{s2}/z_0)/Z_1] \sinh(bd) \qquad \langle 8 \rangle$$

Using the expressions for propagation constant and material available [10] the resonant frequency of the system can then be derived from <7> as;

$$f_{res} = \frac{1}{2\pi} \left[\frac{E'}{h} \left(\frac{1}{m_{s1}} + \frac{1}{m_{s2}} \right) \right]^{1/2} \qquad \langle 9 \rangle$$

The insertion loss of the added foam and septum can be readily calculated from equation <9>. For modelling purposes we assume that R_{panel} is given from the limp mass law.

$$IL = R_{system} - R_{panel} \qquad \langle 10 \rangle$$

3. Experimental Test Rig and Measurement

The test-rig used for experimental work is illustrated in Figure 1. It has dimensions of approx. $1m^3$, with an aperture of 0.87m x 0.87m (the size of commercially available moulded PUR foam). A 1mm mild steel sheet is clamped rigidly onto the top surface. Structural vibration is produced by an electrodynamic shaker, and airborne excitation via a loudspeaker within the test-rig cavity. The PUR foam is placed upon the panel and a septum layer upon it, if required. Care must be taken to ensure that the system is well sealed from leakage.

Intensity measurements were made by sweeping the intensity probe above the surface of the top layer. This was carried out for the bare panel and also with the composite in place. The insertion loss of the foam composite system could then be obtained by subtracting the two measurements. Vibration response measurements were carried

out with miniature accelerometers on the plate surface.

4. Results

The insertion loss for the foams in Table 1 was obtained using the procedure outlined in Section 3 above. A septum layer of 3.2 kgm^{-3} was used. Material properties are detailed in table 1.

The experimentally determined insertion losses for the plate + PUR foam are shown in figures 4 and 5. The insertion losses for the three layer system are shown in figures 6 and 7. The cross-over frequency, f_s can be obtained from figures 4 and 5. These are compared with the predicted values by equation <1> in table 2. Likewise, for the three layer system, the resonant frequency of the minima can be obtained from figures 6 and 7. These are compared with those predicted by equation <9> in measured values of resonant frequencies with those predicted by equation <9> in table 3.

The vibration response for foam A is shown in figure 2.

5. Discussion

Figure 2 illustrates the effect of an unbonded foam layer (no septum) on the vibration response of the steel panel. It is seen that the layer reduces the intensity of the modal response. This effect is enhanced by the addition of the septum, and with foams of relatively high damping (approx. 0.3) the modal response is eliminated The effective loss factor, as measured by the decay method, is shown in figure 3. It is seen that the general characteristic is one of decreasing damping with increasing frequency. This behaviour agrees with that previously reported by Reddy et al [6] for bonded systems. Placing the foam layer on the panel increased the system loss factor by an order of magnitude.

The predictions by Schultz for the airborne noise insertion loss of a panel + foam layer system is that the IL is zero where the wavelength of the incident wave is larger than ten times the foam thickness. Figures 4 and 5 demonstrate that this behaviour does occur in practice. Table 2 shows that the predictions of this crossover frequency correlate reasonably well with those measured in practice. The predicted IL above the crossover frequency does not agree so well with the measured values, although the trends are predicted correctly. This could be attributed in part to the differences in flow resistance of the foams layers.

The introduction of a septum layer effectively produces a damped double leaf partition with viscoelastic foam core. Around the minimum in the response the measured IL values are in reasonable agreement with those predicted from equations <8> and <10>. The resonance frequencies predicted by equation <9> using measured values of material properties agree with those found in practice, as seen from table 3. Although the overall response found experimentally is in general agreement with with that predicted by equations <8>

and <10>, at frequencies away from resonance the quantitative agreement is poor.

The data of figure 4 and equation <8> shows that for a given panel the frequency of the resonance trough can be controlled through the thickness and modulus of the foam core and the area mass of the septum layer. The depth of the trough is influenced by the loss factor of the foam, as expected from simple analysis of damped systems.

6. Conclusions

The work reported in this paper has demonstrated some of the fundamental material properties that affect the IL performance of unbonded PUR foam cored systems. A theoretical approach has been introduced, preliminary results presented, and these compared with those obtained experimentally.

7. References

[1] Au A.C.K., Byrne K.P.
J.Acoust.Soc.Am.82(4),pp.1325-1333, (1987)
On The Insertion Losses Produced By Plane Lagging Structures

[2] Beranek L.L., Work G.A.
J.Acoust.Soc.Am. 21(4),pp.419-428, (1949)
Sound Transmission Through Multiple Structures Containing Flexible Blankets

[3] Oberst H.
Acustica 6(1), pp.144-153, (1956)
Werkstoffe Mit Extrem Hoher Innerer Dampfung

[4] Trochidis A., Kalaroutis A.
J. Sound & Vibration, (1986)
Sound Transmission Through Double Partitions With Cavity Absorption

[5] Satter M.A., Ahmadi C.
Applied Acoustics (10),pp.113-120, (1977)
Experimental Investigation of Noise Radiation From A Circular Plate Covered By Polyurethane Foam

[6] Reddy R.C.U., Gamesan N., Rao B.U.A.
J. Sound and Vibration, 75(4),pp.481-494, (1981)
Response of Clamped Sandwich Panels With Viscoelastic Core Under Random Acoustic Excitation

[7] Gahlau H.K.
Proc. Polyurethanes World Congress, pp.712-726, (1987)
Fortschrittliche Schallisolationen In Der Automobiltechnik
Advanced Noise Control In Automotive Engineering

[8] Mangiarotty R.A.
J. Acoust. Soc. Am. 35,pp.1023-1029, (1963)
Optimisation Of The Mass Distribution And The Air Spaces In Multiple-Element Soundproofing Structures

[9] Schultz T.J.
Noise And Vibration Control, Ed. Beranek L.L., (Reprinted I.N.C.E. 1988)
Ch.15, Wrappings, Enclosures, and Duct Linings

[10]Bies D.A.
Noise And Vibration Control, Ed. Beranek L.L., (Reprinted

I.N.C.E. 1988)
Ch.10, Acoustical Properties of Porous Materials
[11]Qunli W.
Applied Acoustics, 25, pp.141-148, (1988)
Empirical Relations Between Acoustical Properties and Flow Resistivity of Porous Plastic Foams

Foam	Thickness \mm	Density \kgm^-3	Modulus \10^5Pa	Loss Factor @200 HZ	Flow Resistance \10^3 Rayls
A	14	29	2.2	0.18	1.5
B	25	31	1.9	0.15	4.5
C	38	31	1.9	0.14	10.5
D	29	86	1.5	0.21	26.9 (14)*
F	29	84	2.5	0.65	109.6 (19)*

Table 1 Material Properties
(* skin removed)

Symbols

α = attenuation constant (dBm_{-1})
A = area of sample (m_2)
b =propagation constant of core (m_{-1})
h = core thickness (m)
m_{s1} = surface mass of base panel (kgm^{-2})
m_{s2} = surface mass of septum layer (kgm^{-2})
R_1 = flow resistivity (Nsm^{-4})
R = sound Reduction index (dB)
T = transmission coefficient
w = angular frequency ($rads^{-1}$))
z_0 = specific impedance of air (415 Nsm^{-3})
Z_1 = acoustic impedance of the core layer (Nsm^{-3})

Sample	Cut-off Frequency \Hz	
	Measured 1/3 Oct.	Theory Eqn<>
A	3150	2450
B	1250	1372
C	630	903
D	1000	1183
F	630	1183

Table 2 Crossover Frequency

Sample + Septum	Resonant Frequency \Hz	
	Measured 1/3 Oct.	Theory
A	315	420
B	250	292
C	200	237
D	250	241
F	315	311

Table 3 Resonant Frequencies of Composite System

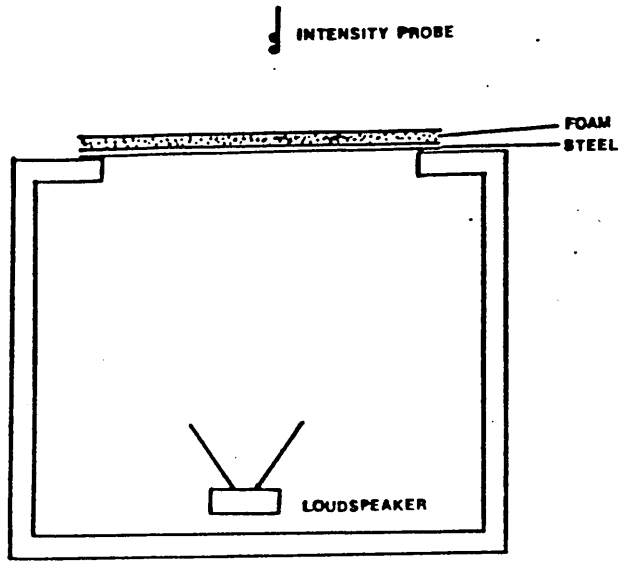

Fig. 1 Small Scale Test-Rig

FIGURE 2 FREQUENCY RESPONSE

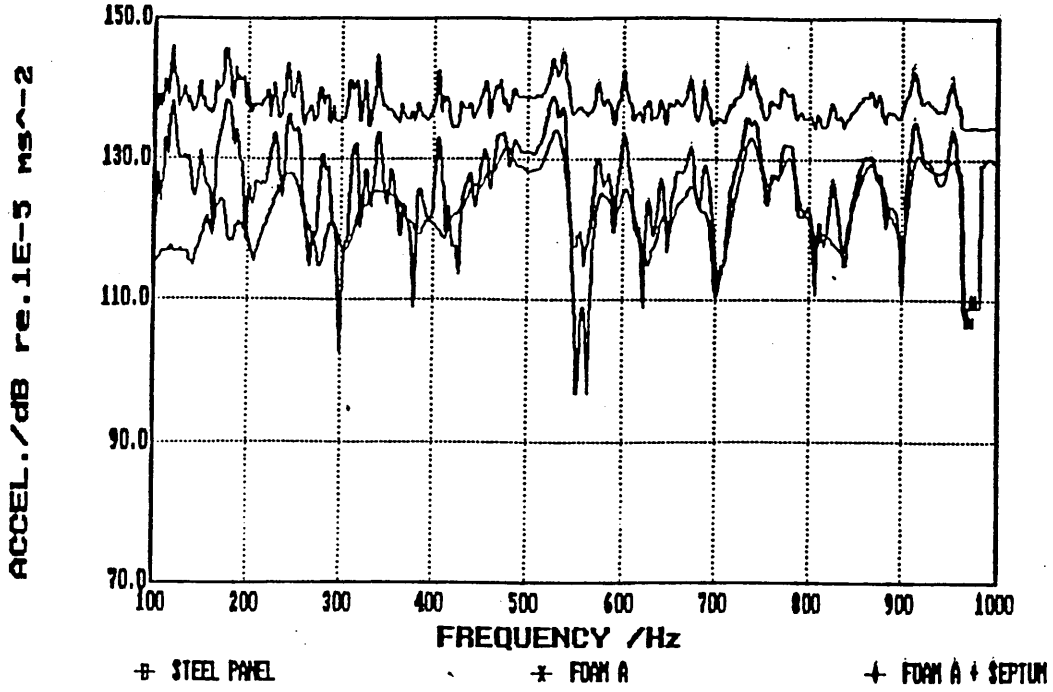

FIGURE 3 LOSS FACTOR

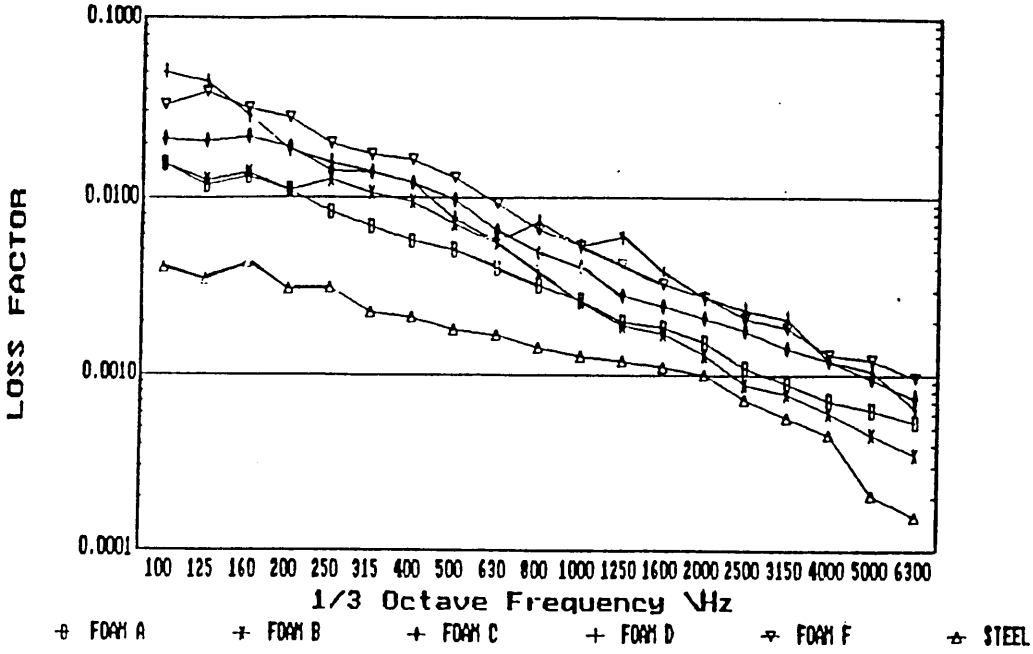

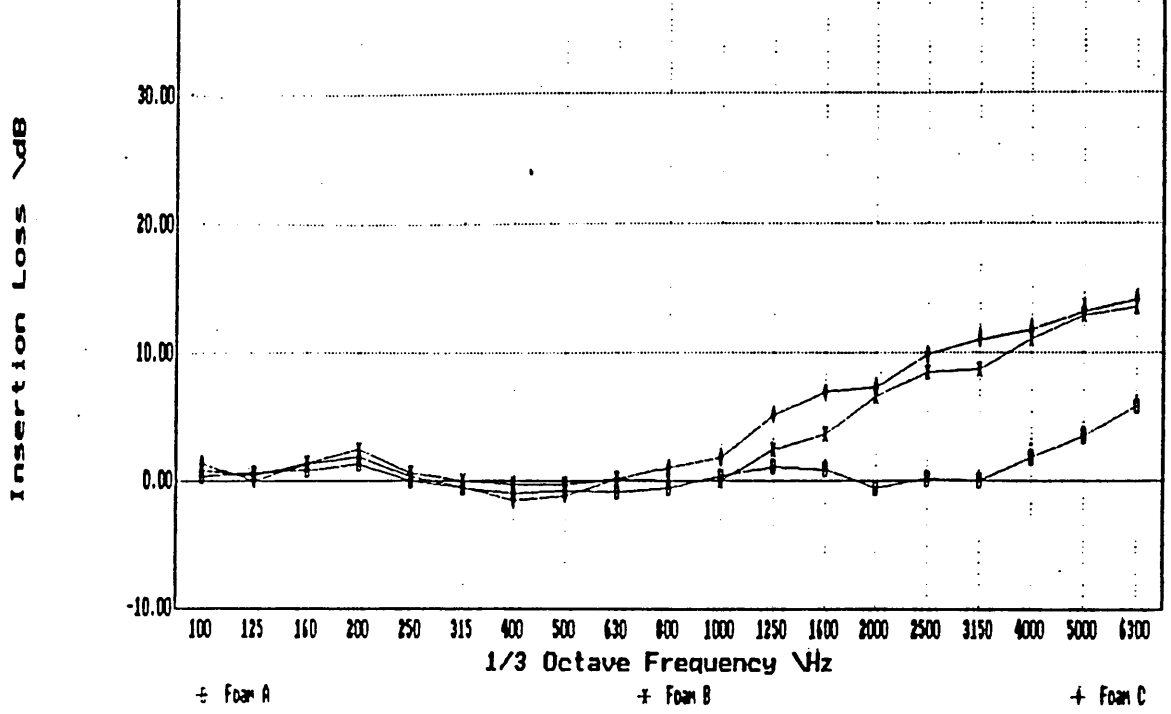

FIG.5 Insertion Loss

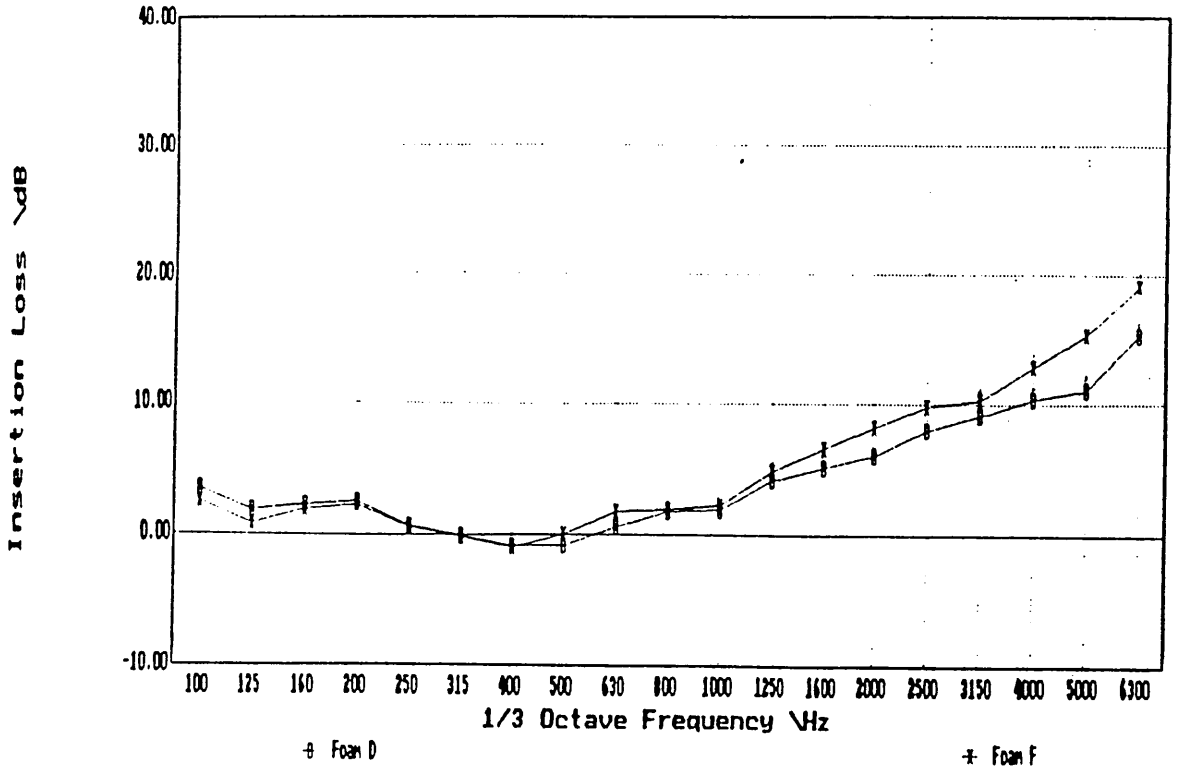

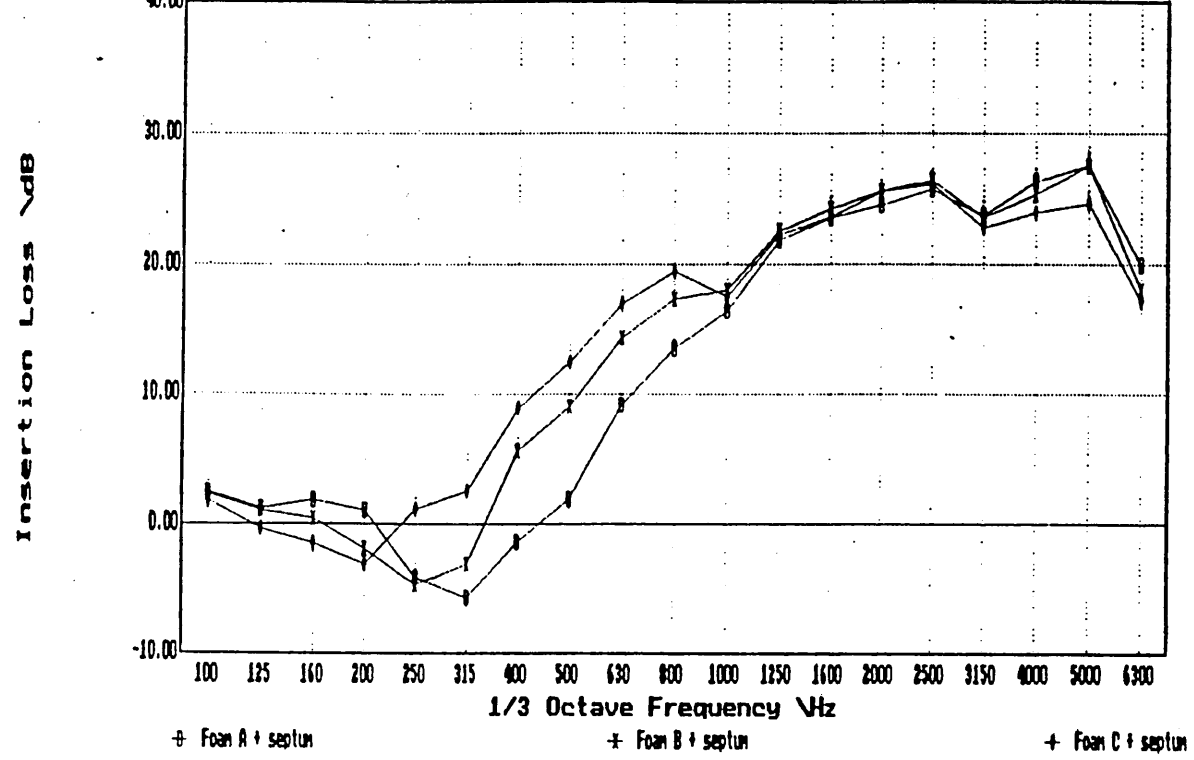

FIG.7 Insertion Loss

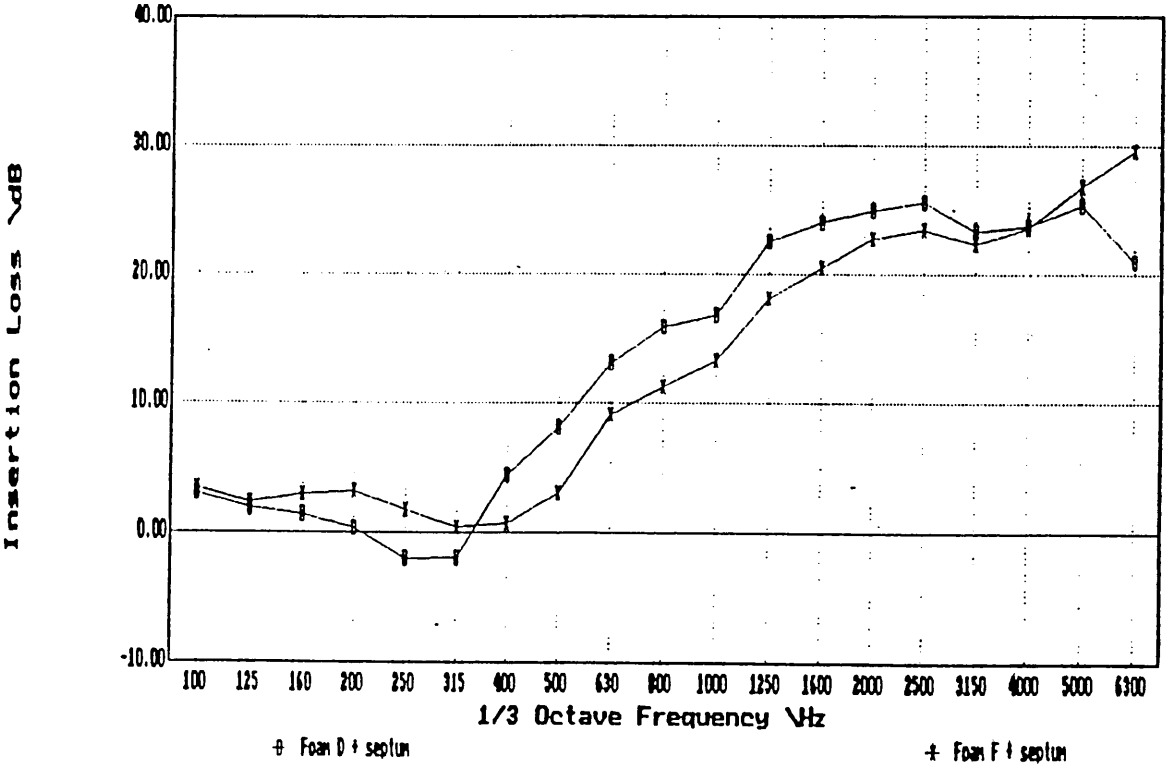

FIGURE 8 Insertion Loss

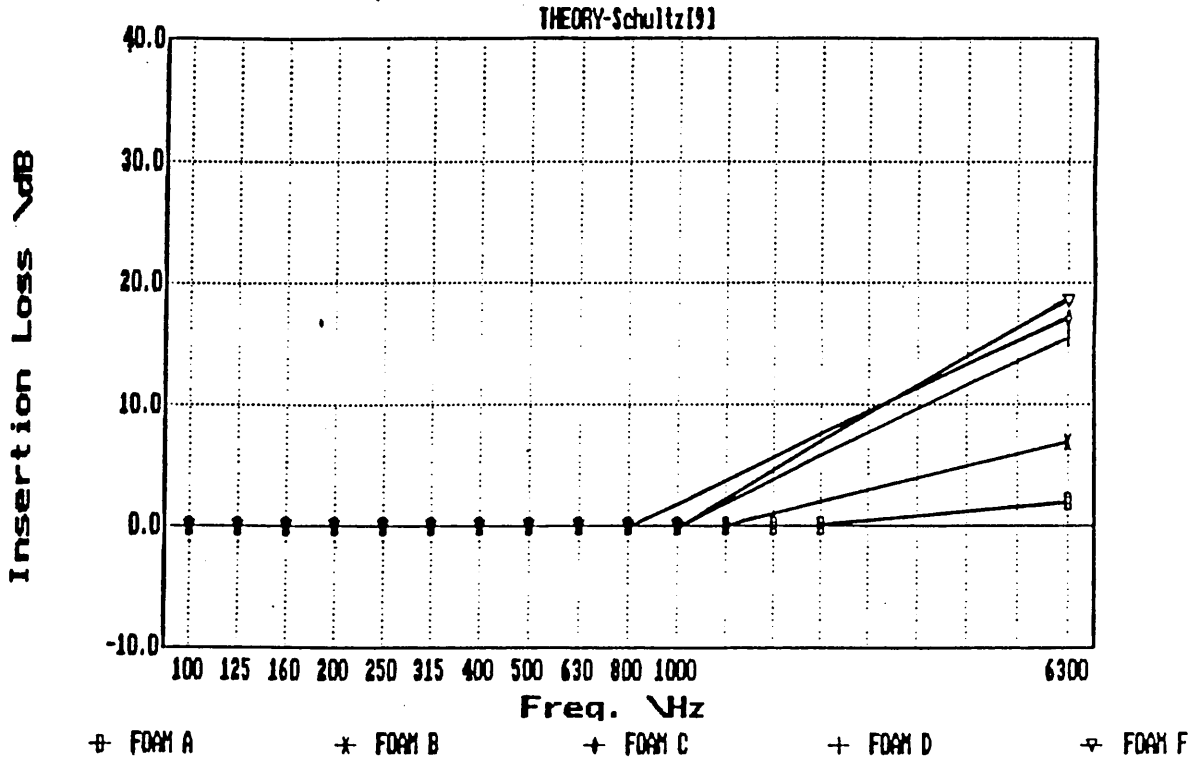

2 Proceedings of Cellular Polymers, London, 20-22 March 1991

FUNDAMENTAL STUDIES OF THE ACOUSTIC BEHAVIOUR OF FOAM BACKED FLOOR COVERING

M K LING
Division of Applied Physics, Sheffield City Polytechnic,
Pond Street, Sheffield, S1 1WB, UK

N C HILYARD
Materials Research Institute, Sheffield City Polytechnic,
Pond Street, Sheffield, S1 1WB, UK

A CUNNINGHAM
ICI Polyurethanes Group, Everslaan 45, B-3078 Kortenberg,
Belgium

SUMMARY

Moulded foam backed carpet composites are being introduced into production vehicles to reduce interior noise levels. However, little information has been published in the literature on their performance characteristics. In this paper we examine the fundamental aspects of two important facets of the problem. (a) The damping created by non-bonded foam layers and its influence on the modal response and transmission of airborne noise through a finite clamped panel and (b) the influence of design and material parameters on the airborne noise insertion loss of carpet composites. Theoretical models are described and their predictions compared with experimental data.

INTRODUCTION

Noise enters a vehicle through two main pathways (a) transmitted airborne noise and (b) radiated structure-borne noise. About one half of the acoustic energy is transmitted through the floor pan and bulkhead [1] so that increasing the acoustic efficiency of automotive floor coverings could lead to a reduction in interior noise with lower added weight. Although we have studied cut slabstock foam isolating layers our attention has been focused mainly on all-MDI water blown moulded units. These are CFC free, and offer the opportunity of one step assembly and they provide the acoustic engineer with the design flexibility needed to tailor the composite to meet the needs of a particular type of vehicle.

To establish how system design parameters and material property values influence the performance of a noise reduction composite it was necessary to develop methods of system evaluation - both laboratory based and in-car. This paper concentrates on the dynamics of panel motion and the airborne noise insertion loss of foam based composites determined from laboratory investigations. Other aspects of our work, such as the structure-borne insertion loss behaviour,

and single point rating of composites will be described elsewhere.

THEORETICAL BASIS

(a) Panel Vibration

A structure which is vibrating freely exhibits a number of resonances typical of the system. For a steel panel these can be obtained by a number of methods. Firstly, the panel equations of motions can be solved or secondly by using the finite element method (FEM). This second method predicts the response by describing the system by a mesh, and then considering the motion of the elements. The panel used in this work was clamped mild steel of dimensions 0.87x0.87x0.001m. The analytical solution by Warburton [2] gives the first three mode frequencies as 11.5, 23.4 and 23.4Hz, whilst the FE analysis gives 10.6, 21.3, 21.9Hz. The differences are accounted for by the small mesh used in the FE method. The finite element method is illustrated for the clamped steel panel used in Fig. 1.

{Figure 1 Finite element based visualisation of the modes of a clamped (4C) panel }

A panel undergoing forced excitation will exhibit a response that depends upon the exciting force. For most practical applications the force is acting at a point (e.g. the engine mounts in a vehicle). The theoretical analysis presented here therefore limits itself to such a system. The response of a point excited panel is complicated. There are two types of wave propagated which are important in radiation of airborne noise. Firstly, there is the direct field. This is the near field vibration. Secondly, away from the excitation point, there is resonant (far-field or reverberant) vibration. This is dependent upon system damping. The total sound radiated from the panel is the sum of the contribution of these two wave types. This is given by Cremer *et al* [3] as;

$$P = \frac{\rho F^2}{2\pi m_s^2}\left(1 + \frac{U}{2Sk_b\eta}\right) \quad \text{Watts} \qquad (1)$$

near reverberant

where m_s is area mass of the panel
F is r.m.s. exciting force
k_b is bending wave number
S is panel area
U is panel circumference
η is panel damping
ρ is the density of air

Examination of equation (1) shows that the radiated power is only

significantly reduced by additional damping if $2\eta k_b S/U<1$. This expression gives us the optimum loss factor above which extra damping will have a minimal effect.

(b) Airborne Transmission

{Figure 2 Transmission line model for airborne transmission through a composite}

The transmission loss (TL) for the composite in fig. 2 is given by;

$$TL = 20 \log_{10} \frac{P_i}{P_t} \quad dB \qquad (2)$$

where P_t and P_i are the transmitted and incident sound pressures.

The system performance can also be represented by the insertion loss (IL) of the added foam and septum layer.

$$IL = TL_{composite} - TL_{panel} \quad dB \qquad (3)$$

This expression allows experimental measurements to be conducted more easily.

The addition of a PUR foam to a vibrating panel affects the transmission loss [4]. Where the foam area density is low compared with the panel area density, at low frequencies the motion of the foam is similar to that of the panel. Thus the TL of the panel is relatively unaffected. At higher frequencies, the wavelengths of sound become comparable to the system dimensions, and thus energy dissipation mechanisms occur, reducing radiated sound energy. The TL of the composite thus becomes greater than the panel alone.

The addition of a septum layer to the panel and foam introduces a mass-spring-mass resonance to the system. This is important when designing a system as the improvement in TL at this frequency is small, or in some cases negative, i.e. the transmitted noise intensity with the foam and septum is greater than with the panel alone. Thus, if an incorrect choice of material is made a degradation in performance can result. The theoretical analysis is based upon the impedance of the layers that make up the composite. The technique was first used to analyse and predict the performance of aircraft sidewalls by Beranek [5], with fibreglass cores. The analysis has been extended here for PUR foam cores. Figure 2 shows the system configuration.

The pressures p_i, p_r, p_t and p_1 to p_n are represented in the exponential form $p_n=A_n\exp[j(\omega t-k_n x)]$. The velocities are given by $u(x,t)_+=P_n(x,t)/z_n$ and $u(x,t)_-=-P_n(x,t)/z_n$, where the suffix + or - indicates a positive or negative going wave. The values of the

complex wave numbers, k_n, are related to the wave frequency and the speed of sound within the medium by $k_n=\omega/c_n$. The layer impedance $z_n=\rho_n c_n$.

Now, there is continuity of pressure and velocity at the interface boundaries. Substitution of values in the continuity equations leads to the formulation of simultaneous equations. These equations can then be solved and an expression for the ratio of the transmitted pressure wave amplitude, A_t, to the incident pressure wave amplitude, A_i, obtained. This leads to a complicated expression which can be simplified to give;

$$R = 10\ LOG_{10}\ \{\ x_1 \cosh \Gamma d_1 + x_2 \sinh \Gamma d_1\ \} \qquad (4)$$

where $x_1 = j(m_s/\rho c + \omega m_{s1}/\rho c)$ (5)

and $$x_2 = \frac{z_3}{\rho c} - \frac{\omega^2 m_s m_{s1}}{z_3 \rho c} + \frac{j\omega m_s}{z_3} \qquad (6)$$

where m_{s1} is the area mass of the septum
Γ is the propagation constant for the foam

The propagation constant Γ, and impedance z_3, for the foam are dependent upon material properties. The values can be obtained from impedance tube measurements [6]. In this analysis they are found from the expression given by Bies [7];

$$\Gamma = j\omega \sqrt{(Y\rho'/K)} \qquad (7)$$

and the characteristic impedance given by ;

$$z_3 = \sqrt{(\rho' K/Y)} \qquad (8)$$

where Y is the porosity
K is the foam bulk modulus, related to Young's modulus by $K=E/[3(1-\gamma)]$, γ is Poisson's ratio equal to zero when the foam is in compression.

$$\rho' = (\rho_3 + \rho_0)\left(1 - \frac{jR_2}{\rho_{tot}\,\omega}\right) \qquad (9)$$

The complex density, $\rho'$is used as it combines the density of the enclosed air and the porous structure, as well as incorporating the effect of viscous and inertial motion. R_2 is approximately $1.2R_1$, where R_1 is the foam flow resistivity. The factor 1.2 takes into account the combination of isothermal and adiabatic compression and rarefaction of the air enclosed by the foam matrix.

The system resonance is given by equation (10);

$$f_R = \frac{1}{2\pi}\left[\left(\frac{K^*}{d}\right)\left(\frac{1}{m_s} + \frac{1}{m_{s1}}\right)\right]^{1/2} \qquad (10)$$

The expressions in equations (4) and (10) allows airborne IL of the composite to be examined as functions of material and system parameters. The performance of the composite can thus be optimised.

EXPERIMENTAL

The laboratory test facility used to study the effects of non-bonded foam layers and composites on panel motion and the insertion loss of composites has been described previously [8,9]. The facility consists of a small brick/concrete box enclosing an array of loudspeakers. These are connected via a power amplifier to a Bruel & Kjaer broadband noise source. Structure-borne excitation is provided by a loosely coupled electromagnetic shaker, again supplied by random noise by a power amplifier. Samples are mounted horizontally on a 1mm steel panel. Loss factor measurements are obtained by measuring the reverberant decay of the panel, when excited by an impulse. Radiated intensity is measured by the Norwegian Electronics 830 analyser and intensity probe 216. The probe is scanned close to the measurement surface to obtain a spatial average of the radiated intensity. The insertion loss of the composite is obtained by two measurements. First, the intensity radiated by the steel panel and second, the intensity radiated through the composite. The composite insertion loss is simply the first intensity value subtracted from the second. It is essential to ensure that samples are well sealed to prevent sound leakage.

The foams were characterised by measuring the small strain dynamic modulus and loss tangent using DMTA at 1Hz, and a modified form of the BMW [10] test. Airflow resistivity was obtained through a modified form of the BS4443 test, and normal incidence absorption using the standard test described in ASTM C384.

RESULTS AND ANALYSIS

The material properties are shown in Table 1.

Foam	Area Density	Storage Modulus	Loss Modulus	Flow Resistivity
	kgm^{-2}	$x10^5Pa$		Nsm^{-4}
A	1.69	4.21	0.25	74
B	1.71	1.25	0.42	28
C	1.33	0.84	0.44	18
D	1.84	1.17	0.41	36
E	1.69	4.21	0.25	74

Table 1 Material properties

The frequency response in Fig. 3 is for a constant acceleration of 5g. The panel displays a high modal density, as expected. This is important as subsequent analysis is to be carried out in frequency bands rather than at discrete frequencies. The non-bonded foam significantly reduces the modal resonances. We would thus expect this modal damping to enhance the IL of the composite. (This is later shown not to be the case).

{Figure 3 The effect of a non-bonded MDI foam layer on the modal response of the 4C panel for point vibration excitation}

Fig. 4 compares the effective loss factor of the clamped steel panel with the effective loss factor of the panel and foam. The steel panel loss factor is approximately ten times that of a freely supported panel, and it decreases with frequency. This agrees with other reported work [11]. However, it should be noted that slightly higher values of loss factor are obtained with other measurement methods [12].

The loss factor values predicted by the Oberst model [13] for bonded unconstrained damping treatments is in reasonable agreement with that observed for the non-bonded foam, in the frequency range for which foam loss tangent values are available.

{Figure 4 Effective loss factor of the 4C panel and panel, as a function of frequency}

Equation (1) gave an expression which gives the maximum added damping for a reduction in the noise radiating from a point excited structure. The predictions are substantiated by subjective observations that in some cases the addition of damping increases radiated noise [3]. This is attributed to the change in resonance due to added mass. The optimum loss factor is shown in Fig. 4 for the steel panel under test, and indicates that at 100Hz there is little reason to increase the panel loss factor above 0.04 and at 1kHz above 0.015.

{Figure 5 The optimum effective loss factor of the panel and composite predicted by Cremer *et al* (Equation 1)}

Figure 6 compares the airborne IL of the panel and foam, and panel with foam and septum layer of 5.9kgm^{-2}. It can be seen that in the range 100-1000Hz that the foam layer alone has little influence on the system IL, although it does has a marked effect on the panel effective loss factor as shown above.

{Figure 6 Comparison of the airborne noise insertion loss of a foam layer and foam and heavy layer}

The influence of septum unit mass is illustrated in Fig. 7. It can be seen that increasing the unit mass of the septum moves the resonance frequency to lower values, as expected, and increases the IL at resonance. It is seen that there is reasonable agreement between the model predictions and experiment.

{Figure 7 (a) Experimental data showing the influence of septum unit mass on the airborne insertion loss of a composite and (b) the behaviour predicted by the model (Equation 4)}

Increasing the modulus of the foam causes the resonance frequency to increase, as expected, and the insertion loss at resonance to increase. There is reasonable agreement between the theory and the experiment. It should also be noted that at higher frequencies the IL curves cross over.

{Figure 8 (a) Experimental data showing the influence of foam modulus on the airborne insertion loss behaviour and (b) behaviour predicted by the model }

The model can be used to examine the influence of material and system parameters. Fig. 9 shows the predicted influence of foam thickness. It can be seen that increasing the foam thickness reduces the resonance frequency, and also increases the IL at resonance. At low frequencies (approximately 100Hz) there is little difference between the insertion losses.

{Figure 9 Influence of foam thickness as predicted by the theoretical model}

CONCLUSIONS

This paper has presented theoretical and experimental data concerning the behaviour of panel vibration and the influence of foam layers upon this panel vibration.

We have shown that there is an optimum system loss factor, above which added damping has negligible effect upon radiated noise. Also, the prediction of effective system loss factor for bonded layers has been shown to agree with those measured experimentally for unbonded foam layers.

Experimental data has demonstrated the influence of septum unit mass and foam modulus upon the insertion loss and the resonance frequency.

A theoretical model has been described to predict system performance and has reasonable agreement with measured data. The theoretical model also enables investigation of the influence of system and material parameters on system performance. This is an important as a tool for the optimisation of system performance for a design application.

REFERENCES

[1] GAHLAU H.K.
Advanced Noise Control in Automotive Engineering, (Dr. Alois Stankievicz GMBH), Proc. Polyurethanes World Congress 1987

[2] WARBURTON G.B.
Proc. Inst. Mech. Eng., Ser. A, 168(12), pp. 371-384, 1954

[3] CREMER L., HECKL M., UNGAR E.E.
Structure-Borne Sound, 2nd Edition, Springer-Verlag, 1988

[4] SCHULTZ T.J.
Wrappings, Enclosures and Duct Linings, Chapter 15, Noise and Vibration Control, Edited by L.L. Beranek, Institute of Noise Control Engineering, 1988

[5] BERANEK L.L., WORK G.A.
Sound Transmission Through Multiple Structures Containing Flexible Blankets, J. Acoust. Soc. Am., 21(4), pp.419-428, 1949

[6] KUTRUFF H.
Applied Science Publishers, 2nd edition, 1978

[7] BIES D.A.
Acoustical Properties of Porous Materials, Chapter 10, Noise and Vibration Control, Edited by L.L. Beranek, Institute of Noise Control Engineering, 1988

[8] LING M.K., HILYARD N.C., HENG R.B.W.
Performance of Polyurethane Cored Carpet Composites for Vehicle Interior Noise Control, Proc. Inst. of Acoustics '90, Southampton, March 27-30, Vol. 12, Part 1, pp.307-316, 1990

[9] HILYARD N.C., ELLIOT A.M., CUNNINGHAM A., MACFARLAND D.
Tailor-Made All MDI Based Moulded Floor Systems for the Automotive Industry, Proc. 33rd Annual Polyurethane Technical/Marketing Conference, Sept.30-Oct.3, 1990

[10] BMW INFORMATIONSPAUSE
Drawing No. 1 933 613, 16 August 1984

[11] TARNOCZY T.
Vibration of Metal Plates Covered With Vibration Damping Layers, J. Sound and Vibration, 11(3), pp.229-307, 1970

[12] BIES D.A., HAMID S.
In Situ Determination of Loss and Coupling Loss Factors by the Power Injection Method, J. Sound and Vibration, 70(2), pp.187-204, 1980

[13] OBERST H.
Über die Dampfung der Biegeschwingungen Dunner Bleche Durch Fest Haftende Belage, Acustica (Beihefte), 1954, 4, pp. 181-194

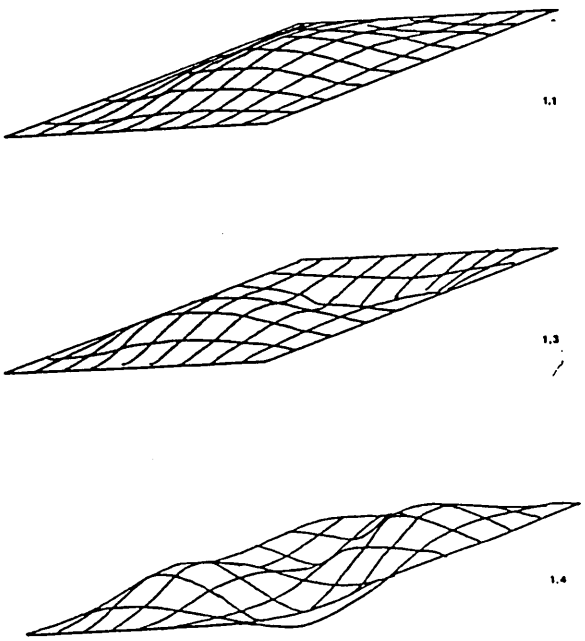

Figure 1

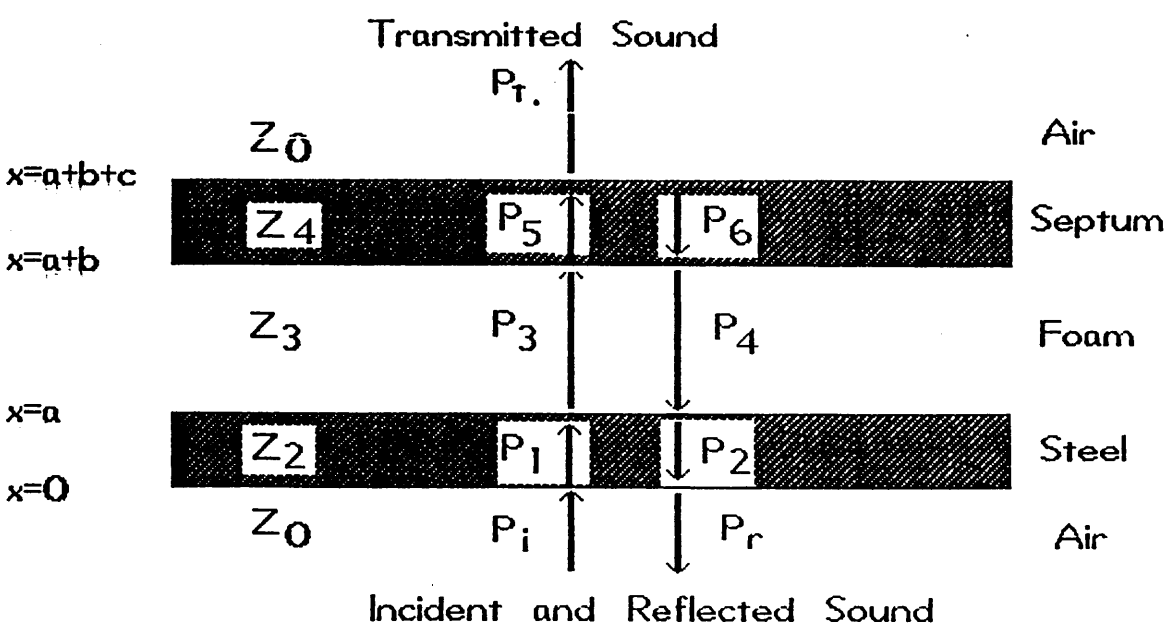

Figure 2

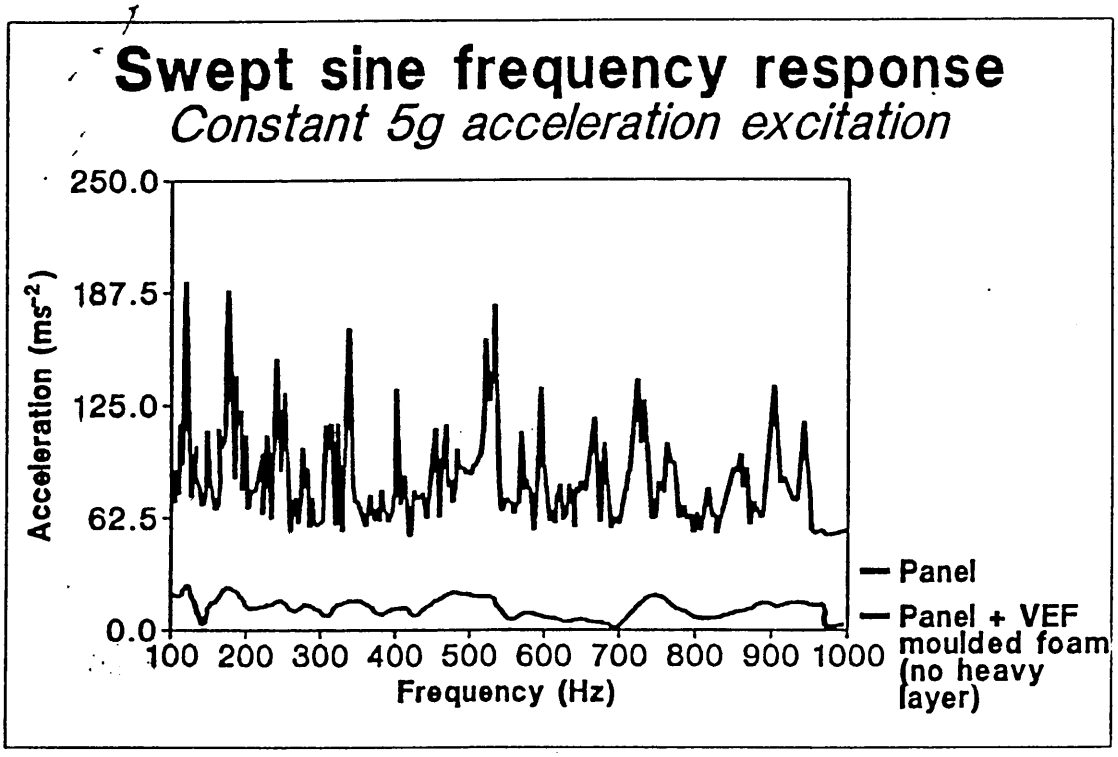

Figure 3

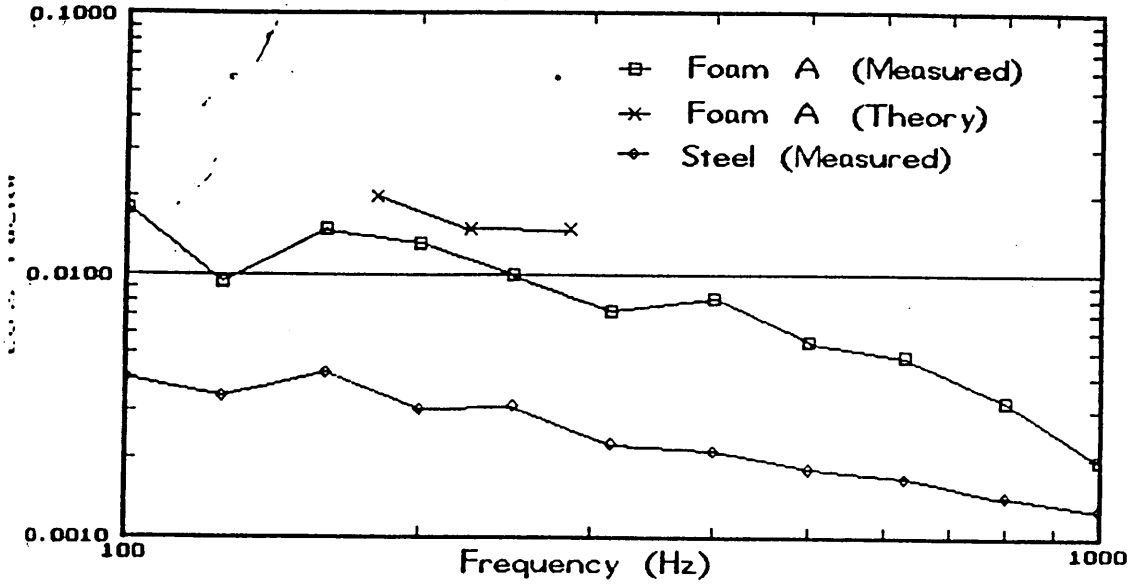

Figure 4

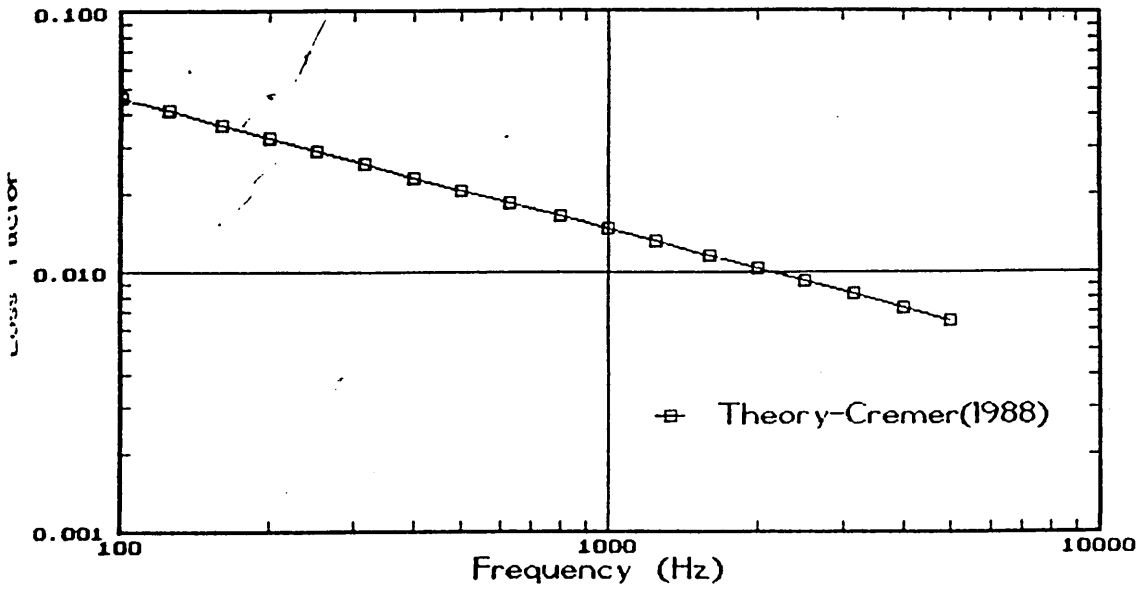

Figure 5

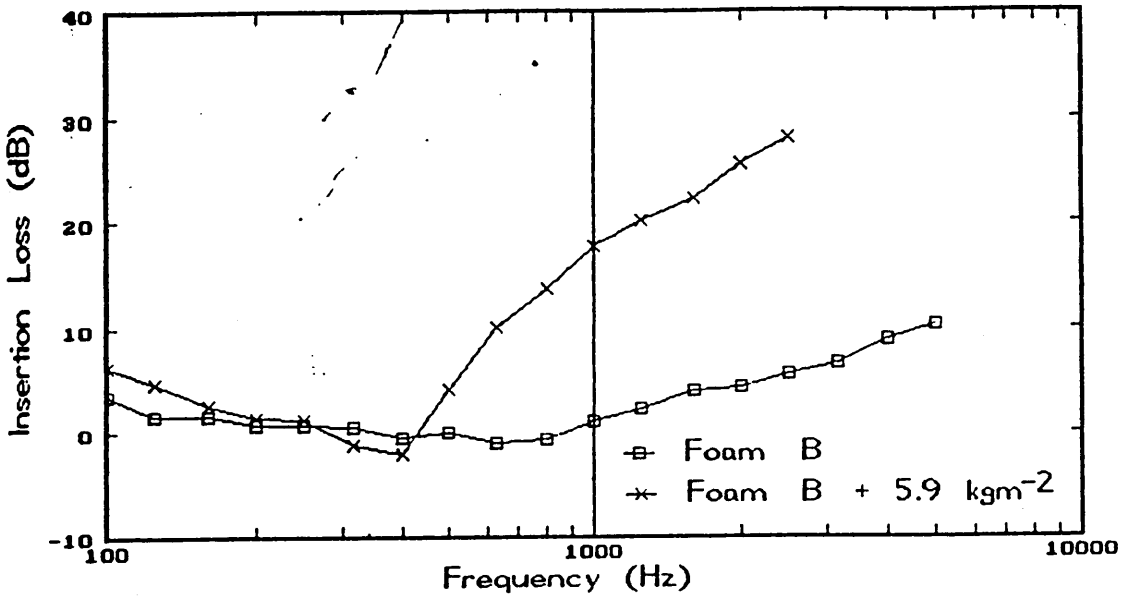

Figure 6

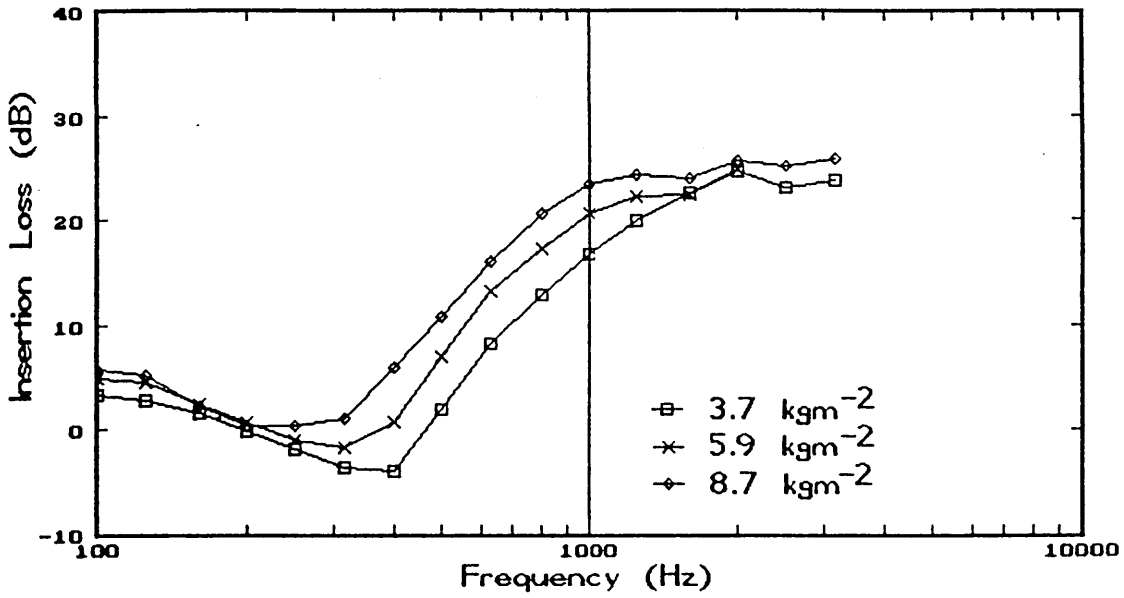

Figure 7a

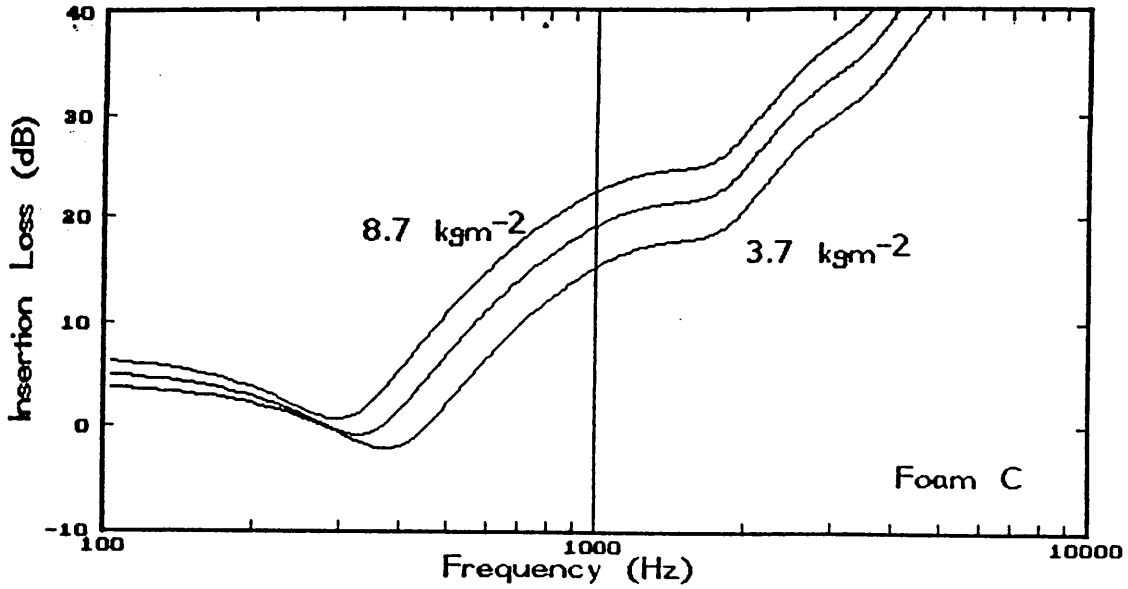

Figure 7b

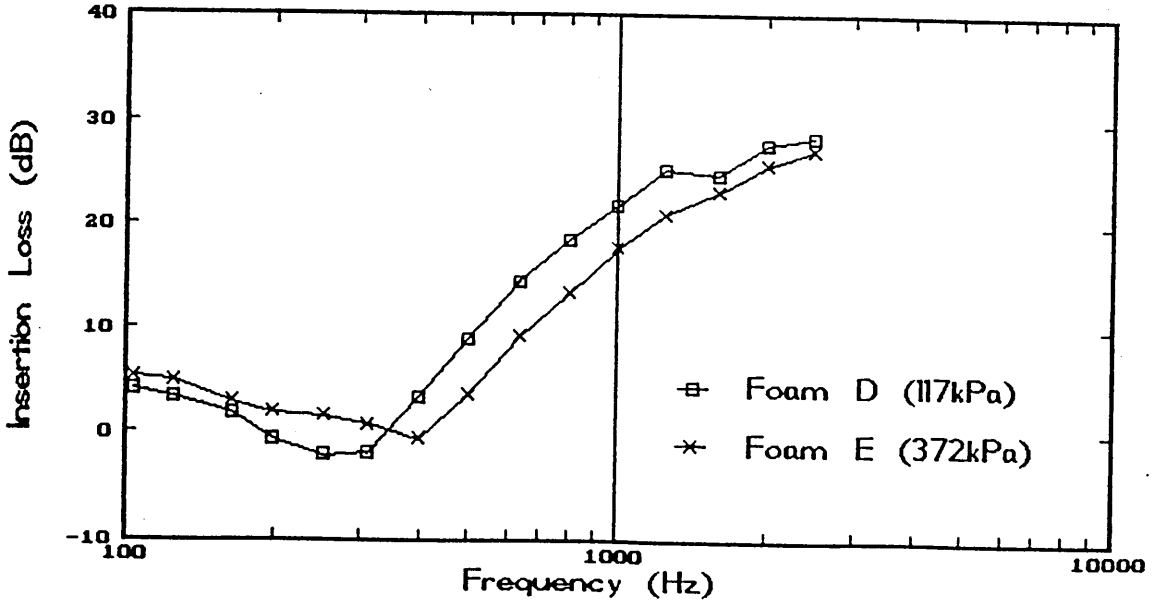

Figure 8a

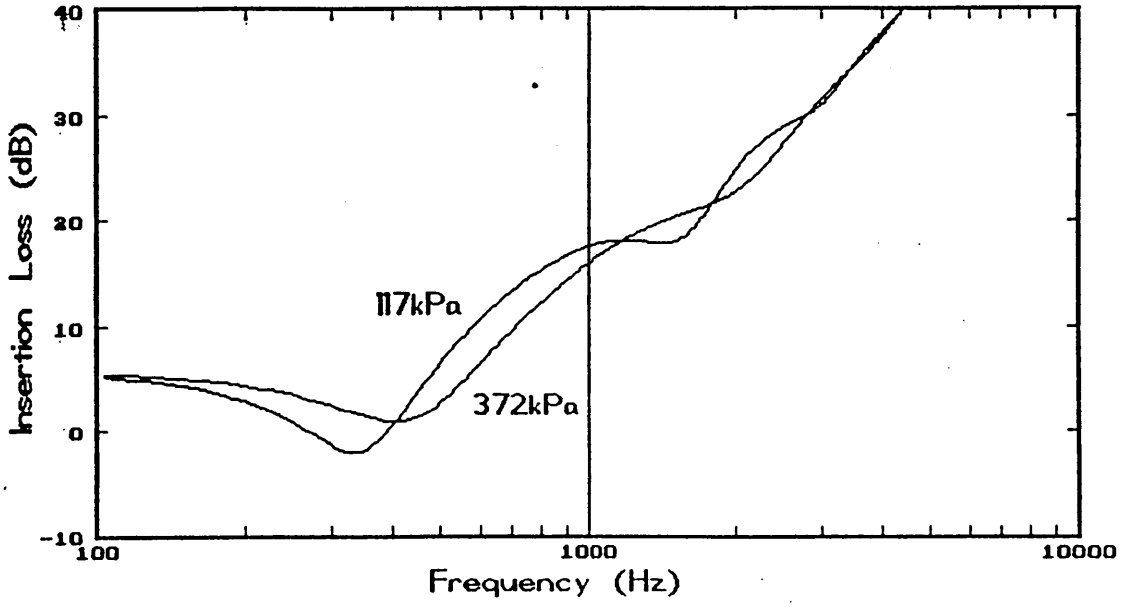

Figure 8b

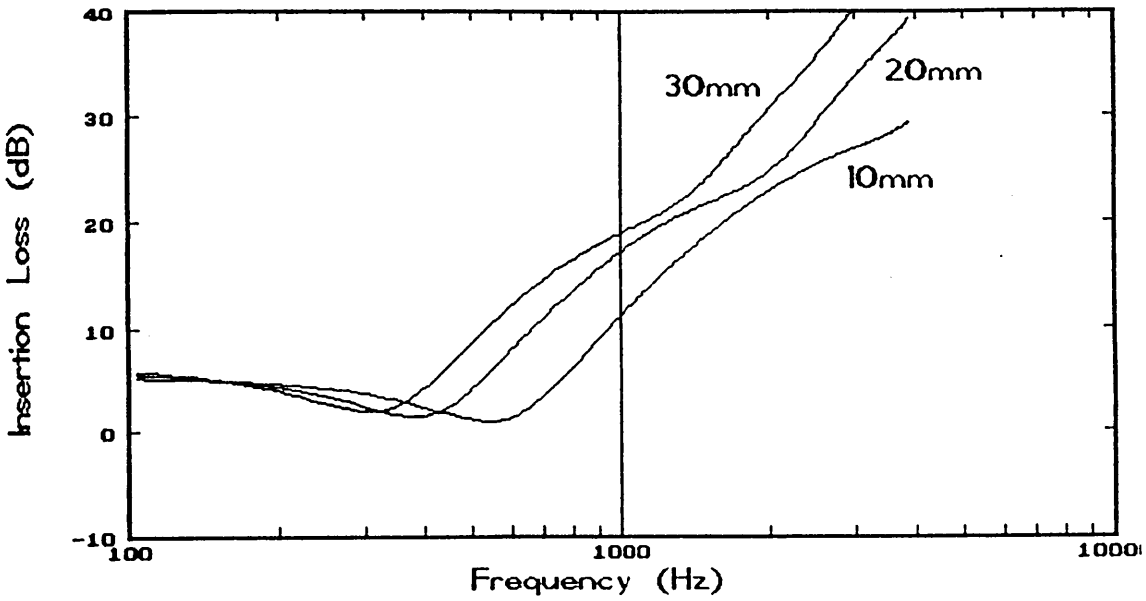

Figure 9

3. Journal of Sound and Vibration, 158(1) 1992

VEHICLE INTERIOR NOISE CONTROL USING THREE LAYER COMPOSITES WITH POLYURETHANE CORES

M.K. LING

Division of Applied Physics, Sheffield City Polytechnic, Sheffield, S1 1WB, United Kingdom

Insertion loss results are presented for a series of small scale laboratory tests on three layered polyurethane cored systems. These systems are utilised in under-carpet treatments, applied to vehicle floor pans. Experimental insertion loss values are compared for a number of configurations differing in material and system parameters. A theoretical approach is presented, with predictions showing good correlation with those obtained experimentally below 2kHz. The small-scale test facility used to obtain the system insertion loss is also briefly described.

1. Introduction

The studies by Priede and Jha [1,2] highlighted the sources of vehicle interior noise. They reported that the main noise sources originate from the engine, the tyre/road interface and aerodynamic effects of the body. At low frequencies the dominant source is the engine noise and due to the periodic nature of the combustion process this contributes a discrete frequency component to the overall noise spectra. As the other sources have a broad frequency spectra, it is this low frequency noise which causes the most annoyance to the vehicle occupants.

Within this paper are detailed results and discussion of the insertion loss measurements and theoretical predictions for three layered foam cored systems. These systems, illustrated in Figure 1, are now widely used in the automotive industry as vehicle under-carpet noise control treatments [3], to attenuate airborne noise and damp out structural vibration. If the composite is considered as a damped mass-spring-mass system a resonance is introduced. For most common polyurethane (PUR) foams this resonance occurs in the same frequency range as the engine firing frequency, 100-300Hz. If insufficient care is taken in the choice of materials a carpet system could thus be detrimental to interior noise reduction. This work therefore aims to optimise the system attenuation at resonance, whilst maintaining performance at the higher frequencies. Experimental evaluation of system performance was achieved using the insertion loss measurement technique described in Section 3. The theoretical approach [4] is based upon a transmission line formulae and is described in Section 2. The theoretical predictions from this analysis are presented in Section 4 and compared with experimental data. These results demonstrate that control of system insertion loss can be achieved by careful choice of material and system properties. Experimental studies establish that this is also achievable in practice. The application of the analysis is not restricted to the automotive industry as similar structures occur elsewhere, e.g. the lagging of ducts [6].

2. THEORETICAL TREATMENT OF THE THREE LAYERED SYSTEM

The theoretical system used is illustrated in Figure 2. The configuration consists of a steel base panel, a polyurethane foam core layer, and a heavy septum layer. A further carpet layer is used in the vehicle, but experimental work has shown it is only significant at frequencies above 2500 Hz, and is therefore outside the main frequency range of interest. This is also true of the frequency at which coincidence occurs, which is typically 50kHz.

The analytical approach towards the system is by applying the condition of continuity of pressure and particle velocity at the interfaces. The solution of the resulting simultaneous equations yields the system transmission loss. This technique, utilising the layer impedances, has been used by a number of authors [4-6] for analysis of fibrous blanket materials.

The analysis can be simplified for normal incidence by a set of general equations [4] which when applied to the three layer system reduce to;

$$R = 10\ LOG_{10}\ \{\ x_1 \cosh \Gamma d_1 + x_2 \sinh \Gamma d_1\ \} \qquad \langle 1 \rangle$$

$$\text{where } x_1 = j(\omega \rho_{s1}/\rho c + \omega \rho_{s2}/\rho c) \qquad \langle 2 \rangle$$

$$\text{and} \quad x_2 = \frac{z_3}{\rho c} - \frac{\omega^2 \rho_{s1}\, \rho_{s2}}{z_3\, \rho c} + \frac{j\omega \rho_{s1}}{z_3} \qquad \langle 3 \rangle$$

d_1 is the foam thickness

ρ_{s1} and ρ_{s2} are the surface densities in kgm^{-2} of the panel and

septum respectively.

The propagation constant of a wave though a porous material [9] is

$$\Gamma = j\omega \sqrt{(Y\rho'/K')} \quad \langle 4 \rangle$$

and the characteristic impedance,

$$z_3 = \sqrt{(\rho' K'/Y)} \quad \langle 5 \rangle$$

The complex density, ρ' in equation <6> combines the density of porous structure and the enclosed air, and includes the effects due to viscous and inertial motion, which cause it to be complex.

$$\rho' = \rho_{tot} \left(1 - \frac{jR_2}{\rho_{tot}\,\omega}\right) \quad \langle 6 \rangle$$

The bulk compression modulus K^* is also represented as the combination of the foam modulus and the contained air modulus, i.e. $K^* = (K'_{foam} + K'_{air})(1+j\eta)$. The bulk compression modulus, K^*, is related to Young's modulus by $K^* = E^*/[3(1-2\sigma)]$.

The system resonance frequency, f_R, can be obtained by setting the imaginary part of equation <1> to zero, to give;

$$f_R = \frac{1}{2\pi}\left[\left(\frac{K^*}{d}\right)\left(\frac{1}{\rho_{s1}} + \frac{1}{\rho_{s2}}\right)\right]^{1/2} \quad \langle 7 \rangle$$

Experimental results were obtained in terms of the insertion loss of

the added foam and septum. This can be theoretically calculated using the relationship in equation <8>. The transmission loss of the steel panel, R_{panel}, is calculated from the mass law, and the composite transmission loss, R_{system} from equation <1>.

$$IL = R_{system} - R_{panel} \qquad <8>$$

3. MEASUREMENT PROCEDURE

The measurement procedure is illustrated in Figure 3. The test facility [8] enables the insertion loss of unbonded horizontal samples to be obtained, important as the trend is for unbonded carpet systems [11]. The broadband random noise source is provided by an array of loudspeakers, connected to a B&K 1024 sine/random noise generator. The radiated intensity was measured using the Norsonic AS 830 analyser with 216 p-u intensity probe. Scanned measurements were used to obtain a single value spatial average intensity. The scan speed was $0.4ms^{-2}$, and the probe to surface distance 0.1m in line with draft standards [12]. The use of intensity measurements obviates the need for a diffuse receiving environment. The pressure-intensity (p-I) index was monitored to ensure that an active sound field was present, and that the measurement data was valid. The p-I values were typically 4-5dB for the steel panel and 8-9dB when the composite was in place. Two measurements of radiated intensity are required to obtain the system insertion loss. The first measurement from the bare steel panel, and the second from the steel + foam + septum layer. The insertion loss is simply the difference of the two measurements. Comparison between the behaviour

predicted by equation <10> can thus be made with experimental data.

4. RESULTS

The mechanical and material properties of the foam cores are contained in Appendix II. Theoretical results are presented which examine the influence of two important parameters (foam modulus, and septum mass). These results are compared with measured insertion losses.

(a) Septum Mass

Three septum surface masses (3.7, 5.9, 8.7 kgm^{-2}) were used with foam A. The theoretical and experimental data is shown in Figures 4 and 5. The experimental data agrees with the predicted results below 2kHz. It is seen that with increasing septum area mass the resonance frequency, f_R decreases and the IL level increases above resonance.

(b) Foam Modulus

This was investigated using foams B, C and D. These had moduli of 0.41, 1.17 and 3.72 $x10^5 Pa$. The theoretical predictions are shown in Figure 6, and the measured data in Figure 7. Once again there is good agreement between theoretical and measured data. The theoretical predictions show two phenomena. Firstly that an increase in foam modulus causes an increase in the resonance frequency, and a consequent decrease in IL level. Secondly, with decreasing f_R the IL at

resonance decreases, indicating that the effect of foam damping is reduced.

5. CONCLUSIONS

This short paper has introduced a theoretical treatment of foam cored composites as used in vehicles. Experimental measurements of the system insertion loss for a number of PUR foams have been presented, and compared with theoretical predictions. Good agreement between the data was observed below 2kHz. The importance of system and material properties has been demonstrated theoretically and experimentally. It can be concluded that by careful choice of system parameters the composite can be designed so that the resonance occurs at an optimum position. This is obviously dependent upon the noise source signature.

6. ACKNOWLEDGEMENTS

The author would like to thank Dr. N.C. Hilyard of Sheffield City Polytechnic, Sheffield, I.C.I. Polyurethanes, Blackley, Manchester and Mr. R. Rodwell, Gracey and Associates, Chelveston, Northants for their assistance in this work.

7. REFERENCES

[1] T. PRIEDE, S.K. JHA, 1970 Low Frequency Noise in Cars, Journal of Automotive Engineering, July pp. 17-21

[2] T. PRIEDE, 1971, Origins of Automotive Noise, J. Sound and Vibration, vol.15(1), pp.61-73

[3] N.C. HILYARD, A.M. ELLIOT, A. CUNNINGHAM, D. MACFARLAND, 1990, 33rd Annual Polyurethane Technical/Marketing Conference, Sept.30-Oct.3, pp.631-638

[4] L.L. BERANEK, G.A. WORK, 1949, Sound Transmission Through Multiple Structures Containing Flexible Blankets J. Acoust. Soc.

Am., vol.21(4), pp.419-428
[5] R.A. MANGIAROTTY, 1963, Optimisation Of The Mass Distribution And The Air Spaces In Multiple-Element Soundproofing Structures J. Acoust. Soc. Am., vol.35,pp.1023-1029
[6] A.C.K. AU , K.P. BYRNE, 1987, On The Insertion Losses Produced By Plane Lagging Structures, J.Acoust.Soc.Am., vol.82(4),pp.1325-1333
[7] M.E. DELANY, E.N. BAZLEY, Nat. Phys. Lab. Aerodyn. Div. NPL Aero Report AC37
[8] M.K. LING, N.C. HILYARD, R.B.W. HENG, 1990, Performance of Polyurethane Cored Carpet Composites for Vehicle Interior Noise Control, Proc. Institute of Acoustics, vol.12, Part I, pp.307-316
[9] D.A. BIES, 1988, Acoustical Properties of Porous Materials, Chapter 10, Noise and Vibration Control, ed. L.L. BERANEK, pub. Inst. of Noise Control Engineering
[10] P.A. MORSE, 1986, Vibration and Sound, pub. Acoust. Soc. Am.
[11] I.C.I. Polyurethanes Newsletter, 1990, Vol. 4, No.7
[12] ANSI S12.21, Engineering Method for the Determination of Sound Power Levels of Noise Sources Using Sound Intensity

APPENDIX I LIST OF SYMBOLS

A amplitude of incident or transmitted intensity
d foam core thickness
E^* Young's modulus
f frequency
f_R mass-spring-mass resonance frequency
j complex operator ($\sqrt{-1}$)
k wave number
K^* bulk modulus
K' storage modulus of porous material
K'_{foam} foam storage modulus
K'_{air} air storage modulus
P,p pressure
R transmission loss
R_1 flow resistivity
R_2 approx. $1.2R_1$ (see ref. [9] and [10])
x axial distance
Y porosity of foam
z impedance

η loss factor
ρ_0 density of air
ρ_3 density of foam
ρ_{tot} combined density of air and foam
ρ_{s1} area density of steel panel or floor pan
ρ_{s2} area density of septum
ω angular frequency
Γ propagation constant
σ Poisson's ratio

APPENDIX II MATERIAL PROPERTIES

Foam	Thickness	Area Density	Storage Modulus	Loss Modulus	Flow Resistivity
	mm	kgm^{-2}	$x10^5Pa$		Nsm^{-4}
A	20	1.26	0.63	0.62	182
B	20	1.67	0.41	0.43	26
C	30	1.73	1.17	0.35	36
D	20	1.58	3.72	0.27	74

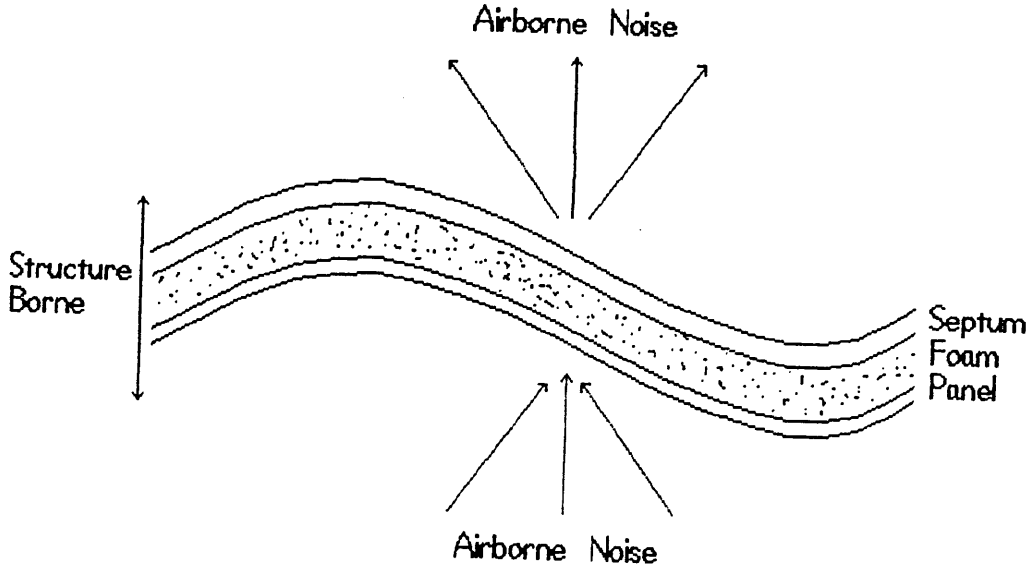

Figure 1 Foam cored composite system

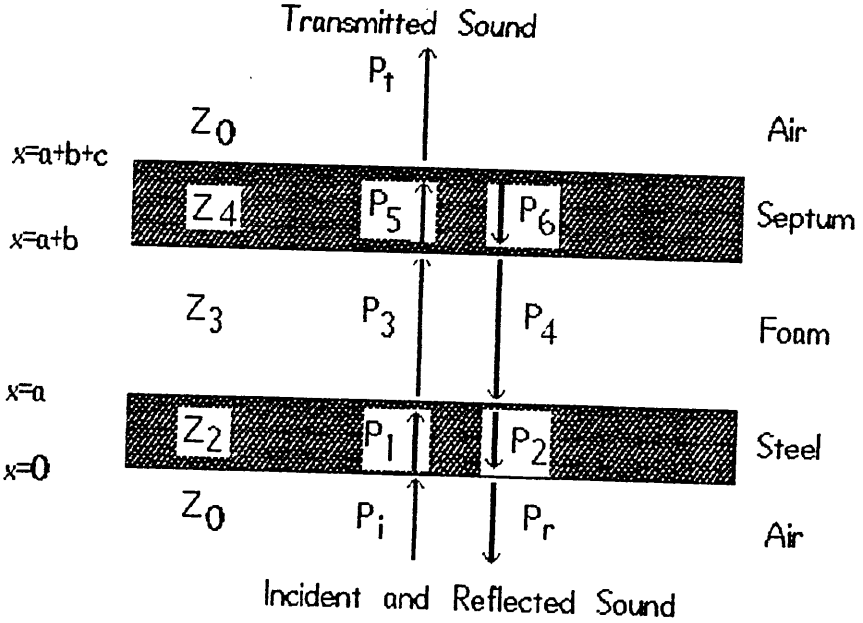

Fig. 2 Theoretical composite system

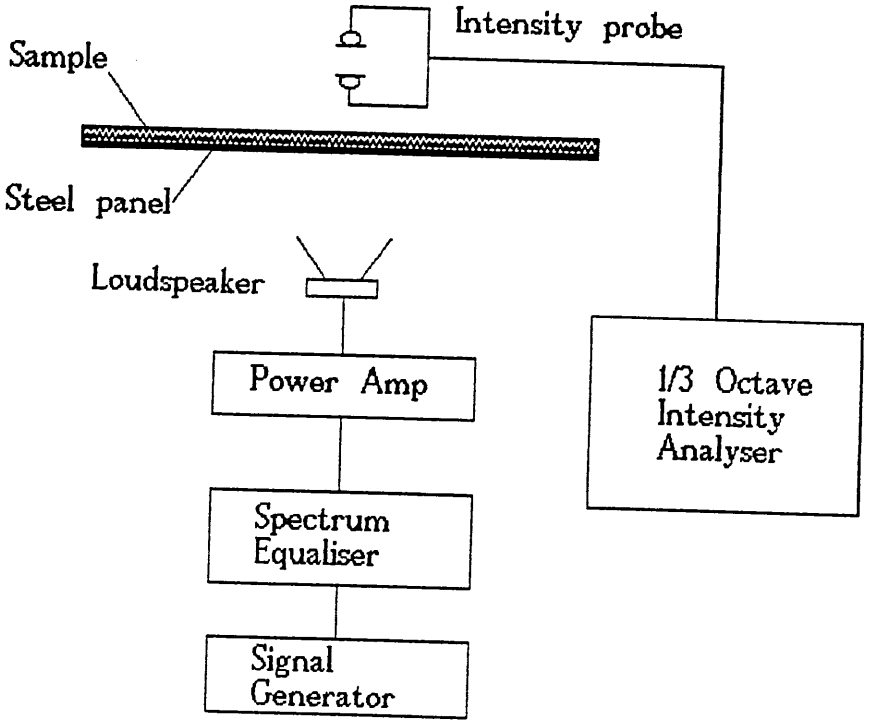

Figure 3 Experimental measurement of insertion loss

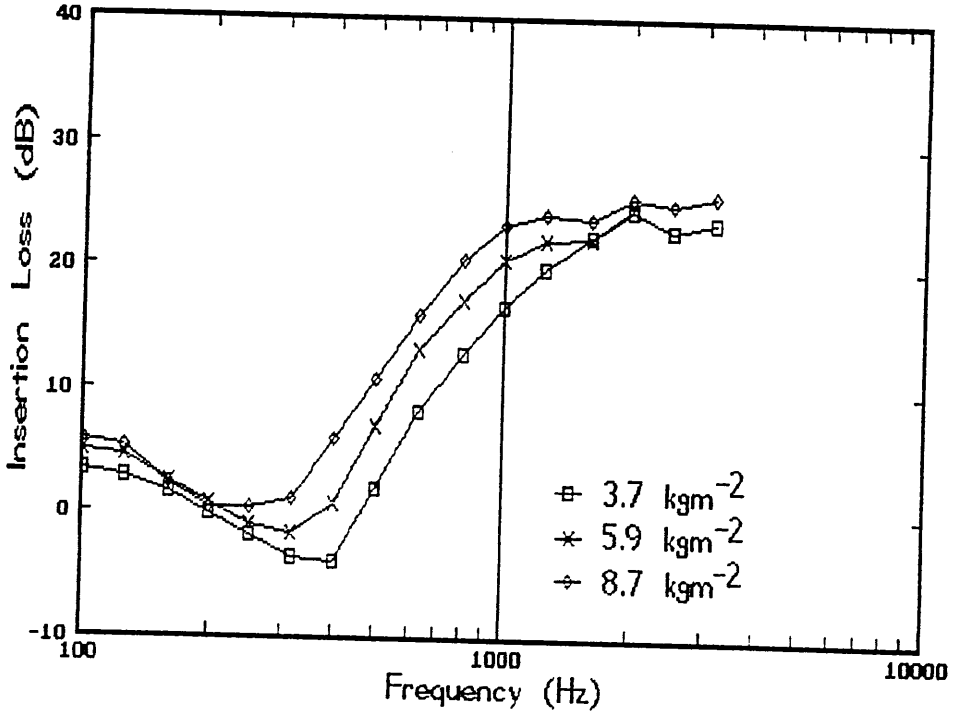

Fig. 4 Measured influence of septum mass-3.7, 5.9, 8.7kgm^{-2} (foam A)

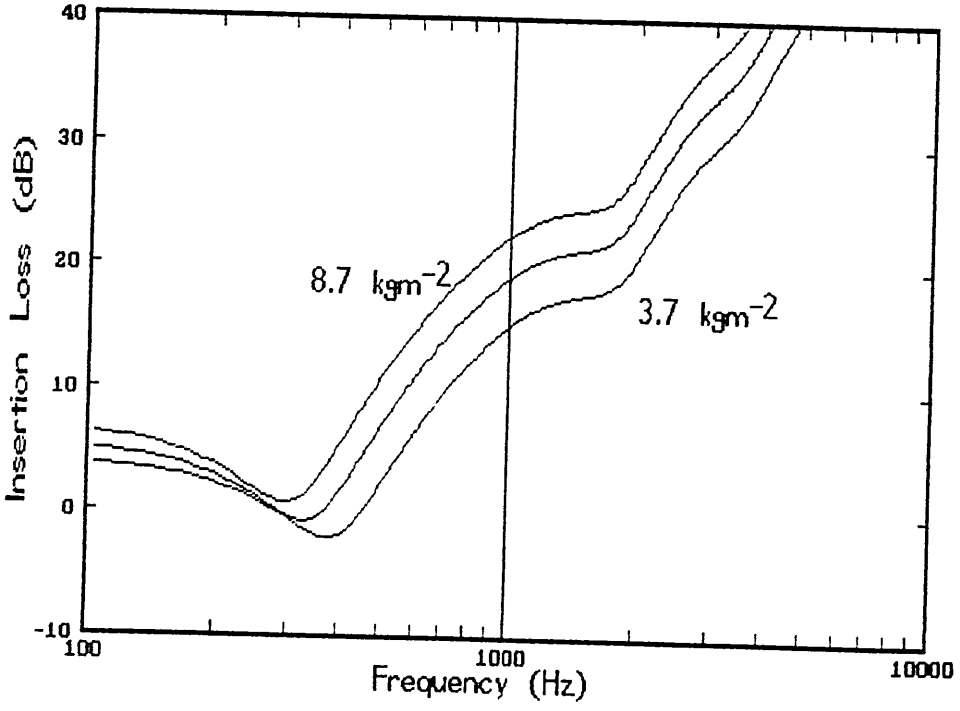

Fig. 5 Predicted influence of septum mass - 3.7, 5.9, 8.7kgm^{-2} (foam A)

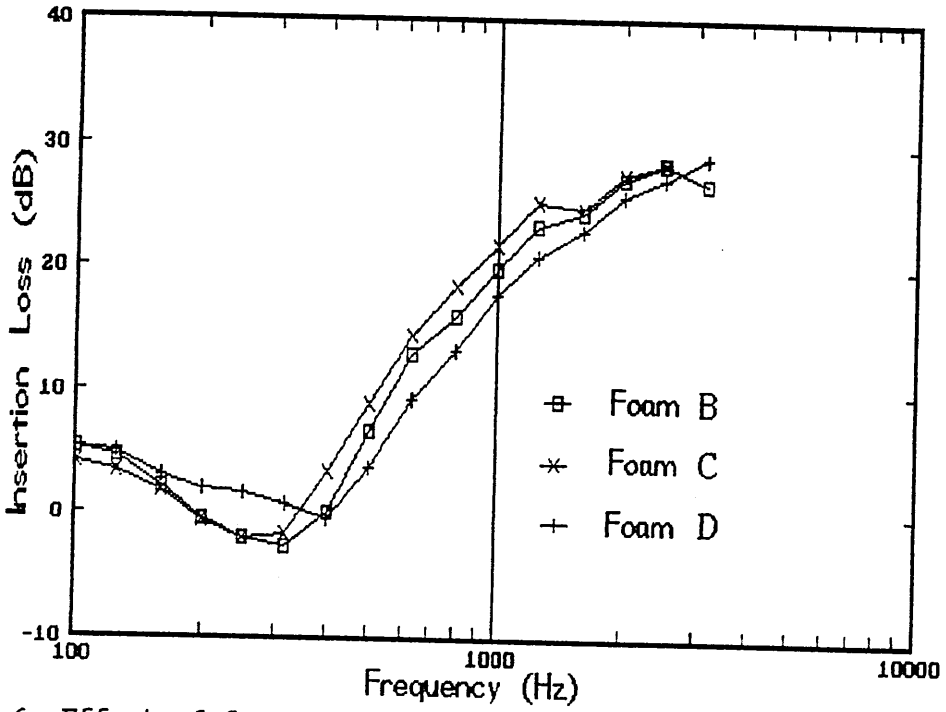

Fig. 6 Effect of foam modulus on measured IL

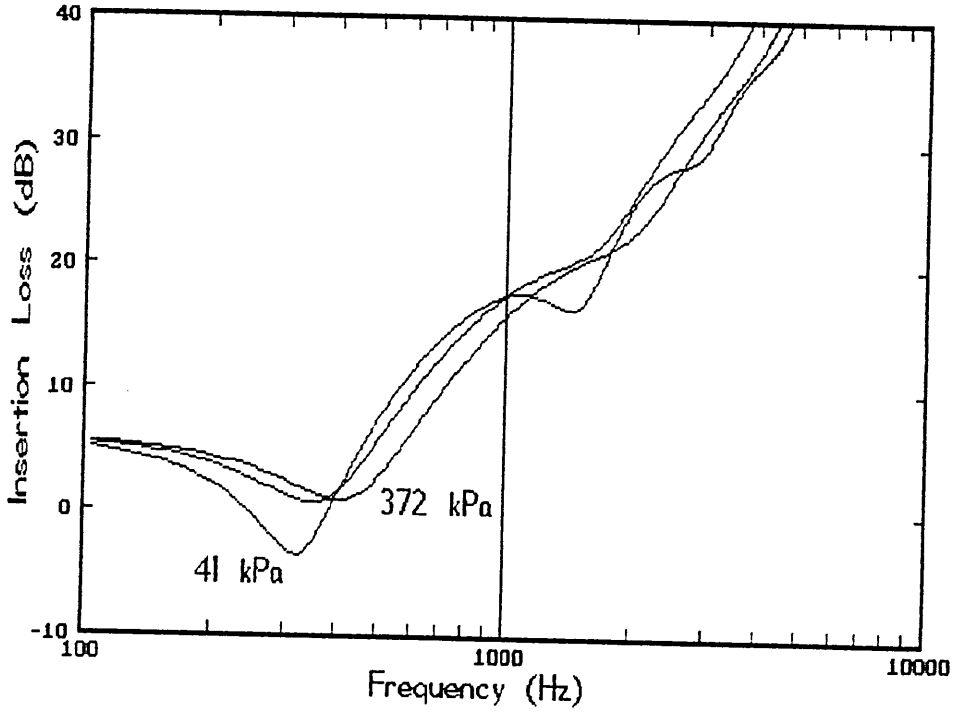

Fig. 7 Predicted IL for foams B, C and D

4. Journal of Automotive Engineering, Proc. I.Mech.E. Part D, Vol. 206, 1992

Measurement of Sound Insulation of Automotive Body Components using Sound Intensity

Matthew K. Ling, BSc

Division of Applied Physics, Sheffield City Polytechnic,
Pond Street, Sheffield, S1 1WT

(Now at Building Research Establishment, Garston, Watford, Hertfordshire, WD2 7JR)

Synopsis

A small scale test facility is described which enables manufacturers to assess the sound insulation of noise reduction treatments. Designed to provide a cheap and quick alternative to standard test methods, the technique uses sound intensity to measure the insertion loss of noise reduction treatments when subjected to airborne noise.

1. Introduction

Automotive noise reduction composites are normally assessed using in-car tests (1), large scale transmission loss (2) or small scale facilities e.g. APAMAT II (3). These tend to be costly with time consuming procedures. The test facility and measurement technique described here provide the manufacturer with a method that enables

fast and reproducible measures of insertion loss to be made. It was designed to allow the testing of foam backed carpets to examine the effect of various parameters (e.g. foam thickness, density etc.) upon the system insertion loss (4), but has application to the testing of other vehicle body components (e.g windows). This would obviously require a modification of the test-rig to allow mounting of the component.

The need for a small scale laboratory test facility, which satisfied the requirements of economical, but effective, evaluation of material attenuation properties has been an attractive proposition for many years. A number of small scale test facilities have been employed. The earliest appears to be that described by Wallace (5) and Nichols (6). This measured transmission loss for small section (18" x 18") aircraft panels, and was later modified by Beranek (7). It provided a measure of transmission loss for the materials under test. More recently GM and Bridgestone (Japan) have used a similar facility for their transmission measurements. Existing facilities utilise sound pressure measurements. These are unreliable in the near field and subject to large fluctuations over small distances (8). The technique described here utilises sound intensity instrumentation to overcome these near field effects.

The technique allows the insertion loss of a sound reduction treatment to be assessed. The insertion loss of a material is often more useful than its sound reduction index. It is a measure of the reduction of radiated noise when the material is applied to the radiating surface. It thus enables ranking of performance. If a conventional

transmission loss suite was used, sound reduction indices would be measured for the complete system i.e. steel + foam composite. The relationship between sound reduction index and insertion loss is detailed in Appendix 1.

2. Test Facility and Instrumentation.

The test facility is illustrated in Figure 1 below. It has approximate external dimensions of $1m^3$. The walls are of a sand/lime brick and mortar construction, upon a reinforced concrete base. These provide high density walls to minimise radiation from the test rig sides. The base rests upon four TICO anti-vibration mounts. The top is also of reinforced concrete, with an aperture of 870x870mm cut out. A 2.5cm thick chipboard baffle with a small array of loudspeakers is located 300mm above the base. The loudspeakers consisted of a 100W woofer (Celestion, type G12H-100T3597 CE 8Ω) with a frequency response from 50 Hz to 3.5 kHz, and two piezoelectric tweeters with a frequency response from 2.2 kHz to 33 kHz. A 1mm steel sheet was placed over the aperture, and secured with a 4mm angle iron framework and toggle clamps. These enable quick access to be made to the source chamber. A thin self-adhesive foam layer is attached to the edges of the steel panel to ensure good sealing from acoustic leakage when clamped. (The 1mm thick mild steel panel was used as being representative of vehicle panels). Access holes in the sides allow cabling from the loudspeaker and monitoring microphone to be routed. These are easily sealed to prevent leakage during measurements.

Broadband excitation was provided via a B&K 1024 Sine/Random generator, shaped by a Sony graphic equaliser, and amplified by a Sony power amplifier (type TA-1130). The internal level was monitored by a 1/2" microphone connected to a B&K 2031 narrow band real time analyser. The radiated intensity was measured using a Norwegian Electronics (Norsonics) 830 1/3 octave real time analyser with intensity probe (type 216). The Norsonics 216 is a p-u type, measuring the pressure,p and air particle velocity, u directly. The instantaneous product of p and u gives the intensity. The probe geometry limits the frequency range to f<3150 kHz for a measurement accuracy of 1dB. Alternatively a two microphone probe (e.g. B&K type 4177) with appropriate spacers could be used for a wider operational frequency range.

3. Measurement of Insertion Loss

The insertion loss of the treatment is obtained using the following method. First the radiated intensity from the steel panel is measured, to give a value I_1. With the treatment in place a second intensity level measurement, I_2 is made. The insertion loss, IL, is the difference of these two measurements (see Appendix 1);

$$IL = \bar{I}_1 - \bar{I}_2 \qquad \text{dB} \qquad 1$$

The intensity can be measured either by sweeping the probe close to the surface, or by using a number of fixed positions to obtain an average. A swept measurement gives a single value spatial average intensity. Obviously care needs to be taken to sweep the probe at a

constant rate, and to cover the surface equally. This ensures that a good average of radiated sound intensity is obtained. Swept measurements were used in this work as they give a better approximation of the space integral (9,10). ANSI S12.21 (11) recommends that scan speeds should be preferably in the range $0.1ms^{-1}$ and $0.5ms^{-1}$ with a maximum of $3ms^{-1}$. The draft standard also recommends a surface to probe distance of between 0.1m and 0.2m, with a scan area of less than $1m^2$.

The radiated intensity was measured using scanned measurements at a distance of 0.1m from the sample surface, and a scan speed of $0.4ms^{-2}$. A fifteen second average was used. This value was chosen on the basis of radiated intensity being measured over a range of averaging times from 5 to 90 seconds. It was found that a measurement time of 15 seconds gave both a repeatable intensity value and agreed with the 90 second averaged value within 0.5 dB. The procedure is illustrated in Figure 2.

The measured data was stored onto floppy disc by the Norsonic analyser. This data was then transferred to a PC in ASCII format, and manipulated using a spreadsheet to obtain the system insertion loss.

In sound power measurements using sound intensity the power is obtained by summing the intensity over a surface enclosing the radiating object (12). Extraneous noise will contribute an intensity component that is measured as negative when entering the volume and positive on exiting. Thus the net effect is zero (9,13). This is not

the case in insertion loss measurements because the sound intensity is not measured over the surface of an enclosed volume. However if the external noise environment is stationary over the insertion loss measurement period, it can be shown that the net contribution to the insertion loss is also nil (see Appendix 2).

There are a number of field indicators which gauge the validity of an intensity measurement (12). The most widely used one is the pressure-intensity (p-I index) or reactivity index (L_k) where the local index δ_{pI} is given by;

$$\delta_{pI} = L_p - L_{Ii} \qquad \text{dB} \qquad 2$$

The global pressure-intensity index, (this is also known as the negative partial power indicator) Δ_{pI} (or F_3) is given by;

$$\Delta_{pI} = F_3 = \bar{L}_p - 10\log[1/N \; \Sigma_{i=1}^{N} I_{ni}/I_0]$$
$$= \bar{L}_p - \bar{L}_I \qquad \text{dB} \qquad 3$$

where I_{ni} is a sample normal intensity, $\bar{L}_p$ is the sample average mean square sound pressure level, $\bar{L}_I$ is the sample mean square sound intensity level, and N is the number of samples.

The F_3 index provides information about the sound field present. A high value indicates that external sources are present, and appropriate action should then be taken. The accuracy of an intensity measurement can be assessed by the dynamic capability index, L_d (12);

$$L_d = \delta_{pOIO} - K \qquad dB \qquad 4$$

where the error factor K depends upon the desired grade of accuracy. For an accuracy of 1 dB the p-I index must be less than the residual p-I index by at least 7dB (9) i.e. K=7dB and

$$\delta_{pIO} - \Delta_{pI} > 7 \text{ dB} \qquad 5$$

4. Results

To investigate the measurement reproducibility the analysis procedure for a number of foam composites was repeated (**4,14**) and the insertion loss recalculated. The results are shown in Figures 3 to 5. These graphs are for a foam of density 77.9kgm^3, storage modulus 1.24x10^5 Pa and thickness 20mm, with three different septum area densities (3.7, 5.9 and 8.7 kgm^{-2}). It can be seen that the difference in IL between the two datasets is of the order of 1.5dB, except at high frequencies (f>2kHz). This reproducibility of measurements was seen both on a day to day and month to month basis. The error can be attributed to the variability in measurement and slight differences in the installation. Larger variations that were observed could be attributed to leakages of sound on the composite perimeter i.e. poor sealing, or sudden extraneous noises. In both these cases the measurement could be repeated once the identified problem was remedied. The high level of reproducibility shows that the test facility and method can be used in the long-term to assess the performance of under-carpet composites without degradation in

measurement accuracy beyond that of experimental error.

The pressure-intensity index was used to assess the validity of a measurement. The criteria of a low global p-I (low F_3) index was easily met in the intensity measurements. This is shown in figure 6 for the same foam. The p-I values are for one set of the measurements in the above measurements. For the conditions of steel panel and steel panel plus foam the index is low, 4-6dB. With the addition of septa the index increases at higher frequencies but still remains less than 10 dB (f<4kHz).

The experimental data exhibits two phenomena. Firstly, the insertion loss of the composite system increases with increasing septum surface density. Secondly, the resonance dip due to the mass-spring-mass system behaviour decreases with increasing septum surface density. This behaviour is to be expected from the theoretical analysis (14).

5. Conclusions

A small scale test facility has been described, and used to obtain the insertion loss of sound reducing materials when subjected to airborne noise. The intensity measurement technique was introduced and measurement accuracy briefly discussed. Experimental results demonstrated that the use of the sound intensity technique enables the insertion loss to measured with a high level of reproducibility to an accuracy within that specified by current draft standards.

6. References

1 Gahlau H.K., Fortschrittliche Schallisolaten in der Automobiltechnik, Proc. Polyurethanes World Congress, 1987, 712-726

2 BS2750

3 Kingenberg H., Automobil-Meßtechnik, 1988 (Springer-Verlag, Berlin)

4 Ling M.K., Hilyard N.C., Heng R.B.W., Performance of Polyurethane Cored Composites for Vehicle Interior Noise Control, Proc. Inst. Acoustics, 1990, 12(1), 307-316

5. Wallace R.L., Dienel H.F., Beranek L.L., 31st Meeting of the Acoustical Society of America, J. Acoust. Soc. Amer., 1946, 18, 246 (Abstract only)

6. Nichols, Sleeper, Wallace, Ericson, J. Acoust. Soc. Amer., 1947, 19, 428-443

7. Beranek L.L., Work G.A., Sound Transmission Through Multiple Structures Containing Flexible Blankets, J. Acoust. Amer., 1949, 21, 419-428

8. Noise and Vibration Control, Edited by L.L. Beranek, 1988 (Institute of Noise Control Engineering)

9. BRUEL & KJAER, Sound Intensity, 1986, DK 2850 Nærum, Denmark

10. MCGARY M.C., Separation of Airborne and Structure-borne Noise Radiated by Plates Constructed of Conventional and Composite Materials with Applications for the Prediction of Interior Noise Paths in Propeller Driven Aircraft, 1986, PhD Dissertation, Dept. Aeronautics and Astronautics, Stanford University

11. ANSI S12.21 Engineering Method for the Determination of Sound Power Levels of Noise Sources using Sound Intensity

12. ISO 9614-1, 1990, Acoustics-Determination of Sound Power Levels of Noise Sources using Sound Intensity-Part 1:Measurement at Discrete Points

13. Fahy F., Sound Intensity, 1988 (Elsevier Applied Science)

14. Ling M.K., Vehicle Noise Control Using Three Layer Composites with Polyurethane Cores, J. Sound and Vibration, 1992, 158 (to be published)

Appendix 1 Sound Reduction Index and Insertion Loss

The technique described in this paper measures the insertion loss of a sound reducing treatment. The insertion loss can be simply related to its sound reduction index as described in the following
The sound reduction index, R of a panel is defined in Equation 6.

$$R = 10 \log_{10} [I_t/I_i] \qquad 6$$

where I_i and I_t are the incident and transmitted intensities on a panel.

Insertion loss, L_{IL}, is the difference in sound levels (measured in dB) at a specified receiver position before and after a treatment is applied, or a barrier is inserted. This is illustrated in Figure 7. The insertion loss is given by;

$$IL = L_1 - L_2 \quad dB \qquad 7$$

where, L_1 is transmitted level in the receiving room with the base panel alone, and L_2 is the transmitted level with base panel + treatment.

It can be shown (4) that the sound reduction index is related to the insertion loss to give equation

$$IL = L_1 - L_2 = - (R_{panel} - R_{composite}) \quad dB \quad 8$$

where R_{panel} is the sound reduction index of the steel panel and $R_{composite}$ is the sound reduction of the steel panel and treatment.

Appendix 2 Errors due to Background Noise in Insertion Loss Measurements

The influence of an external noise source upon an insertion loss measurement can be shown to be nil. It is assumed that the external noise source is stationary with respect to the measurement time.

If the first intensity measurement, in the presence of an external noise source, is $\bar{I}_1'$ which is related to the actual intensity value $\bar{I}_1$ by

$$\bar{I}_1 = \bar{I}_1' + \bar{I}_e \quad dB \quad 9$$

where $\bar{I}_e$ is the intensity due to the extraneous stationary sound

source, and if the intensity with the composite in place is given by;

$$\bar{I}_2 = \bar{I}_2' + \bar{I}_e \qquad \text{dB} \qquad 10$$

then the insertion loss is given by;

$$IL = \bar{I}_1' - \bar{I}'_2 \qquad \text{dB} \qquad 11$$

which is of the form in equation 1 above.

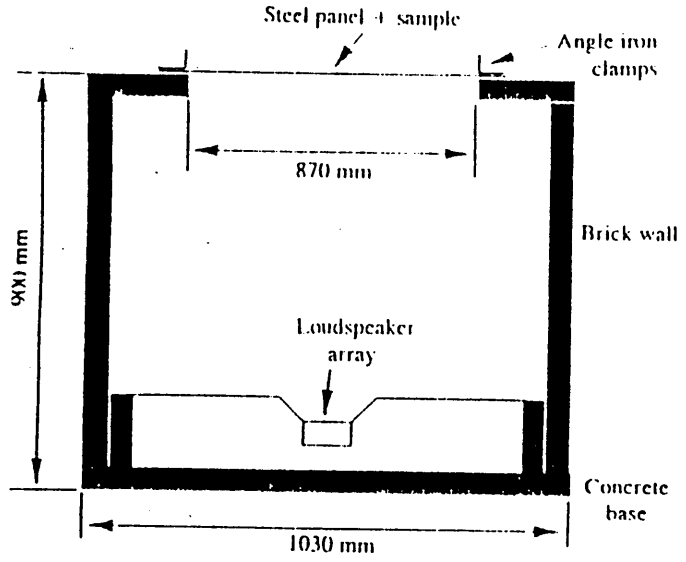

Figure 1 Test facility

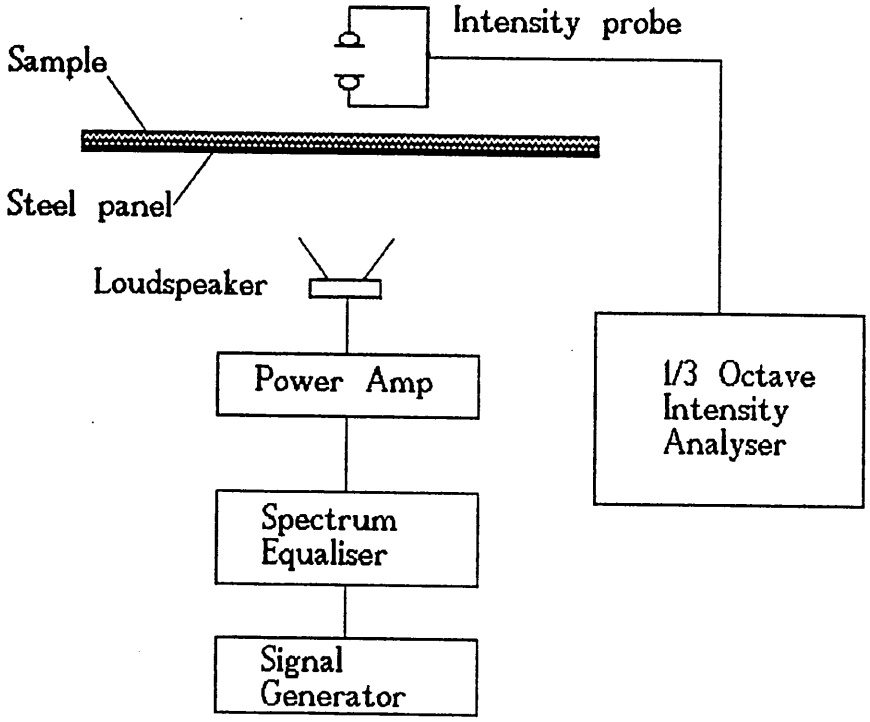

Figure 2 Measurement of radiated intensity

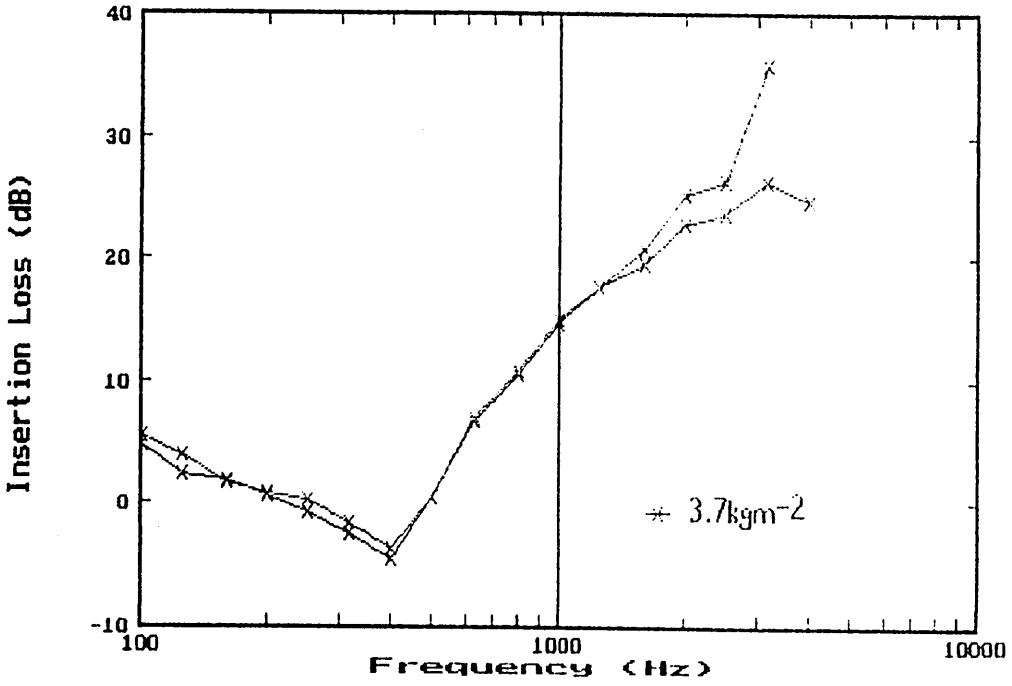

Figure 3 Repeatability of Insertion Loss Measurements ($3.7kgm^{-2}$ Septum)

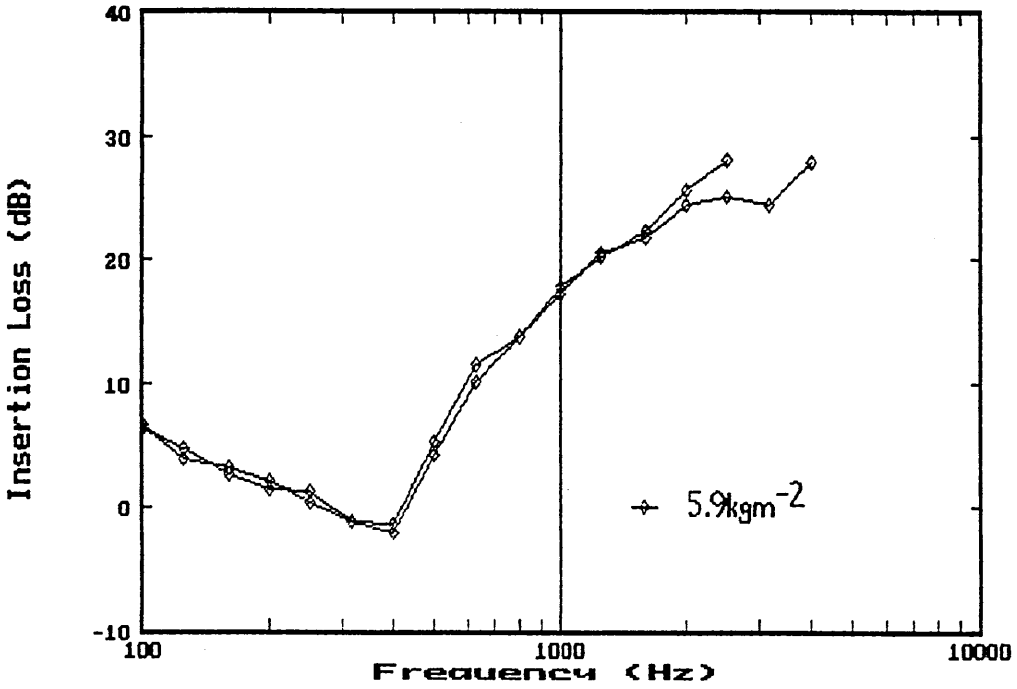

Figure 4 Repeatability of Insertion Loss Measurements (5.9 kgm^{-2} Septum)

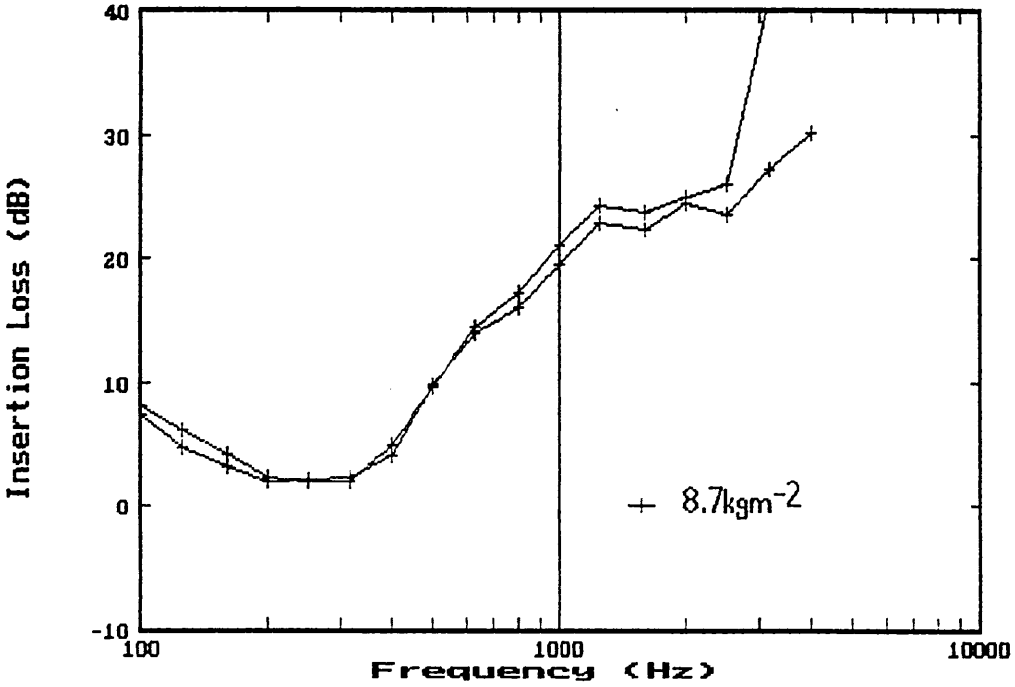

Figure 5 Repeatability of Insertion Loss Measurements (8.7 kgm^{-2} Septum)

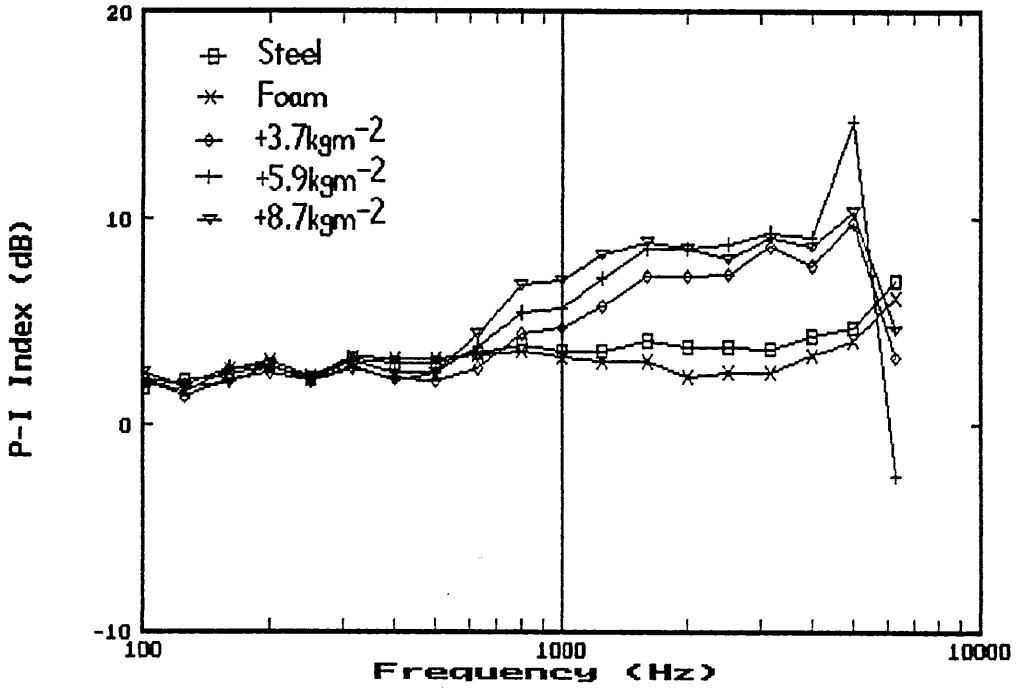

Figure 6 Typical Pressure-Intensity Index Values

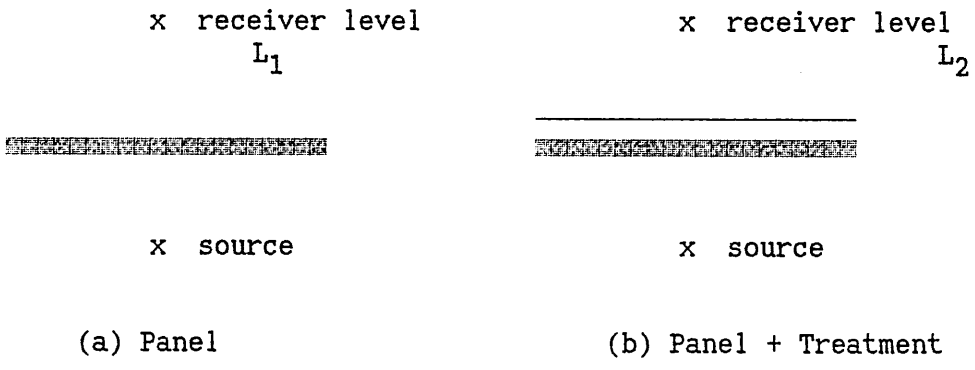

(a) Panel

(b) Panel + Treatment

Figure 7 Insertion Loss

APPENDIXB PROGRAMME LISTINGS

1. Structure-Borne Insertion Loss

```
#include <math.h>
#include <stdio.h>
#include <stdlib.h>
#include "complex1.c"

/*variable declarations*/
double ratio,omega1,omega01,temp1,k0,omega,omega2,fres,
     freq,h,h2,e2,e3,h3,h31,y,etaratio,
          eta,IL,transmissibility,x0,BSYS,lb,p,gfoam,x;

int i;

char out_name[14],data_name[14],ch[12];

complex hfoam,efoam,etafoam,etacomp,mfoam,rho,cair,eair,R1,
          zair,kair,nu1,mass1,mass2,z0,area,e1,temp2,temp3,temp4,temp5,
     prop,force,veloc1,veloc2,x1x2,etot;

const double  MASS1=7.7,MASS2=5.9,ESTEEL=19.7E10,
                    ETASTEEL=0.001,RHO=1.21,CAIR=343,KAIR=1E5,
                    NU1=0.27,HSEPT=0.0027,ESEPT=1e6,
          ZAIR=415,AREA=0.7569;
FILE*out_file;
FILE*data_file;

/* start of the program*/

main()
{

/* complex constants */

rho=cmplx(RHO,0.0);
cair=cmplx(CAIR,0.0);
kair=cmplx(KAIR,0.0);
nu1=cmplx(NU1,0.0);
mass1=cmplx(MASS1,0.0);
mass2=cmplx(MASS2,0.0);
zair=cmplx(ZAIR,0.0);
area=cmplx(AREA,0.0);
e1=cmplx(ESTEEL,ETASTEEL*ESTEEL);
eair=cmplx(1.2E5,5e3);

 /* input the data required*/

 printf("What is data input filename\n");
 scanf("%s",data_name);
 data_file=fopen(data_name, "r");
 if (data_file==NULL)
```

```
    return(1);
    }

printf("What is output filename\n");
scanf("%s",out_name);
out_file=fopen(out_name, "w");
if (out_file==NULL)
   {
    printf("Can't open file %s\n", out_name);
    return(1);
    }

fgets(ch,15,data_file);
temp1=atof(ch);  /*foam thickness*/
hfoam=cmplx(temp1,0.0);

fgets(ch,15,data_file);
temp1=atof(ch);  /*foam modulus*/
efoam=cmplx(temp1,0.0);

fgets(ch,15,data_file);
temp1=atof(ch);  /*foam flow resistance*/
R1=cmplx(temp1,0.0);

fgets(ch,15,data_file);
temp1=atof(ch);  /*foam loss  factor*/
efoam.y=temp1*efoam.x;
etafoam=cmplx(temp1,0.0);

fgets(ch,15,data_file);
temp1=atof(ch);/*  mass  of the foam*/
mfoam.x=temp1*hfoam.x;

fclose(data_file);


/* print out all the variables*/

printf("Steel surface  mass=");
PRINTCOMP(mass1);printf("\n");
printf("Septum  Mass=");PRINTCOMP(mass2);
printf("Steel Storage  Modulus=");PRINTCOMP(e1);
printf("Foam Storage  Modulus=");PRINTCOMP(efoam);
printf("Foam thickness=");PRINTCOMP(hfoam);
printf("Foam Loss  Factor=");PRINTCOMP(etafoam);
printf("Foam flow resistance=");PRINTCOMP(R1);
printf("Output filename is  %s\n",out_name);

etot=comp_div(comp_add(eair,efoam),hfoam);

/*main programme  calculations*/

for (i=1; i<=150; i++)
   {
```

```
    omega=2*M_PI*freq;
    k0=omega/CAIR;
    omega2=omega*omega;

/* two degree of freedom system */
/*etaratio=eta/ETASTEEL*/
etaratio=2091.4*pow(freq,-0.923265);
temp1=(etaratio)*pow((mass1.x+mfoam.x+mass2.x)/mass1.x,2);
temp2=cmplx(0.0,omega);

/*K/jw*/
temp3=comp_div(etot,temp2);

/*jwm2+K/jw*/
x1x2=comp_add(comp_mult(temp2,mass2),temp3);

veloc1=comp_div(x1x2,temp3);

IL=10*log10(temp1)+20*log10(cabs(veloc1));

/*That would appear to be the bulk of the calculations*/
/*Write the data to a file*/
    fprintf(out_file,"%G\n",IL);
    }
    fclose(out_file);
    }
```

2. Airborne Insertion Loss

```
#include <math.h>
#include <stdio.h>
#include <stdlib.h>
#include "complex1.c"

/*variable declarations*/
 double temp1,k0,omega,omega2,sri,fres,
      itau,freq,h,f1,f2,s;
 int i;

 char out_name[14],data_name[14],ch[15];

complex x1,x2,prop,hfoam,efoam,etafoam,R1,comega,rho,cair,
zair,kair,nu1,mass1,mass2,z0,area,e1,temp2,temp3,temp4,
prop,c_omega2,rho,ktot,eair,rhofoam;

 const double  MASS1=7.7,MASS2=5.9,ESTEEL=19.7E10,
                      RHO=1.21, CAIR=343,KAIR=1E5,
                      NU1=0.27,
       ZAIR=415,AREA=0.7569;

 FILE*out_file;
 FILE*data_file;
```

```
/* start of the program*/

main()
{

/* complex constants  */

rho=cmplx(RHO,0.0);
cair=cmplx(CAIR,0.0);
kair=cmplx(KAIR,0.0);
nu1=cmplx(NU1,0.0);
mass1=cmplx(MASS1,0.0);
mass2=cmplx(MASS2,0.0);
zair=cmplx(ZAIR,0.0);
area=cmplx(AREA,0.0);
e1=cmplx(ESTEEL,0.0);
eair=cmplx(1.2e5,5e3);

 /* input the data required*/

 printf("What is data input filename\n");
 scanf("%s",data_name);
 data_file=fopen(data_name,  "r");
 if (data_file==NULL)
    {
     printf("Can't open file %s\n", data_name);
     return(1);
     }

 printf("What is output filename\n");
 scanf("%s",out_name);
 out_file=fopen(out_name,  "w");
 if (out_file==NULL)
    {
     printf("Can't open file %s\n", out_name);
     return(1);
     }

fgets(ch,15,data_file);
temp1=atof(ch);  /*foam thickness*/
hfoam=cmplx(temp1,0.0);

fgets(ch,15,data_file);
temp1=atof(ch);  /*foam modulus*/
efoam=cmplx(temp1,0.0);

fgets(ch,15,data_file);
temp1=atof(ch);  /*foam flow resistance*/
R1=cmplx(temp1,0.0);

fgets(ch,15,data_file);
temp1=atof(ch);  /*foam loss  factor*/
efoam.y=temp1*efoam.x;
etafoam=cmplx(temp1,0.0);
```

```
fgets(ch,15,data_file);
temp1=atof(ch);  /*foam density*/
rhofoam=cmplx(temp1,0.0);

fclose(data_file);

/*include contribution of air stiffness here - if required*/
ktot=comp_add(efoam,eair);
ktot=scal_mult(1.7,ktot);
/* print out all the variables*/

printf("Steel surface mass=");
PRINTCOMP(mass1);printf("\n");
printf("Septum Mass=");PRINTCOMP(mass2);
printf("Steel Storage Modulus=");PRINTCOMP(e1);
printf("Foam Storage Modulus=");PRINTCOMP(efoam);
printf("Foam thickness=");PRINTCOMP(hfoam);
printf("Foam Loss Factor=");PRINTCOMP(etafoam);
printf("Foam flow resistance=");PRINTCOMP(R1);
printf("Foam density=");PRINTCOMP(rhofoam);
printf("Ktot=");PRINTCOMP(ktot);
printf("Output filename is %s\n",out_name);



/* Calculate the resonant frequency*/
temp2=cmplx(1.0,0.0);

temp3=comp_div(efoam,hfoam);
temp4=comp_add(comp_div(temp2,mass1),comp_div(temp2,mass2));
fres=sqrt(cabs(comp_mult(temp3,temp4)))/(2*M_PI);

/*sqrt(EFOAM/HFOAM)*sqrt(1/MASS1+1/MASS2))/(2*M_PI);*/
printf("The Mass-Spring-Mass resonant frequency is %G Hz\n",fres);

/*start of all the wonderful calculations*/

 for (i=1; i<=300; i++)
    {
     freq=pow(i,1.5);
     omega=2*M_PI*freq;
     k0=omega/CAIR;
     omega2=omega*omega;
     c_omega2=cmplx(omega2,0.0);

     h=RHO*freq/R1.x;

/*Calculate the values for propagation constant*/
/*b=alpha+ j beta*/

      temp2=cmplx(0.0,1.0);

      /*rho=jw(rho/ktot)^1/2*/
```

```
    rho.y=-1.2*R1.x/(omega*s);

    prop=comp_mult(temp2,comp_sqrt(comp_div(rho,ktot)));
    prop=scal_mult(omega,prop);

/*Calculate the value of complex impedance*/
/*z=R+jX*/

/*The approximation of z0=sqrt(rho*ktot);*/
z0=comp_sqrt(comp_mult(rho,ktot));

/* calculate cosh(a+jb)*/
/* and sinh(a+jb) terms*/

x1=comp_add(mass1,mass2);
temp2=cmplx(0.0,omega/ZAIR);
temp3=cmplx(1.0,0.0);
x1=comp_add(temp3,comp_mult(temp2,x1));

temp2=comp_div(z0,zair);
temp3=comp_mult(mass1,mass2);
temp4=comp_mult(z0,zair);
temp3=comp_div(temp3,temp4);

x2=comp_sub(temp2,comp_mult(c_omega2,temp3));
temp2=cmplx(0.0,1.0);
temp3=scal_mult(omega,comp_div(mass1,z0));
x2=comp_add(x2,comp_mult(temp2,temp3));

temp2=comp_mult(prop,hfoam);
x1=comp_mult(x1,comp_cosh(temp2));
x2=comp_mult(x2,comp_sinh(temp2));

itau=cabs(comp_add(x1,x2));
sri=20*log10(itau);

/*That would appear to be the bulk of the calculations*/
/*Write the data to a file*/
    fprintf(out_file,"%G  %G\n",freq,sri);
    }
    fclose(out_file);
    }
```

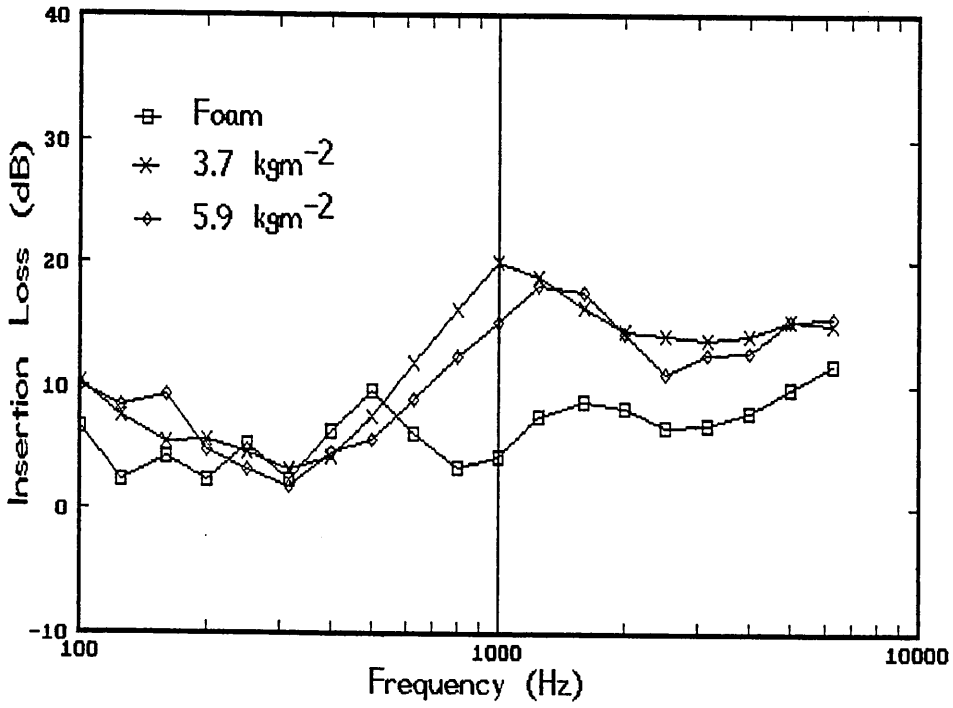

Fig. C1 Foam 1

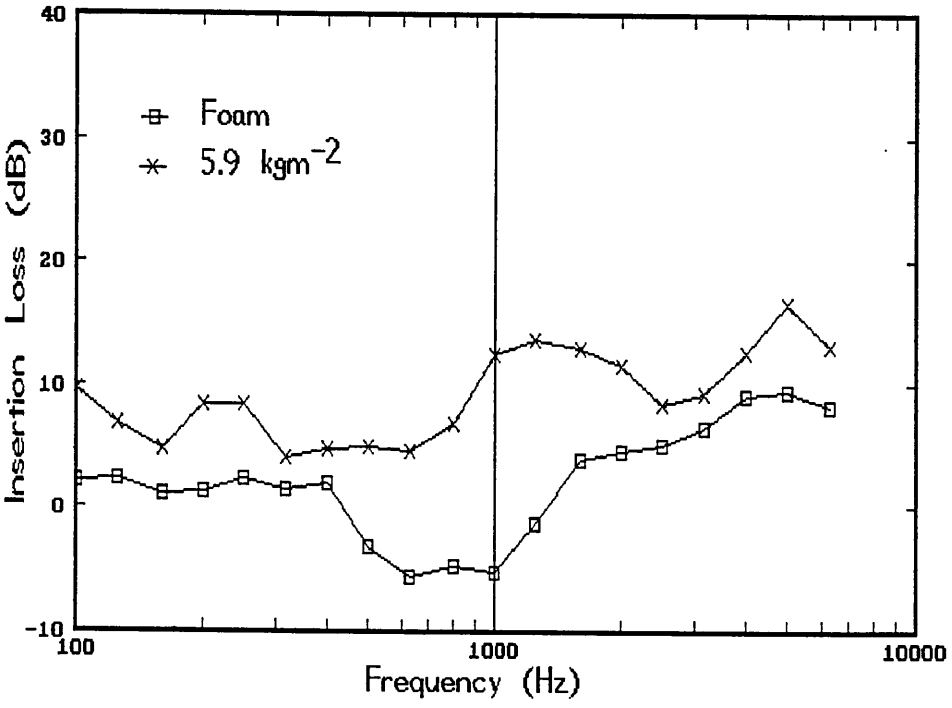

Fig. C2 Foam 2

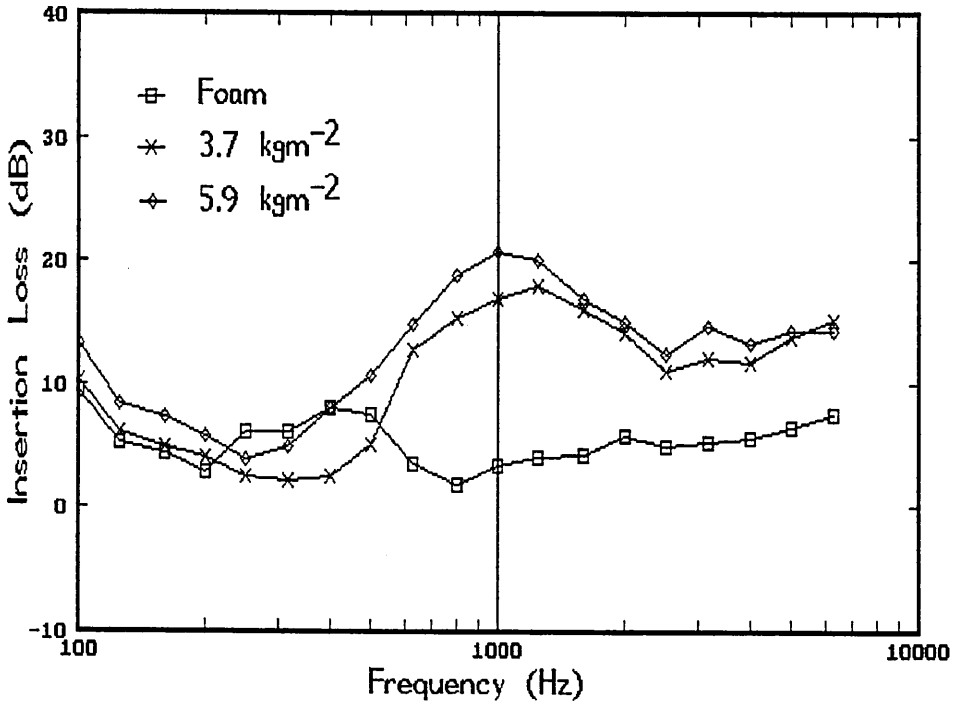

Fig. C3 Foam 3

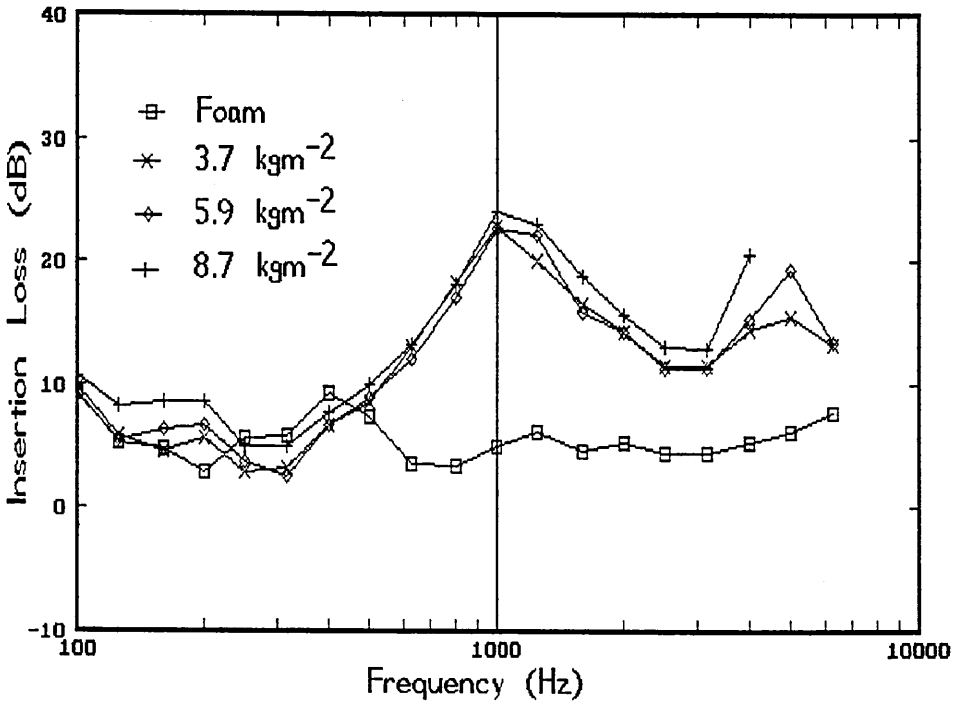

Fig. C4 Foam 4

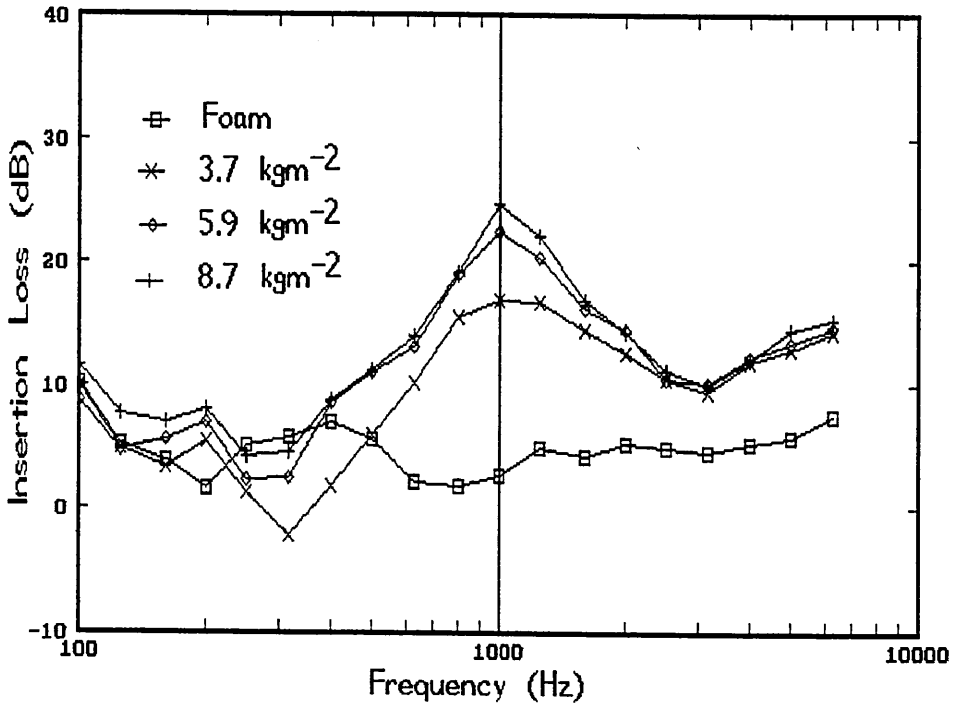

Fig. C5 Foam 5

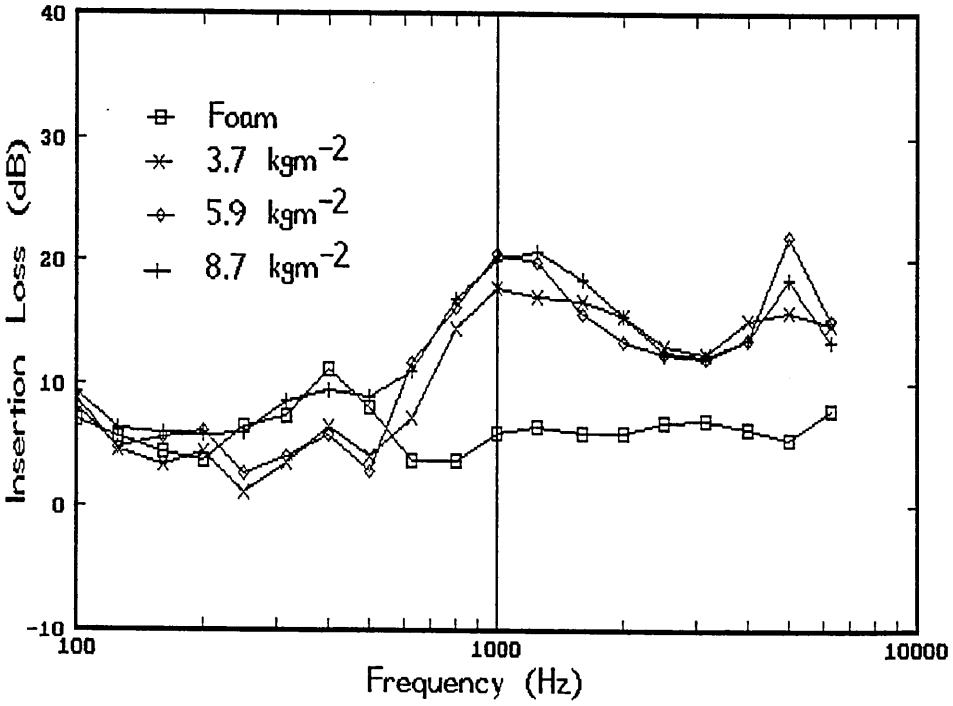

Fig. C6 Foam 6

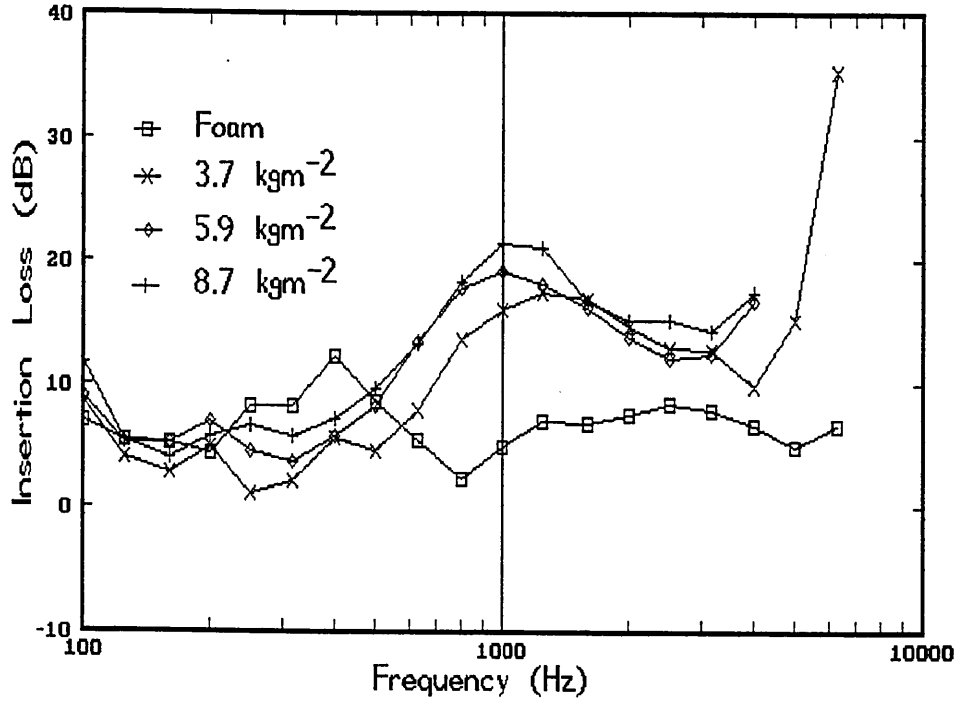

Fig. C7 Foam 7

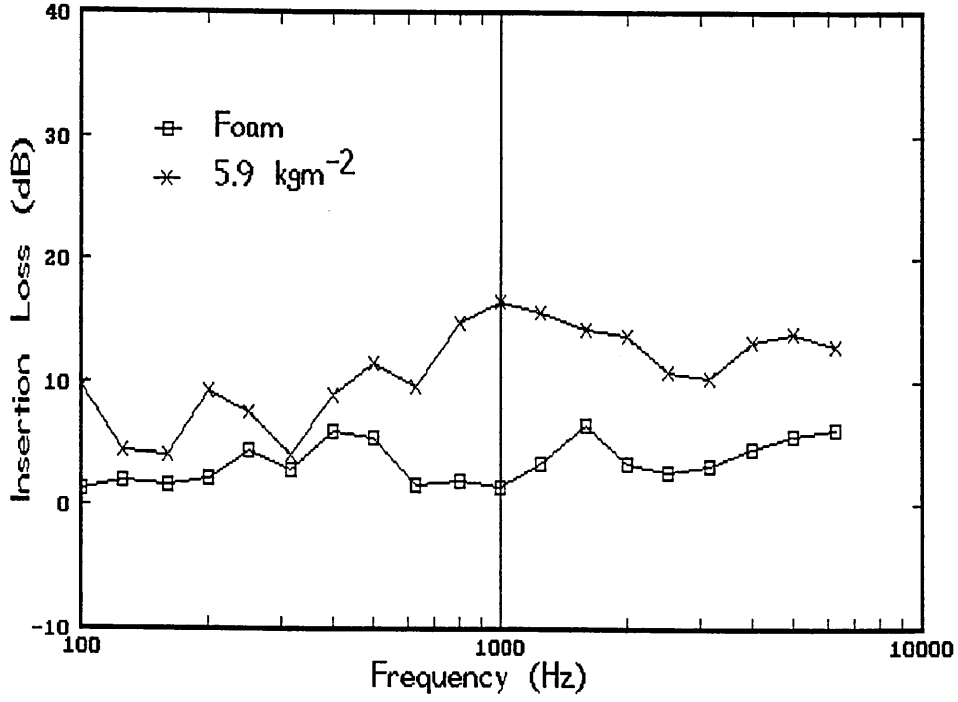

Fig. C8 Foam 8

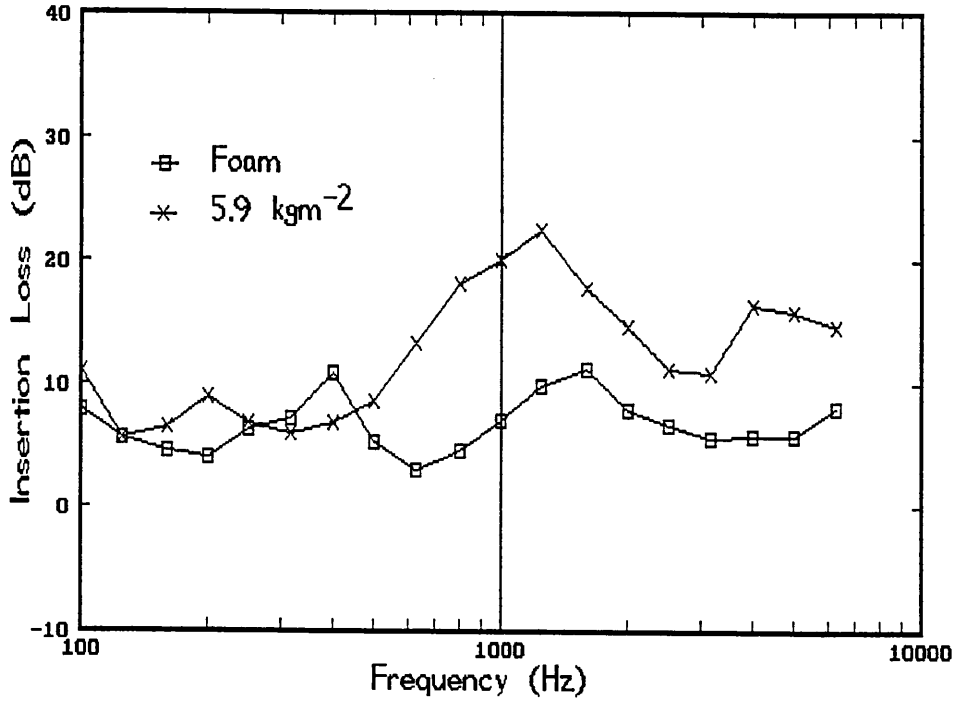

Fig. C9 Foam 9

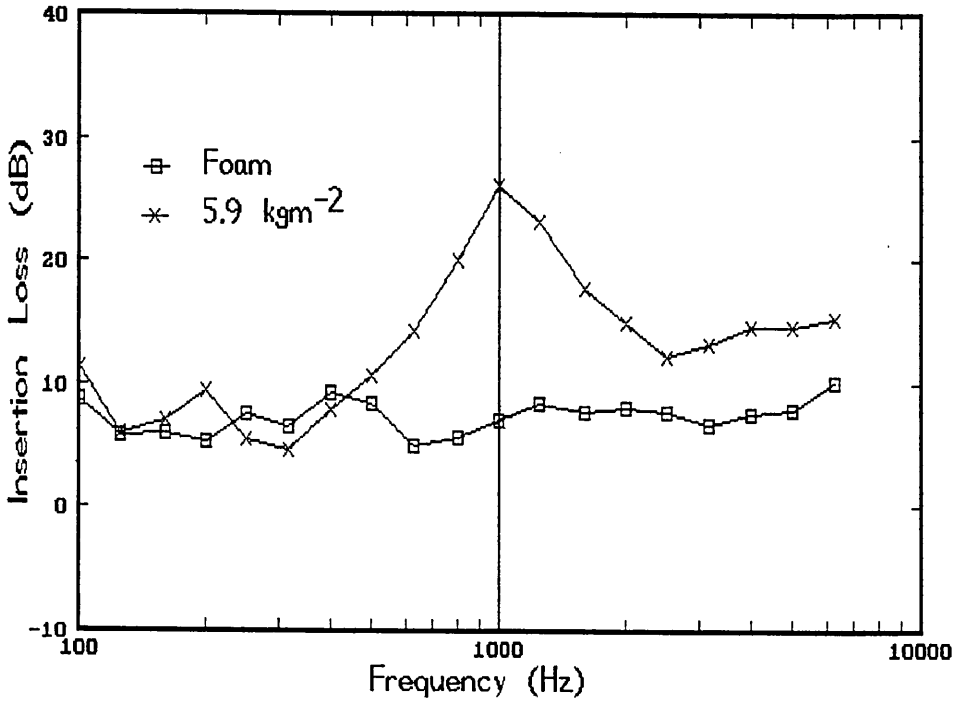

Fig. C10 Foam 10

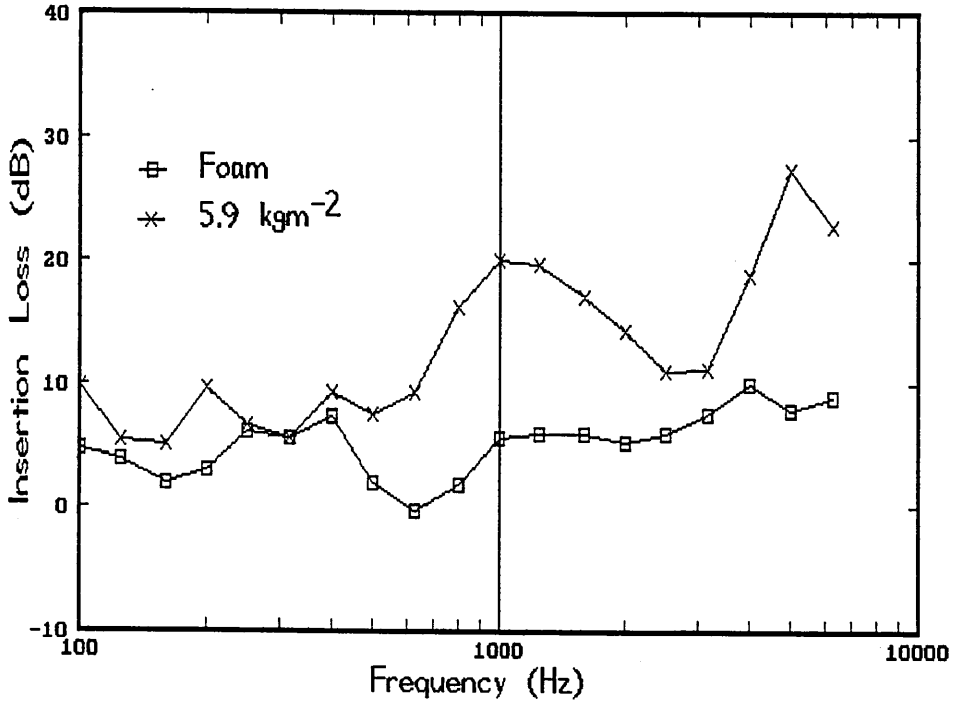

Fig. C11 Foam 11

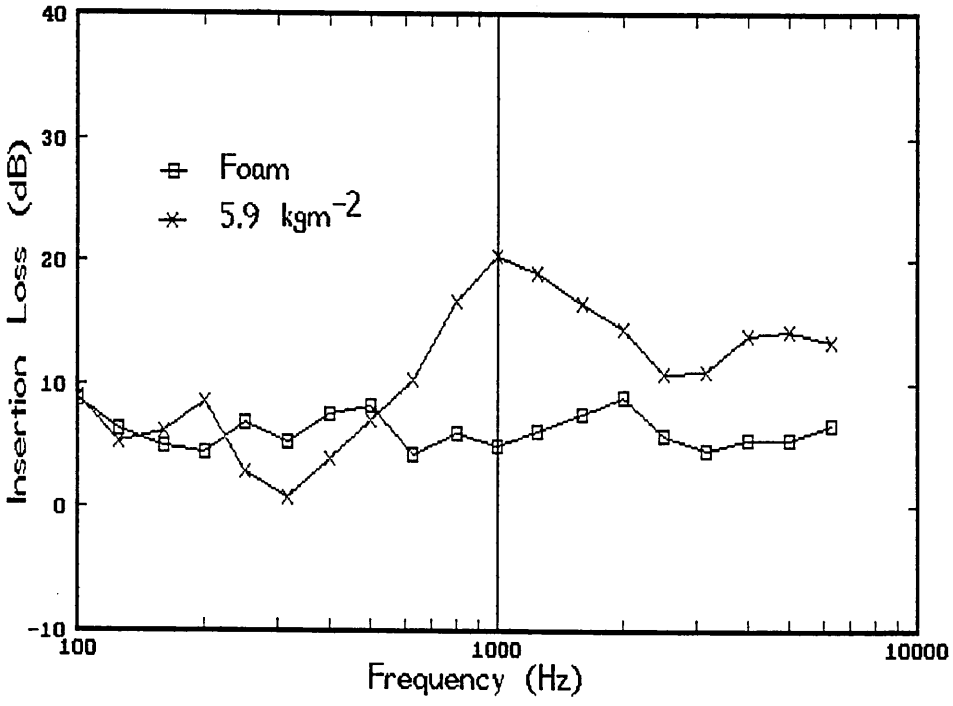

Fig. C12 Foam 12

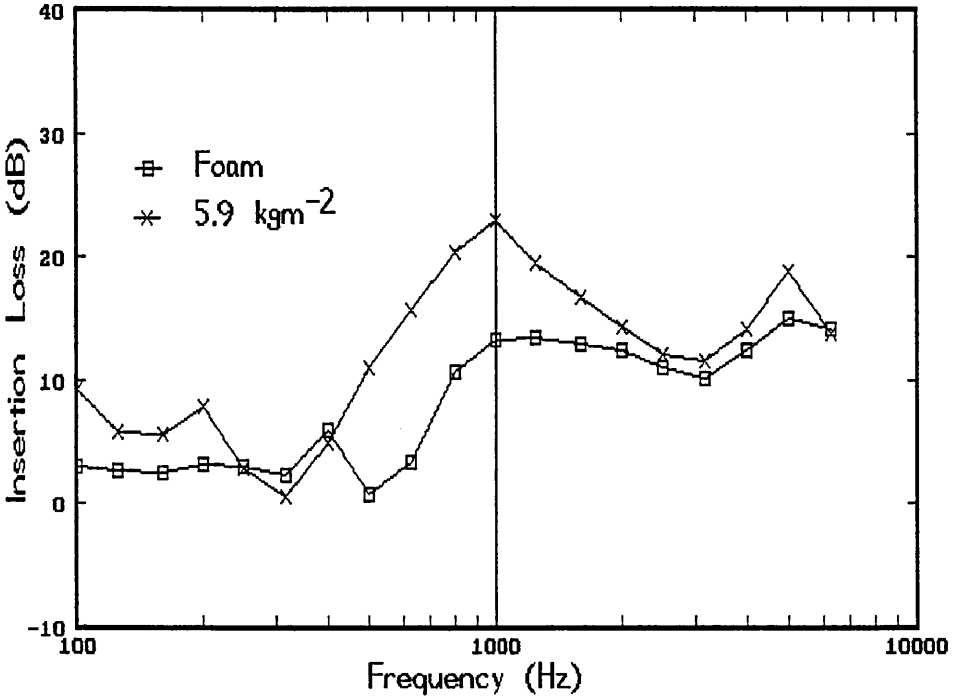

Fig. C13 Foam 13

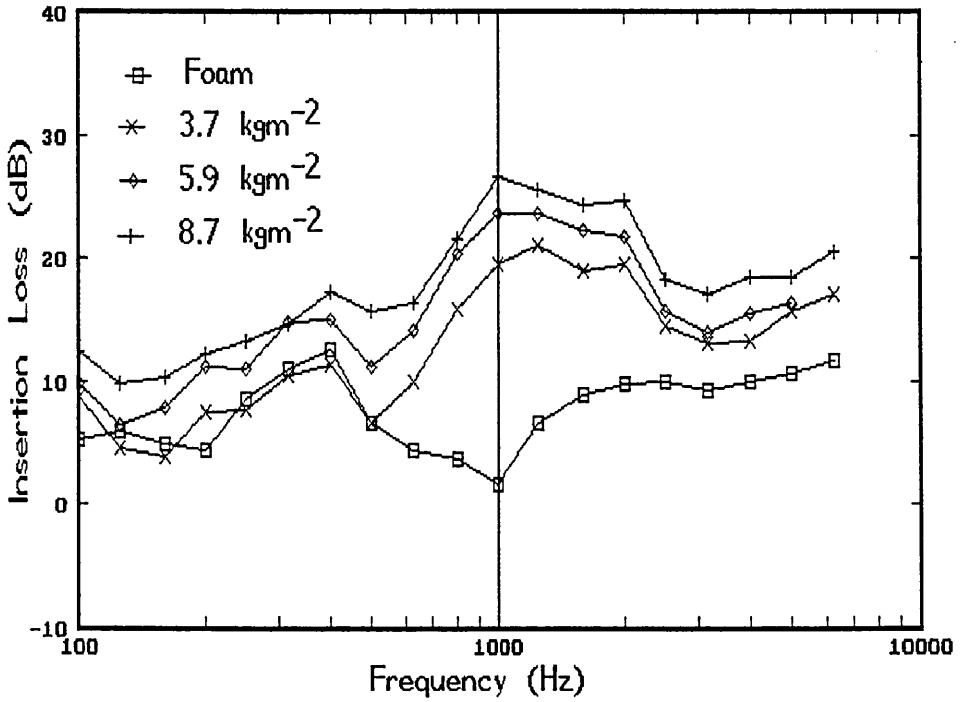

Fig. C14 Foam 14

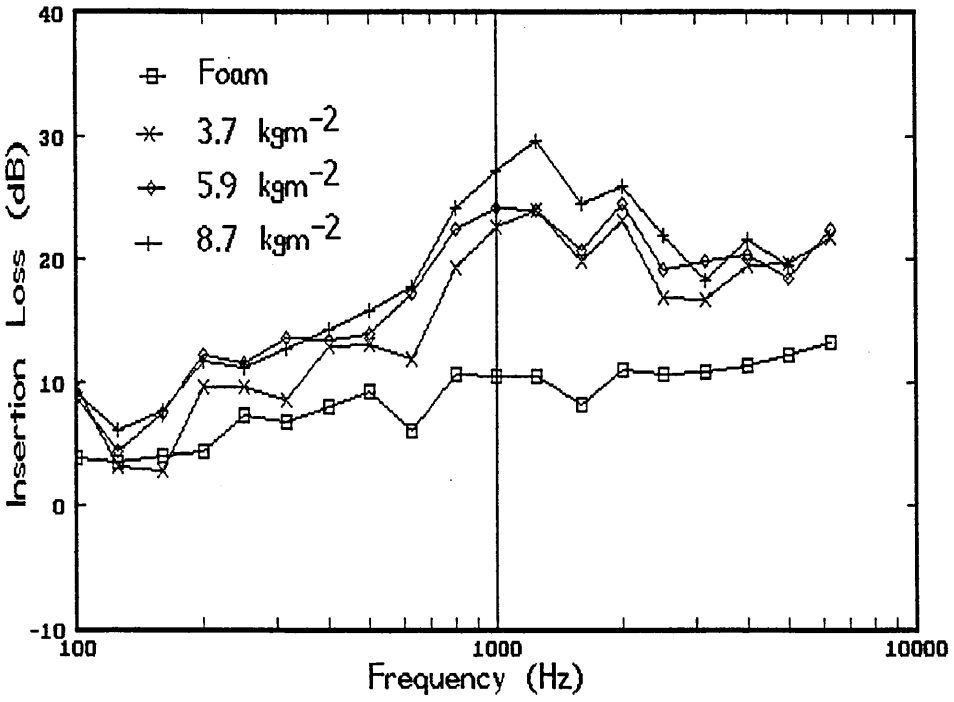

Fig. C15 Foam 15

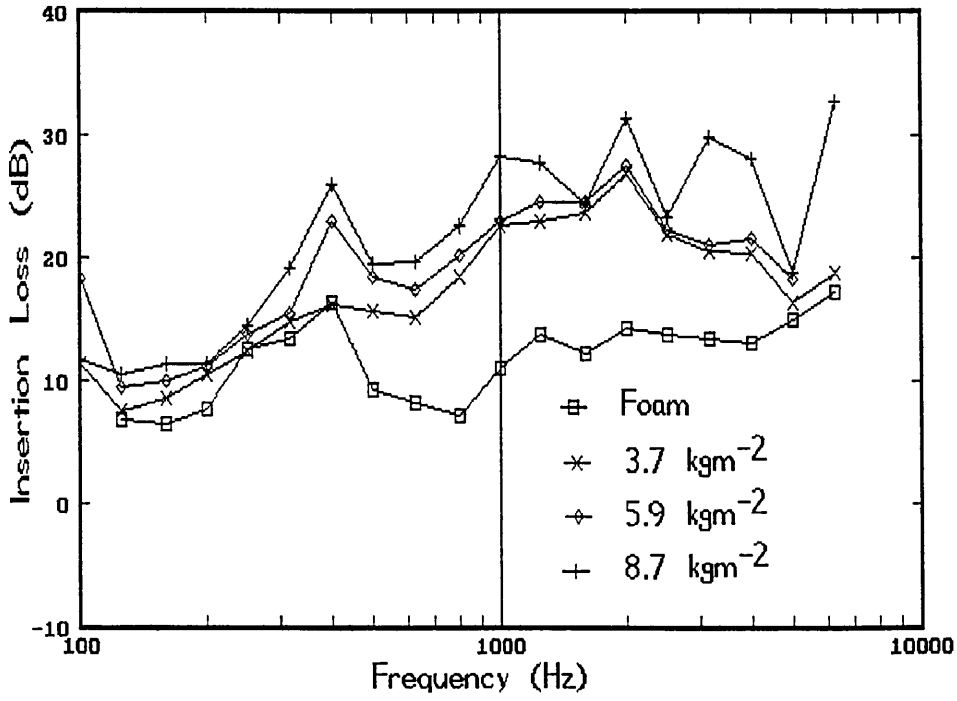

Fig. C16 Foam 16

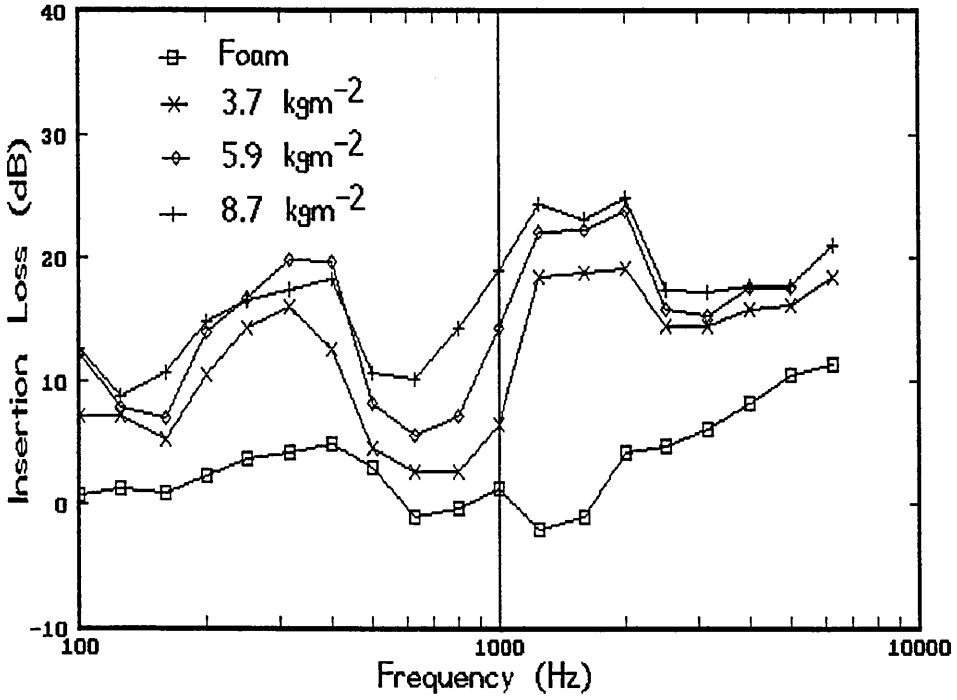

Fig. C17 Foam 17

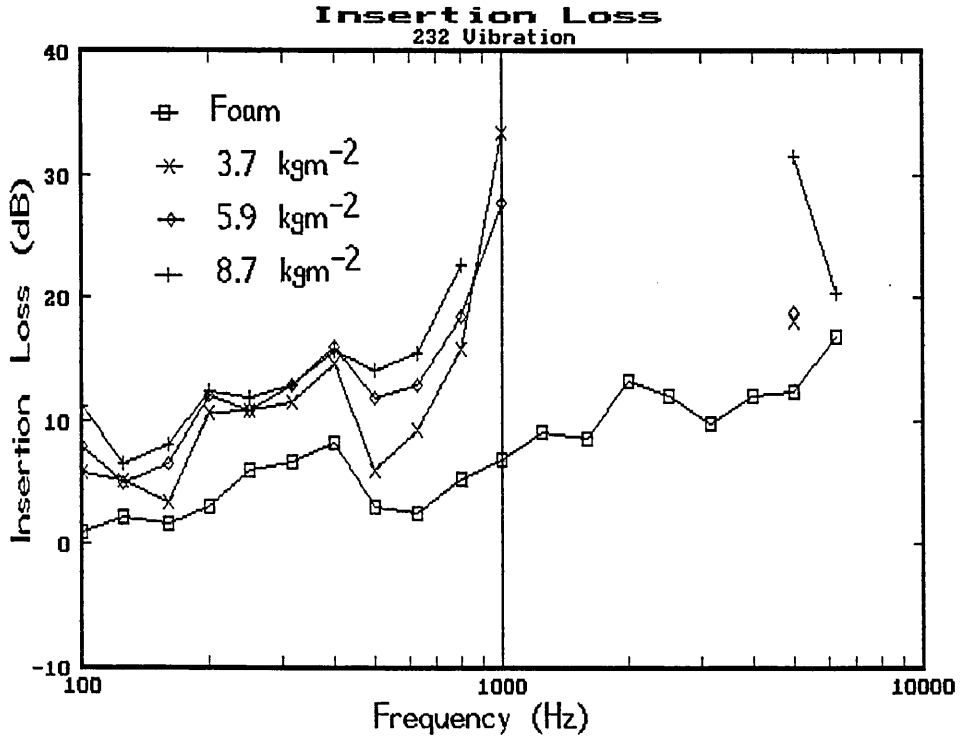

Fig. C18 Foam 18

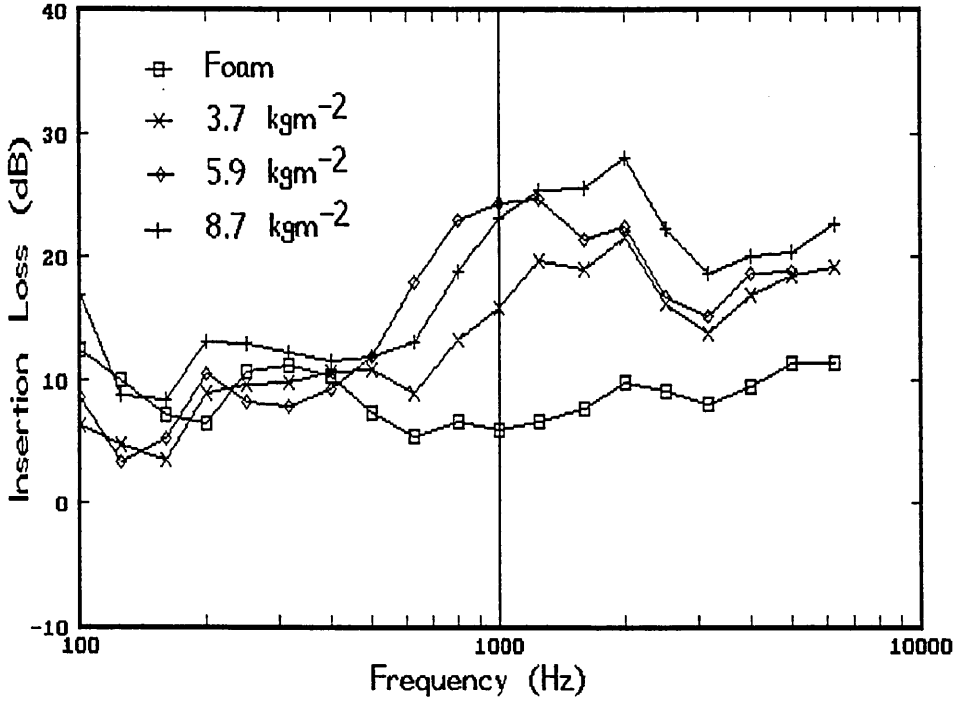

Fig. C19 Foam 20

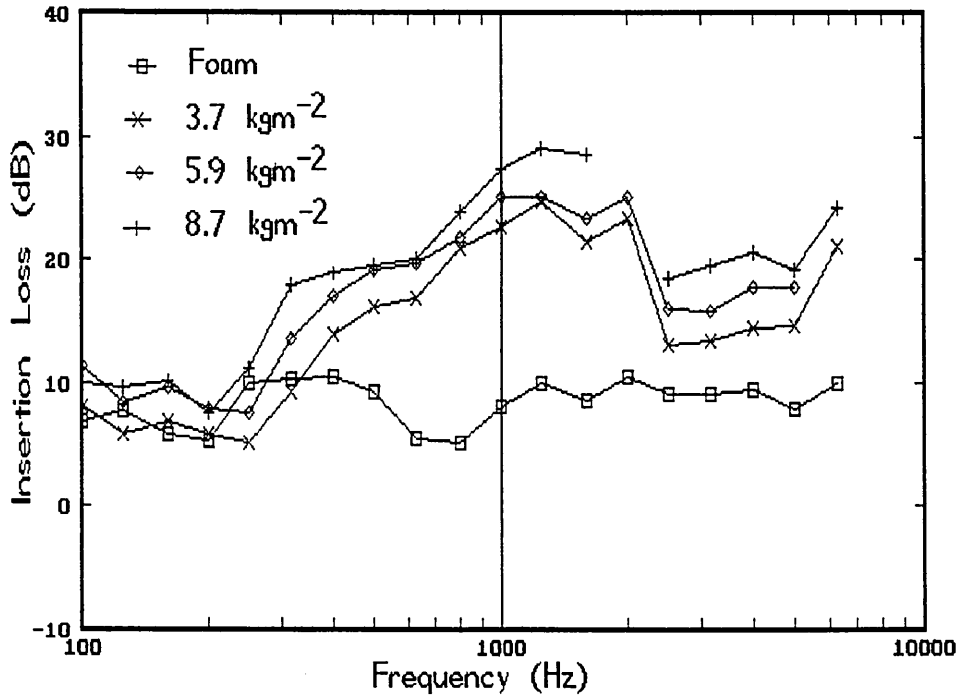

Fig. C20 Foam 21

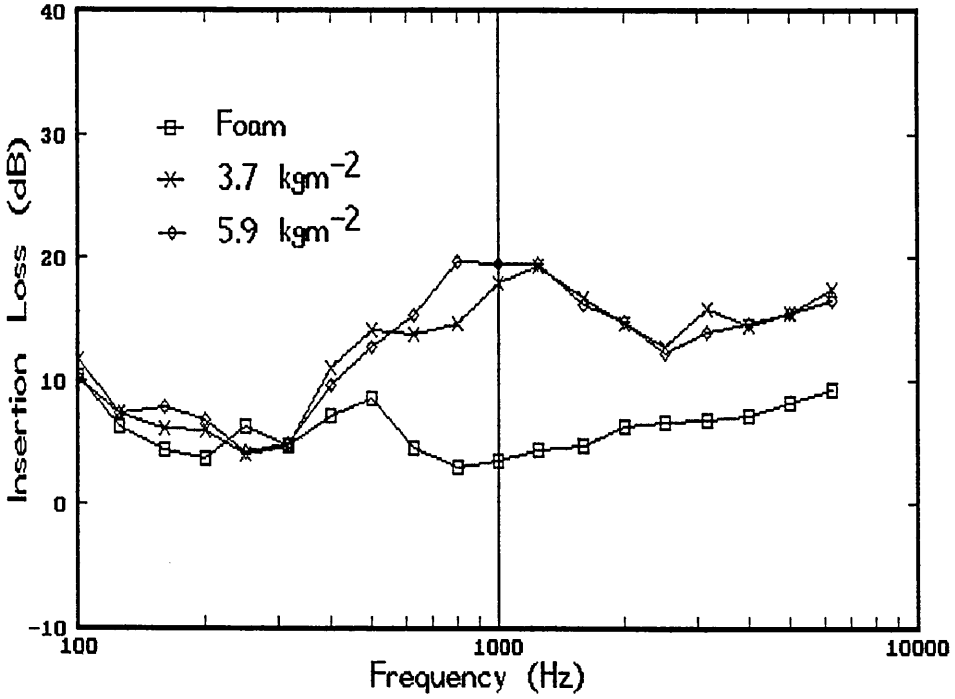

Fig. C21 Foam 22

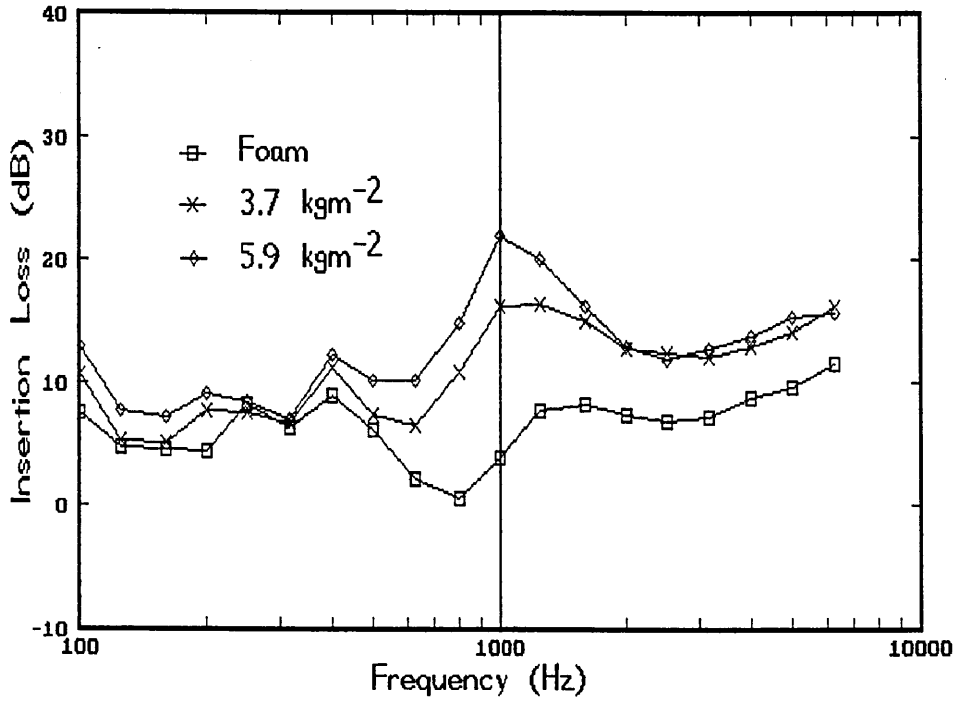

Fig. C22 Foam 23

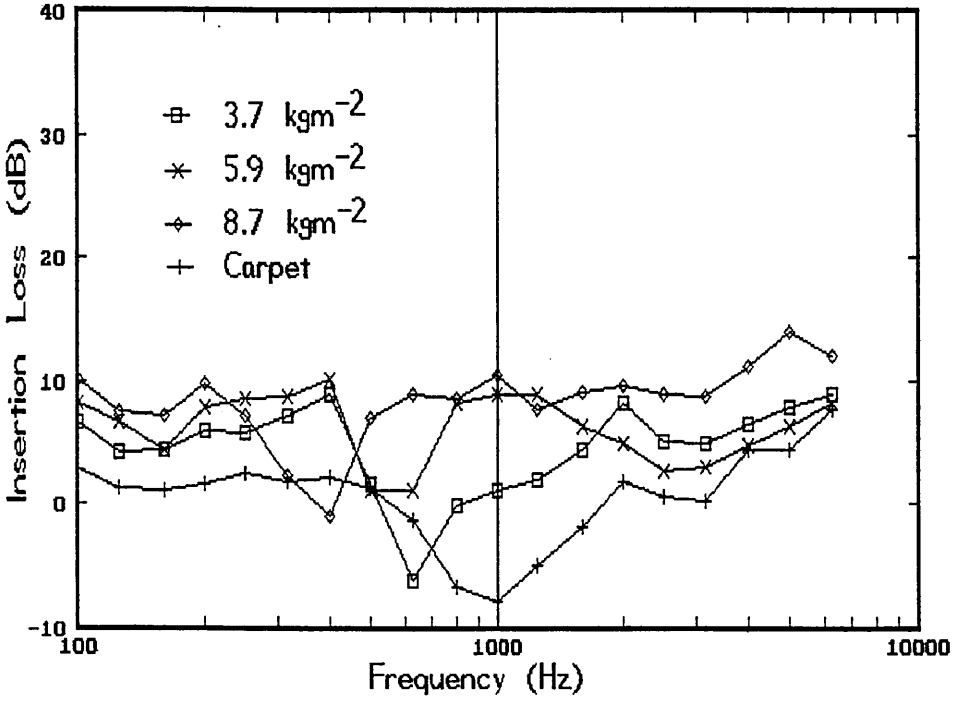

Fig. C23 Septum layers

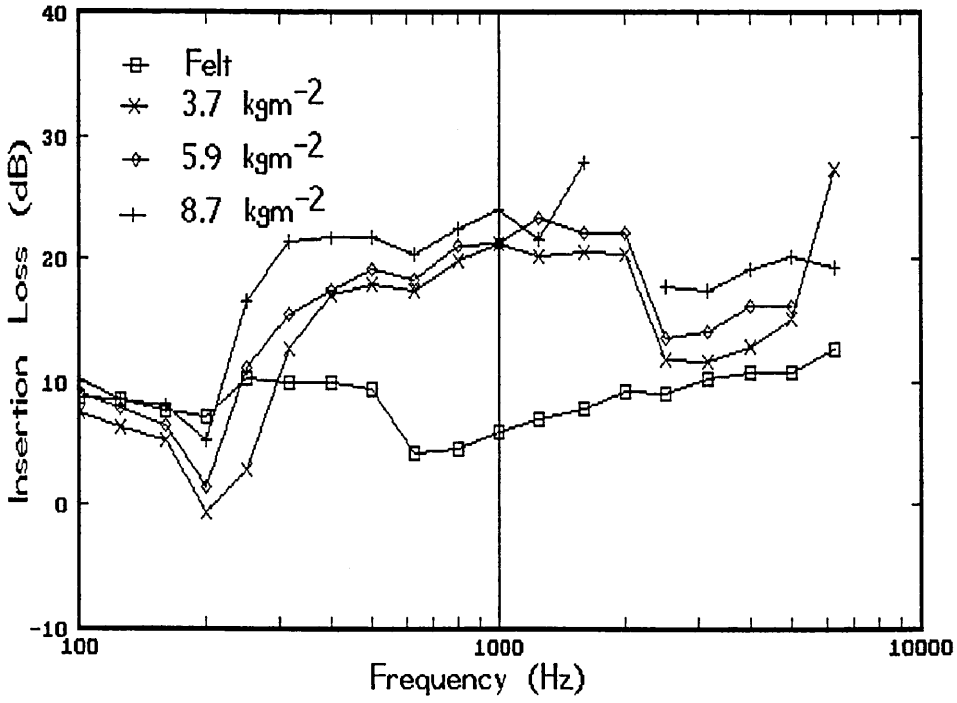

Fig. C24 Felt

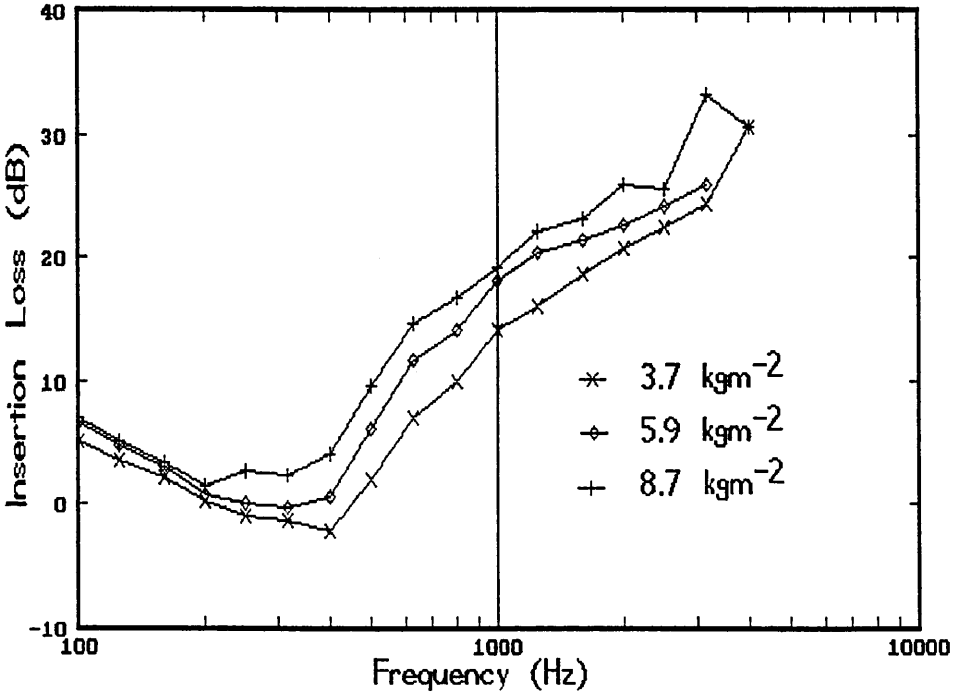

Fig. D1 Foam 1

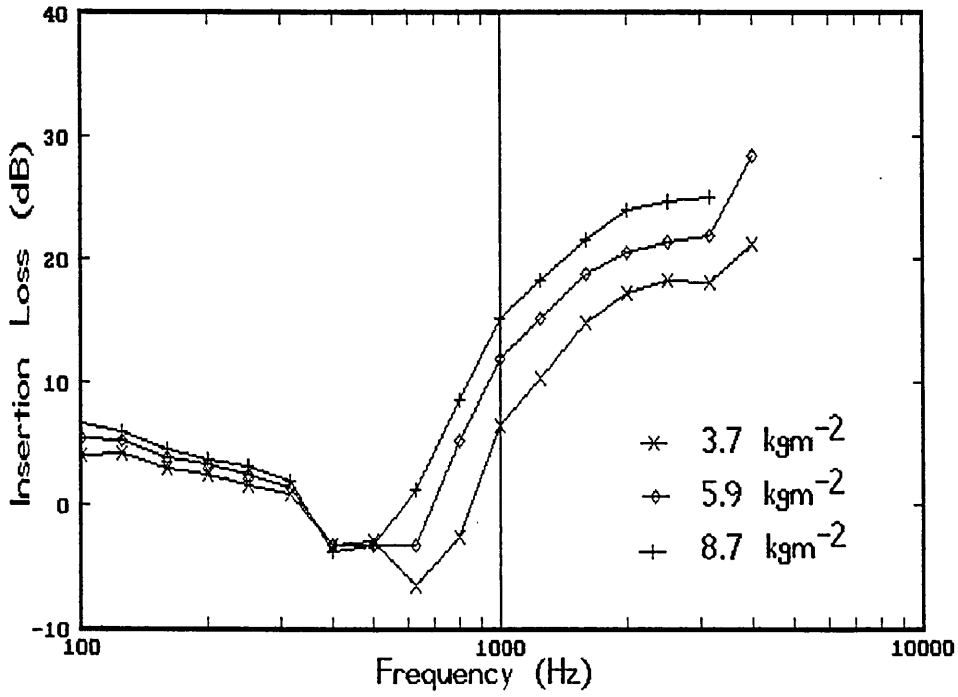

Fig. D2 Foam 2

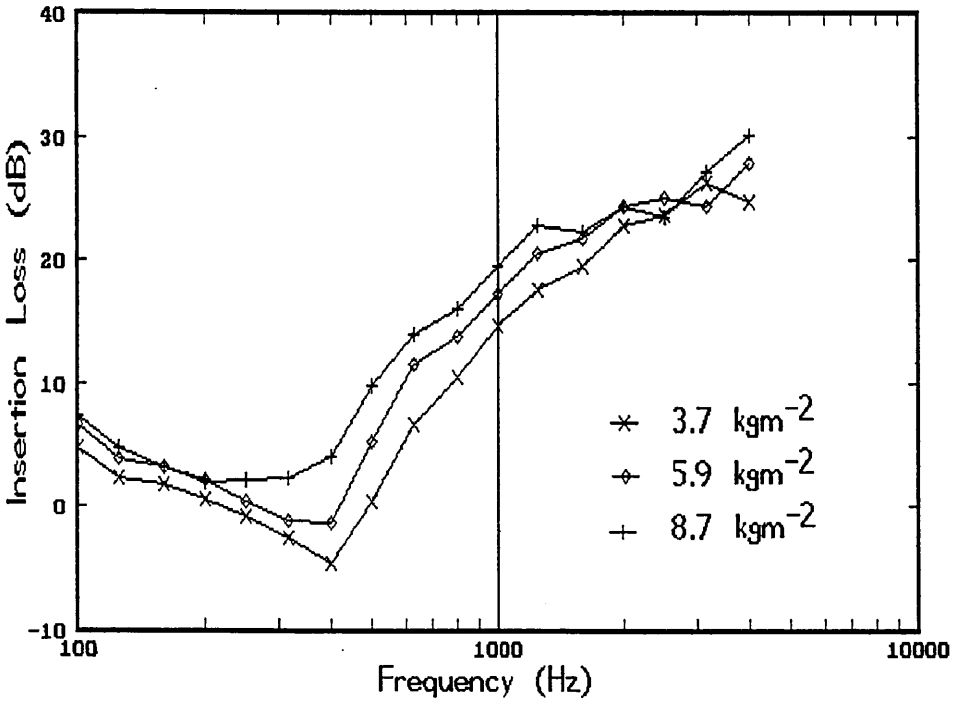

Fig. D3 Foam 3

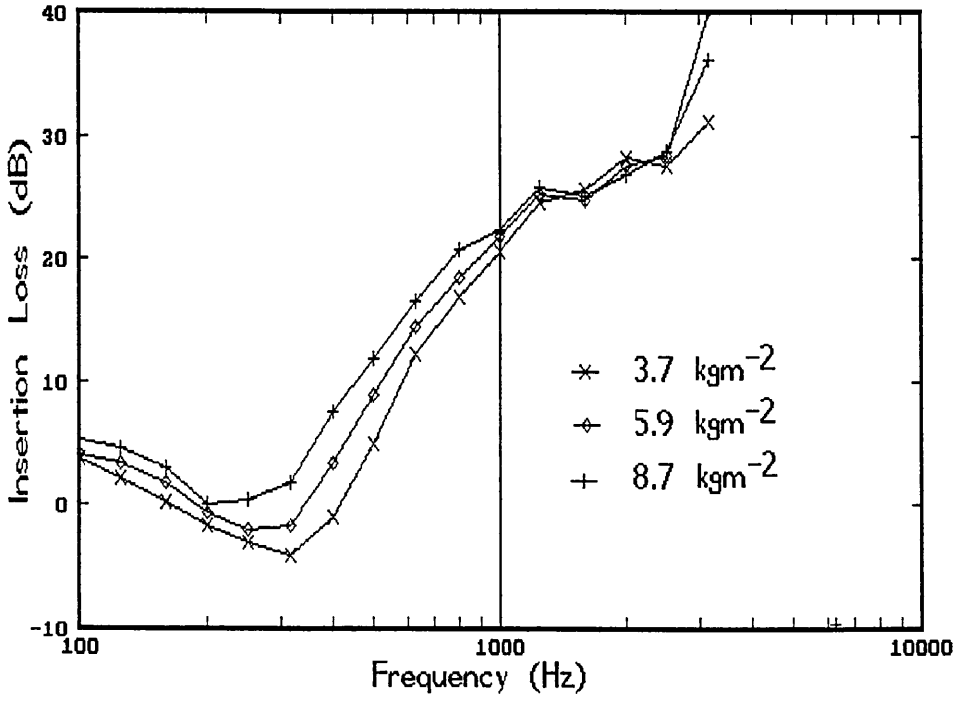

Fig. D4 Foam 4

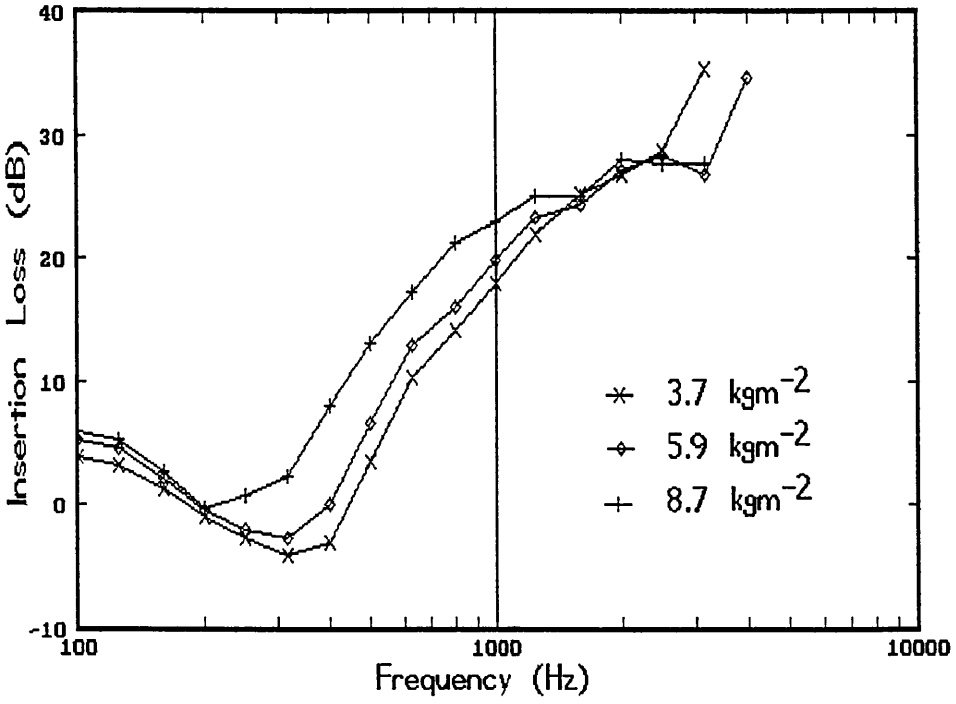

Fig. D5 Foam 5

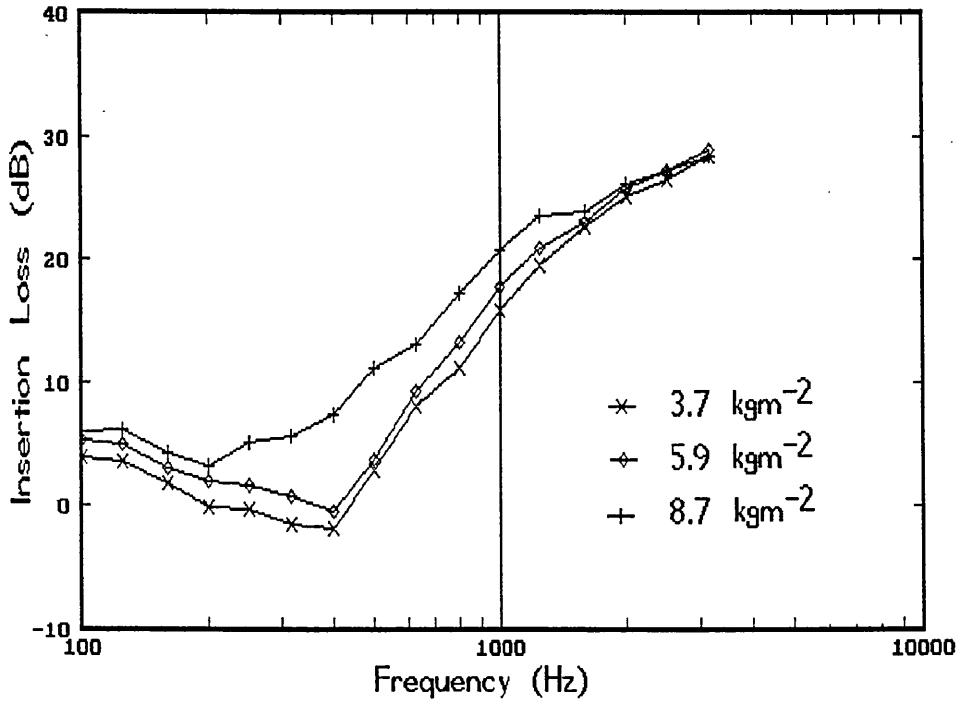

Fig. D6 Foam 6

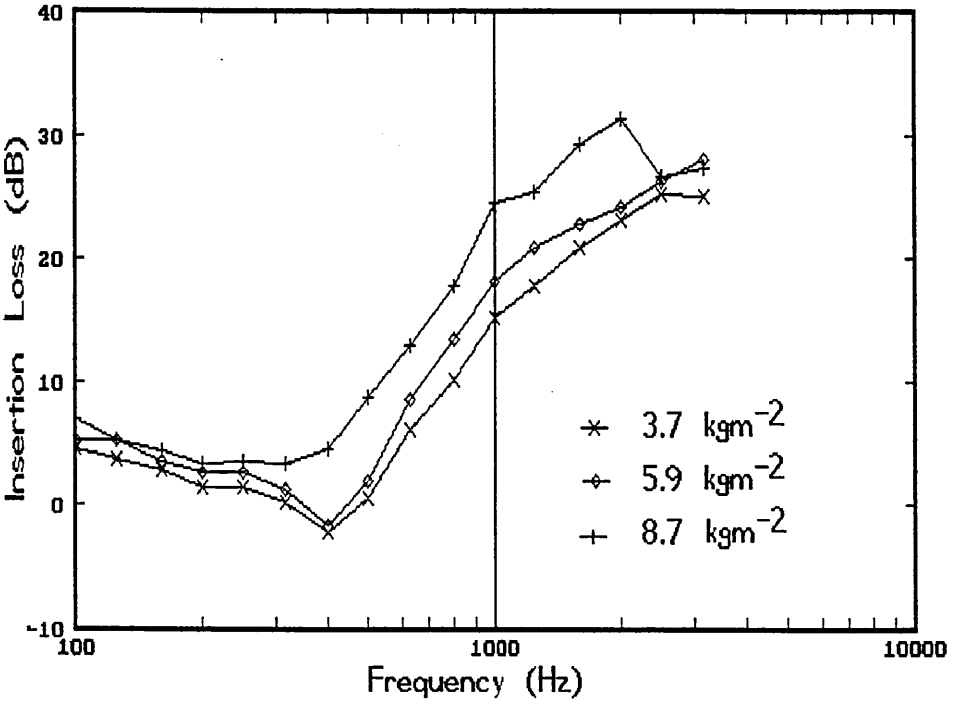

Fig. D7 Foam 7

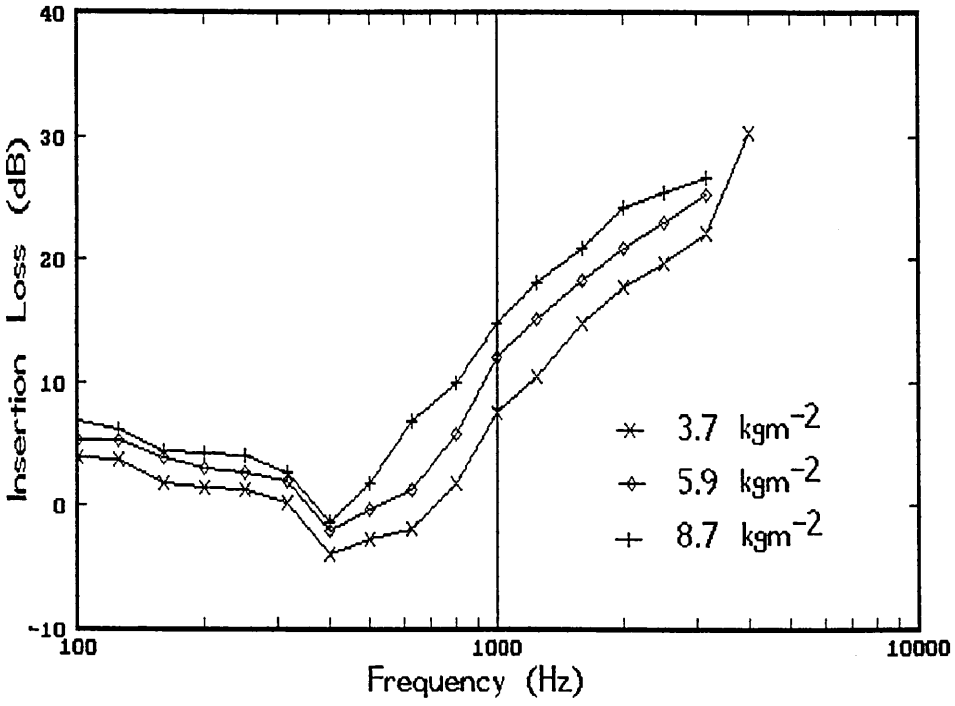

Fig. D8 Foam 8

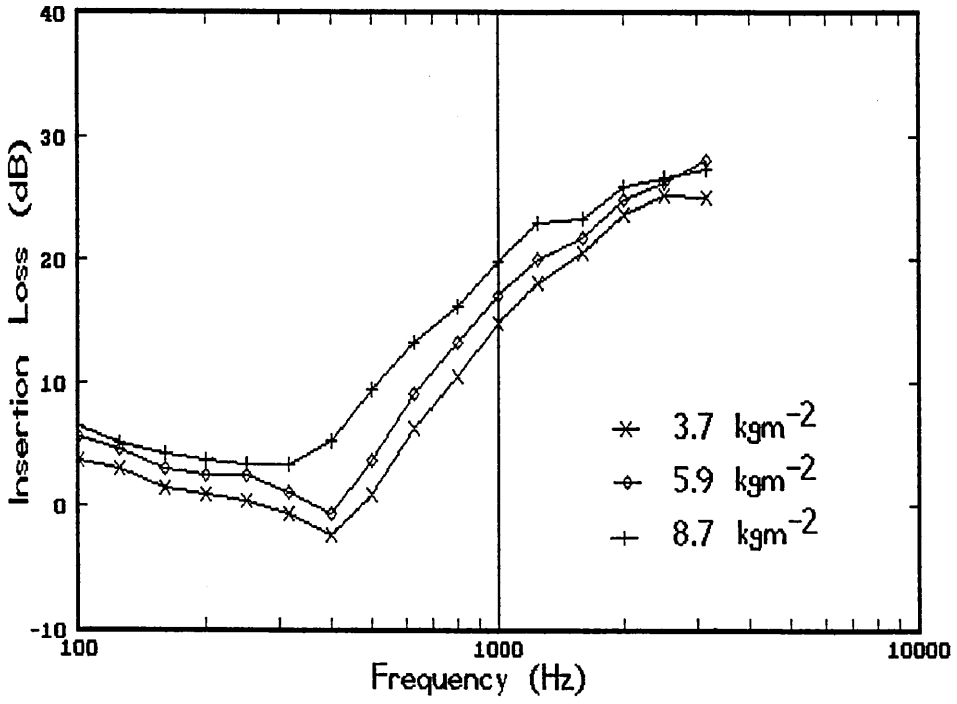

Fig. D9 Foam 9

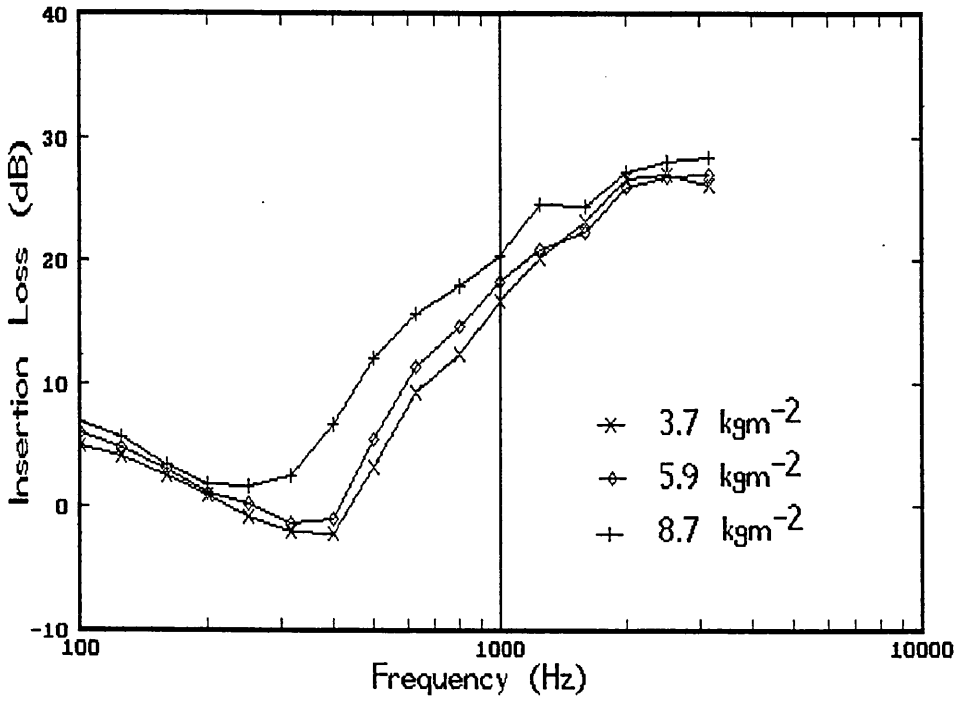

Fig. D10 Foam 10

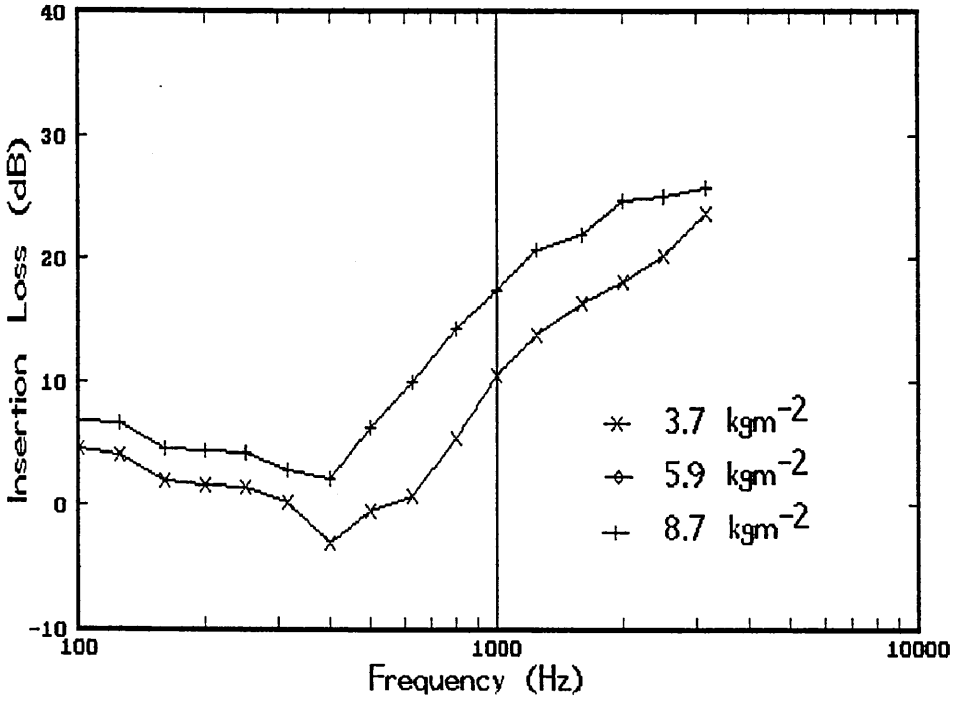

Fig. D11 Foam 11

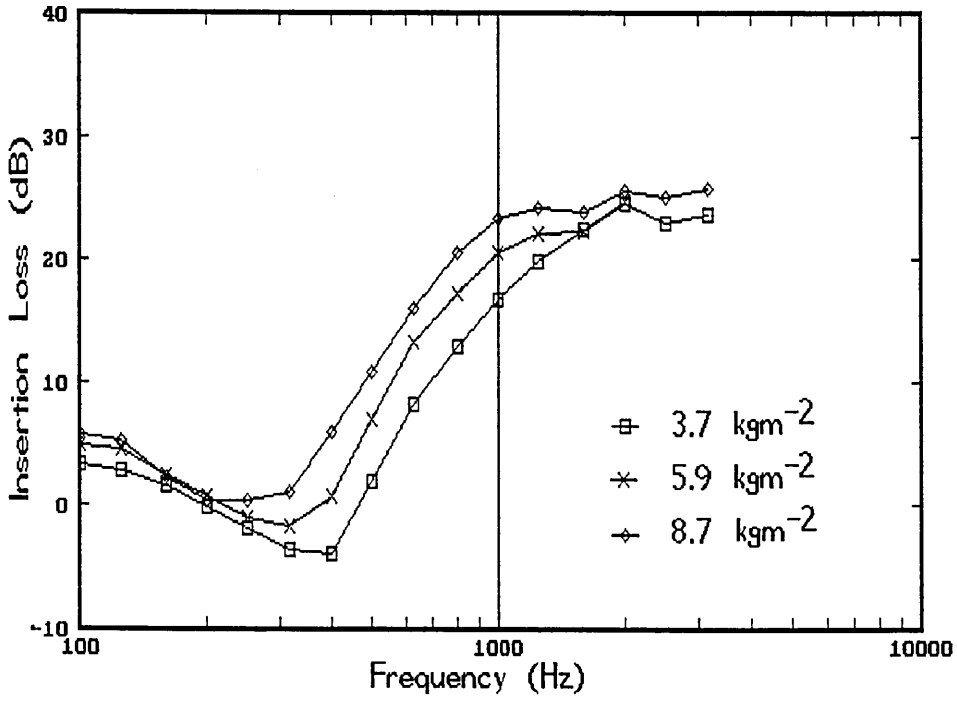

Fig. D12 Foam 12

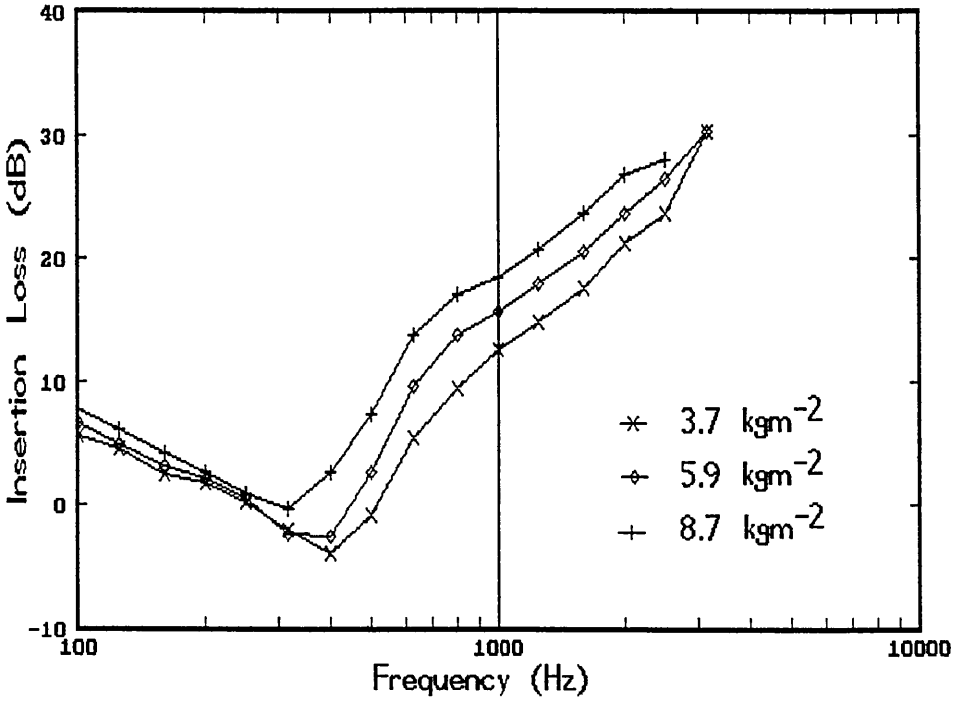

Fig. D13 Foam 13

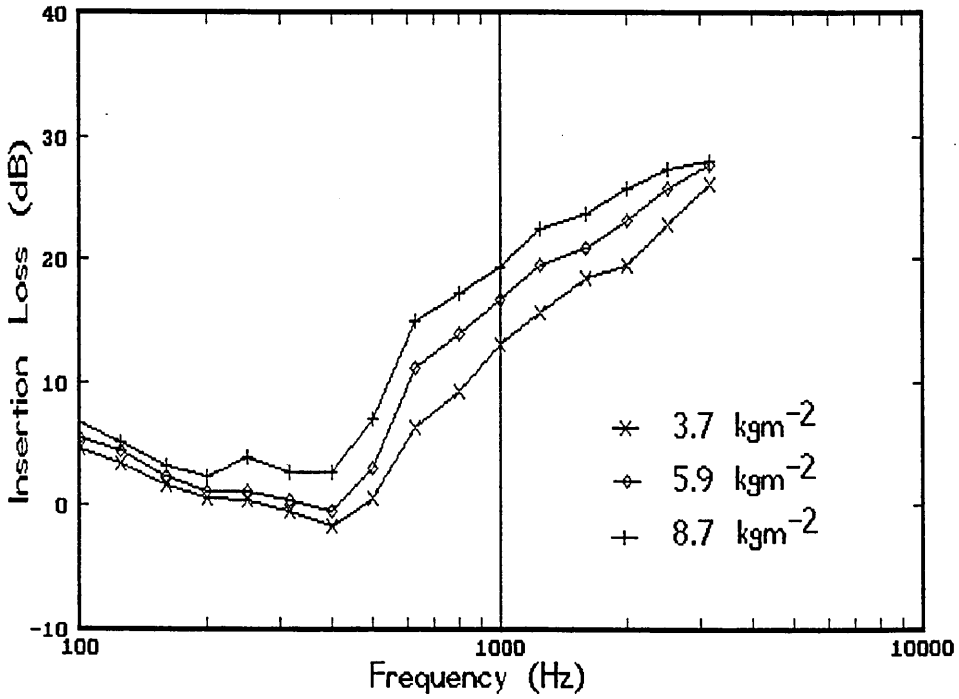

Fig. D14 Foam 14

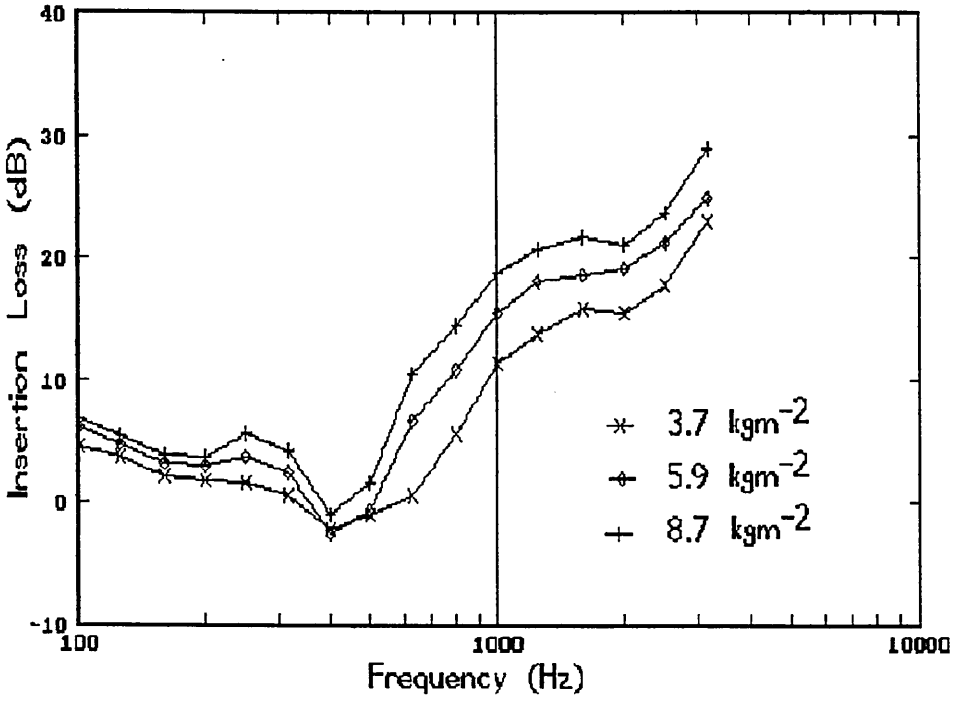

Fig. D15 Foam 15

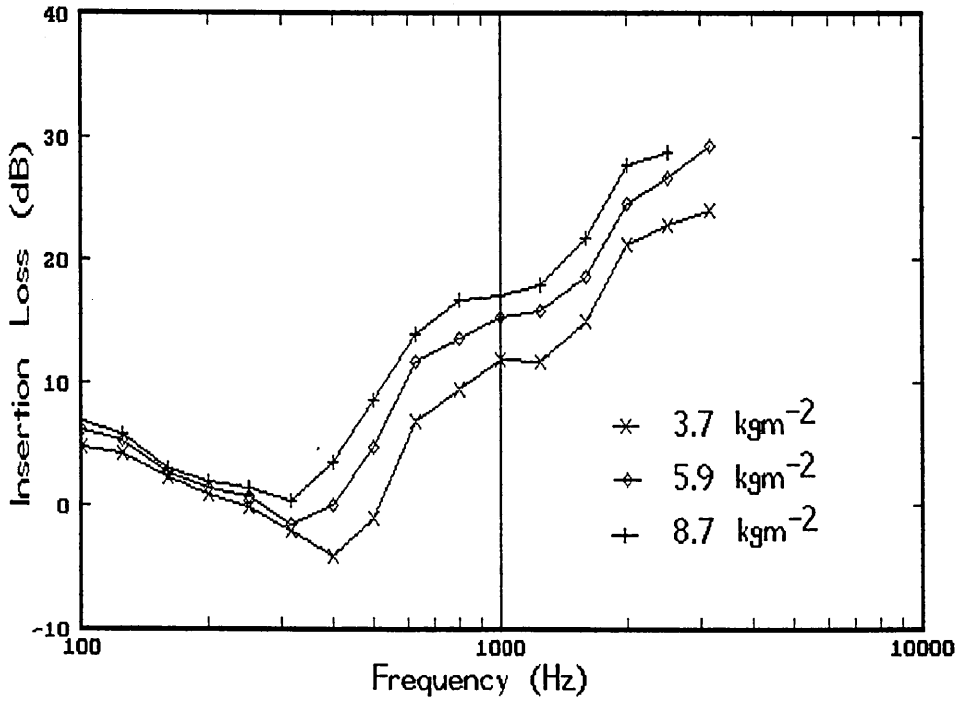

Fig. D16 Foam 16

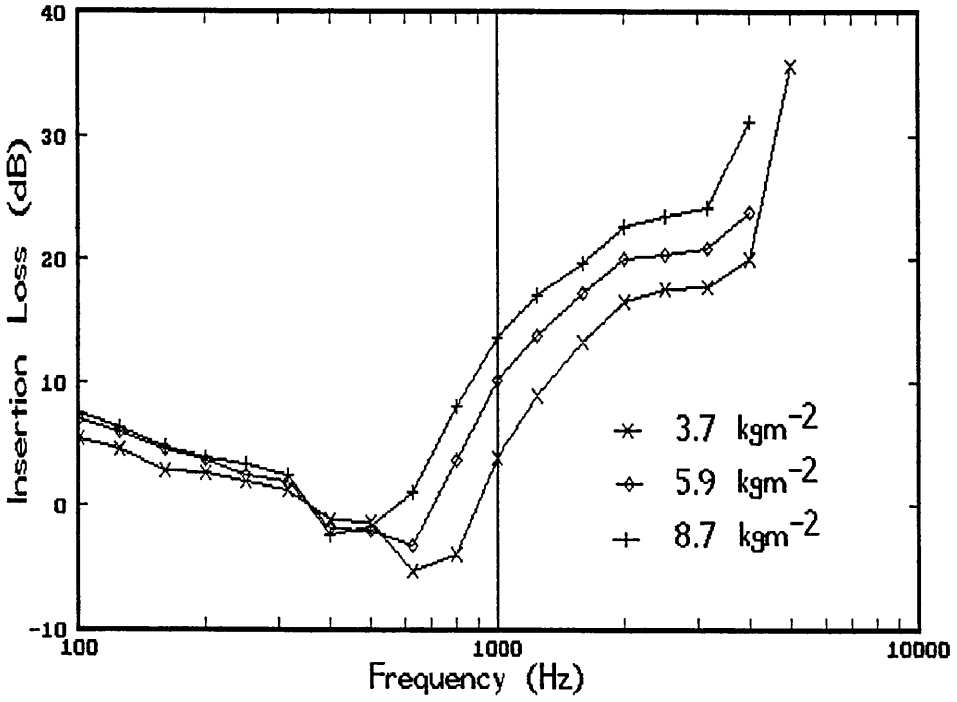

Fig. D17 Foam 17

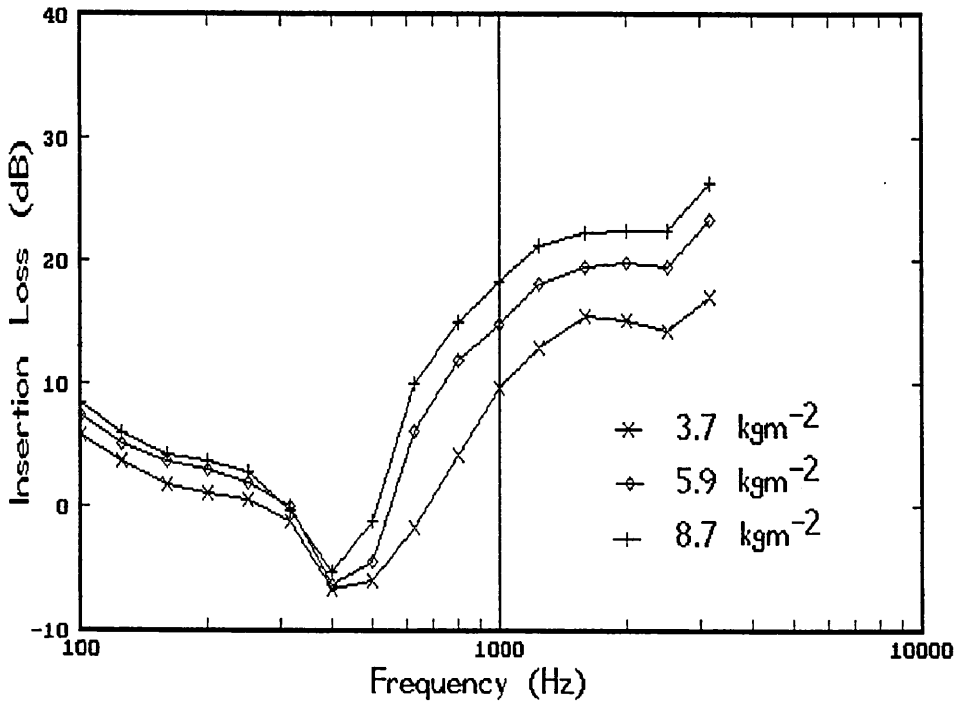

Fig. D18 Foam 18

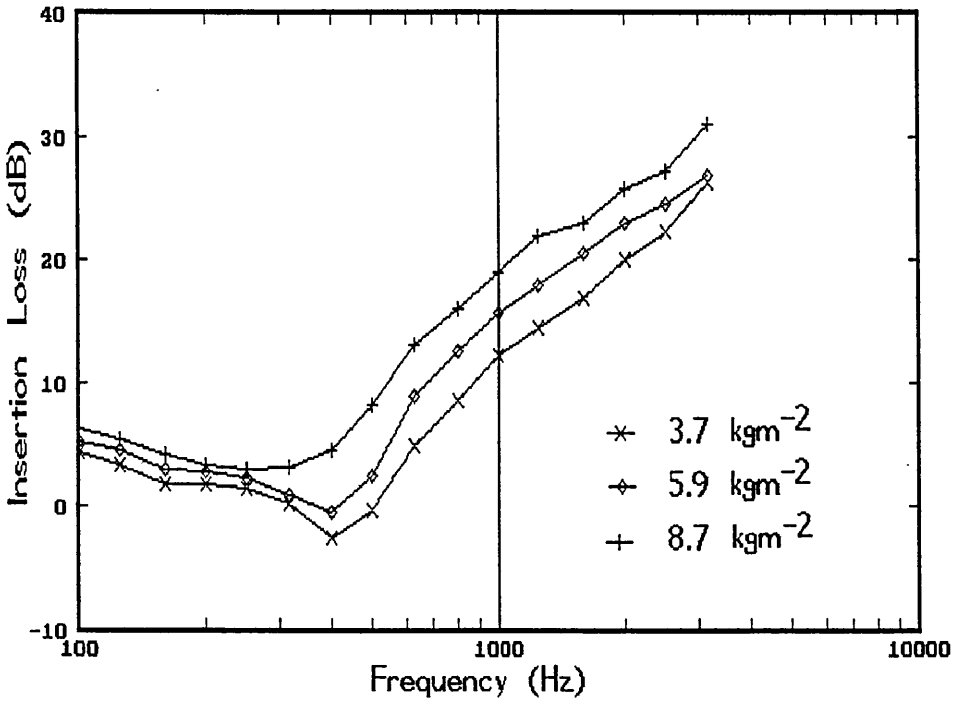

Fig. D19 Foam 19

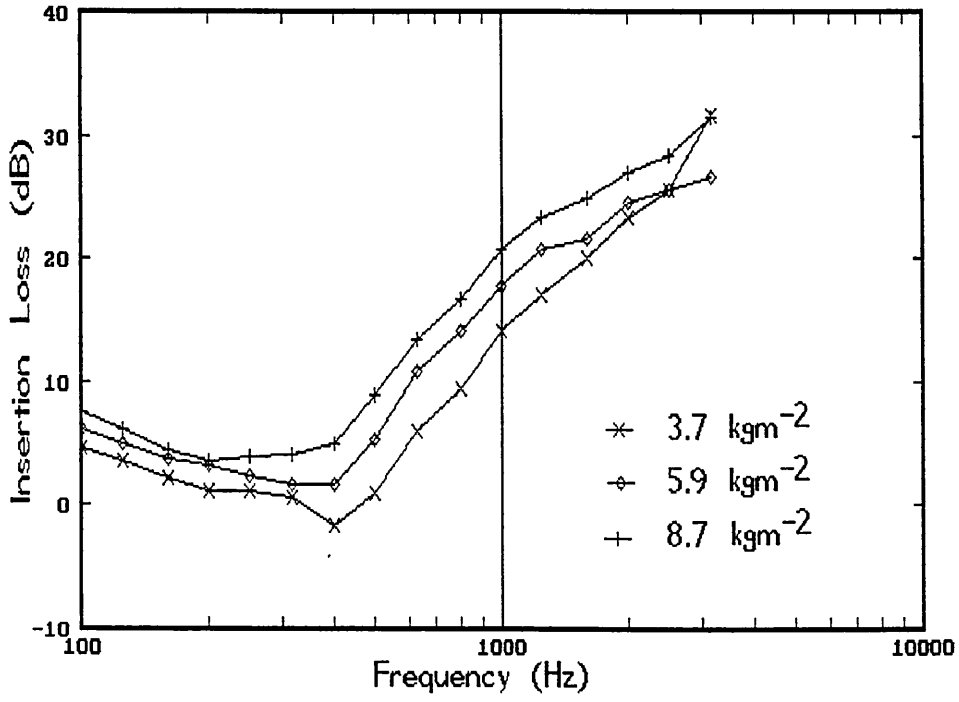

Fig. D20 Foam 20

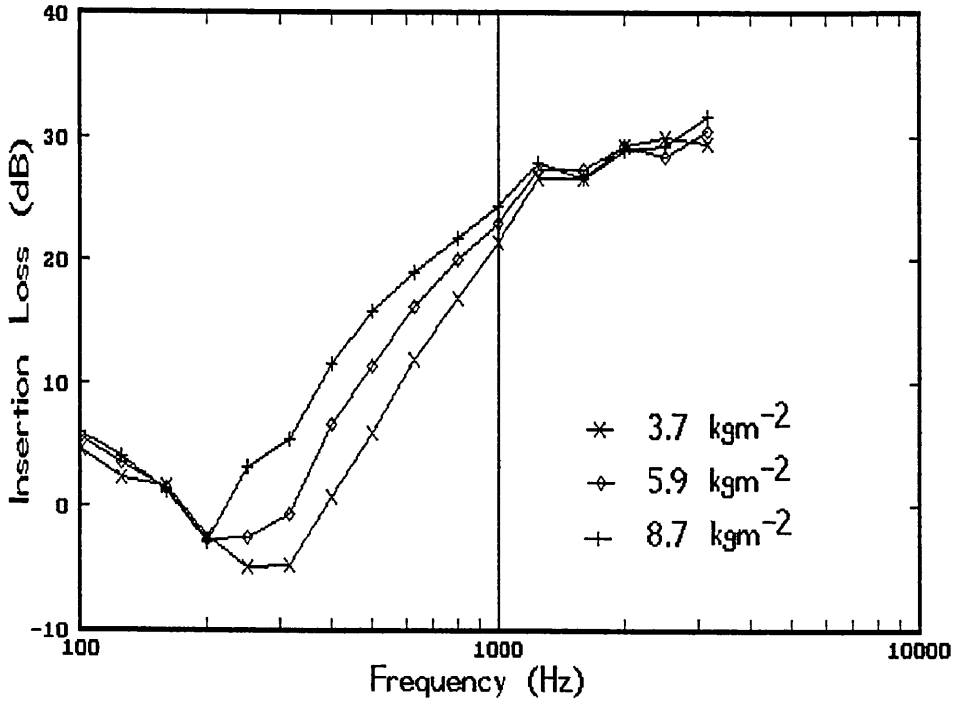

Fig. D21 Foam 21

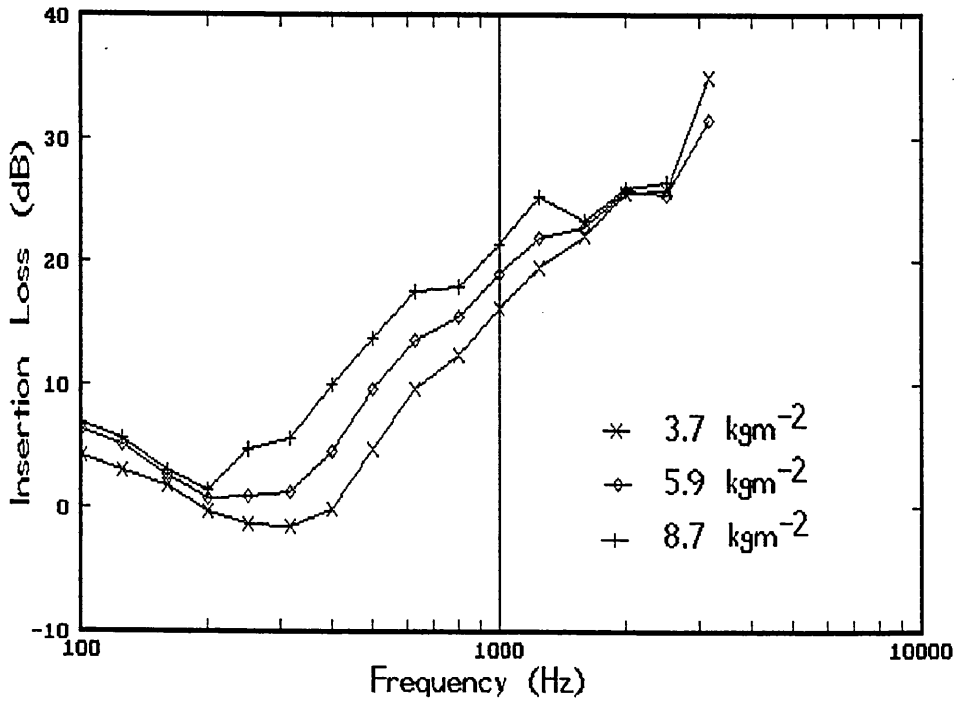

Fig. D22 Foam 22

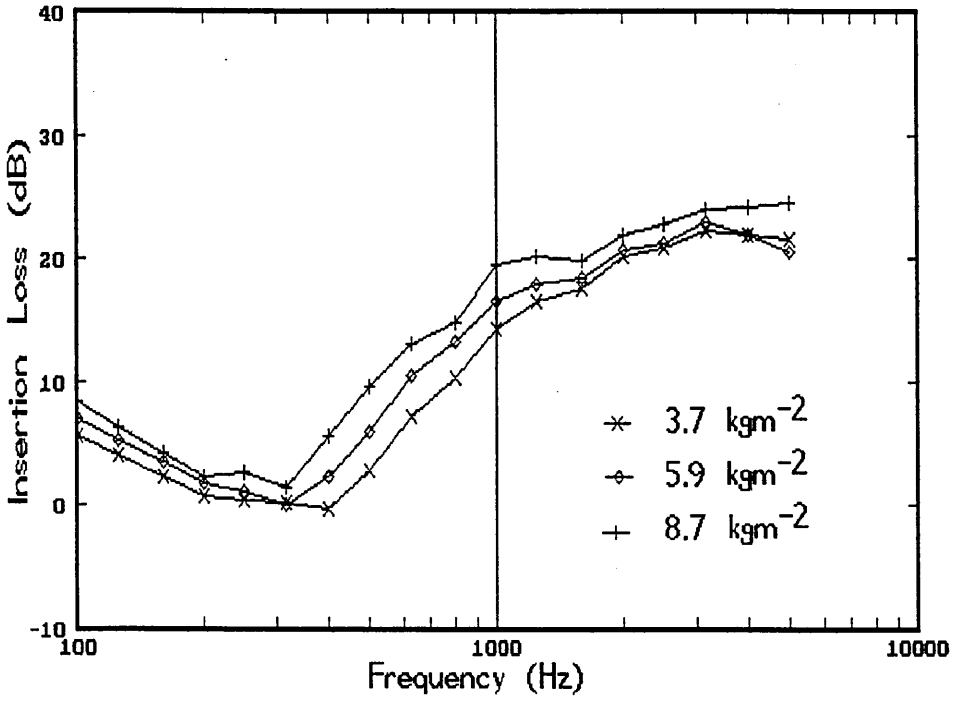

Fig. D23 Foam 23

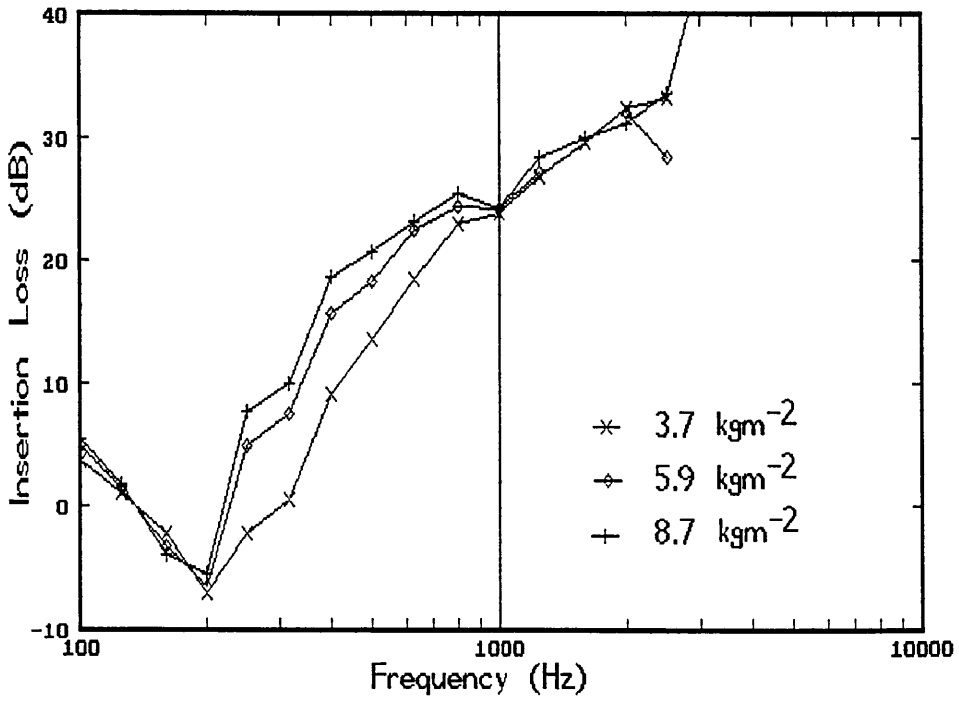

Fig. D24 Felt

APPENDIX E LOSS FACTOR

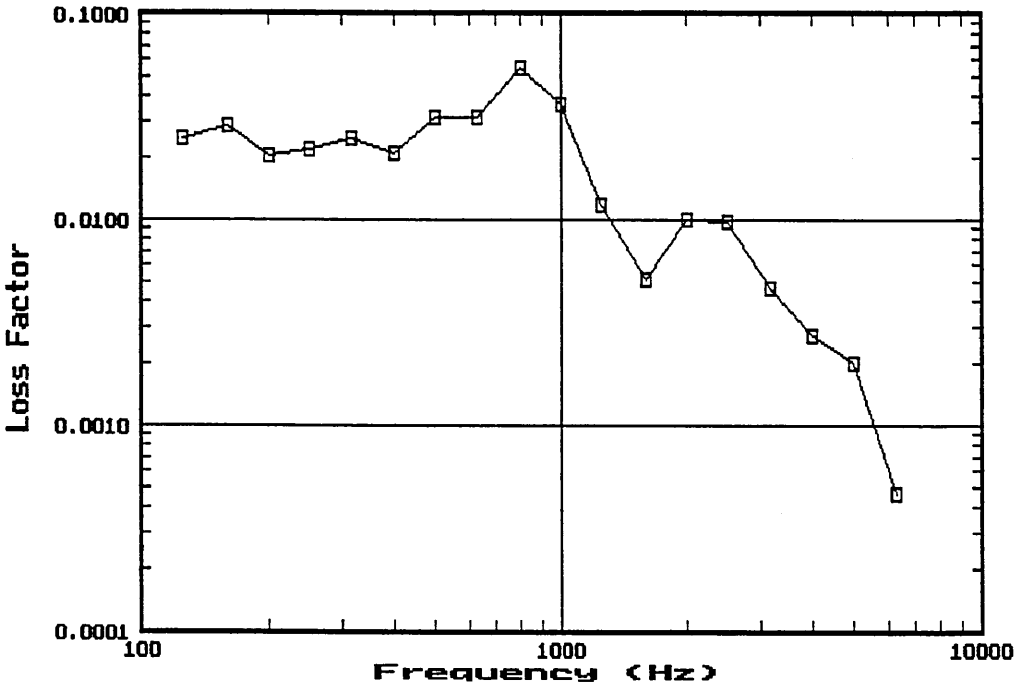

Fig. E1 Foam 1

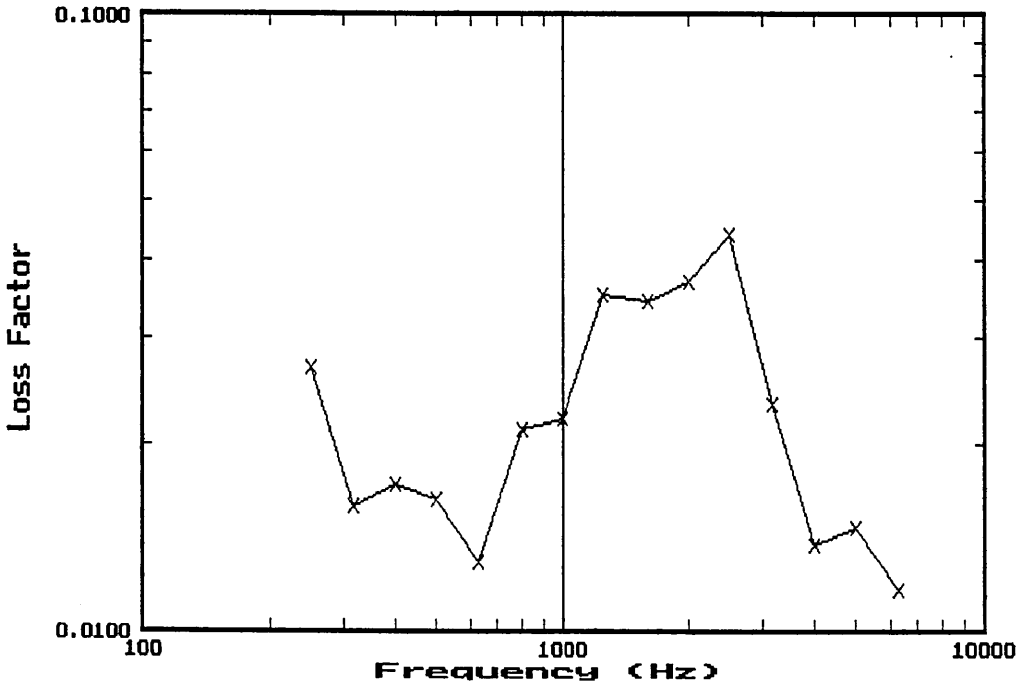

Fig. E2 Foam 2

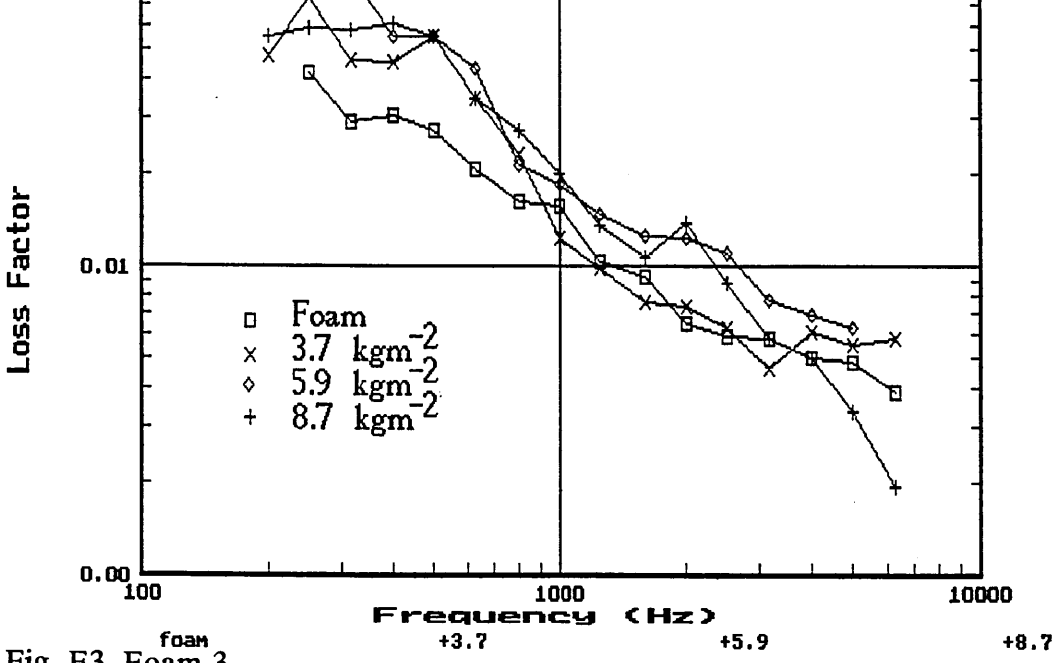

Fig. E3 Foam 3

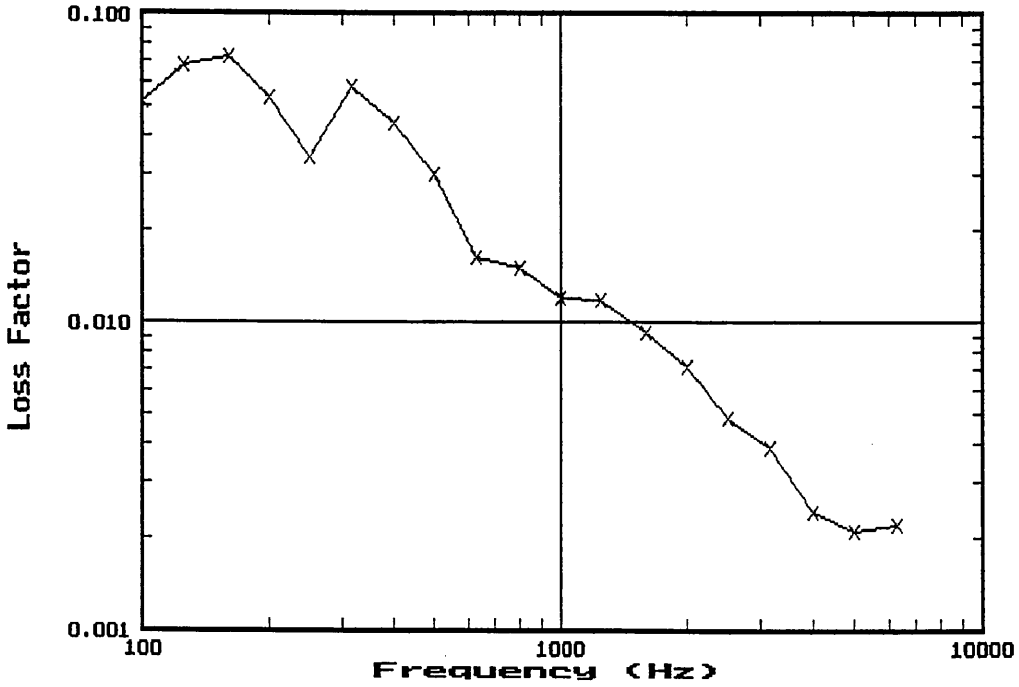

Fig. E4 Foam 4

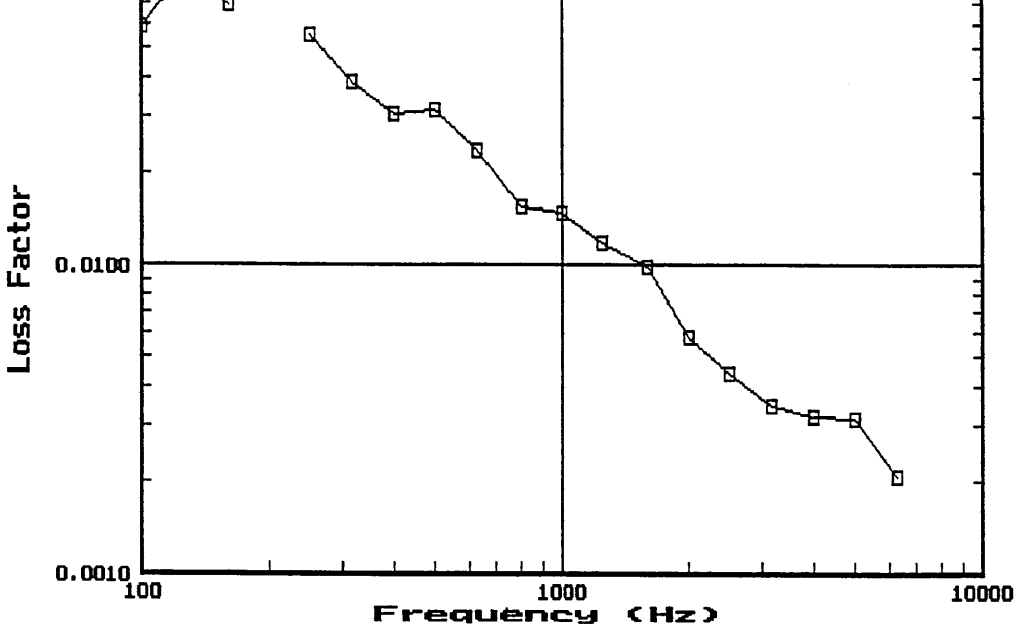

Fig. E5 Foam 5

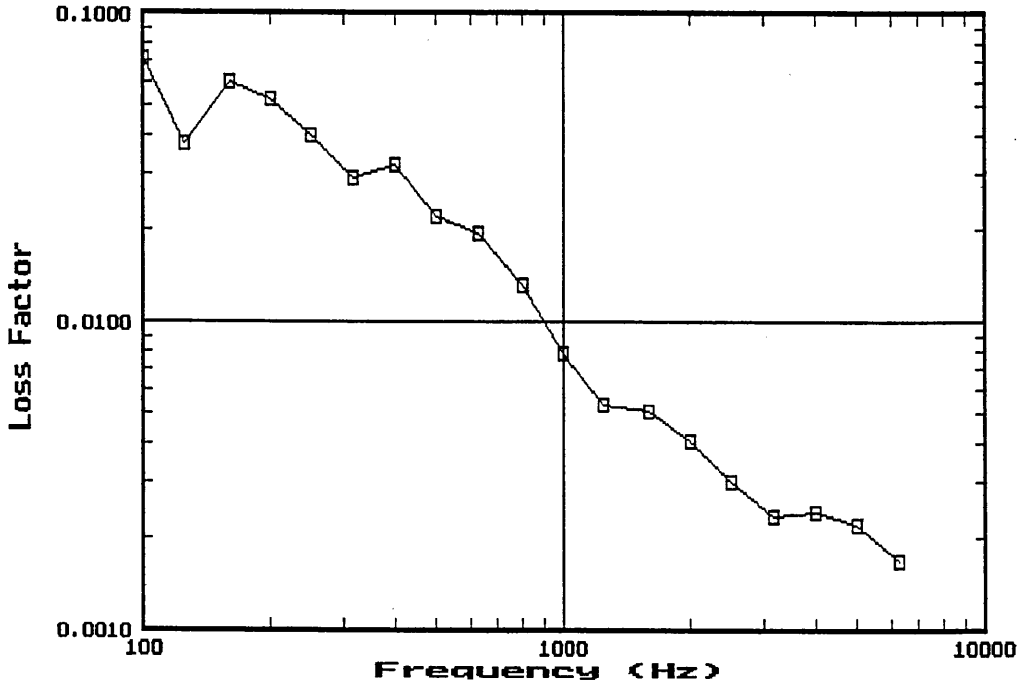

Fig. E6 Foam 6

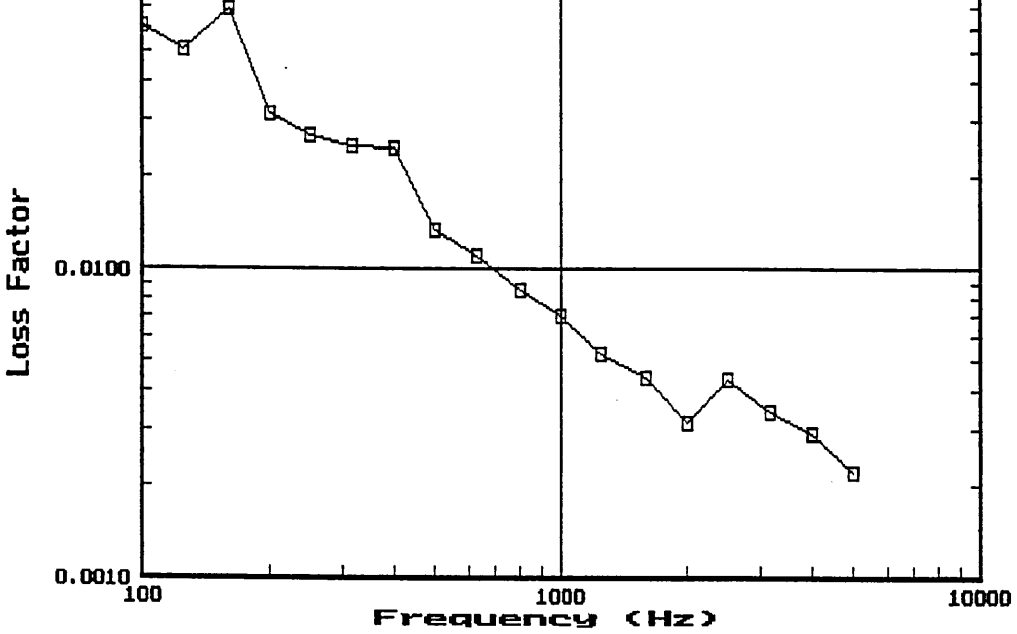

Fig. E7 Foam 7

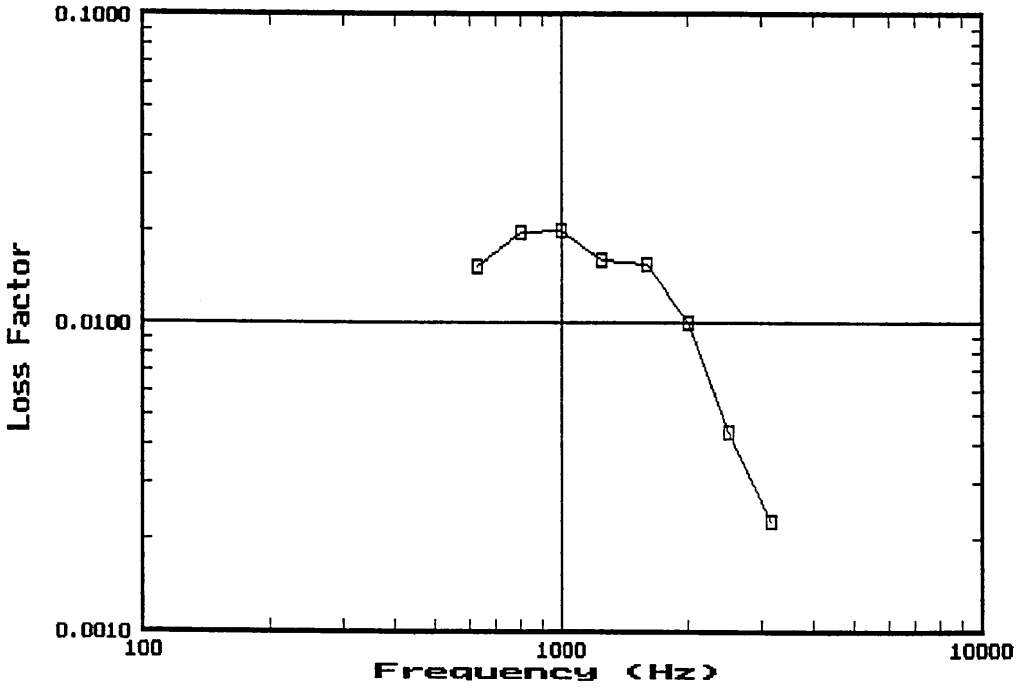

Fig. E8 Foam 8

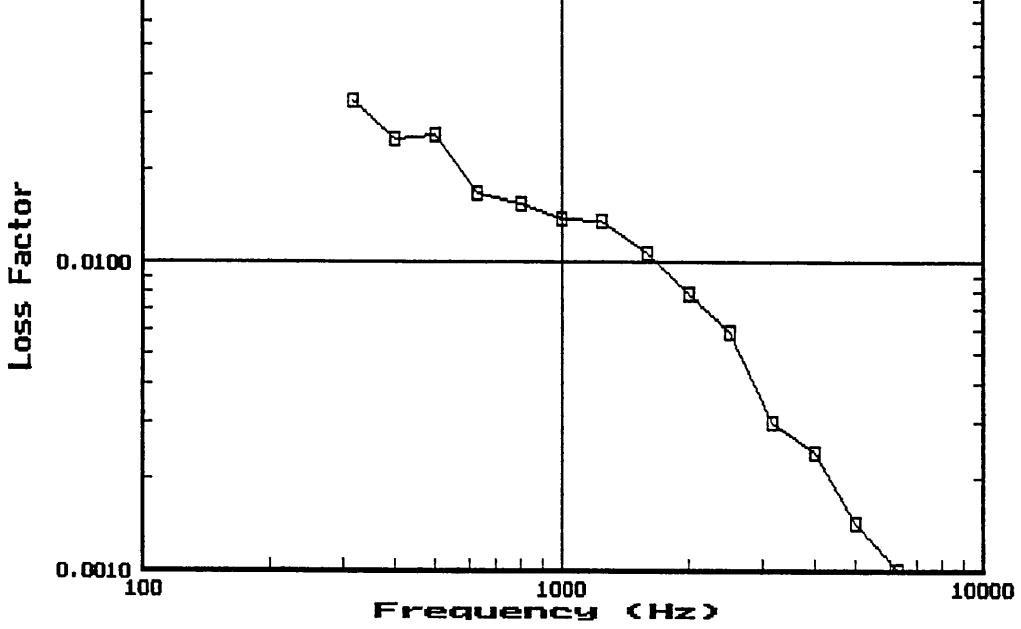

Fig. E9 Foam 9

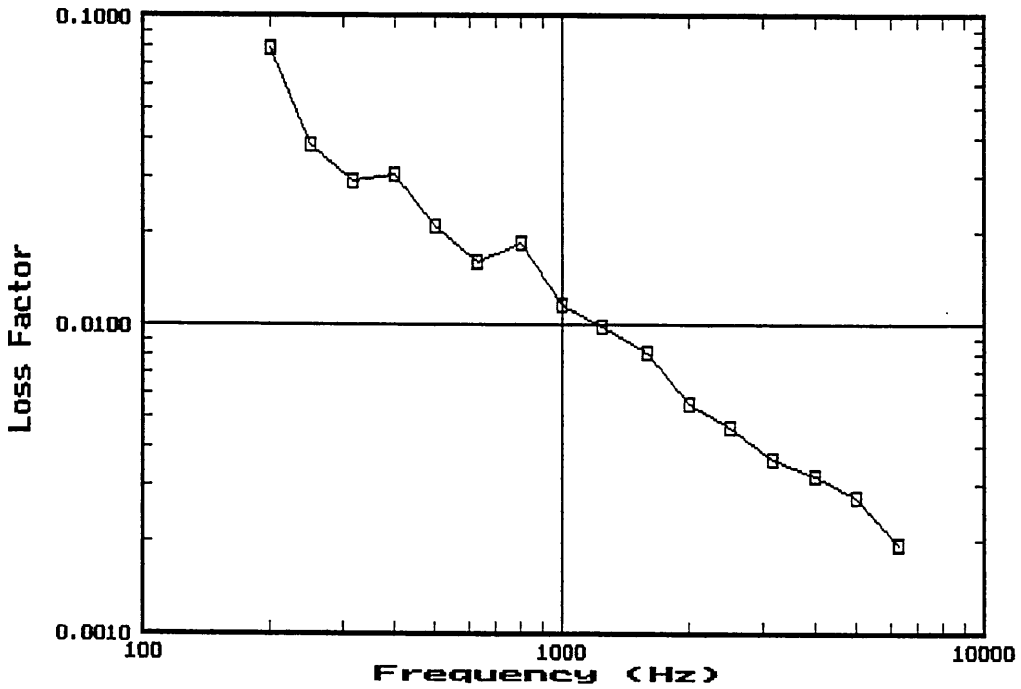

Fig. E10 Foam 10

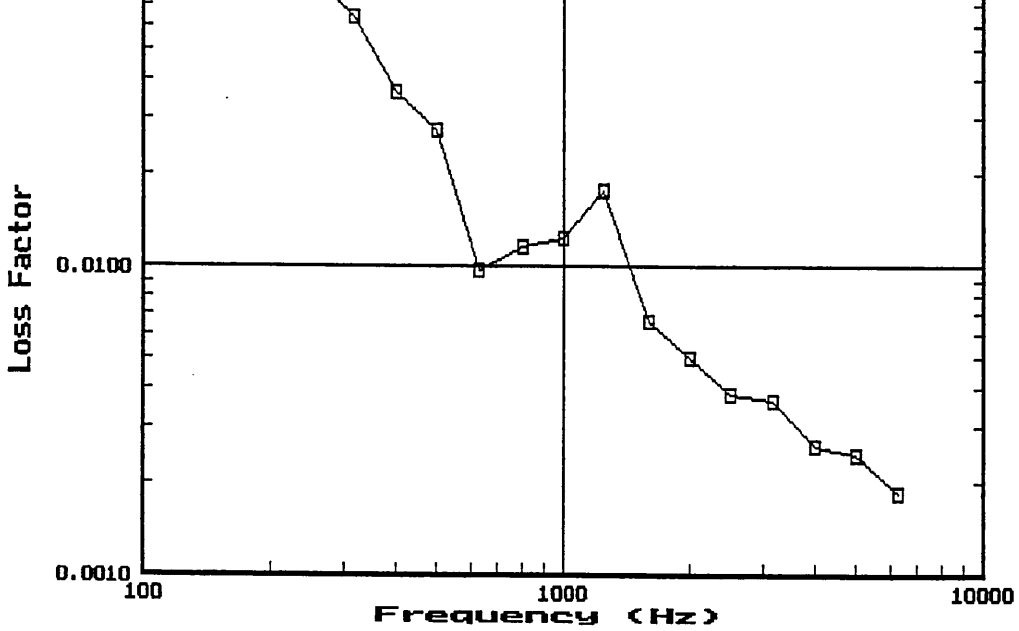

Fig. E11 Foam 11

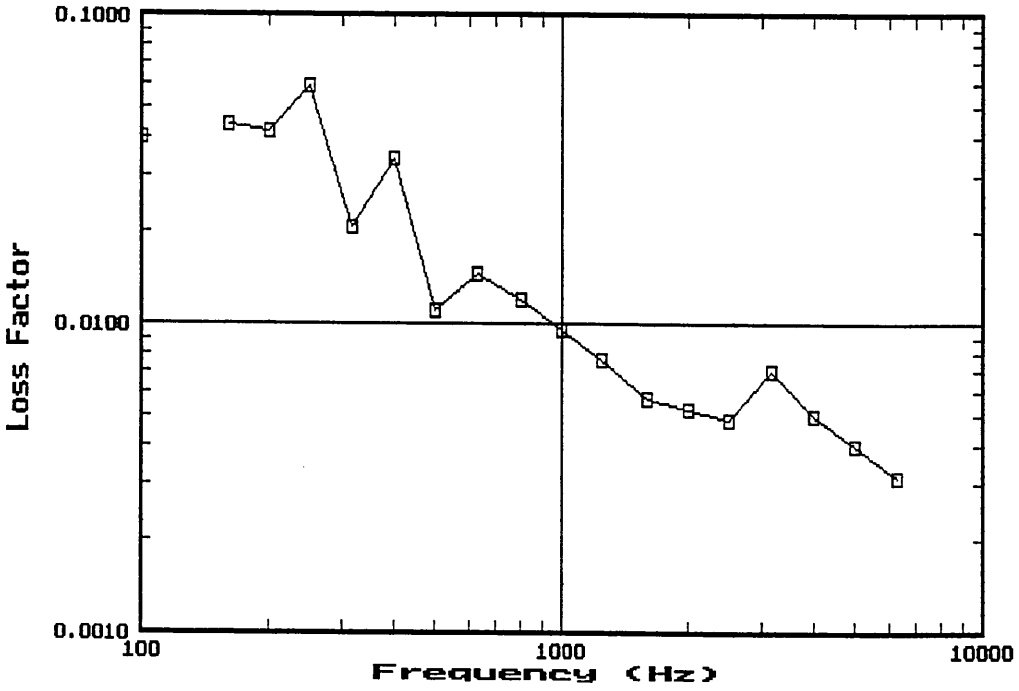

Fig. E12 Foam 12

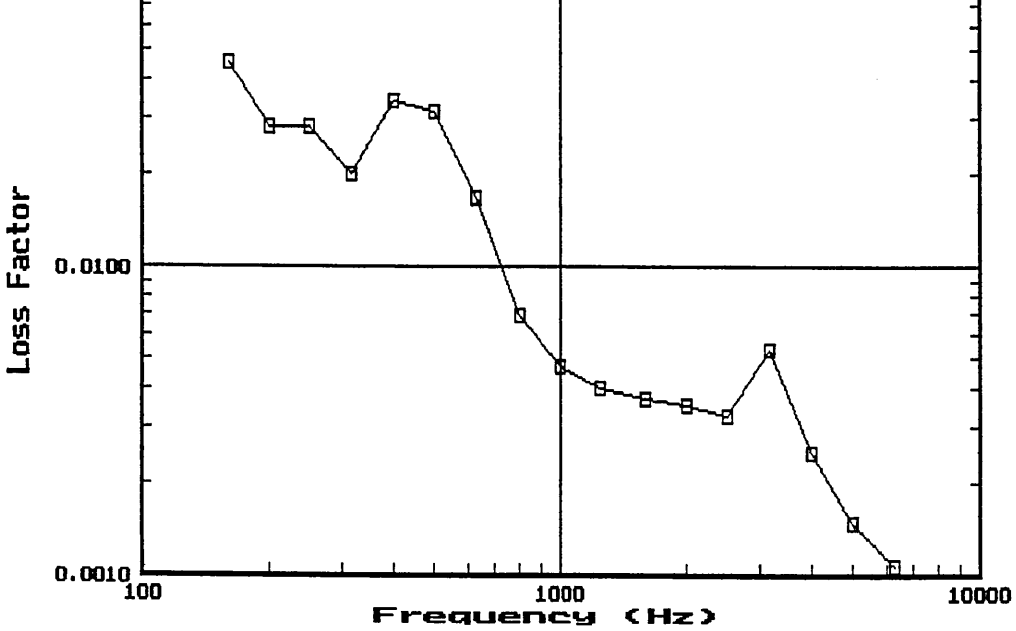

Fig. E13 Foam 13

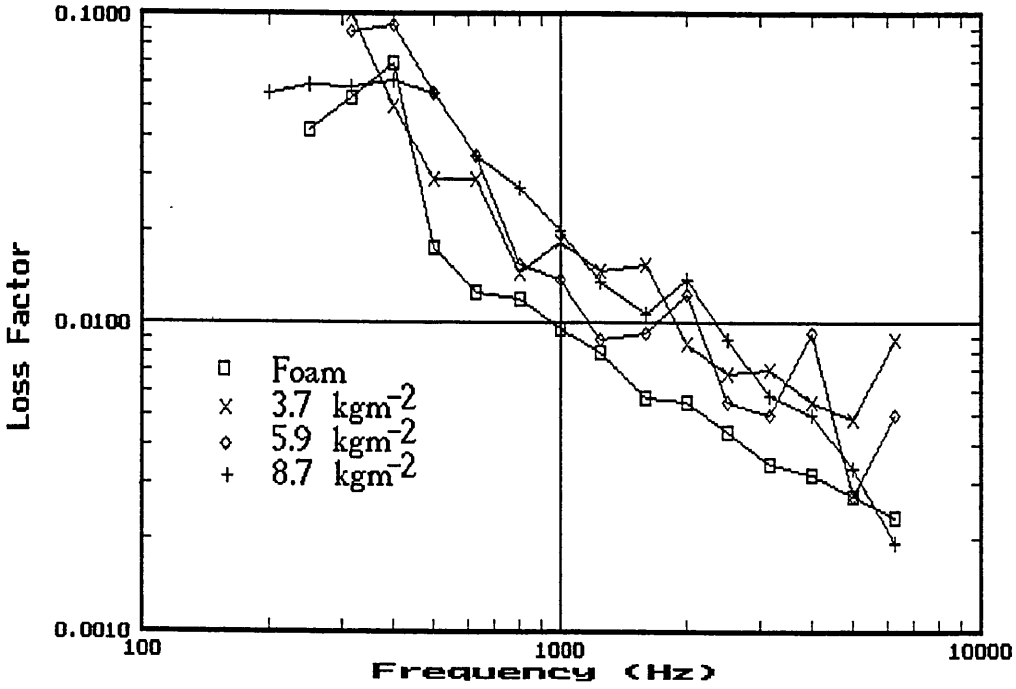

Fig. E14 Foam 22

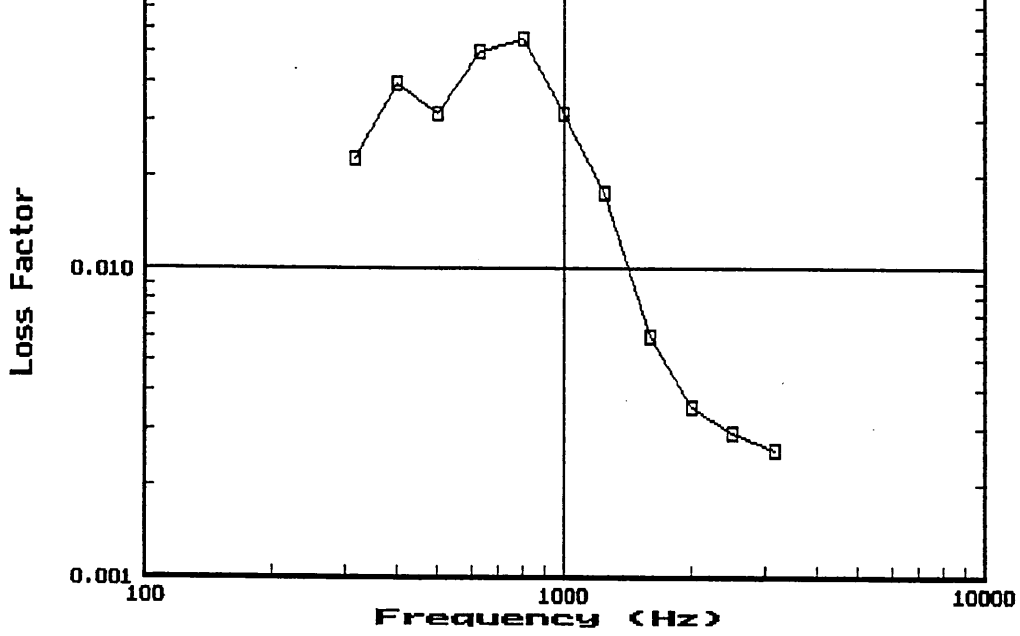

Fig. E15 Foam 23

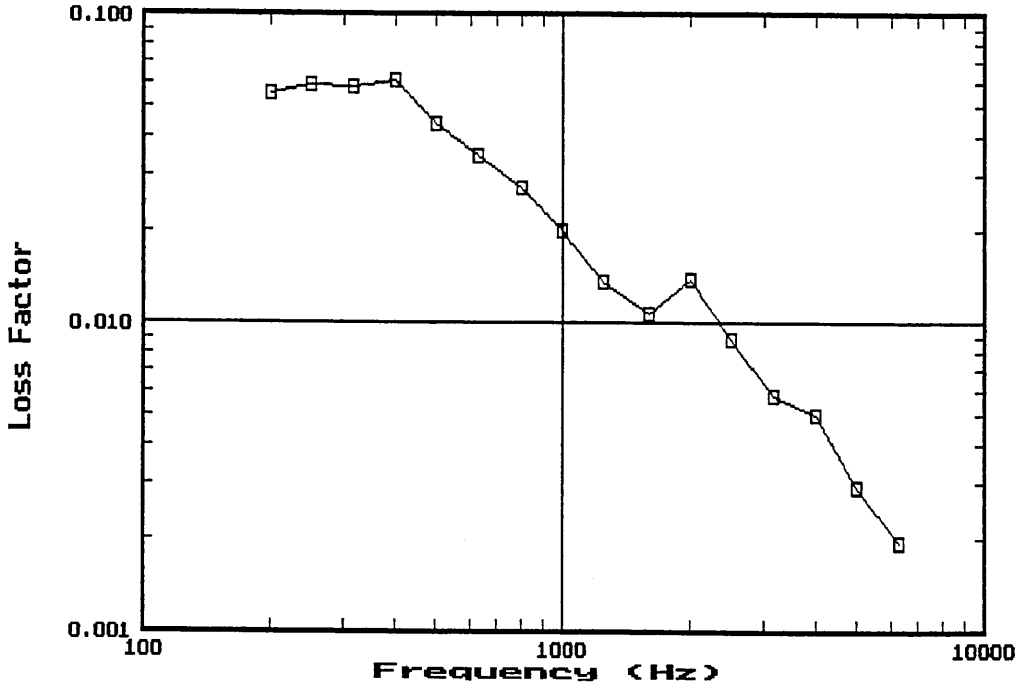

Fig. E16 Felt

Foam	Surface Density	Density	Thick-ness	Storage Modulus	Loss Factor	Freq	Flow Resistivity	
	kgm^{-2}	kgm^{-3}	mm	$x10^5Pa$		Hz	$kNsm^{-4}$	
							1	2
1	1.65	84.8	19.5	0.63 0.47 0.32	0.16 0.16 0.24	122 94 64	31	50
2	0.93	86.0	10.8	0.36 0.36 0.35	0.18 0.15 0.21	123 103 76	85	107
3	1.52	77.9	19.5	1.25 1.24 0.44	0.42 0.39 0.43	155 130 58	39	28
4	1.73	88.5	19.5	1.17 1.17 1.08	0.41 0.35 0.44	153 125 90	40	36
5	1.67	85.6	19.5	0.47 0.41 0.33	0.46 0.43 0.44	95 75 50	29	26
6	1.58	80.8	19.5	4.21 3.72 4.25	0.25 0.27 0.31	285 225 180	84	74
7	1.56	80.2	19.5	1.87 1.88 1.59	0.40 0.38 0.37	190 160 110	56	44
8	0.89	89.6	9.9	2.35 1.87 1.57	0.40 0.43 0.44	315 235 160	215	56
9	2.00	102.7	19.5	1.27 1.07 0.89	0.42 0.48 0.44	155 120 82	43	47
10	2.01	103.1	19.5	0.89 0.90 0.69	0.45 0.41 0.47	130 110 72	43	44
11	1.24	63.6	19.5	2.36 2.48 2.55	0.30 0.35 0.32	215 185 140	312	122

Table 6 Material properties

Data No.	Surface Density	Thick-ness	Storage Modulus	Loss Factor	Flow Resistivity
	kgm^{-2}	mm	$x10^5Pa$		$kNsm^{-4}$
1	2.0	20	1.1	0.5	50
2	1.6	20	1.1	0.5	50
3	1.2	20	1.1	0.5	50
4	0.8	20	1.1	0.5	50
5	0.8	10	1.1	0.5	50
6	1.6	20	1.1	0.8	50
7	1.6	20	1.1	0.2	50
8	1.6	20	0.5	0.5	50
9	1.6	20	1.8	0.5	50
10	1.6	20	1.1	0.5	20
11	1.6	20	1.1	0.5	100
12	1.6	20	1.1	0.5	130
13	2.4	30	1.1	0.5	50
14	2.4	30	1.1	0.2	50
15	0.8	10	1.1	0.2	50
16	1.6	20	0.2	0.5	50
17	1.6	20	0.2	0.2	50
18	1.6	20	0.5	0.2	50
19	1.6	20	1.8	0.2	50

Table 4 Material property values of test pieces used in the theoretical study

Foam	Surface Density	Density	Thick-ness	Storage Modulus	Loss Factor	Freq	Flow Resistivity	
	kgm^{-2}	kgm^{-3}	mm	$x10^5Pa$		Hz	$kNsm^{-4}$	
							1	2
12	1.26	64.6	19.5	0.84 0.63 0.46	0.44 0.62 0.50	128 93 60	20	182
13	1.99	101.8	19.5	0.82 0.63 0.61	0.22 0.28 0.31	125 92 68	403	378
14	1.65	85.7	19.2	1.00 0.99 1.00	0.18 0.11 0.14	137 115 87	137	61
15	2.00	101.2	19.8	1.90 1.80 1.60	0.14 0.17 0.11	185 150 108	268	115
16	2.45	83.2	29.4	0.89 0.80 0.83	0.16 0.12 0.14	102 82 63	99	63
17	0.88	87.7	10.0	1.10 1.40 1.20	0.23 0.21 0.19	200 192 135	272	88
18	1.32	69.2	19.0	0.87 0.92 1.10	0.15 0.18 0.14	130 112 90	348	59
19	1.66	86.0	19.3	0.90 0.95 0.90	0.49 0.42 0.51	130 112 82	113	50
20	1.60	84.8	18.9	0.88 0.67 0.61	0.50 0.56 0.47	130 95 68	78	53
21	1.60	84.8	18.9	0.21 0.17 0.21	0.22 0.21 0.20	64 48 40	31	29

Table 7 Material properties

Foam	Surface Density	Density	Thick-ness	Storage Modulus	Loss Factor	Freq	Flow Resistivity	
	kgm^{-2}	kgm^{-3}	mm	$x10^5Pa$		Hz	$kNsm^{-4}$	
							1	2
22	1.65	103.3	19.4	0.38 0.33 0.21	0.92 0.80 0.76	85 67 40	35	35
23	1.31	69.5	18.9	0.45 0.38 0.31	0.41 0.41 0.43	94 72 49	235	77
FELT	1.41	76.2	18.5	0.04 0.05 0.06	0.24 0.35 0.53	29 26 22	17	
24	0.40	29.6	14.0	2.20	0.18	200		1.5
25	0.78	31.2	25.0	1.90	0.15	200		4.5
26	1.12	29.5	38.0	1.90	0.14	200		10.5
27	2.49	85.9	29.0	1.50	0.21	200		27
28	2.44	84.1	29.0	2.50	0.65	200		110

Table 8 Material properties